Organic materials for photovoltaic devices

by

John le Quesne, B. Sc.

Thesis submitted to the University of Nottingham for
the degree of Doctor of Philosophy, March 1997

Acknowledgements

The completion of this thesis has involved help from a number of people to whom thanks must be offered.

Firstly, I would like to thank my supervisor, Dr. M.R. Willis, for his constant encouragement, advice and ideas throughout this research. It has been a pleasure to work with him over the last three years.

I would also like to thank my laboratory colleagues, Adam Loveday, Dr. Steve Kinge, Stafford Burt, Susan Appleyard and Dr. Hitoshi Fujimoto for their supervision, guidance and friendship. I wish them all well.

Thanks are due to the technical staff in the department. To Neville Brown and Neil Barnes for repairing broken equipment, the glassblowers, Ron and Tony and the members of the Cripps Computing Centre for helping to install the EH program.

Running the EH program required atomic coordinates from the Daresbury database and I would like to acknowledge the help of Dr. Sandy Blake in transferring these and the help in adjusting the program given by Dr. Wheatley.

Finally, I would like to thank Prof. Maruyama, Dr. Atsushi Suzuki and Dr. Shoali Fang for their help during my time at the Institute for Molecular Science, Okazaki, Japan and to the British Council and Japanese government for funding me for this.

Contents

Abstract

This thesis is a contribution towards the understanding of the operation of bilayer solar cells, and the development of a theoretical basis for the selection of suitable pairs of materials for the fabrication of such cells.

The work is divided into two main areas:
(a) theoretical calculations on materials used in solar cells
(b) fabrication of devices to test the calculations.

Practically, many devices were made using some previously untried materials, the most successful of which was formed from dibromoanthanthrone and titanyl phthalocyanine. This sample was 0.30% efficient under incident white light of intensity $20mW/cm^2$ and had an open circuit voltage of 0.39V. Measurements of the response time of the sample were also recorded which provided information on the quality of the device made.

Theoretically, calculations were performed using the extended Huckel method on potential materials for photovoltaic devices. Initially, these provided information on the variation of bandwidth with inter-ring separation for cofacially stacked phthalocyanines. They were also used to predict the position of the HOMO/LUMO for different materials. Then by deducing the position of the Fermi level, it is possible to simulate the junction formed between the two materials. Predicted behaviour for the phthalocyanine/perylene interface agreed with that found experimentally from UPS and optical absorption measurements of the ionisation potentials, work functions and band gaps for a similar junction. The calculations have also demonstrated how substituting or changing the two layers alters the performance of the device. This allowed a set of criteria to be established that should enable a more systematic approach to choosing potential pairs and then optimising their performance in future solar cells.

Glossary of abbreviations

χ	Electron affinity of the material
σ	Conductivity
μ	Mobility of electrons/holes
τ	Response time of device
λ	Wavelength (of light)
e	Charge on the electron
ε	Electrical permittivity of the material
ΔE_C	Magnitude of discontinuity in the conduction band
ΔE_V	Magnitude of discontinuity in the valence band
E_C	Energy of conduction band
E_F	Fermi level
E_G	Band gap
E_V	Energy of valence band
Eff	Efficiency of device (%)
FF	Fill Factor of device
H_{ii}	Diagonal elements of the Hamiltonian matrix
H_{ij}	Off diagonal elements of the Hamiltonian matrix
HOMO	Highest Occupied Molecular Orbital
LUMO	Lowest Unoccupied Molecular Orbital
ITO	Conducting glass
J_{sc}	Short curcuit current (density)
J_{np}	Current density flowing across a p-n junction from the n-type material to the p-type material
J_{pn}	Current density flowing across a p-n junction from the p-type material to the n-type material
k_B	Boltzmann constant
k_1	Pre-exponential term in the formula for the off-diagonal elements of the Hamiltionian matrix proposed by Marynick
k_2	Exponetial term in the formula for the off-diagonal elements of the Hamiltonian matrix proposed by Marynick
n	Concentration of electrons/holes
R_s	Series resistance of device
R_{sh}	Shunt resistance of device
S	Overlap matrix
V_{bi}	Built-in voltage of a junction
V_{app}	Applied voltage
V_{oc}	Open circuit voltage
W_d	Width of depletion region

Glossary of molecular structures

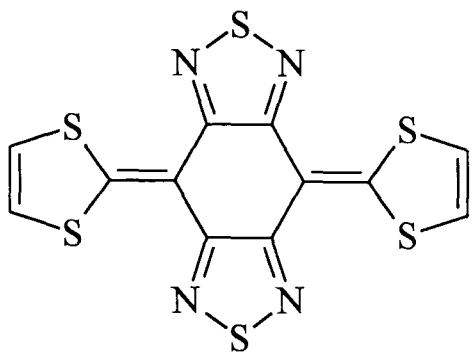

BTQBT: bis [1,2,5]thiadiazolo-*p*-quinobis (1,3-dithiole)

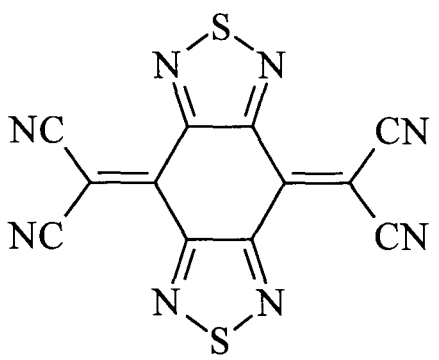

BTDA: bis (1,2,5-thiadiazolo) tetracyanoquinodimethane (sometimes referred to as BTDA-TCNQ)

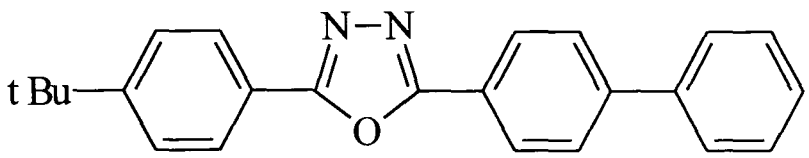

PBD: biphenylyl-*tert*-phenyl-1,3,4-oxadiazole

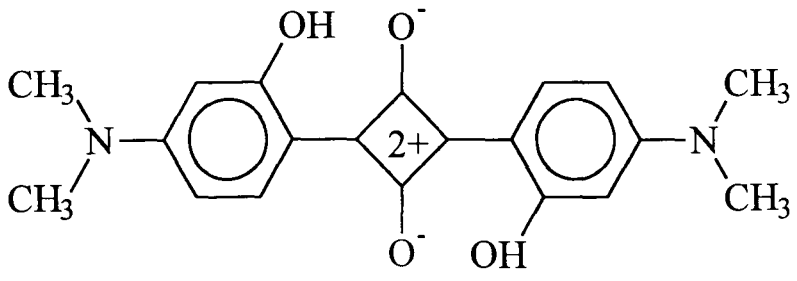

Sq5 (Squaraine 5) according to the nomenclature proposed by Law.

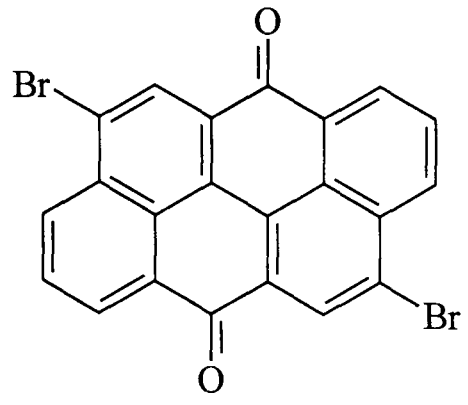

DBA: Dibromoanthanthrone

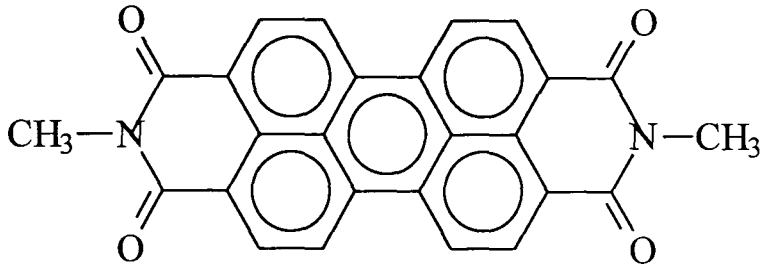

MPCI: dimethyl perylenetetracarboxylic acid diimide

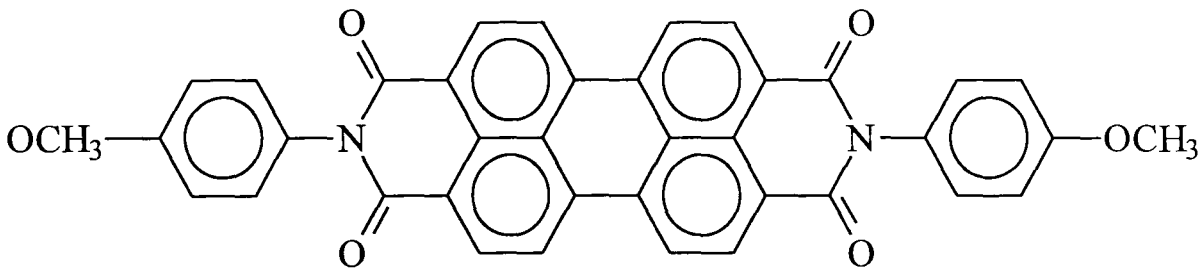

MOPPCI: dimethoxyphenyl perylenetetracarboxylic acid diimide

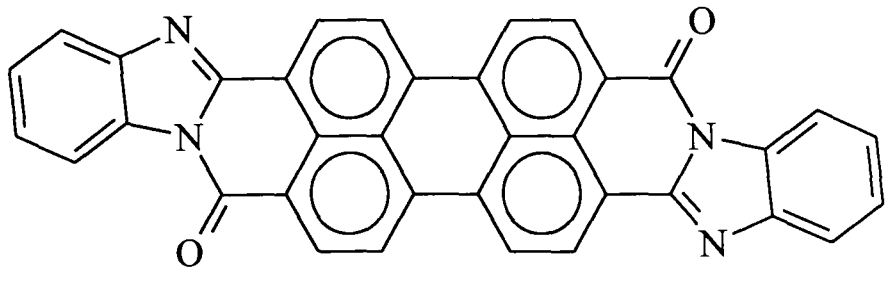

ImPCI: Perylenetetracarboxylic acid benzimidazole

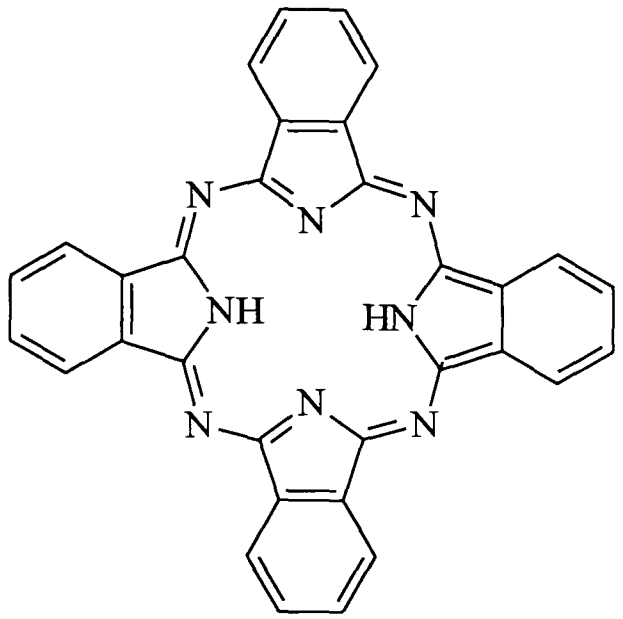

H_2Pc: Metal free phthalocyanine

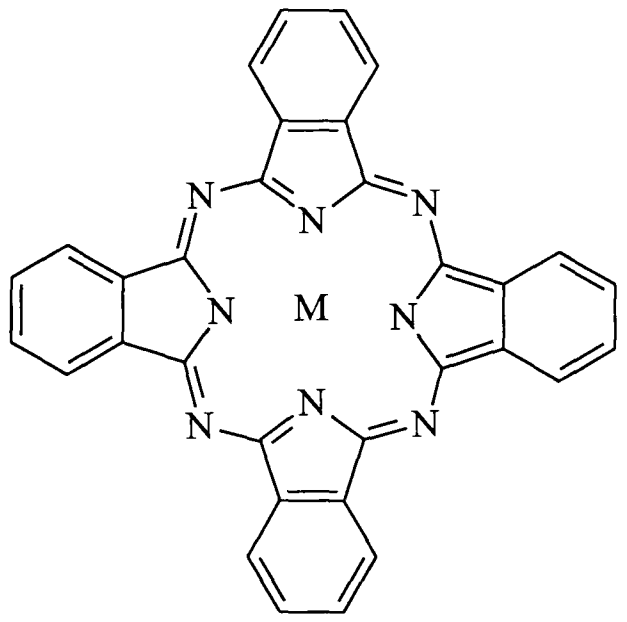

MPc: Metal phthalocyanine where M is the central metal atom (e.g. TiOPc, ZnPc, AlFPc)

TPyP: 5,10,15,20-tetra(4-pyridyl) 21H,23H-porphine

DMQ: 2,9-dimethyl quinacridone

Chapter 1:- Conduction in solids

1.1 Historical perspective

The conversion of light quanta into electricity was first shown by Becquerel[1] in 1839 when he discovered that the potential of an electrode in an electrolyte is varied when the electrode is exposed to light. Adams and Day[2] observed a similar effect in a solid material, selenium. Subsequent work followed on the photovoltaic effect in selenium and cuprous oxide led to the development of cells which were 1% efficient. Renewed interest was stimulated in 1954 when Chapin et al[3] reported a solar cell with an efficiency of around 6% made from a silicon single crystal. Twenty years of development increased the efficiency to about 10%. In 1956, Jenny et al[4] proposed a cell with an efficiency of 4% based on gallium arsenide. Improvements in technology have improved this figure to approaching 24%.

1.2 Solid state background[5-7]

The transport of electrical charges in a material is dependent upon the number of free charge carriers (i.e. electrons and holes) and their mobility. The simplest way of expressing this is to define the conductivity of a material.

$$\sigma = n_e . e . \mu_e + n_h . e . \mu_h \qquad (1)$$

where σ = conductivity.

n = concentration of electrons/holes.

μ = mobility of the electrons/holes.

The conductivity of a material represents the amount of charge that will be transported per second per unit area per unit applied electric field. Thus the conductivity gives a measure of the number of free charge carriers and their ability to move through a lattice. When there is more than one type of charge

carrier present, then the conductivity is the sum of the contributions as long as the interactions between these charge carriers are negligible. Chemically, electron transport in organic materials requires two processes: the creation of free charges and their ability to migrate. The conductivity domain of metals, semiconductors and insulators is shown in fig 1.1. Whereas inorganic compounds span the entire scale, undoped organic derivatives mostly belong to either metals or insulators.

The mobility of charge carriers is dependent upon their ability to move freely through the lattice. Transient states located within the band gap (more commonly known as traps) can act as centres which inhibit the carrier from moving freely through the crystal. When a trapped carrier is released, it is free to move through the crystal unless it recombines with another carrier or is trapped again. Traps are usually split into two groups. Shallow (electron) traps lie just below the conduction band at an energy less than the thermal energy, kT. Electrons caught in these traps can be easily released and have little effect on the conductivity of the material. Deep traps lie too far below the conduction band to be emptied by thermal energy, so electrons caught in these traps tend to be held for a long time. This causes a reduction in the conductivity. The effect of traps is seen most clearly in the rise and decay profiles for the photocurrent and it causes an overall reduction in the number of charge carriers, so reducing the dark conductivity. As traps are usually caused by lattice disorder or impurity sites, films which are more ordered are expected to display a larger dark conductivity.

In order to make more quantitative predictions, a model needs to be employed which takes the structure of the individual molecule and information on its stacking and returns information on the density of free charges and their mobility. The band model has been frequently used effectively on monocrystalline materials and provided useful insights into their properties so it will provide a framework for discussing the properties of organic thin films.

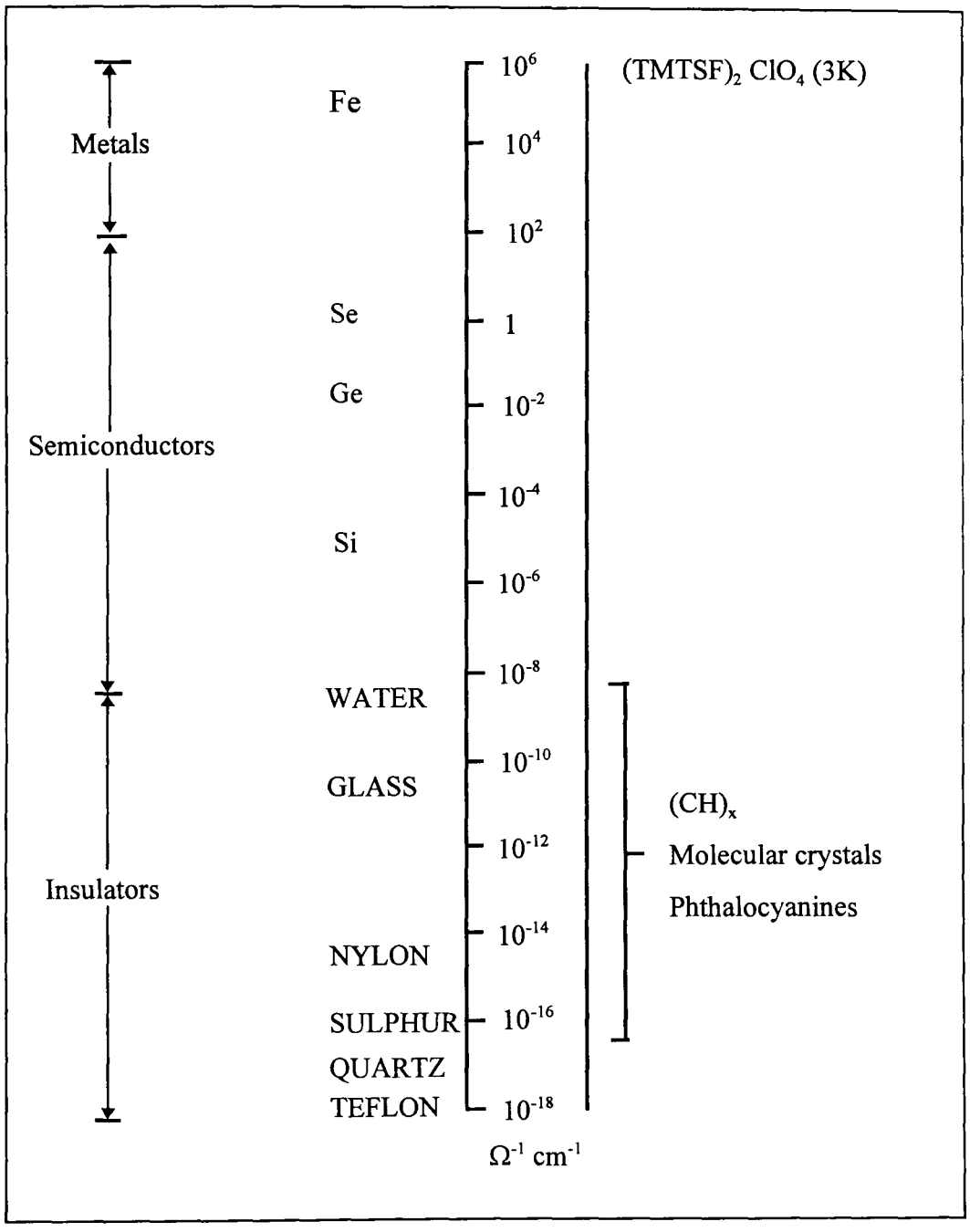

Fig 1.1: Conductivity domains of metals, semiconductors and insulators.

1.2.1 Free electron model

This model was proposed by Sommerfield[8] to describe the conduction in metals where the electrons are only restricted by the confines of the edge of the solid. The following assumptions/approximations are made:

1. Each atom 'releases' valence electrons which are free to migrate throughout the crystal.
2. There is a lattice of positively charged ions which do not interact with the electrons (the free-electron approximation)
3. Electrons do not interact with each other (independent electron approximation)
4. Electrons obey Fermi-Dirac statistics. i.e. the probability of an electron state of energy, ε, being occupied at a temperature, T, is

$$f(\varepsilon) = \left[e^{\beta(\varepsilon-\mu)} + 1\right]^{-1} \tag{2}$$

where $\beta = (k_B T)^{-1}$

μ = chemical potential of an electron

This allows the Schrodinger wave equation to be solved for a free particle in three dimensions,

$$-\frac{\hbar^2}{2m}\left(\frac{\partial}{\partial x^2} + \frac{\partial}{\partial y^2} + \frac{\partial}{\partial z^2}\right)\Psi_k(r) = \varepsilon\Psi_k(r) \tag{3}$$

If the particle is in a cube of length, L, the wavefunctions which satisfy this equation are:

$$\Psi_k(r) = \exp(ik.r) \tag{4}$$

where the wavevector, k, satisfies the condition,

$$k_x = 0, \pm\frac{2\pi}{L}, \pm\frac{4\pi}{L} \tag{5}$$

The solution of the equation for the energy, ε_k, of an orbital with wavevector, k, is

$$\varepsilon_k = \frac{\hbar^2}{2m}k^2 = \frac{\hbar^2}{2m}\left(k_x{}^2 + k_y{}^2 + k_z{}^2\right) \tag{6}$$

In the ground state of a system with N free electrons, the occupied orbitals can be represented by points in a sphere in k space. The energy of the surface of the sphere is defined as the Fermi energy. So by determining the Fermi wavevector, k_f, in terms of the electron concentration (N/V), it is possible to define the Fermi energy, ε_f.

$$k_f = \left(\frac{3\pi^2 N}{V}\right)^{1/3} \tag{7}$$

so

$$\varepsilon_f = \frac{\hbar^2}{2m}\left(\frac{3\pi^2 N}{V}\right)^{2/3} \tag{8}$$

The density of states, $D(\varepsilon)$, can also be found by arranging to get N in terms of ε then differentiating with respect to ε.

$$D(\varepsilon) = \frac{dN}{d\varepsilon} = \frac{V}{2\pi^2}\left(\frac{2m}{\hbar^2}\right)^{3/2}\varepsilon^{1/2} \tag{9}$$

So by using Fermi-Dirac statistics to describe the occupancy of the states, it is possible to define the number of states that are occupied between energies ε and $\varepsilon+d\varepsilon$,

$$N(\varepsilon)d\varepsilon = D(\varepsilon)f(\varepsilon)d\varepsilon \tag{10}$$

At T=0K, all the levels below E_F will remain occupied with the rest empty. Fig 1.2 shows how the occupation varies with density at a range of temperatures. This model was used to make predictions on the specific heat capacity and thermal conductivity of materials and was successful in the case of metals. But it was clearly in need of modification as it had no way of explaining insulators (or semiconductors) as the distribution of electrons was always continuous.

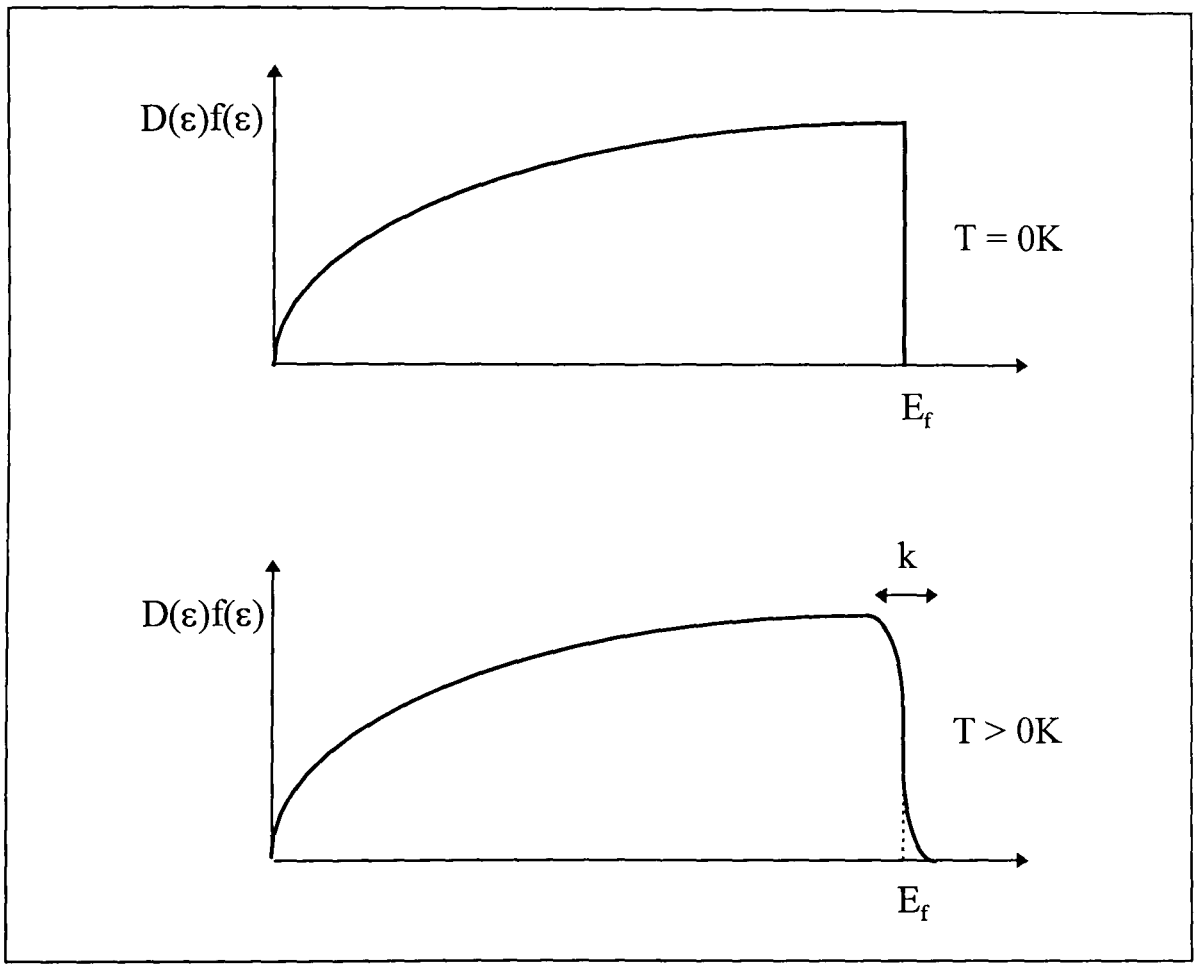

Fig 1.2: Plot of population of states against energy for a 3D free electron gas at T = 0K and T > 0K.

This method was improved by including an interaction with the nuclei (in the form of an array of positive ions) whilst keeping the independent electron approximation. This meant introducing a term to represent the periodicity of the lattice. So in the nearly free electron theory, the band electrons are treated

as if they are perturbed by the periodic potential caused by the positive ion cores.

To solve the Schrodinger wave equation, it was necessary to find a form of the wavefunction that represented the periodicity of the lattice. This was achieved by Bloch who proved that

$$\Psi(r) = u(k,r)e^{ik.r} \tag{11}$$

where u(k,r) has the periodicity of the lattice

so u(k,r) = u(k,r+a) where a is the lattice constant

The solutions of the Bloch equation give a function that is periodic in k by $2\pi/a$ where a is the lattice constant and it is multivalued. This means that there are intervals in the energy which separate each solution of the equation. Thus the results show that there are certain energies where electrons cannot be found in a crystal (bandgaps) and energies where electrons can exist, called bands (see Fig 1.3).

1.2.2 Metals, semiconductors and insulators

If a calculation is performed on a crystal, then a series of bands where electrons can exist are formed. As the number of electrons that exist in the system is known, these bands can be filled up from those lowest in energy until an array of filled and empty bands results. Then, by assuming that a completely full or an empty band carries no current, it is possible to comment on the conductivity of different materials. (see Fig 1.4)

Metals: Metals have a partially filled band even at 0K. This means that the charge carrier concentration is always large. Thus, the temperature dependence of the conductivity depends on the variation of mobility with temperature. As the lattice vibrations increase with temperature, the scattering of charge

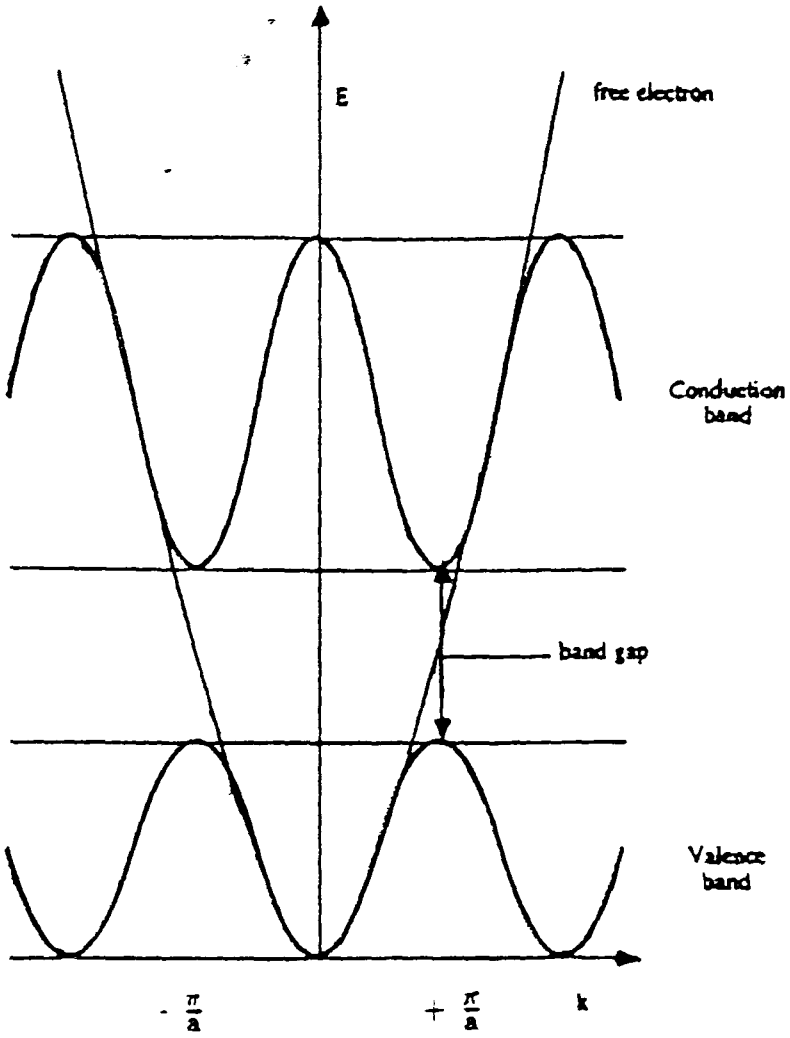

Fig 1.3: Energy against wavevector, k, plot for an electron in a linear monatomic lattice of constant, a.

carriers increases causing the mobility to drop and so hence also the conductivity.

Insulators: These materials are semiconductors with a large bandgap (usually taken to be larger than 2.5eV though the distinction between the two is arbitrary). These have similar properties to semiconductors though the large band gap means that carriers are unlikely to be generated thermally which means that carrier density (and hence the conductivity) is low.

Semiconductors: These materials have a totally filled valence band at 0K. The band gap is small enough to allow thermal excitation of charge carriers across the band gap into the conduction band. Thus the conductivity increases with temperature as more charge carriers are promoted. Thus the dark conductivity is usually described by the following equation:

$$\sigma = \sigma_0 e^{-\left(\frac{\Delta E_G}{2k_B T}\right)} \qquad (12)$$

where ΔE_G = band gap energy.

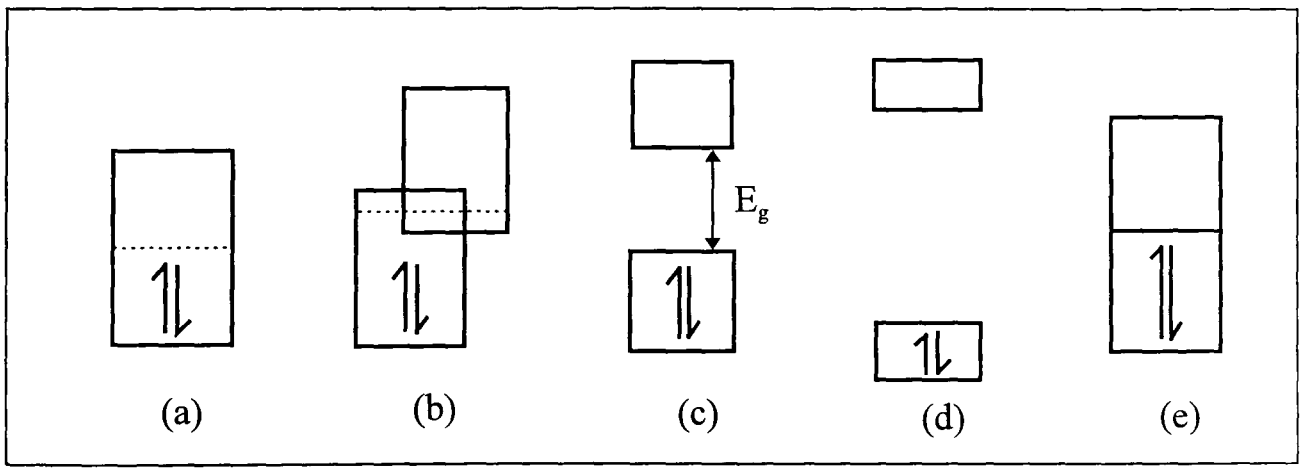

Fig 1.4: Relationship between electrical properties of solids with the location and filling of the energy bands. (a) Metal with a partially filled band. (b) Metal generated by the overlap of filled and empty bands. (c) Semiconductor characterised by a small gap between the filled and empty bands. (d) Insulator with a large gap between the filled and empty bands. (e) Semi-metal where the filled and empty bands just touch from ref. 149.

1.2.3 The position of the Fermi level

From the condition of thermal equilibrium between the conduction and valence bands, the total density of free electrons in an n-type material, n_0, can be written[9]

$$n_0 = N_c e^{\left[-(E_C - E_V)/kT\right]} \tag{13}$$

where $N_c = 2M_c\left[2\pi m_e^* kT/h^2\right]^{3/2}$ (14)

M_c = number of equivalent minima in the conduction band

m_e^* = electron effective mass

Similar equations can be written for the total hole density, p_0. From these, the position of the Fermi level in an intrinsic semiconductor can be defined as

$$E_{F,\text{int}} = \left(E_C + E_V\right)/2 + \left(kT/2\right)\ln\left(N_V/N_C\right) \tag{15}$$

In this case, the Fermi level lies very close to the middle of the band gap. The Fermi level for extrinsic semiconductors can then be defined relative to the intrinsic Fermi level, E_i, from the total density of free electrons, n_0, or holes, p_0:

$$n_0 = n_i e^{\left[(E_F - E_i)/kT\right]} \tag{16}$$

$$p_0 = n_i e^{\left[(E_i - E_F)/kT\right]} \tag{17}$$

where $n_i^2 = n_0 p_0$

This form of the equation shows that the carrier concentration is equal to the intrinsic concentration, n_i, when E_f is at the intrinsic level E_i. This then increases exponentially when the E_f moves towards the conduction band.

1.2.4 Intrinsic conductivity

If enough energy is absorbed, then an electron can transfer directly from the valence band to the conduction band. The vacancy that it leaves behind acts as a single positive charge carrier and is called a hole. As population of the conduction band is usually due to thermal excitation, the conductivity is temperature dependent.

However, photons of energy greater than the band gap can be used and the increase in conductivity due to the absorption of light is termed photoconductivity.

1.2.5 Extrinsic conductivity

An extrinsic semiconductor is a material in which additional electrons are present in the conduction band (or holes in the valence band) due to ionised donor imperfections (or ionised acceptor imperfections). This means that the electrical properties of semiconductors can be controlled by the addition of donor or acceptor imperfections.

Generally, n-type semiconductors are characterised by impurity levels just below the conduction band. These are usually electron donor states which are readily excited so promoting an electron into the conduction band. The increase in the number of electrons found in the conduction band results in the Fermi level moving towards the conduction band as the probability of finding an electron there is greater than in the intrinsic case.

The opposite happens in p-type semiconductors where impurities create acceptor states just above the valence band. Electrons are then promoted from this band to the bound state leaving free holes in the valence band. The Fermi level is then lowered towards the valence band.

In both cases, the number of mobile charge carriers is increased leading to an increase in the conductivity. Intrinsic materials can be made extrinsic by doping with either donors or acceptors. In practice, organic semiconductors are readily doped and so are rarely intrinsic. However, by changing the dopant it is possible to convert n-type into p-type semiconductors (or vice versa) e.g. for MPCI [10,11].

1.2.6 Photoconductivity

The photoconductivity of a material is defined as the increase in the conductivity of the sample resulting from the absorption of electromagnetic radiation. For an intrinsic semiconductor, the incident radiation causes an electron to be promoted from the valence band into the conduction band, increasing the conductivity. There are a number of physical characteristics that affect photoconductivity and as a detailed study of these is not required, they are listed below:

- The magnitude and polarity of the applied field
- The wavelength and intensity of the incident light
- The surface of the illuminated solid
- The purity of the illuminated solid
- The ambient atmosphere
- The temperature of the illuminated solid
- The degree of order found in the illuminated solid

The amount of photoconduction is usually defined by quoting the photosensitivity i.e. the change in conduction caused by excitation divided by the incident illumination intensity. This is sometimes termed as the photoconductivity gain, G, where

$$G = \frac{\Delta I}{eF} \tag{18}$$

where ΔI is the increase in current

F is the incident photon flux.

In materials were there is a low quantum yield, there are some special mechanisms of photoconduction. These are deduced from the electric field and temperature dependence of the quantum yield. The model says that the diffusion of electrons and holes which have been produced by the absorption of a photon may happen under the influence of an applied electric field or a Coulombic field. This is because in the absence of a field, the number of carriers is low due to geminate recombination (i.e. the immediate recombination of generated charge carriers due to Coulombic attraction). This is the Onsager model for carrier generation and a distance is defined as the mean distance between generated charge carriers.

1.2.7 Carrier generation

Charge carriers can be generated in two different ways. The first of these is by a direct interband process where a photon of energy larger than the band gap is absorbed. This directly generates an electron/hole pair, thus electrons in the conduction band and the holes in the valence band contribute to the conduction. The other method is that proposed by Frenkel where the absorption of a photon causes the creation of a tightly bound state. This is considered as a tightly bound, yet mobile, electron/hole pair called an 'exciton'. Charge carriers are usually generated from excitons by one of the following processes:

- Exciton interaction with a trap
- Exciton interaction with a surface state
- Exciton-exciton annihilation
- Exciton dissociation by thermal processes.

1.2.8 Recombination

Recombination is the process which attempts to restore the equilibrium carrier densities. Carrier recombination in an organic semiconductor can result from direct recombination or via an interaction at an imperfection. When the carrier density is large then direct recombination dominates whereas at low carrier densities, recombination at imperfections is the important process. The resulting energy released when carriers recombine is dissipated either as a photon (electroluminescence), phonons or to a third carrier in a three body process.

The rate of recombination of carriers may vary between the surface and the bulk of the material. This is a result of the surface of a crystal being more prone to lattice imperfections than the bulk. Also, foreign molecules can diffuse into the first few layers of a crystal and increase the number of traps. A large difference in the relative trap densities at the surface compared to the bulk is usually recognisable from a plot of photocurrent against the wavelength of incident light and comparing it to the absorption spectra.

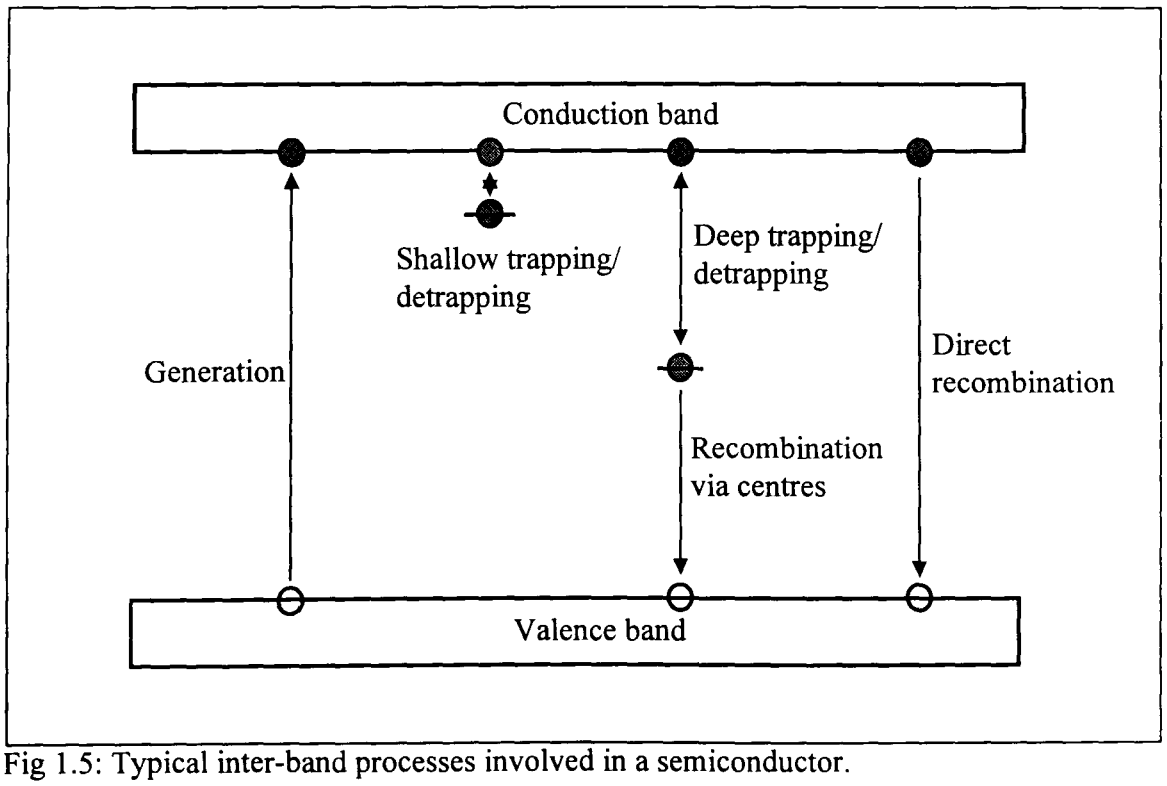

Fig 1.5: Typical inter-band processes involved in a semiconductor.

Chapter 2:- The Photovoltaic Effect

2.1 Background

There are three main kinds of photovoltaic effects in solids. These are

(a) bulk effects - a Dember photovoltage arises in the bulk of the solid due to the diffusion of photogenerated charge carriers with different electron and hole mobilities.

(b) surface effects - these arise from a potential barrier such as a Schottky barrier at the surface of the semiconductor (i.e. at the interface between the metal and the semiconductor).

(c) depletion layer effects - a photovoltage can arise from the built in field at the semiconductor-semiconductor junction which drives the two types of photogenerated charge carriers in opposite directions.

Generally, the second two processes are more efficient than the generation in the bulk. However, in all cases, the photovoltaic effect requires

(i) light absorption in the solid

(ii) mobile charge carriers to be generated from the absorbed light

(iii) an internal electric field to separate the charge carriers

(iv) electrical contacts.

The following sections will explain in more detail processes (b) and (c) by referring to p-n junctions, heterojunctions and metal-semiconductor contacts.

2.2 p-n junction

This is formed when two portions of the same material are brought into contact with one being doped to become n-type and the other p-type. A large volume of work[12] has been done characterising junctions based on doped silicon and whilst a large number of equations exist describing its behaviour,

they are not relevant to an organic junction as the assumptions are no longer valid. However, the principles that will be explained here can be carried forward to heterojunctions which more accurately describe the situation between two different organic semiconductors.

Firstly, take two portions of the same intrinsic semiconductor and dope them so that one becomes p-type and the other becomes n-type. Then when they are brought together so that they are intimately joined, the Fermi levels equalises causing an exchange of charge to take place. Thus holes flow from the p-type material to the n-type material and electrons do the reverse. Electrons that flow from the n-type material into the p-type material then tend to recombine with holes thus removing charge carriers from the region adjoining the junction (called the depletion region for this reason). This makes the depletion region an area of higher resistance than the bulk of the two semiconductors.

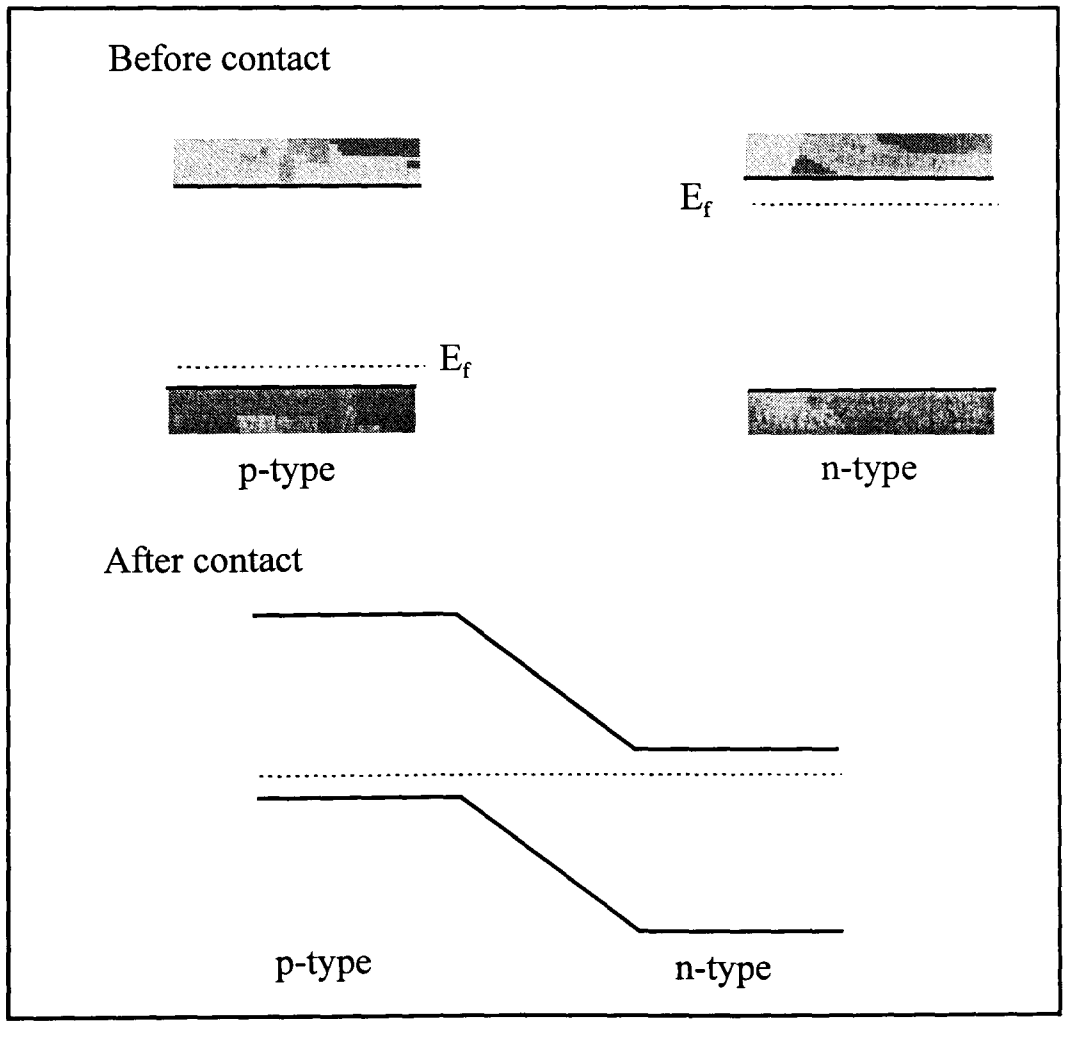

Fig 2.1: Figure showing the formation of a p-n junction.

Fig 2.1 shows the formation of a p-n junction. The junction is drawn by fixing the position of the edges of the bands where they contact and moving the position of the bands in the bulk so that the Fermi levels equalise. i.e. in this case the position of the bands in the n-type material go down and the p-type material move up. In an inorganic material, the edges of the depletion region are well defined because of the high mobility and lifetime of charge carriers. This also explains why the field is approximately constant within the depletion region resulting in a straight line being drawn between the valence bands in the bulk.

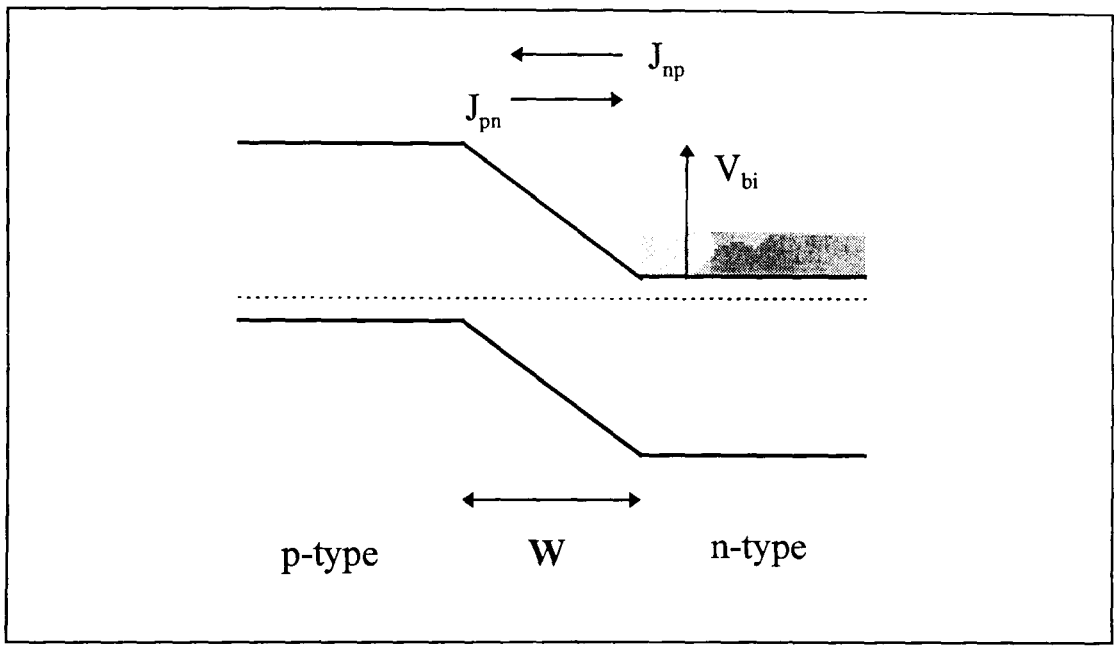

Fig 2.2: A p-n junction at equilibrium.

When a p-n junction has been formed and the charge has been redistributed, it is said to be at equilibrium. At this point the current flowing across the barrier in either direction is equal. J_{np} is made up of electrons in the conduction band of the n-type material that have enough thermal energy to overcome the barrier (V_{bi}) and cross into the p-type layer. J_{pn} is formed from electrons in the conduction band of the p-type material that diffuse to the junction. As there are more electrons in the conduction band of an n-type material than a p-type one (by definition), the two currents can be equal at equilibrium. The magnitude of the barrier height (V_{bi}) is equal to the difference in the Fermi

levels of the two doped semiconductors and this is the theoretical maximum open circuit voltage of the device.

2.2.1 p-n junction under bias

When a voltage is applied to a p-n junction, the barrier height changes from being V_{bi} to (V_{bi} - $V_{applied}$). The resulting change in the barrier height means that the junction is no longer in equilibrium. When a negative voltage is applied, the height of the barrier increases. This causes J_{np} to decrease as more thermal energy is now required to overcome the barrier, making this event less probable. J_{pn} is largely unchanged as the increase in the barrier height does not affect the number of electrons reaching the barrier. This means that the net flow of electrons is from the p- type to the n- type layer. If a positive voltage is applied, then the barrier height is decreased. Again J_{pn} is unchanged, but this time J_{np} is increased as it is easier to overcome the barrier. This causes an overall flow of electrons from the n- type to the p- type layer. The shape of the current-voltage (I-V) plot is shown in Fig 2.4. This shows how the a negative applied voltage causes a small decrease in the current whilst a positive applied voltage causes a considerable increase in the forward current. The effectiveness of a junction at allowing current flow in one direction is measured by the rectification of the system. This is defined as the ratio of the current at $+V_{app}$ against $-V_{app}$.

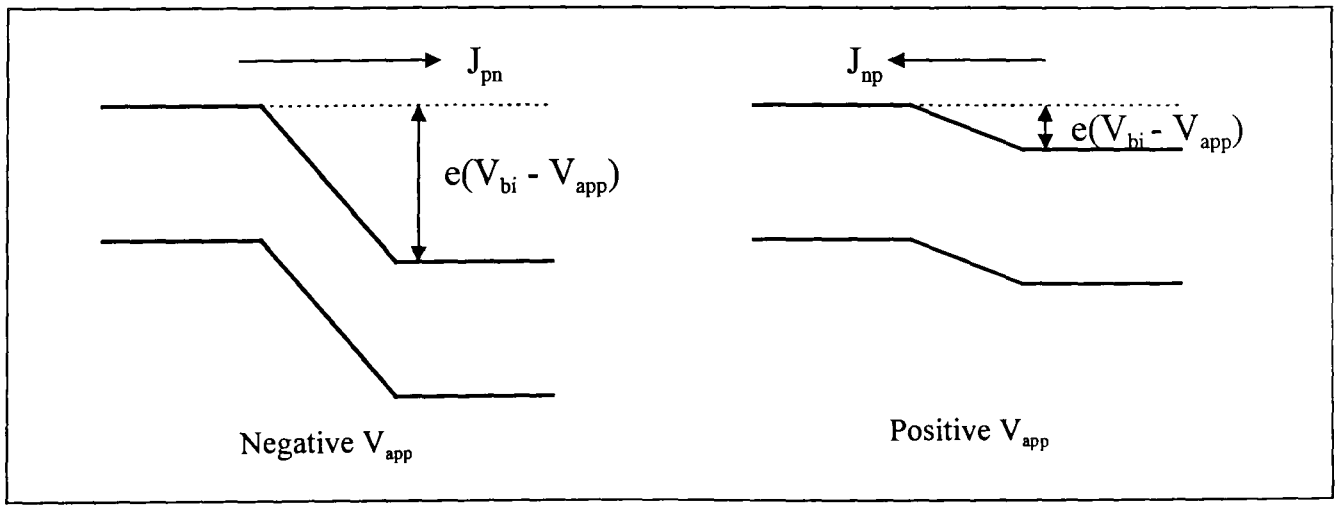

Fig 2.3: A p-n junction under bias.

2.2.2 p-n junction under illumination

When the p-n junction is illuminated, photons absorbed with an energy greater than the band gap will create an exciton than can dissociate into charge carriers (an electron and a hole). Excitons that dissociate in the depletion region will be split by the internal field causing a current to flow. The direction of this photocurrent is for electrons to flow from the p- type to the n- type layer. This has the effect of shifting the I-V plot downwards (see Fig 2.4). In inorganic systems where the diffusion lengths of excitons and electrons/ holes are much longer than for organic thin films, light absorbed anywhere in the solid can contribute to the photocurrent. This is because excitons generated in the bulk can diffuse to the depletion layer before dissociating into an electron/ hole pair. In organic systems, the major contribution to the photocurrent comes from light absorbed at the interface as typical exciton diffusion lengths are much shorter. The overall efficiency of p-n junctions is limited by the amount of light absorbed (any photon with energy less than E_G will not be absorbed by the device) and that most of the light is absorbed at the front of the first layer requiring the exciton to diffuse to the depletion region before dissociating. These problems are overcome in heterojunction devices.

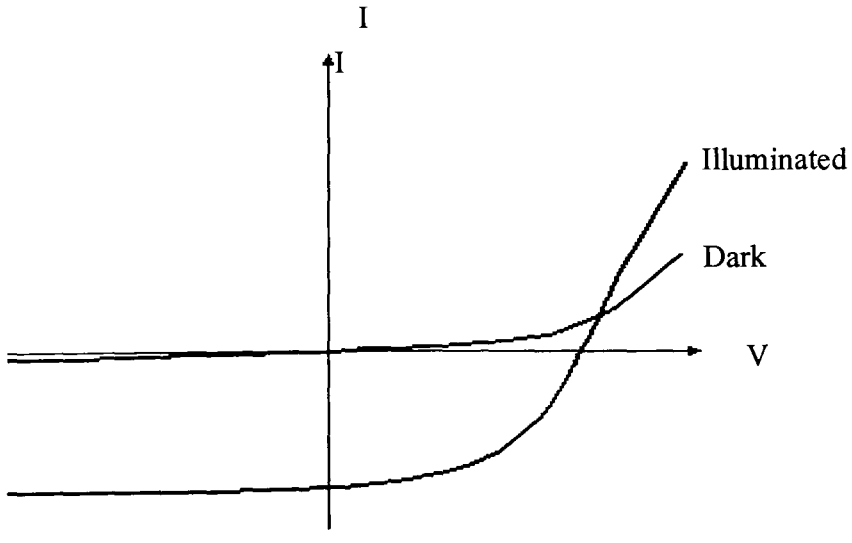

Fig 2.4: I-V plot for a rectifying junction in the dark and when illuminated

2.3 Heterojunctions

A junction formed between two materials with different band gaps is called a heterojunction. In inorganic systems, heterojunction solar cells are usually formed between two materials whose lattices match closely with one having a small band gap whilst the other has a large one. These cells are then illuminated through the large band gap material. Thus, most of the light is absorbed near the front of the second layer making the active region the interface of the two layers. As the materials have different bandgaps and electron affinities, χ, discontinuities will inevitably appear in the conduction and valence bands. These yield results that are easy to visualise though are more problematic theoretically. The first, and simplest, discussions on the formation of heterojunctions were described by Anderson[13] in 1960.

2.3.1 The Anderson model

The same rules are used for forming a heterojunction as a p-n junction. The discontinuity in the relative dielectric constant is dealt with by requiring that the electric displacement be constant across the interface; i.e. $\varepsilon_1 E_1 = \varepsilon_2 E_2$ where ε is the electrical permittivity of the layer and E is the electrical field across the layer. The shape of the junction is determined by the values of E_{G1}, E_{G2}, χ_1 and χ_2 which permits a large variety of different junctions to be formed. Fig 2.5 shows the formation of an n-p anisotropic heterojunction (so termed because the first layer is n-type and the second p-type) with positive discontinuities in the conduction and valence bands. The top layer (the layer the light passes through first) is the n-type material so the sample is illuminated from the left.

From the diagram of the schematic Anderson heterojunction formed between an electron acceptor as the front layer and an electron donor as the second layer, the relationship between various quantities can be defined. Firstly, the

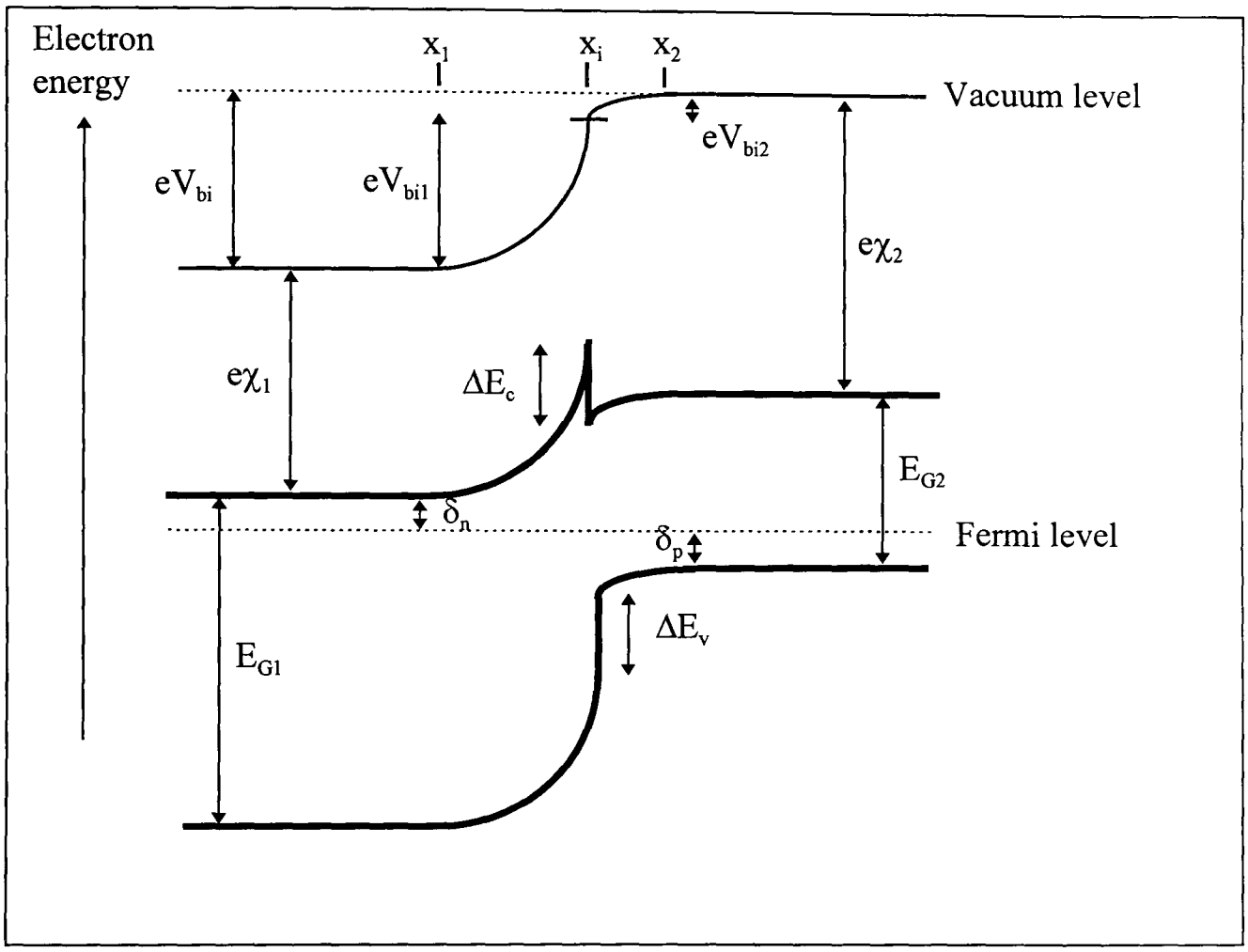

Fig 2.5: Formation of an Anderson n-p heterojunction with $\Delta E_c > 0$ and $\Delta E_V > 0$ (from ref. 14)

where E_G = Band gap

χ = electron affinities

V_{bi} = built in voltage for the junction

x = edge of depletion region

δ = position of Fermi level from conduction/valence band

size of the discontinuities can be found in terms of the electron affinities, χ, and band gaps, E_G, of the materials:

$$\Delta E_C = e(\chi_2 - \chi_1) \tag{1}$$

$$\Delta E_V = e(\chi_1 - \chi_2) + E_{G2} - E_{G1} \tag{2}$$

From this the size of the built in voltage (V_{bi}) for the junction (this is sometimes called the diffusion voltage) can be determined:

$$eV_{bi} = eV_{bi1} + eV_{bi2} = E_{G2} - \delta_n - \delta_p + \Delta E_C \tag{3}$$

ΔE_C does not affect the size of V_{bi} for a junction as this originates from the difference in the Fermi levels. The ratio of the number of free carriers and the width of the depletion region on each side of the junction is determined by the relative permittivities.

$$V_{bi2}/V_{bi1} = \varepsilon_1 W_{d2}/\varepsilon_2 W_{d1} = \varepsilon_1 N_A/\varepsilon_2 N_D \tag{4}$$

When a voltage, V, is applied to the junction, the width of the depletion region, W_d, can be shown to equal,

$$W_{d1} = x_1 - x_i = \left[\frac{2 N_D \varepsilon_1 \varepsilon_2 (V_{bi} - V)}{e N_A (\varepsilon_1 N_A + \varepsilon_2 N_D)} \right]^{1/2} \tag{5}$$

$$W_{d2} = x_2 - x_i = \left[\frac{2 N_A \varepsilon_1 \varepsilon_2 (V_{bi} - V)}{e N_D (\varepsilon_1 N_A + \varepsilon_2 N_D)} \right]^{1/2} \tag{6}$$

where N_A = acceptor concentration

N_D = donor concentration

ε_1 = permittivity of layer 1

ε_2 = permittivity of layer 2

V_{bi} = built-in voltage

The configuration described above is the common one used for a solar cell, with E_{G1} chosen to be considerably larger than E_{G2} so maximising the band gap window. Recombination is low in these systems because photogenerated electrons are swept towards the n-type layer which has a low hole density. There is also a large barrier in the valence band which prevents the holes from the front layer crossing into the depletion region of the second layer. Photogeneration is considered to come exclusively from the second layer as the first layer is thicker than the exciton diffusion length. So if diffusion dominated transport exists and if we assume that the electron and hole quasi-Fermi levels are constant across the depletion region then the I-V relation can be written,

$$I \cong e\left(D_1/L_1\right)\left(N_{C1}N_D/N_{C2}\right)\exp\left(-eV_{bi}/kT\right)\left[\exp\left(eV/kT\right)-1\right] \qquad (7)$$

where D_1 = diffusion coefficient of electrons in the front layer.

L_1 = diffusion length of electrons in the front layer.

N_C = Effective density of states in the conduction band.

V = Applied voltage.

$V_{bi} = V_{bi1} + V_{bi2} - \Delta E_C$

The effect of the discontinuity in the conduction band is restricted to the current flow. The magnitude of ΔE_C has little effect on the transport until the flat band condition is reached ($V_{app} \approx V_{bi1} + V_{bi2}$). But as the I-V characteristics only need to be known over a small range between $0 \leq V_{app} \leq V_{oc}$ for solar cell applications, this barrier cannot always be ignored though it is sufficient for our purposes to say that any barriers in the conduction band will alter the motion of electrons so affecting the magnitude of the short circuit current. The Anderson model is successful at predicting the configuration of the bands at the junction though the nature of the I-V relationship is often inaccurate. Values of I_0 (found by extrapolating a log I versus V curve to V = 0) for a Ge/GaAs heterojunction have been found to be six decades larger than the value predicted by theory[15]. The model has also

had trouble predicting the size of the discontinuity expected from the values for the electron affinities of the materials although it is unclear whether this is a fault of the model or due to practical difficulties in separating out the effects of interface states.

The Anderson model relies on a perfectly abrupt metallurgical junction, whereas in real systems where the junction is fabricated at a high enough temperatures then interdiffusion occurs sometimes, causing solid solutions of the semiconductor components to be formed. Cheung[16] et al have shown that junction grading over a distance of 100Å can smear out conduction band spikes so that carrier flow is unimpeded. Thus in systems without good lattice matching, any discontinuity in the conduction band will be smoothed out so it will not interfere with the carrier flow.

2.3.2 The effect of interface states

The Anderson model makes no allowance for any interface states that exist. Extrinsic imperfection energy levels in the vicinity of the interface arise from either the effects of a lattice mismatch between the two materials or from impurities introduced during fabrication. In inorganic systems, interface states often arise from a periodic array of dangling bonds arising from the lattice mismatch of the two materials. These bonds may be electrically active or act as sites of impurity segregation. Impurities at the interface are unavoidable as even 0.001 monolayer of electrically active impurity atoms can change the electrical properties of a junction. A wider discussion of the effects of intrinsic and extrinsic imperfections in heterojunctions are discussed by Fahrenbruch and Aranovich[17].

Electrically active interface states can alter the properties of a junction in two ways:

1. The charge stored in these interface states can distort the band profile, altering the position of the conduction band at the interface. This will then change the shape of the junction hence its properties (i.e. V_{bi} etc.)
2. The states provide a large number of recombination centres. This alters the shape of the I-V curve and will change the photogeneration characteristics of the junction.

When using organic semiconductors, the lower conductivity of the materials requires that the layers be thinner to reduce the internal resistance of the device to acceptable values. The width of the 'photoactive region' in organic junctions is typically 10-40nm making the most efficient devices those with layers 25-50nm thick[18]. As the materials are chosen to have complementary absorption spectra, the action spectra largely follows the absorption spectra of the second layer as light of this wavelength is absorbed in the photoactive region. Owing to the imperfect nature of vacuum deposited thin films, any barriers in the conduction band will not result in spikes appearing in the current-voltage plot as these will be smoothed out.

2.4 Semiconductor-Metal contacts

When a semiconductor comes into contact with a metal, there are two different outcomes depending on the respective positions of the Fermi levels.

2.4.1 Ohmic contacts

For the contact between an n-type semiconductor and a metal, if the workfunction of the semiconductor is greater than that of the metal, then an ohmic contact is formed. This is characterised by a symmetric current-voltage plot. When the materials are brought into contact, electrons flow from the metal to the semiconductor. As the semiconductor is n-type, it cannot accept electrons so a space-charge region does not develop. In the semiconductor

close to the metal interface, an electron accumulation layer results though the extent of this layer is less than space charge layers. It has no effect on the shape of the I-V plot for the junction which remains linear.

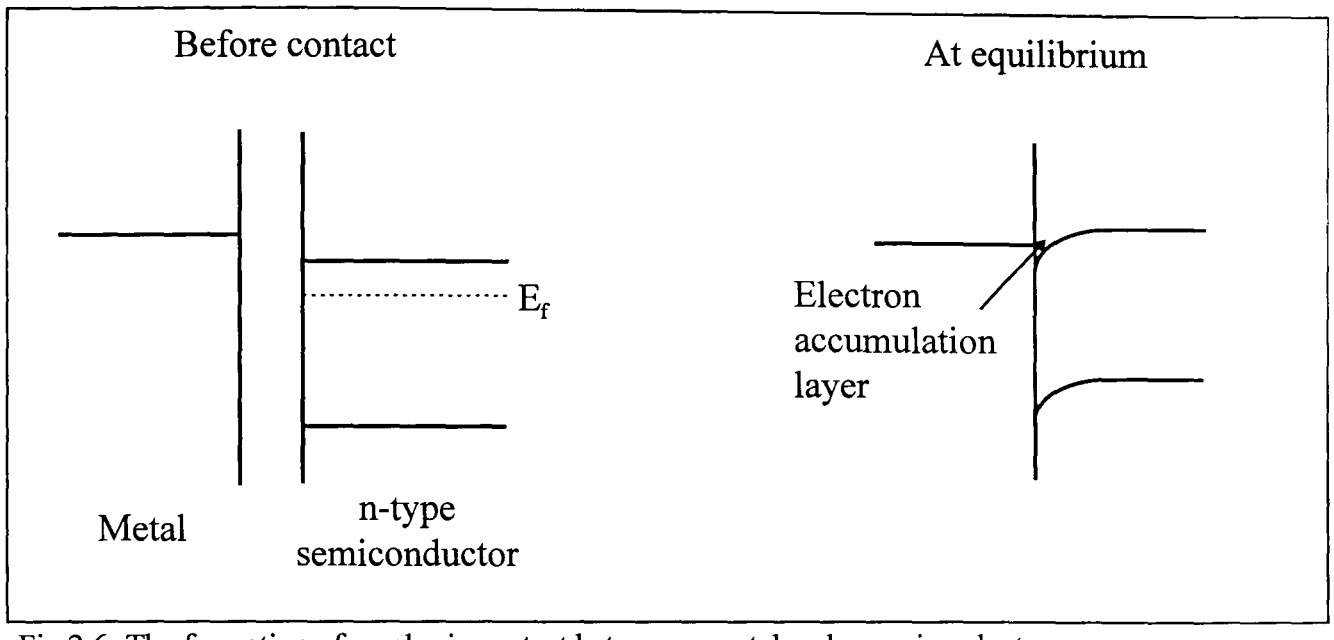

Fig 2.6: The formation of an ohmic contact between a metal and a semiconductor.

2.4.2 Barrier contacts

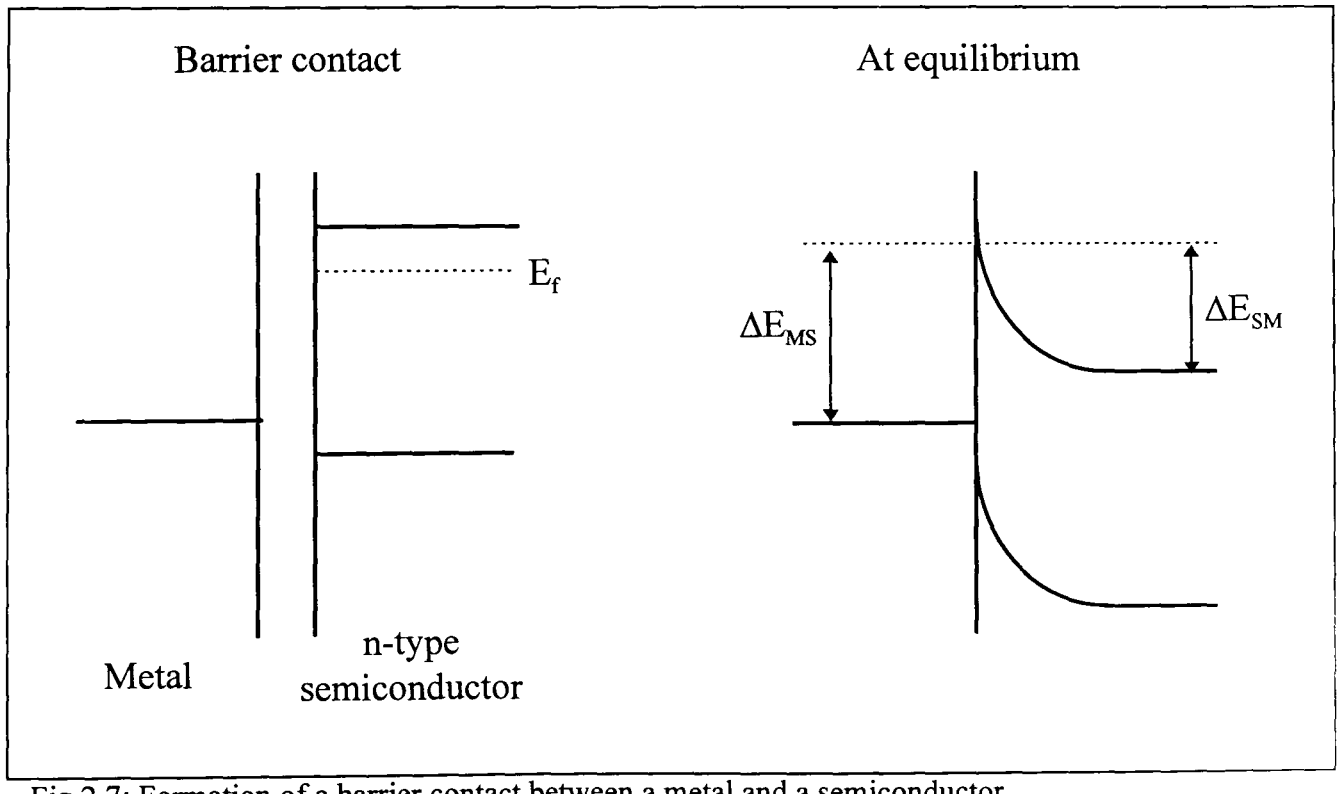

Fig 2.7: Formation of a barrier contact between a metal and a semiconductor.

where ΔE_{SM} = height of energy barrier between semiconductor and metal

ΔE_{MS} = height of energy barrier between metal and semiconductor

The opposite case occurs when the workfunction of the metal is larger than that of the semiconductor, when a barrier contact (sometimes called a Schottky contact) is formed (see fig 2.7). These are characterised by a rectifying I-V plot. For bilayer solar cells, the electrodes are usually chosen to form ohmic contacts with the semiconductor layer as the separation of the generated charge carriers is performed at the semiconductor-semiconductor interface.

2.4.3 Schottky barrier solar cells

Schottky barrier solar cells are formed between two metals with different workfunctions and a single organic semiconductor layer. The metals are chosen to form a barrier (Schottky) contact and an ohmic contact with the semiconductor, making the electrical properties dominated by the workfunctions of the metal electrodes and the semiconductor layer[19]. These devices are known to display large open circuit voltages though the overall efficiency is often low.

2.5 Measurable quantities

The quantities measured that are used to determine the efficiency of a solar cell are obtained from a current-voltage plot (see fig 2.8).

From the maximum power rectangle, the fill factor (FF) can be defined:

$$FF = \frac{V_{\max} J_{\max}}{V_{oc} J_{sc}} \tag{8}$$

The fill factor is a measure of the 'squareness' of the current-voltage plot. A large fill factor is desirable. The efficiency of the solar cell can then be defined as:

$$Eff(\%) = \frac{J_{sc} V_{oc} FF}{P_{in}} \times 100\% \tag{9}$$

where P_{in} = power of the incident radiation (usually in mW/cm^2)

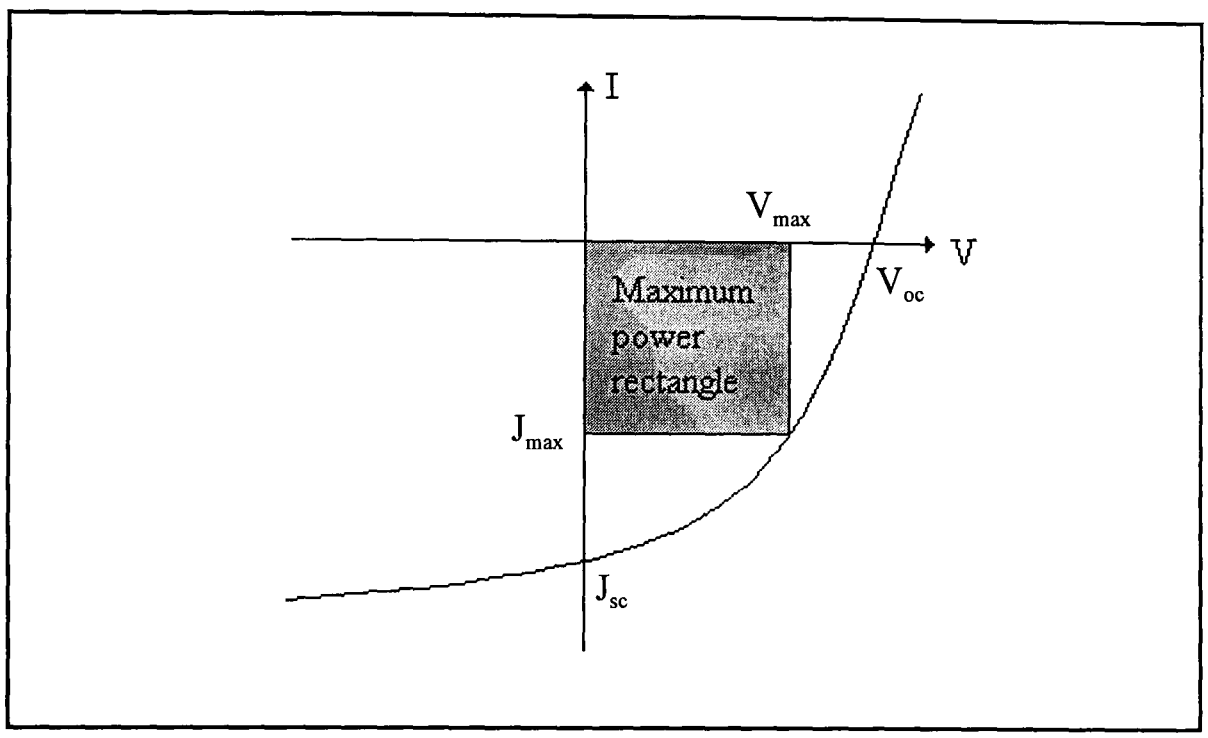

Fig 2.8: A typical I-V plot for an illuminated solar cell.

where V_{oc} = open circuit voltage

J_{sc} = short circuit current

V_{max} and J_{max} are the voltage and current at the maximum power.

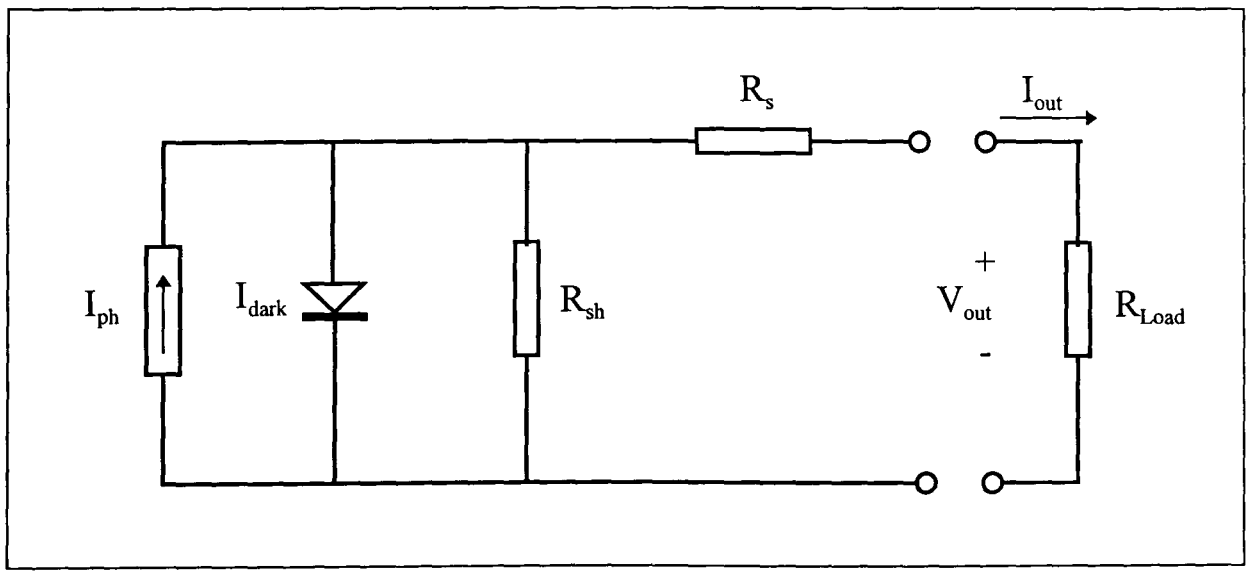

Fig 2.9: Equivalent circuit diagram for a solar cell.

The equivalent circuit diagram for a solar cell is shown in fig 2.9. The photocurrent is represented by I_{ph} which is opposite in direction to the forward bias current of the diode (equivalent to J_{np} in the p-n junction system). The shunt resistance (R_{sh}) may arise from surface leakages, spikes at the interface in the conduction bands or metallic bridges along microcracks. The series resistance (R_s) arises from contact resistances at interfaces, inherently high bulk resistances of organic semiconductors and series resistances of semitransparent electrodes.

2.5.1 Effect of series and shunt resistance on the cell's performance

The magnitude of these resistances can have a large effect on the shape of the current-voltage plot. In an ideal system, R_{sh} is infinite and R_s is zero. The effect of series and shunt resistances on the I-V characteristics of a solar cell are shown in fig 2.10. R_s is defined as the slope of the graph when the curve crosses the x axis (i.e. at $V_{app} = V_{oc}$). Conversely, R_{sh} is found graphically by measuring the gradient at $V_{app} = 0V$. These graphs shows that R_s has no effect on V_{oc}, whilst it has little effect on J_{sc} at small values of R_s. However if R_s is large, the slope ($1/R_s$) is small causing the I-V plot to become linear (FF=0.25). This leads to a subsequent reduction in the size of J_{sc}. If we assume that the cell operates near its maximum and all the power loss is attributable to $J_{max}^2 R_s$ then the power loss fraction, L_s, is given by

$$L_s = \frac{J_{\max}{}^2 R_s}{J_{\max} V_{\max}} = \frac{J_{\max} R_s}{V_{\max}} \approx \frac{J_{sc} R_s}{V_{oc}} \qquad (10)$$

For a 3% power loss at $J_{sc} = 40mA\ cm^{-2}$ and $V_{oc} = 0.6V$, R_s must be less than 0.5Ω per square centimetre. The conductivity of a typical phthalocyanine thin film is of the order $10^{-11}\ \Omega^{-1}\ cm^{-1}$ and the thickness of an organic layer is around 100nm, making the contribution to R_s from the bulk to be $10k\Omega\ cm^{-2}$. Thus it is clear that a typical device made from organic semiconductors will not operate near the maximum power limit. Another contribution to R_s comes

from the contact between a semiconductor and the metal being only 'quasi-ohmic'. This shows up in the dark and illuminated current-voltage characteristics.

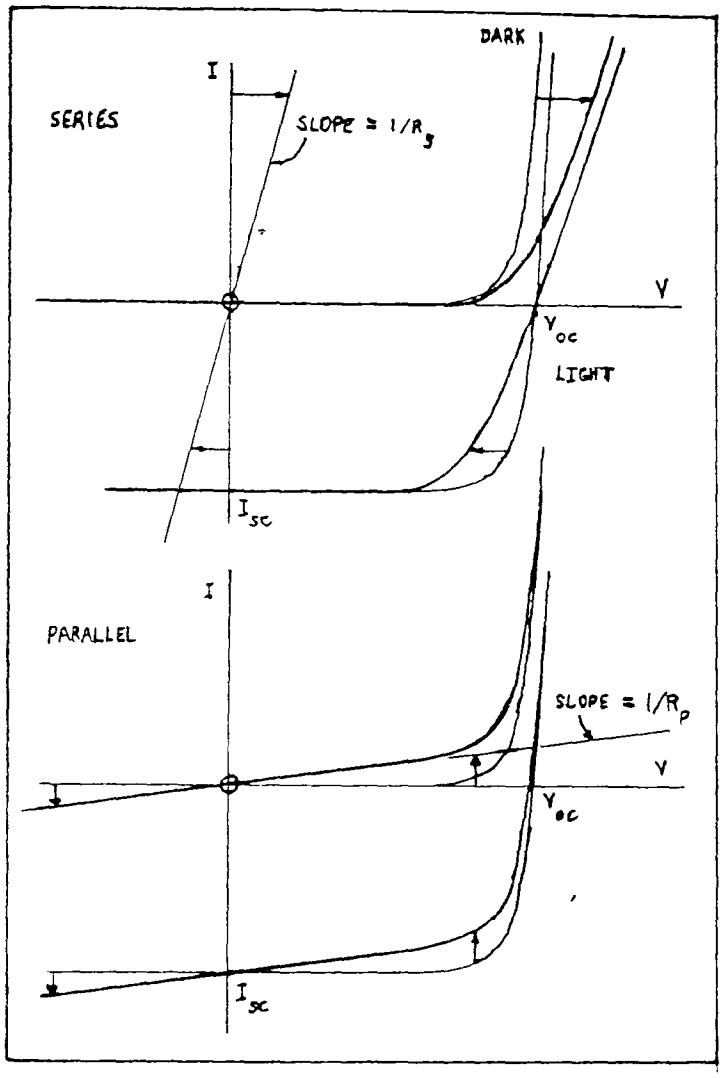

Fig 2.9: Effects of series and parallel resistance on the shape of an I-V plot for an ideal solar cell.

The shunt resistance has the opposite effect as it reduces J_{sc} when R_{sh} is small, whilst leaving V_{oc} unchanged. The power loss fraction in this case, L_{sh}, is

$$L_{sh} \approx \frac{V_{oc}}{J_{sc} R_{sh}} \qquad (11)$$

Using the conditions stated above, the power loss will be less than 3% if R_{sh} is above 500Ω cm^{-2}. If the fill factor of a solar cell falls below 0.25, then the value of R_{sh} will be smaller than R_s.

There has been very little work done adapting the junction theory for organic semiconductors. Wagner et al[18] developed a model to simulate p-n type organic solar cells in order to optimise layer thickness and the design of the cell. The model was based upon the exciton dissociation at the interface only, and due to the typical exciton diffusion lengths being between 5-20nm for different organic dyes[20], optimum layer thickness of 25-40nm were found. This is the compromise between the layers being thick enough to absorb the maximum light possible, whilst being thin enough to allow the photogenerated excitons to diffuse to the interface. The authors suggest using a mixed layer to increase the size of the interface as a possible design improvement. Using this model, light at a wavelength which is absorbed strongly by the front layer will generate an exciton that will dissociate before it reaches the interface and hence will not contribute to the photocurrent. Hence, improvements in the conversion efficiency of these devices requires an increase of the exciton diffusion length (or a decrease in R_s) or a change in cell design that increases the depletion region at the interface of the two layers.

2.6 Action Spectra

By recording the variation of photocurrent with the wavelength of the incident light, it is possible to discover information on where the charge carriers are being generated and the usefulness of the device when operating in sunlight. For a single layer sandwich cell, the field across the semiconductor layer is constant so it is the recombination kinetics that determines the magnitude of response. In this situation, there are two main possibilities. Firstly, symbatic behaviour is when the photocurrent action spectra follows the absorption spectra of the material. Light absorbed at the surface generates carriers that recombine slowly and the excess electrons and holes contribute to the photocurrent. The bulk recombination rate is fast when compared to the surface rate so carriers generated in the bulk do not contribute to the photocurrent. Thus the number of carriers generated

corresponds to the amount of light absorbed hence the action spectra follows the absorption spectra. But if the surface recombination rate is faster than that of the bulk, then it is the charge carriers generated in the bulk that contribute to the photocurrent. Light which is strongly absorbed by the material is absorbed near the surface so does not contribute to the photocurrent but some weakly absorbed light reaches the bulk. Therefore, in antibatic behaviour there is an inverse relationship between the action spectra and the absorption spectra.

In a Schottky barrier, similar behaviour is noted but in this case it is the degree of recombination that is dependent on the rate of separation of the generated charge carriers. As there is no external applied voltage, the generated charge carriers will be separated where there is a large internal field i.e. at a barrier contact making the position of the barrier that is important. If there is a barrier at the surface then symbatic behaviour is recorded but if there is a neutral contact, then antibatic behaviour can be seen. So for a single layer sandwich cell with a barrier contact and a neutral contact, symbatic behaviour will be observed when the cell is illuminated through the barrier contact. Conversely, antibatic behaviour will result when illuminated through the neutral contact because only light that passes through the bulk to the barrier contact contributes to the photocurrent.

For bilayer cells, ideally there is only a barrier at the interface between the two organic layers. Therefore it is light absorbed at the interface that contributes to the photocurrent. Thus the action spectra should follow the absorption spectra of the second layer. However, if a barrier contact exists between an electrode and an organic semiconductor layer, then an additional peak will appear in the action spectra in the region where the first layer absorbs strongly. To prevent light which would be absorbed at the interface by the second layer being absorbed by the first layer and not contributing to the generated photocurrent, it is important to choose two materials that have complementary absorption spectra.

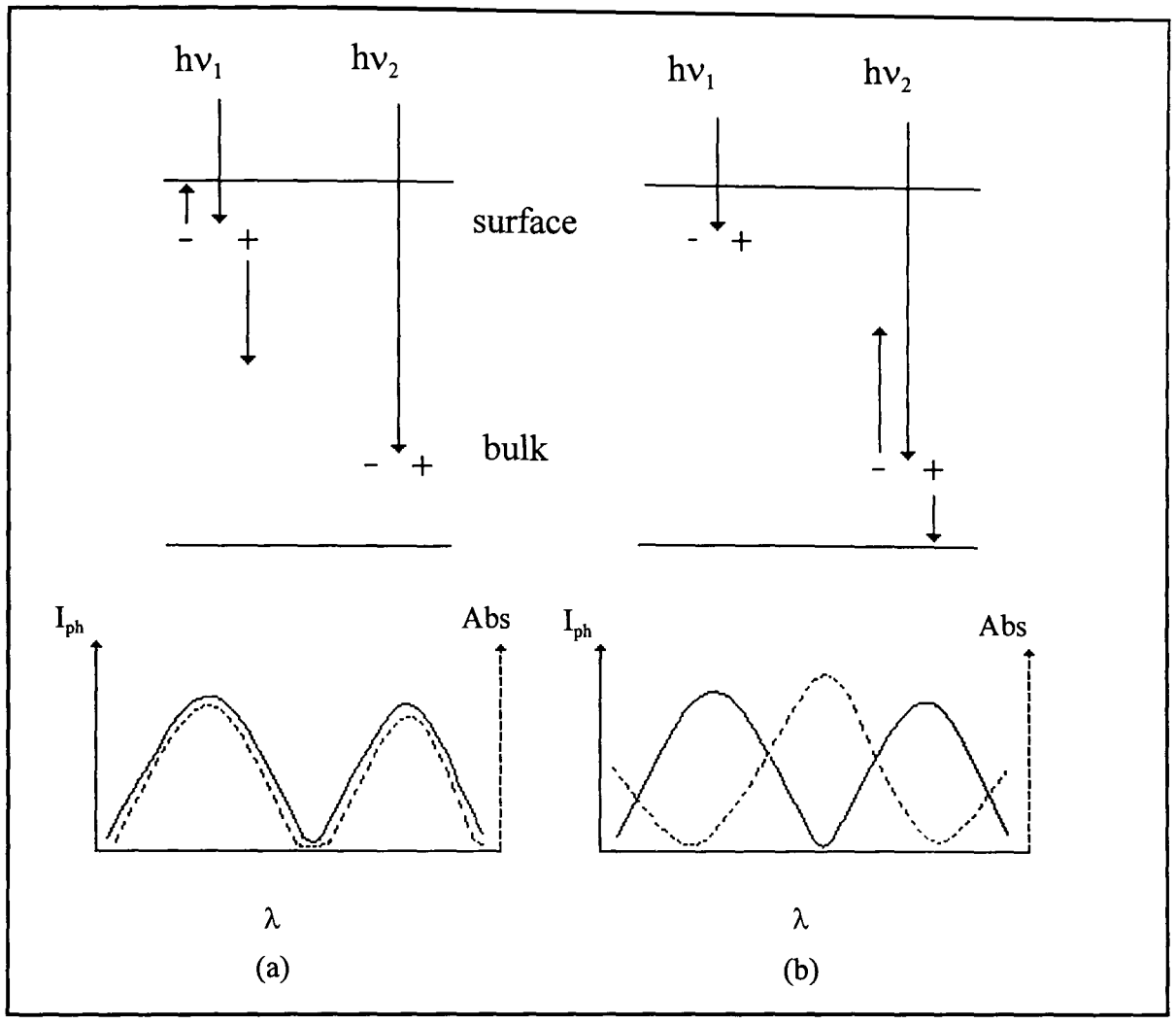

Fig 2.11:- Diagram showing (a) symbatic and (b) antibatic behaviour for the action spectra.

2.7 Chopped light method, Ryvkin analysis

When a sample is illuminated with chopped light, an alternating component of the photoresponse is observed. This process was analysed by Ryvkin[21] assuming that the rise and decay kinetics are purely first order processes with the same rate constant. He found that the steady state photoresponse, $\Delta\sigma$, is a function of the excitation frequency f_c, the carrier lifetime τ, and the observed alternating photoresponse $\Delta\sigma_{\sim}$. The derivation is:

The density of carriers n, present in the sample after an illumination pulse of duration t, is

$$n = f\tau\left(1 - e^{\left[\frac{-t}{\tau}\right]}\right) \tag{12}$$

and after a period of darkness, also of duration t as we are considering a square wave, is

$$n = f\tau e^{\frac{-t}{\tau}} \tag{13}$$

So if $t \gg \tau$ then the current rises to an asymptotic value under illumination and decays to an asymptotic dark current. However, if $t < \tau$ then a saw tooth form is obtained (see fig 2.10). This photocurrent has two different components:

1. A steady state component equal to $\Delta\sigma / 2$
2. An alternating component, $\Delta\sigma_{\sim}$, which oscillates around a value defined by the steady state component.

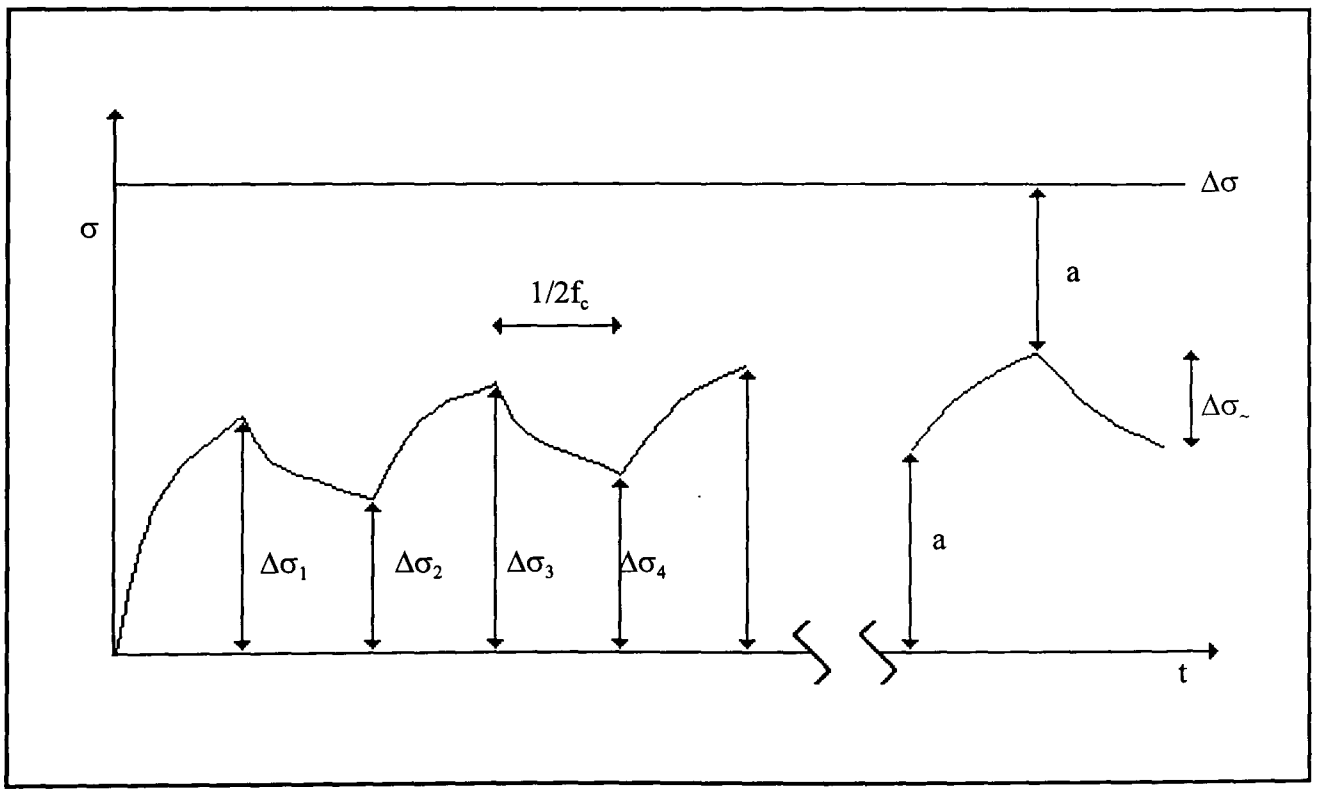

Fig 2.12: Response of a photoconductor to chopped illumination.

From fig 2.12, we can say that

$$\Delta\sigma_{\sim} = \Delta\sigma - 2a \tag{14}$$

and

$$a = (\Delta\sigma - a)e^{\frac{-t}{\tau}} \tag{15}$$

So

$$a = \Delta\sigma \frac{e^{\frac{-t}{\tau}}}{1 + e^{\frac{-t}{\tau}}} \tag{16}$$

By combining equations 14 and 16

$$\Delta\sigma_{\sim} = \Delta\sigma \tanh\left(\frac{t}{2\tau}\right) \tag{17}$$

or in terms of the chopping frequency which equals 1/2t

$$\Delta\sigma_{\sim} = \Delta\sigma \tanh\left(\frac{1}{4\tau f_c}\right) \tag{18}$$

So by measuring the magnitude of the alternating component of the photoresponse at different values of the chopping frequency, f_c, it is possible to fit the results to equation 2.18 so obtaining a value for τ.

The picture is complicated for a bilayer cell as the two different semiconductor layers will have their own values of τ. However, if monochromatic light of a wavelength that is strongly absorbed by one layer is used, then information about the speed of response can be found.

2.8 Literature survey

The first solar cells to be made using organic semiconductors were of the Schottky cell configuration i.e. a thin film of an organic semiconductor sandwiched between two different metal electrodes. Early efficient devices were made with hydroxy squarylium using In_2O_3 and liquid gallium as the electrodes[22]. This cell was 0.1% efficient using white light, partially because of the broad band absorption shown in the visible by squarylium dyes. This efficiency was improved to 0.7% using a merocyanine dye sandwiched between Al-Al_2O_3 and Ag electrodes[23]. The difference in the metal workfunctions produced a value for V_{oc} = 1.2V though the efficiency was limited by the poor absorption of the merocyanine layers in the visible. Schottky cells made from many other materials have been tried including phthalocyanines[24,25,26] and phenothiazine derivatives[27]. For the latter case, the band structures of the different phenothiazine derivatives were estimated from UPS measurements of the ionisation potential and workfunction. The band gaps were predicted from the absorption threshold of the UV-vis spectra. From these, energy diagrams of the cells were proposed and they described the behaviour of the cells well leading the authors to conclude that the photoelectric behaviour of the films could be described using a band model. Other improvements to the photoconversion efficiency have been made by doping the organic layers[28]. These devices demonstrated the advantages of the Schottky cells which are the large values for V_{oc} resulting from choosing electrodes with very different workfunctions. The disadvantage of this arrangement is that there is only one layer to absorb the light so causing some solar radiation to pass through the cell unabsorbed.

In 1986, Tang reported a solar cell made from copper phthalocyanine and dimethyl perylene tetracarboxylic acid diimide which was about 1% efficient[29]. This was a new approach because the charge carrier separation was achieved by the two materials rather than the electrodes. This was a more efficient approach because the electric field at the interface between the two layers is greater than the field across the whole organic layer in the Schottky

diode case. Since then, there has been a lot of work on the performance of bilayer cells made from a phthalocyanine and perylene derivative[30-33], the most comprehensive of which was undertaken by Wohrle[34]. He reproducibly fabricated cells made from zinc phthalocyanine and MPCI finding the best results were obtained using the following conditions:

Purity of materials - materials should be zone sublimed twice
Type of ITO substrate - no noticeable difference (used different manufacturers and values of sheet resistance)
Deposition rate - best in 1-3Å/s range though not vital
Substrate temperature - room temperature as higher temperatures encouraged pinhole formation
Layer thickness - 250-500Å for each layer.

It was also noted that the efficiency decreased at higher light intensities as the efficiency using white light increased by a factor of 3 when the light was $10mW/cm^2$ and 5 at $1mW/cm^2$ when compared to that at $100mW/cm^2$. This can be used to explain some of the differences in the reported efficiencies for similar devices. Another parameter that affected the efficiency of the cell was the area of the device. Enlargement of the active area results in a decrease in J_{sc}, affecting the efficiency as follows: 1 $cm^2 \approx 30\%$, $1.5cm^2 \approx 40\%$, $3.5cm^2 \approx 50\%$ when compared to cells of $0.15cm^2$. Tsutsui et al[36] studied a junction more quantitatively, finding that the low efficiency of the cells was due to a low photon collection efficiency and a low efficiency in the effective use of the incident photon energy (i.e. $V_{oc} \approx 0.5eV$ when the average incident photon energy supplied is 2.19eV).

2.8.1 Changes to phthalocyanine/perylene bilayer cells

There have been various different approaches to improving the efficiency of the basic phthalocyanine/perylene bilayer cell. Hiramoto et al[38] doped a cell made from H_2Pc and MPCI with H_2 and NH_3. This caused a large increase in

the photoconductivity so improving the power conversion efficiency. V_{oc} remained largely unchanged. Tsuzuki et al[39] reported that the conversion efficiency of a cell made with MPCI and TiOPc could be improved if the morphology of the TiOPc layer was changed by exposure to ethanol vapour for 1-3 hours. This caused the TiOPc to change into the α- form which has a higher photoelectric conversion efficiency.

Other approaches have involved using a third layer. Hiramoto[40] compared the performance of a two layer cell (H_2Pc/ImPCI) with a cell which included a third layer made from MPCI. This increased J_{sc} and hence also the overall conversion efficiency. MPCI was chosen because its electron affinity lies between those of H_2Pc and ImPCI. A similar type of device was made with MPCI/DMQ (2,9-dimethyl quinacridone) using H_2Pc as the middle layer[41]. Again the addition of the interstitial layer caused J_{sc} to increase without affecting V_{oc}. However, the overall performance of this device was limited by the poor quantum efficiency of DMQ. Three layer cells have also been fabricated using a codeposited layer as the middle layer[42,43]. The aim of this system is to increase the width of the depletion region so increasing the separation efficiency of the photogenerated charge carriers. Again, this cell design improved J_{sc} without affecting V_{oc}. An attempt to increase V_{oc} by adding a thin layer of gold between two bilayer cells had the effect of almost doubling V_{oc} but reducing J_{sc} by a third as a result of increasing the resistance of the device[44].

2.8.2 Bilayers made from other materials

A range of different materials that have been successfully used as pairs in bilayer cells. A study was done comparing the performance of different naphthalocyanine derivatives with MPCI[45]. It was found that the HOMO energy of the naphthalocyanine derivative strongly affected the size of V_{oc}. Another partner[46] that has been successfully used with a phthalocyanine is 5,10,15,20 - tetra(4-pyridyl)21H,23H-porphine (TPyP) which increased the

conversion efficiency of an ITO/CuPc/Al cell by a factor of 6. The TPyP acted as the electron acceptor. A cell made from ZnPc/TPyP by Harima[47] produced a V_{oc} of 1.0V and a conversion efficiency of 2% for monochromatic light (410nm). However, TPyP has a narrow absorption band which has reduced its use in these systems.

A replacement for the phthalocyanine layer that has been successfully used is the α- thiophene octamer[48] which when coupled with a perylene derivative produced a device that was 0.6% efficient for white light at 105mW/cm^2 with $V_{oc} \approx 0.45V$. Other devices have been made using polymer layers[49-51].

2.8.3 Other related systems

A bilayer cell made from ITO-TPD-MPCI-Ag where TPD is a hole transport layer commonly used in organic electroluminescent devices[52,53] was found to have a value of $V_{oc} \approx 1V$. This large photovoltage was due to asymmetric exciton dissociation as there was little band bending in the system. Another approach suggested[54] was to form a superlattice with the structure donor-acceptor- neither- donor-acceptor- neither- etc. The photocurrent is generated at the donor/acceptor interface.

Another approach is to make a cell with an organic layer grown on top of an inorganic semiconductor[55-58]. This uses the higher absorption coefficients found in organic molecules and the higher conductivity of inorganic species. Alternatively, photoelectrochemical cells have been used effectively[59].

Chapter 3:- Materials

3.1 Phthalocyanines

Phthalocyanines (from the Greek na*phtha* and *cyanide* for rockoil and dark blue) were first produced accidentally in 1907 during a study on 1.2-cyanobenzamide[60]. But it was Linstead in the 1930's who first deduced the structure[61-3]. Since then, a wide range of metal phthalocyanines have been produced resulting in thousands of publications. The reason for this level of interest is a result of several special properties:

- They can be made into exceptionally pure materials by sublimation or crystallisation showing a level of traps which is exceptional in organic chemistry.
- They are exceptionally stable (both thermally and chemically). They show no noticeable degradation up to 400-500°C in air and are unaffected by strong acids (i.e. conc. H_2SO_4) or strong bases.
- They show very intense absorption bands at 400nm and 700nm with high extinction coefficients ($\approx 2x10^5$ in solution).
- There are more than 70 different metal phthalocyanines known (MPc's). As the central metal atom has a profound effect on the physico-chemical properties of the system, a wide variety of different behaviours is reported.

By substituting on the benzene rings, an even wider range of properties can be demonstrated.

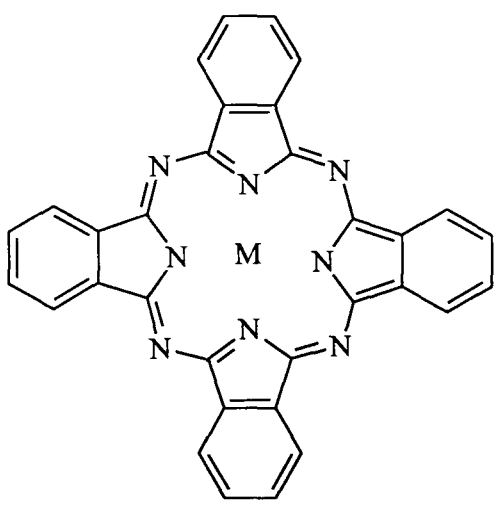

Fig 3.1: Molecular structure of a metal phthalocyanine

3.1.1 Synthesis

Phthalocyanines are usually made in one step by reacting 1,2-dicyanobenzene with a finely dispersed metal. This is carried out at 250-300°C in a high boiling point solvent such as trichlorobenzene. The other routes used to synthesis MPc's are shown in fig 3.2.

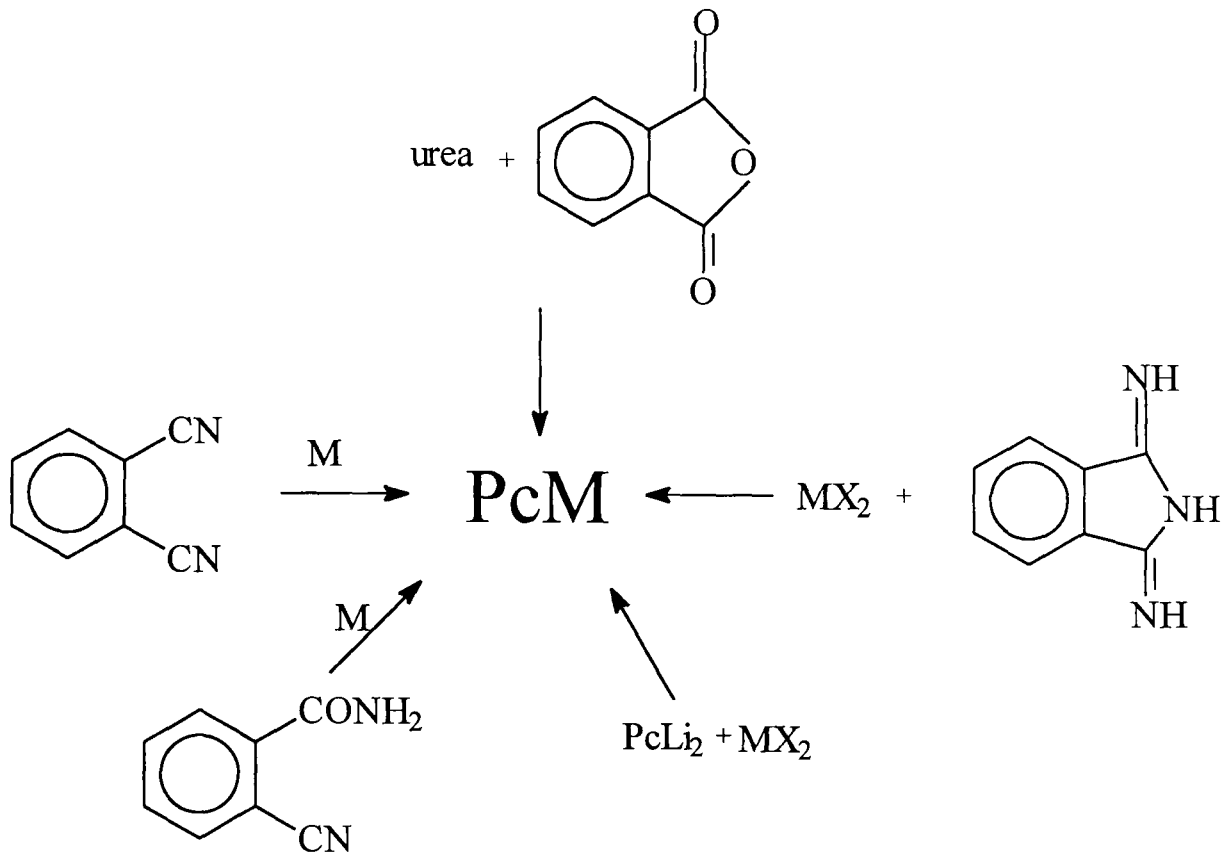

Fig 3.2: The different synthetic routes to a phthalocyanine.

3.1.2 Structure and Morphology

Polymorphism (where a molecule can stack in a variety of ways) is common in phthalocyanines because of the relatively weak interactions between molecules. This has been exploited by the dye industry as polymorphs can exhibit different colours, though the stacking has a profound influence on the photoconductivity as well. Of the different phthalocyanines studied, H_2Pc is known to exist in 4 different polymorphs in the solid state, namely the α, β, X and τ forms. The most thermodynamically stable is the β form which is the form obtained from direct synthesis or recrystallisation[64]. The α form is obtained by acid pasting or

sublimation in thin films[65]. X-H_2Pc is prepared by neat milling α-H_2Pc for 1 week[66] and τ-H_2Pc can be obtained either by milling α-H_2Pc in a solvent[67] or direct synthesis[68]. The different forms of H_2Pc exhibit different absorption spectra and X-ray diffraction patterns. Of the different forms, X- and τ-H_2Pc are found to have the best photoconductivities and the longest wavelength absorption maximum is significantly red shifted relative to the solution absorption.

There has been considerable work in the last few years on the polymorphs of TiOPc as it has shown high photoconductivity which is of considerable interest to the photocopier industry. Besides the α and β forms, several other polymorphs have been reported recently by different authors[69]. As some of the articles were published simultaneously, some of the polymorphs have been assigned different labels. The nomenclature used here is that proposed by Enokida et al[70]. They found that TiOPc had 4 forms, namely α, β, γ and *m*. The processes for treatment of TiOPc to prepare the different forms are shown in fig 3.3. The absorption spectra for films of TiOPc in their different forms is shown in fig 3.4. The spectra were obtained for TiOPc coated on glass with a binding polymer in solution in 1-chloronaphthalene.

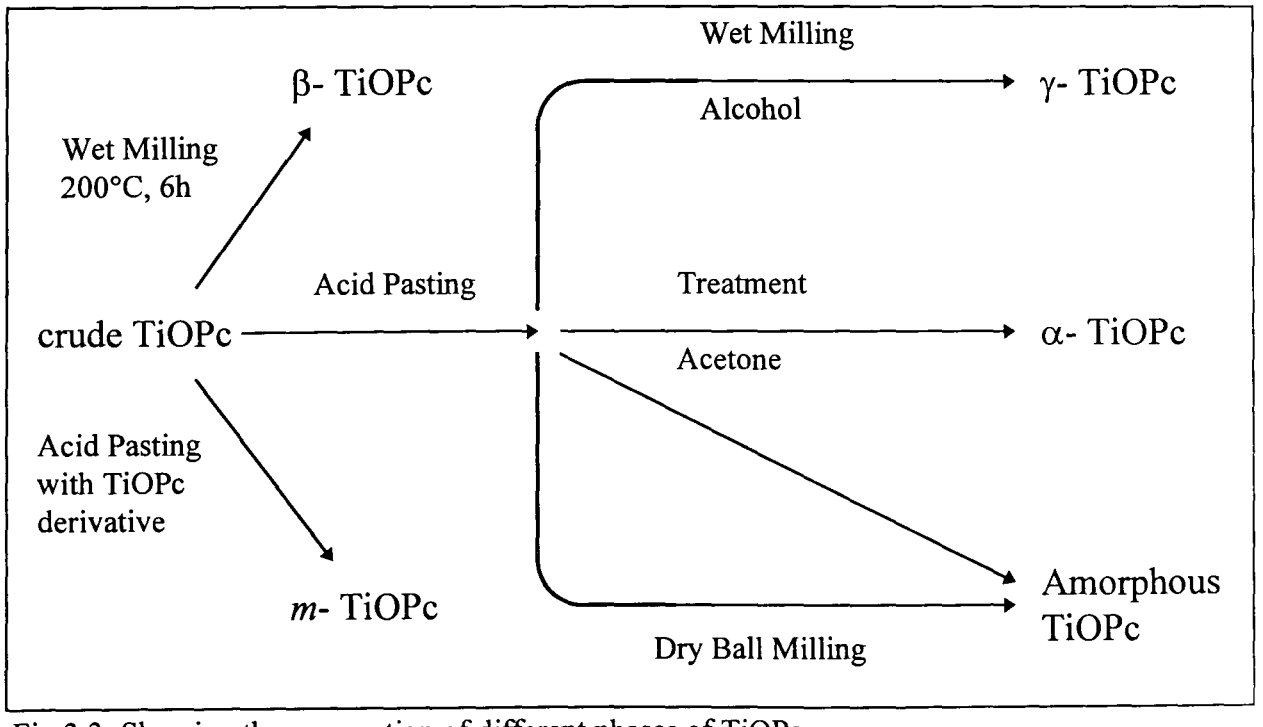

Fig 3.3: Showing the preparation of different phases of TiOPc.

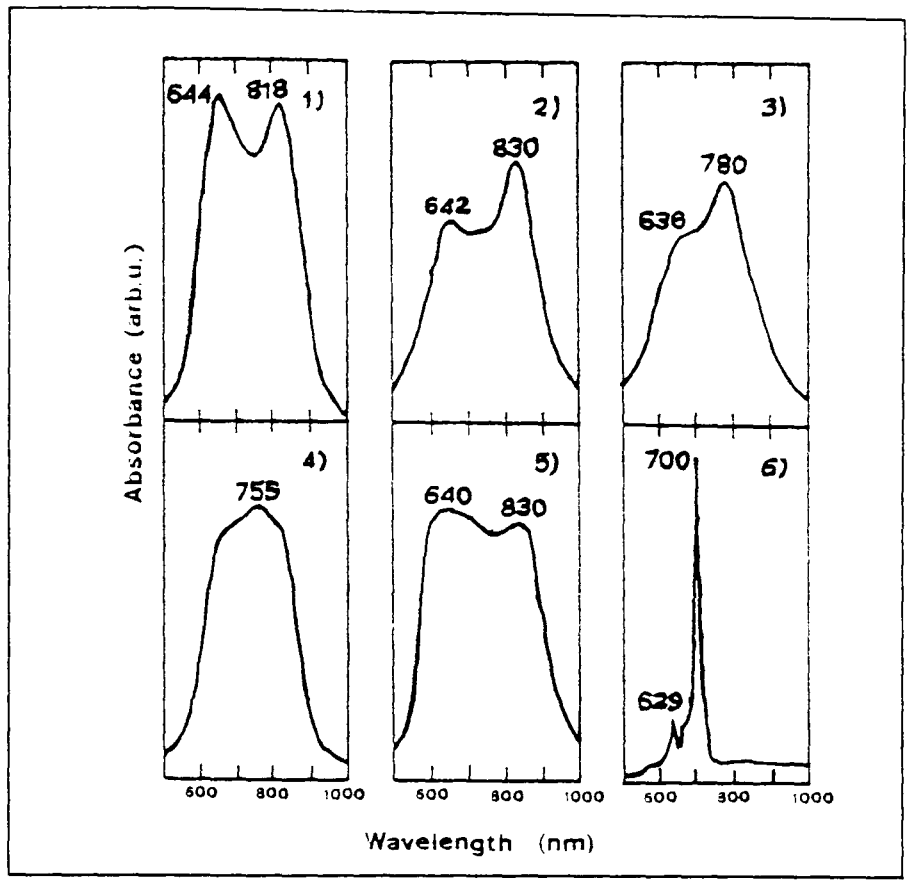

Fig 3.4: The absorption spectra of oxotitanium phthalocyanines on glass. They are (1) amorphous, (2) α-form, (3) β-form, (4) γ-form, (5) *m*-form and (6) is a solution spectrum. From Enokida [70]

Enokida et al measured the ionisation potentials and the photoconductivities of the different forms. The results are shown in table 3.1

TiOPc polymorph	Ionisation potential (eV)	Photosensitivity (erg/cm^2)
amorphous	5.39	1.9
α	5.34	2.6
β	5.27	3.6
γ	5.38	1.8
m	5.35	2.4

Table 3.1: Showing the ionisation potentials and photosensitivity of different polymorphs of TiOPc.

As expected, the values of the ionisation potentials for different polymorphs remain almost constant. The value for the photosensitivity is commonly used by the xerographic industry to describe the response of photoconducting materials. It is written as $E_{0.5}$ and defined as the energy required to photodischarge half of the initial potential. This equals the product of I (the monochromatic light intensity) and t where t is the time for I to photodischarge the device to half its initial value. The units used are ergs cm^{-2}. The definition of the photosensitivity based upon its use as a xerographic device and the values in the table above are for a TiOPc/butadiene derivative photoreceptor at 790nm. As this is a two layer device with the TiOPc layer acting as the charge generation layer and the butadiene derivative being the charge transport layer, the photosensitivity is a measure of the hole injecting properties of the TiOPc layer. Varying the second layer changes the value for the photosensitivity without altering the order of the polymorphs. In terms of use for photovoltaic devices, the polymorph with the greatest photosensitivity will form the most efficient device.

3.1.3 Spectroscopic properties

Most phthalocyanines in solution show a spectrum which exhibits two extremely intense absorption bands at 300-400nm (called the Soret or **B** band) and at 650-700nm (the **Q** band). This makes them useful materials for bilayer devices as the requirement for complementary absorption spectra is more easily met.

The origins of the bands can be explained by considering the symmetry of the molecule. For metal phthalocyanines, the metal atom can coordinate with the nitrogens via in-plane σ orbitals or perpendicular to the plane with the interaction between the metal and nitrogen π orbitals. These π orbitals form a highly conjugated system which dominates the electrical and optical properties.

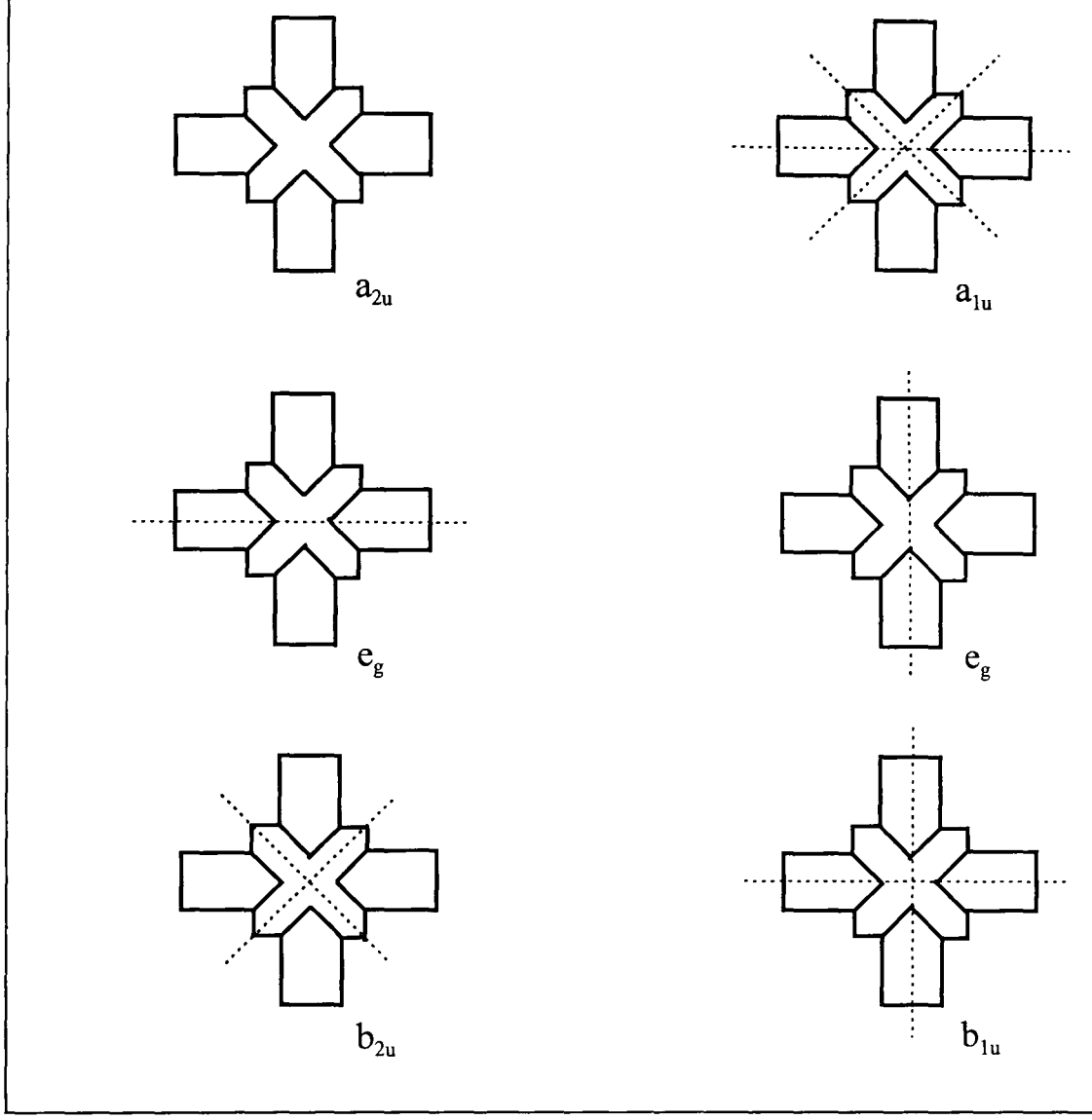

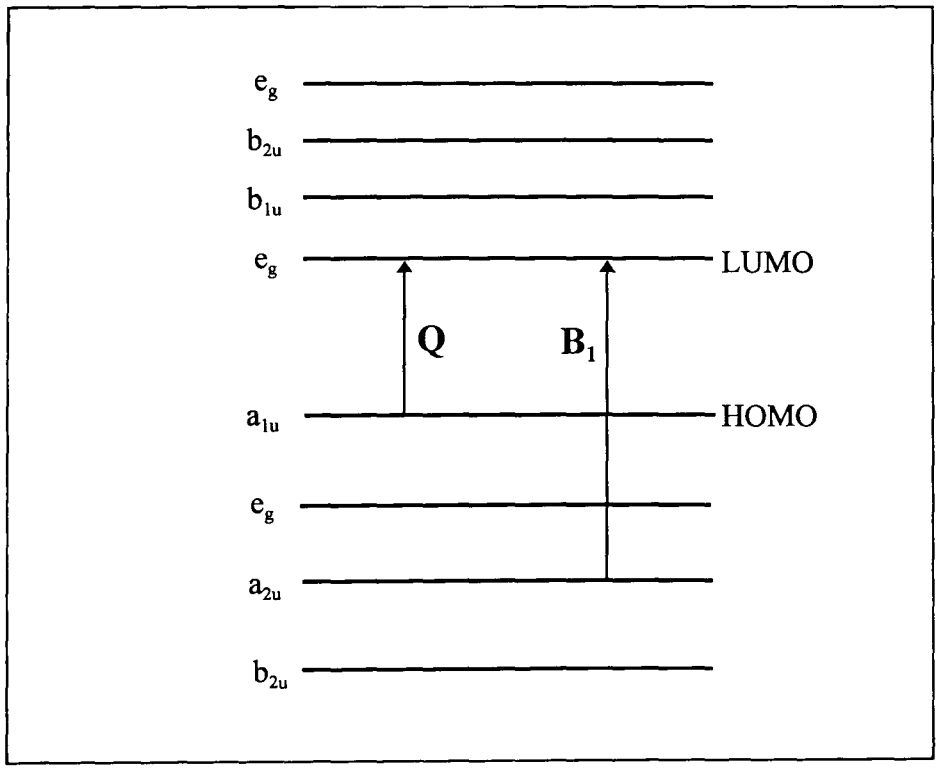

Fig 3.5: Showing the symmetry of orbitals in a D_{4h} phthalocyanine and the origin of the bands observed.

The absorption characteristics have been rationalised most simply by Goutermann's molecular orbital calculations[119] for porphyrins and phthalocyanines. These use the two highest occupied molecular orbitals which are a_{2u} and a_{1u} in symmetry and the doubly degenerate LUMO pair, (e_g). In phthalocyanines, the a_{1u} and a_{2u} levels are widely spaced leading to two transitions, labelled **Q** and $\mathbf{B}_1$ which are both formally allowed (π-π^*) making them strong in intensity (see Fig 3.5). For some other porphyrins, the a_{1u} and a_{2u} levels are close together which allows considerable configuration interaction.

The spectral properties of metal phthalocyanines are more complicated as optical absorptions are not entirely restricted to intra-ring transitions. Thus, electrons associated with the metal can undergo excitation into ring orbitals and vice versa making the energy of the metal orbitals important in the phthalocyanines spectroscopic properties.

3.1.4 Electrical properties

When making measurements of the photoconductive properties of phthalocyanines, it is important to note the effects of the ambients. It was initially thought that the photoconductive properties of α- and β- H_2Pc were very different[72] before it was shown that this arose because the α- form has a greater ability to bind O_2. For MPc's, the effect of O_2 is even more dramatic on the photoelectric properties than on their dark conductivities[73]. Another significant factor is the axial coordination ability of the central metal ion. The ability of MPc's to participate in axial coordination[74] decreases as ZnPc > CuPc > NiPc. This again may be due to the relative ability of the different MPc's to bind O_2 because the photoconductivity of NiPc is low and unchanged in vacuo compared to air whereas the photoresponse of ZnPc decreases by a factor of 40 after being pumped at 10^{-5} Torr for 24 hours[74]. This indicates that the quantum yield of carriers from the excited singlet state is low so an extrinsic process involving oxygen is more likely;

$$(S_0)PcM,O_2 + h\nu \rightarrow (S_0)PcM^*,O_2 \rightarrow PcM^+,O_2^- \rightarrow \text{free carriers}$$

Studies have been carried out on PbPc crystals[75] which show that varying the concentration of oxygen can change the magnitude of the photocurrent by a factor of over 100. This was repeated for CuPc[76] and the thermal activation energy for the photocurrent was found to be 0.41eV. Three conclusions have been drawn on the effects of oxygen on the photocurrent:

- As PcM^+, O_2^- is the likely ionised intermediate with the energy needed to create carriers being 0.4eV
- The photocurrent activation energy is wavelength independent, so the same intermediate is always formed even from different preliminary photoexcited states.
- Energy migration to the PcM, O_2 centres is likely as the overall concentration of O_2 is always low.

The photocarrier generation processes that are involved when thin films of ZnPc are exposed to air have been studied[77]. The distance between the initially formed charged pairs (the Onsager distance) is found to be 9Å. The authors comment that this may correspond to the mean distance between neighbouring phthalocyanine molecules or the mean separation between the PcM^+ and O_2^- formed initially.

Although the phthalocyanine is the most studied class of organic photoconductors, there is still some doubt over the detailed mechanism for the photogeneration process. In 1978, Menzel and Jordan[78] reported the fluorescence emission of microcrystalline x-H_2Pc powder by laser induced fluorescence. Further measurements showed that fluorescence quenching is possible by applying an electric field. This correlation between fluorescence quenching and photogeneration suggests that the first excited singlet state (S_1) is the precursor state for the photogeneration process[79]. Further investigations have been carried out on the photogeneration of x-H_2Pc in the presence of an

electron donor/acceptor, recording both fluorescence quenching and photogeneration efficiency data using sandwich photoelectrical cells[80]. These measurements were carried out by recording the fluorescence quenching of a x-H_2Pc microcrystalline powder which had been surface coated with a variety of electron acceptors and donors to a monolayer coverage. The quenching efficiency was as high as 92% for *o*-chloroanil. The authors proposed that an exciplex was formed at the surface between the H_2Pc and the donor/acceptor. The exciplex then causes the fluorescent quenching. As there is a high degree of fluorescence quenching, this indicates that the exciton migration range is very large. Some authors have measured this[26] to be around 200 - 400Å which is similar to the size of a x-H_2Pc particle (≈1000 x 300 x 300Å). All this leads to a mechanism where the exciton migrates to the particle surface and forms an exciplex so quenching the fluorescence. This exciplex then dissociates to form an electron/hole pair.

The photogeneration mechanism in the absence of an electron donor or acceptor is less well studied. Loutfy and Menzel[80] have studied x-H_2Pc and concluded that O_2 may play a role in the photogeneration process, helping in the formation of the exciplex which dissociates into the electron/hole pair. This conclusion as supported by the work of Ahuja and Hauffe[81] who showed that O_2 is responsible for the photoinjection of charge carriers from x-H_2Pc into inert alkane solvents.

Studies have been performed which have tried to detect the formation of an exciplex in the photogeneration process which was proposed as a precursor state by Loutfy and Menzel. Whilst this was not observed experimentally in x-H_2Pc, Popovic[82] studied β-H_2Pc by delayed-collection-field and delayed fluorescence technique and detected an exciplex intermediate. So far, all the different experimental results found can be explained by using an extrinsic model for photocarrier generation using exciton diffusion and surface ionisation. Whilst this does not mean that all phthalocyanines are extrinsic photogenerators, there is presently no experimental evidence for intrinsic

photogeneration available. As for the dopant, O_2 has commonly been reported as the main dopant though Fujimaki[83] has reported that water molecules which are absorbed on the surface of γ-TiOPc do effect its photoconductivity.

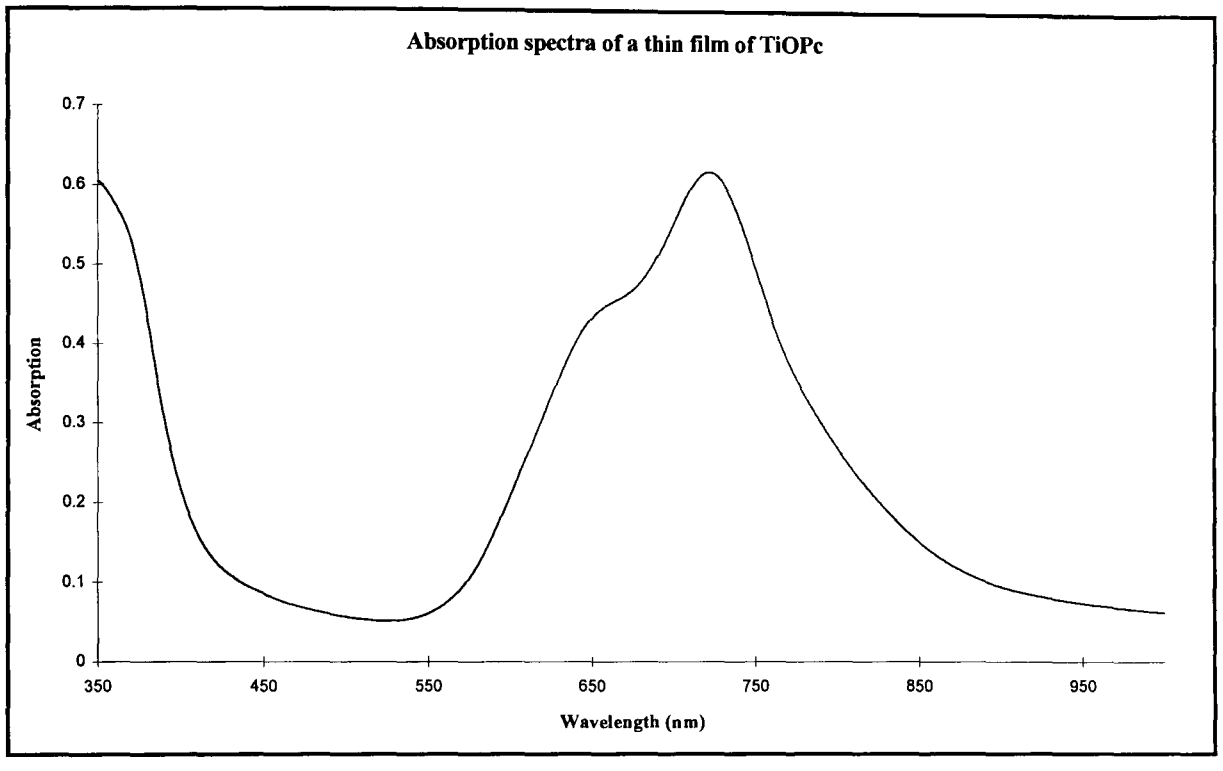

Fig 3.6: Absorption spectra of a thin film (500Å) of TiOPc on a glass substrate

For the photovoltaic devices reported in chapter 5, titanyl phthalocyanine (TiOPc) was used. This is because it shows an exceptionally high quantum photogeneration efficiency (≈90% in the γ-form). An absorption spectrum of a thin film of TiOPc on a glass substrate is shown in Fig 3.6

3.2 Perylene pigments

Perylene pigments are diimides and bis imidazoles of perylene-3,4,9,10-tetracarboxylic acid. These pigments have good light and water fastness and are best known for their use as colourants for car paints and plastics. Their photoconductivity was first noted in 1972 by Regensburger and Jakubowski though their performance was undistinguished[84]. Whilst they were visibly absorbing and readily available, the purity was typically low which reduced their conductivity. However, in 1986 Tang proposed a bilayer solar cell using a perylene pigment with a phthalocyanine layer[29] and this renewed interest in the xerographic industry. Since then, perylene pigments have been at the forefront

of organic solar cell research and have found uses in other novel applications (such as photocurrent multipliers[85] etc.)

3.2.1 Synthesis

Perylene pigments are synthesised by condensation of perylene 3,4,9,10-tetracarboxylic dianhydride with amines in a solvent[86]. This synthesis is extremely efficient with the isolated yields usually greater than 90%. The condensation reaction is stepwise. Since the starting dianhydride, the intermediate (the monoanhydride monoimide) and the product are all insoluble in the reaction solvent, the reaction involves the transformation of one red solid into another. This results in the contamination of the product by starting material and the monoanhydride monoimide form. This is usually removed by washing the perylene pigment with alkaline solutions which dissolve the starting material and the intermediate. Vacuum sublimation is also used. Hiramoto et al[10] have noticed that the position of the Fermi level of a perylene pigment can be altered by reactive sublimation. This is a similar technique to vacuum sublimation but the carrier gas is not inert. As the perylene pigments act as electron acceptors, most of the impurities are thought to be acceptors. So methylamine was used as the carrier gas to react with the unknown impurities. As the position of the Fermi level moved nearer to the middle of the bandgap after sublimation, it was assumed that some of the impurities had been removed.

3.2.2 Structure and morphology

Perylene pigments have either a red, red-brown or purple blue appearance depending on the substituents. They have a very low solubility in common solvents. The solid state absorption properties have been studied by Graser and Hadicke[87]. In the solid state, perylene pigments tend to stack in vertical slipped stacks with only one polymorph. The stacking arrangement is strongly

dependent on the nature of the substituent. As a result, the solution absorption wavelengths of N,N'- dialkyl diimide perylenes are independent of the N-alkyl group whereas the shapes of the solid state absorption bands are very sensitive to the end group. This is due to the end group changing the stacking pattern. As a result, the amount of intermolecular overlap varies so altering the width of the absorption peak. So the blacker the perylene pigment, the wider the absorption peak, hence the larger the intermolecular overlap. This causes the crystallochromy seen in perylene pigments[126].

3.2.3 Electrical properties

The photoconductive properties of perylene pigments are summarised by Law[88]. It has been noted[126] that, generally, the values for the photoconductivity follow the colour of the pigment with the blacker pigments photoconducting better than red pigments. The authors attributed this to increased intermolecular overlap manifested as band broadening which stabilises the separated charges and inhibits recombination.

The photogeneration mechanism in perylenes has been studied[89]. The results show that an extrinsic mechanism involving exciton diffusion is again the most likely. A detailed set of experiments were performed on a bilayer device made from a layer of the perylene and a charge transfer layer (35% hole transporting molecule and 65% polycarbonate polymer). The fluorescence of the film is quenched (by 90%) when the CTL is added and this was shown to be due to the hole transporting material. This quenching follows the photogeneration data which again indicates that the S_1 state is involved in the photogeneration process. Further evidence for the exciton diffusion model comes from the action spectra of the bilayer device. When illuminated through the CTL, the action spectrum follows the absorption spectra whereas the action spectrum is independent to the absorption spectra when illuminated through the perylene layer. The latter case implies that light of a wavelength strongly absorbed by the perylene layer requires a long exciton diffusion length whereas weakly

absorbed light will be compensated for by requiring a shorter exciton diffusion length. From the shape of this graph, Popovic deduced that the exciton diffusion length was ≈2700Å. The field dependence of the photogeneration efficiency was less than that predicted by the Onsager model. This would imply that at low fields, there is direct generation of electron/hole pairs without the formation of an exciplex. No satisfactory model has been proposed for this scenario.

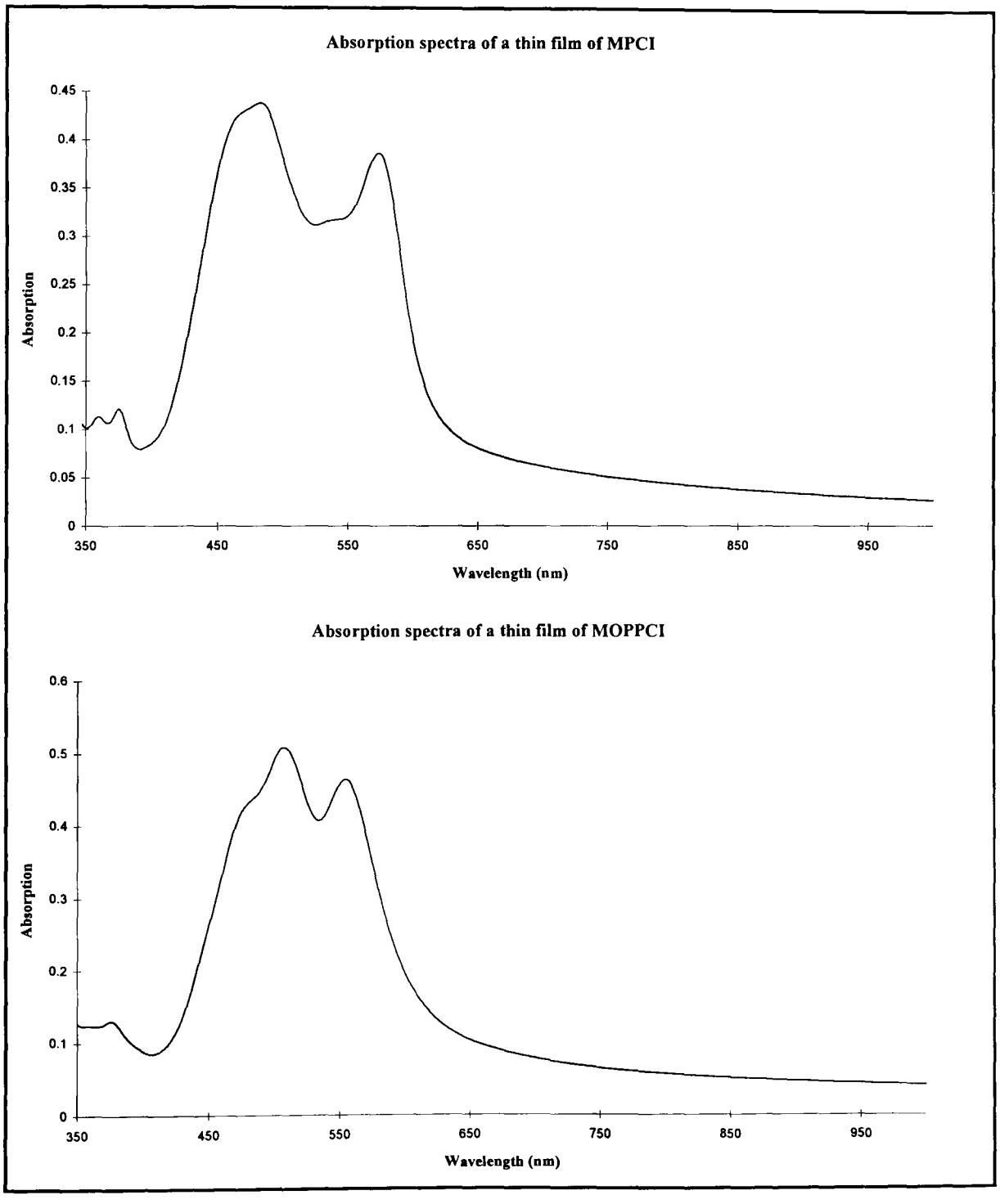

Fig 3.7: Absorption spectra of the perylene pigments used in the bilayer devices reported.

3.3 Squaraines

This class of material was used in early high efficiency solar cells[22] of the Schottky barrier type. To the best of our knowledge, they have not yet been tried in a bilayer system. However, there has been considerable work done on their photoconduction with a view to a use in the xerographic industry, mostly by Law and co-workers. This was initiated because they absorb strongly in the near-infrared (700-850nm) which matches well with the output of diode lasers. A squaraine is shown in fig 3.8

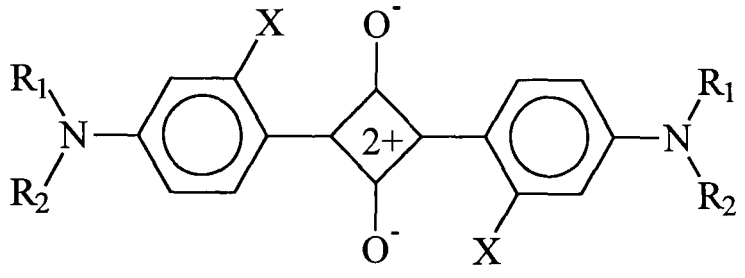

Fig 3.8: A squaraine

A list of the symmetric squaraines along with their absorption maxima and synthetic yield is given by Law[88].

3.3.1 Synthesis

Squaraines are traditionally synthesised by condensing 1 unit of squaric acid to 2 units of N,N-dialkylaniline in an azeotropic solvent[90]. Water is the byproduct and this is removed azeotropically. Structural variations are achieved by using different aniline precursors. An alternative procedure has been suggested by Law and Bailey by an ester route[91]. They noted that although the synthetic yield for this route was lower, squaraines synthesised by this route consistently showed better xerographic properties. This was attributed to the products having a smaller particle size which resulted in a different crystallographic orientation. These morphological changes result in 'purer' squaraines and hence better xerographic properties.

3.3.2 Structure and morphology

Squaraines exist as microcrystalline powders in the solid state, with the highly photoconducting ones being pigmentary. Studies of the x-ray diffraction patterns and absorption spectra of different squaraines with methyl groups attached to the anilino group (positions R_1 and R_2) show that these are largely unchanged by the change in the phenyl group substituent (position X). The absorption spectra contain two broad bands, one at shorter and the other at longer wavelengths compared to the solution absorption spectra. This suggests both that the solid state properties are similar and that substituting the phenyl ring has very little effect on the charge transfer interaction. Similar results were found by Wingard[92] when he reported a crystal structure of Sq-9. The central C_4O_2 was placed 3.5Å above the anilino group. Thus the stacking of squaraines can be displayed schematically (the anilino groups are the donors, D, and the central squarate group is the acceptor, A)

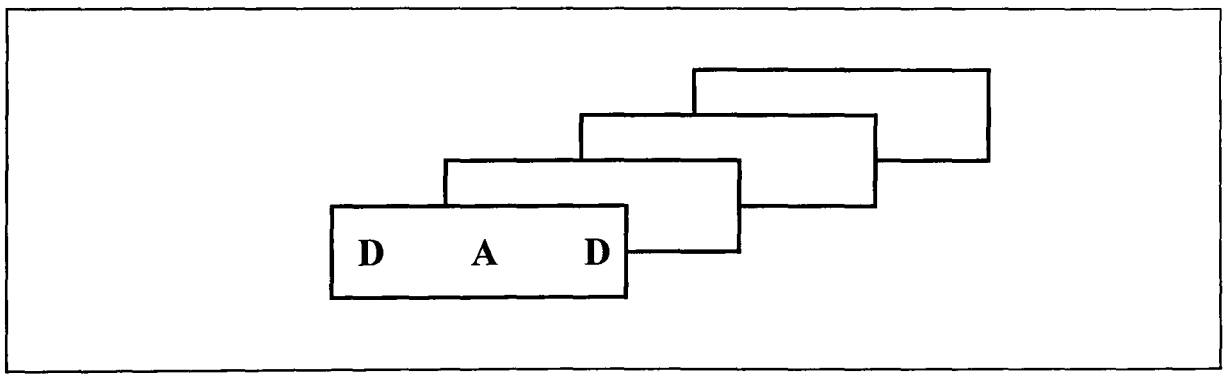

Fig 3.7: Stacking pattern of squaraines

When bulky groups are substituted onto the phenyl rings, then steric effects can disturb the intermolecular charge transfer interaction. This causes a distortion in the absorption spectra which returns to one broad peak centred at the value found in solution.

3.3.3 Electrical properties

Whilst a lot of work has been done measuring the photoconductivities of most squaraines in bilayer devices for xerographic purposes, their response is affected by the purity of the sample even though similar purifying techniques have been used. The response of different squaraines can vary quite dramatically i.e. Sq-5 (where $R_1 = R_2 = CH_3$, X = OH) has a response at 600nm of 5.6 ergs/cm^2 but Sq-6 (where $R_1 = R_2 = C_2H_5$, X = OH) has a response of 314 ergs/cm^2. These values were recorded using a bilayer device where the squaraine layer is covered by a hole transport layer. As a result, the reported photosensitivity depends on the ability of the squaraine layer to inject holes into the hole transport layer. Thus, when the position of the HOMO is lowered, the photosensitivity increases. This means that the magnitude of the photocurrent depends upon three factors: the morphology, purity and hole injecting characteristics of the squaraine layer. As squaraines behave as p-type conductors[22], the value of the HOMO energy should be as low as possible for an efficient bilayer device. Thus the value for the photocurrent gives a combined measure of the photogeneration efficiency and the ionisation potential of the material.

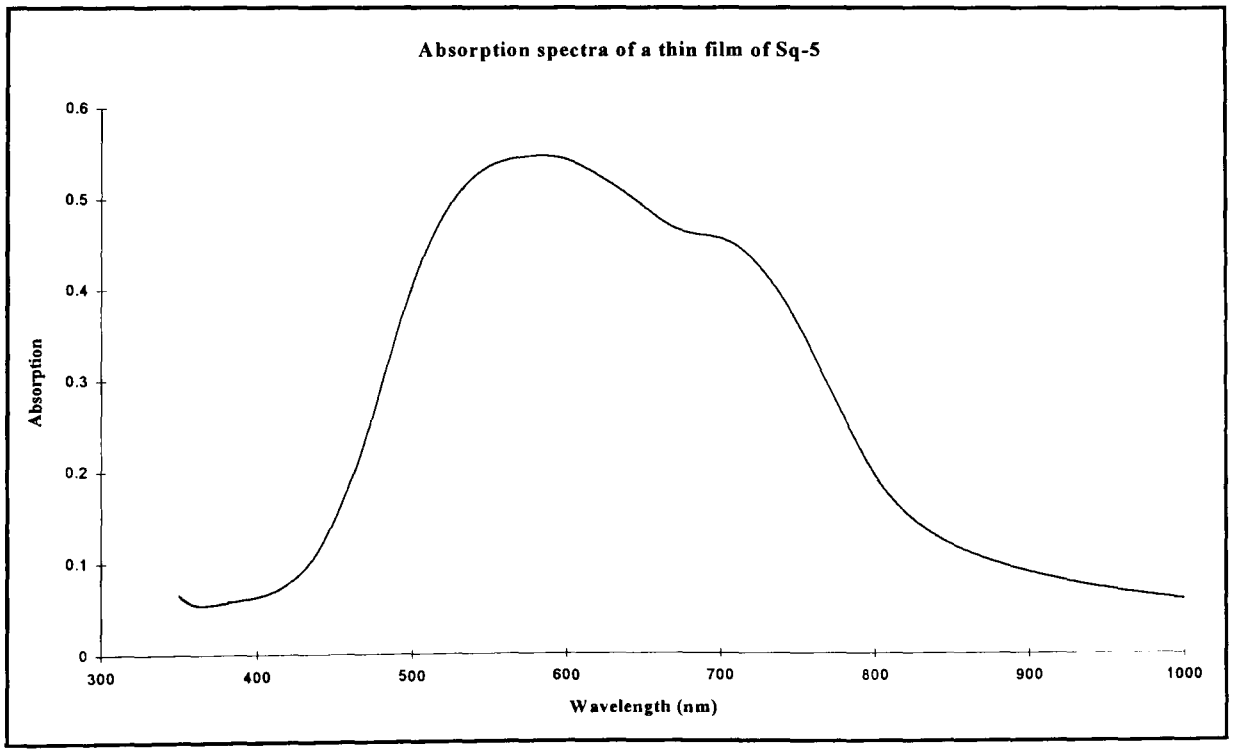

Fig 3.10: Absorption spectrum of a thin film (≈500Å) of Sq-5.

3.4 Anthanthrone pigments

Only occasional studies on the photoconductive properties of this class of materials have been reported. The most comprehensive was by Allen et al[93] who studied the synthesis and photoconductive behaviour of bis-halogenated anthanthrone pigments with a view to their use in the xerographic industry.

3.4.1 Synthesis

The starting material for the preparation of bis-halogenated anthanthrone pigments is the appropriate halogenated naphthostyrils. The preparation of these is described in the literature (for the fluoro- and iodo- forms[94], for the bromo- and chloro- forms[95]). The halogenated naphthostyrils are hydrolysed in sodium hydroxide solution (10M) and coupled via a diazotisation reaction with cuprous chloride. The full pathway is shown in fig 3.11

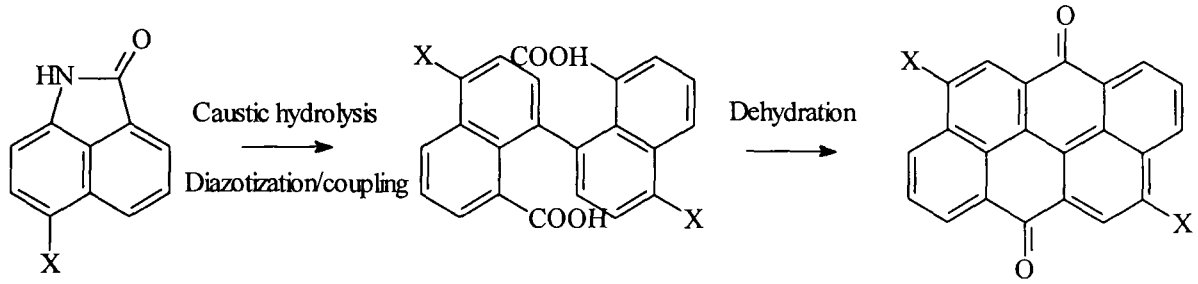

Fig 3.11: Synthetic pathway to 2,7-dihalo-anthanthrones.

3.4.2 Electrical properties

The photoconductivity of the halogenated anthanthrone pigments has been studied by measuring the photodecay rates of a bilayer system made from an anthanthrone layer and a charge transport layer (CTL). In this system, the photodecay rates found for different CTL's follows the order in electron donating power of the layer. This indicates that the anthanthrone layer is an electron acceptor and would behave like an n-type semiconductor. This conclusion is backed up by investigations on the hole injecting properties of the excited state of anthanthrone[96]. It was also noted that the devices operated

better when the anthanthrone layer was vacuum deposited. The authors attributed this to the photoconductive properties being intrinsic to the pigments themselves, with impurities acting as electron traps. Overall, the photoconductive properties of the anthanthrones are reduced by halogenation and dependent on the synthetic route and the purity of the material.

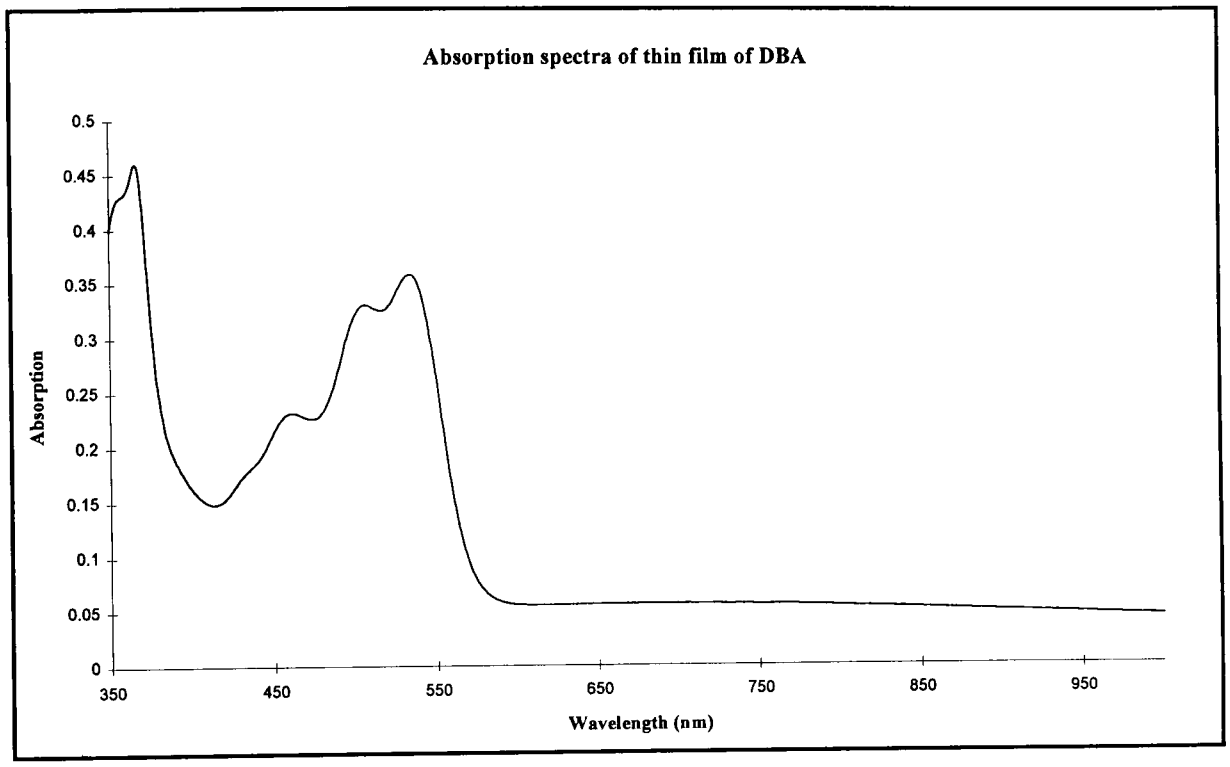

Fig 3.12: Absorption spectra of a thin film of DBA.

Chapter 4:- Experimental

4.1 Sources of materials

The following materials were used for bilayer solar cells: Titanyl phthalocyanine (synthesised by R. Elliot-Martin[97]), dimethyl perylenetetracarboxylic acid diimide (synthesised and donated by Y.Shirota), dibromoanthanthrone (donated by R.Gairns), C_{60} (purchased from Dynamic enterprises), BTDA (synthesised by Yamashita[98]), BTQBT (synthesised by Yamashita[99]), Squaraine 5 and dimethoxyperylenetetracarboxylic acid diimide.

4.2 Synthesis of materials

Dimethoxyperylenetetracarboxylic acid diimide (MOPPCI) and Squaraine 5 (nomenclature used by Law[88]) were synthesised as reported below. All materials were purchased from Aldrich and of the highest purity available. No further purification of the starting materials was attempted.

4.2.1 Synthesis of 2,9- Bis(4-methoxyphenyl)anthra[2,1,9 -*def*:6,5,10 -*d'e'f'*] - diisoquinoline - 1,3,8,10 (2*H*,9*H*)-tetrone (MOPPCI) according to ref 100.

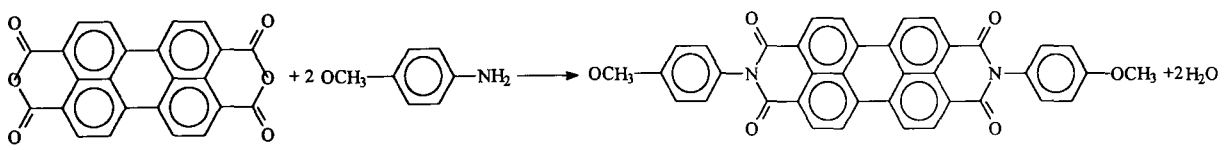

3,4,9,10- Perylenetetracarboxylic dianhydride (5.73g) suspended in *p*- anisidine (60.1g) was heated at 240°C for 2 days under nitrogen. The resulting suspension was suction filtered and washed using 150cm^3 of hot toluene followed by 100cm^3 of acetonitrile. The yield (before sublimation) was 8.04g or 91.3%.

4.2.2 Synthesis of Sq-5

The squaraine was synthesised by the acid route (as proposed by Law[101]) i.e. reacting squaric acid with the appropriate aniline derivative. Thus, 3-hydroxy N,N-dimethylaniline was synthesised according to ref 102.

The preparation of 3-hydroxy N,N-dimethylaniline

32.8g of 3-aminophenol and 28g of pure (99%) trimethyl phosphate were placed in a 500cm^3 round bottomed flask. The mixture was heated gently until a vigorous exothermic reaction took place. When the reaction had subsided, the mixture was refluxed for 2 hours before being allowed to cool. When the temperature had reached 50°C, a solution of 25g NaOH in 100cm^3 water was added and refluxed for 1 hour.

When the mixture had reached room temperature, the oily amine layer was poured off the solid sodium phosphate. Any remaining amine left in the sodium phosphate was removed by adding water and extracting with ether. The combined extract was dried with $MgSO_4$, the ether was distilled off and the residue treated with an equal volume of acetic anhydride and left overnight.

A solution of HCl (20cm^3 in 30cm^3 of water) was added until the base dissolved and extracted with 2x30cm^3 portions of ether. 25% NaOH solution was added to the water layer to liberate the base.

The oil was collected by extracting the mixture with ether, drying the solution with magnesium sulphate then removing the ether on a water bath. The residue was distilled using an air condenser and the product was collected (at 192-193°C).

Preparation of Squaraine 5

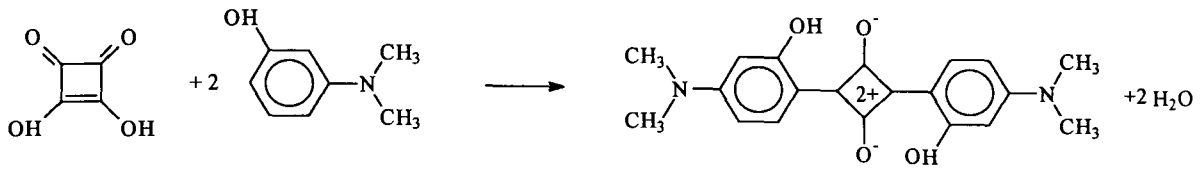

2.28g of Squaric Acid and 5.48g of 3-hydroxy N,N-dimethylaniline were heated with 30cm^3 1-butanol and 12cm^3 toluene under reflux until 0.72cm^3 of water was distilled off azeotropically. The mixture became deep blue and the product was filtered off and washed several times with light petroleum (35-45°C). Yield 3.47g, 49.3%. Chemical analysis: Expected **C** 68.18% **H** 5.68% **N** 7.95% Actual **C** 68.77% **N** 8.16% **H** 5.20%

4.3 Purification of materials

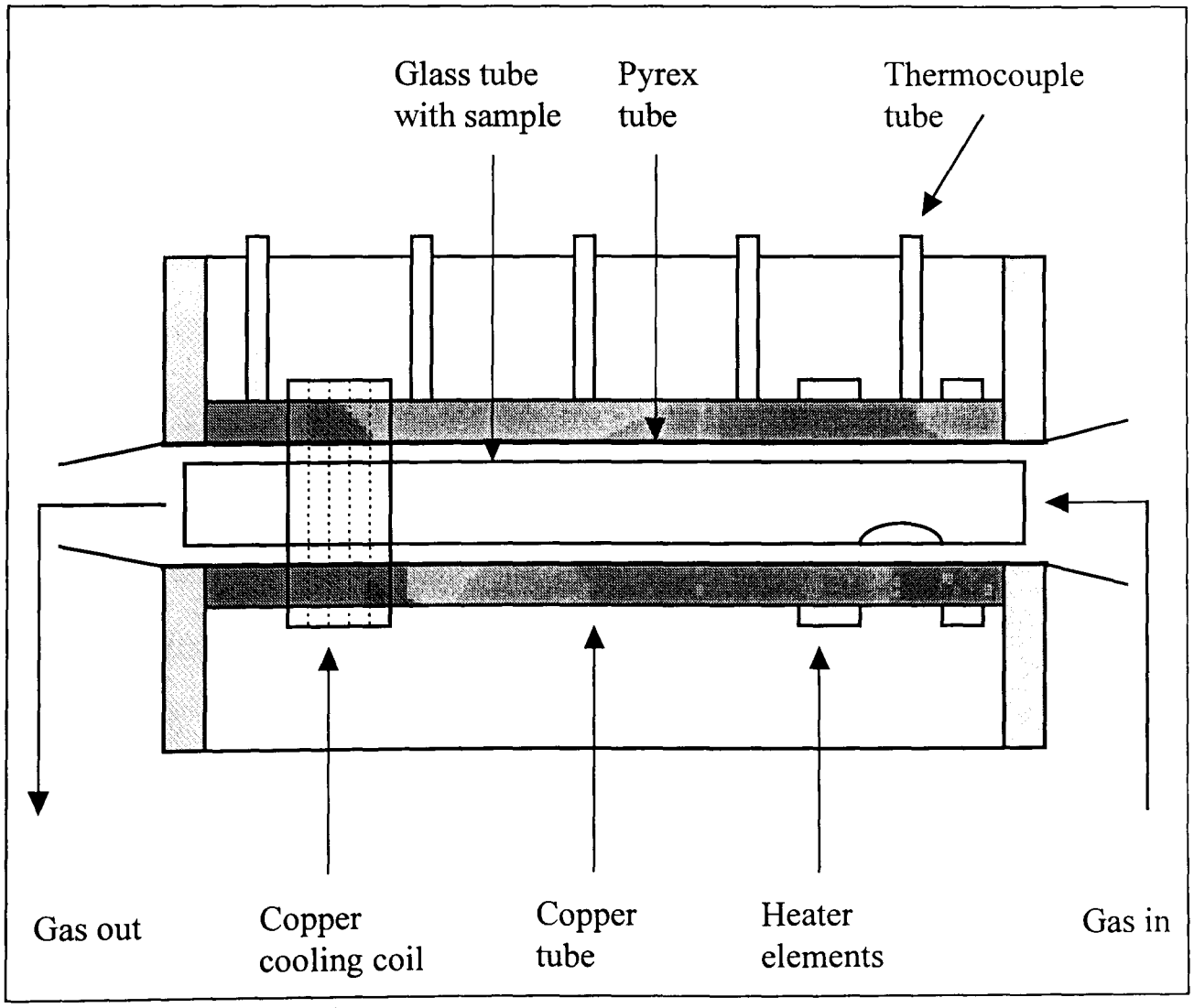

Fig 4.1:- The Entrainer sublimer.

The materials were all purified by entrainer sublimation. The Entrainer sublimer was built by D.C. Davies to a published design[103]. The system consists of a copper furnace tube surrounded by ceramic heating coils at one end and copper cooling coils at the other. This provides a linear temperature gradient along the tube. A Pyrex tube is placed within the furnace tube and this is connected to a rotary pump with a liquid nitrogen trap. The sample is the heated until it sublimes and is carried down the tube by an inert carrier gas (Nitrogen). When the temperature gets cool enough, the sample will solidify on the side of the tube. Hence, it is possible to separate materials which sublime at different temperatures which are thermally stable.

4.3.1 Operation of the Sublimer

About 1g of a sample to be purified was placed in a glass sublimation tube so that the sample was positioned under the heating elements. The system was evacuated to 10^{-2} Torr using a rotary pump and a liquid nitrogen trap was attached. At this point, the nitrogen gas was introduced at a flow rate of 20-30 cm^3 min^{-1} and allowed to stabilise. The heating elements were turned on and allowed to reach a temperature of about 500°C and left for 12-18 hours. The system was allowed to cool and the glass tube was removed, cut at the appropriate point and the purified sample was scraped out. If the sublimation was not successful, then it was repeated at a higher carrier gas flow rate and for a longer time.

4.4 Cell Fabrication

Sandwich cells were made according to the following procedure.

4.4.1 Etching ITO glass substrates

A piece of ITO glass (purchased from Balzers) with a resistance of 20 $\Omega\square^{-1}$ was cut into pieces 40mm x 25mm. It was necessary to etch off the indium tin

oxide layer so that wires could be connected to the gold electrode without shorting the device. This was done using Zn paste and 50% HCl solution. The rest of the slide was protected using Raphaelite hard drying paint which was soluble in acetone so could be easily removed after the etching was complete. It is also possible to use Aqua Regia and Scotch tape.

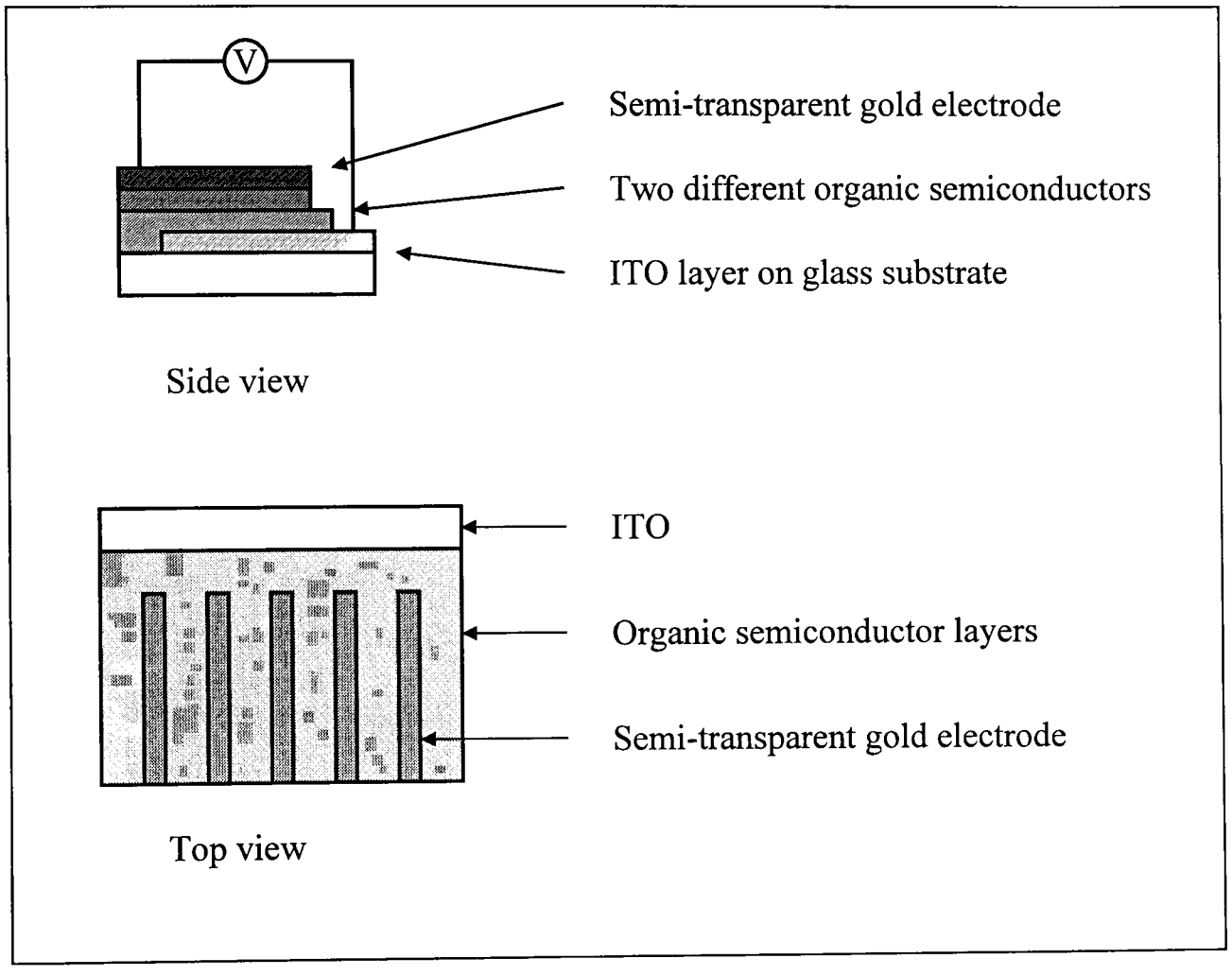

Fig. 4.2: Diagram of a sandwich cell.

4.4.2 Cleaning of glass substrates

Once the slides had been etched and the paint removed, they were cleaned according to the method proposed by Wohrle[37]. Slides were sonicated in Decon 90 solution, acetone and ethanol for 10 minutes, before being put in boiling ethanol for 15 minutes. Cleaned glass slides were stored in ethanol and boiled in ethanol before use.

4.4.3 Deposition by sublimation

All the samples were prepared by vacuum evaporation deposition using an Edwards E306 vacuum coating unit.

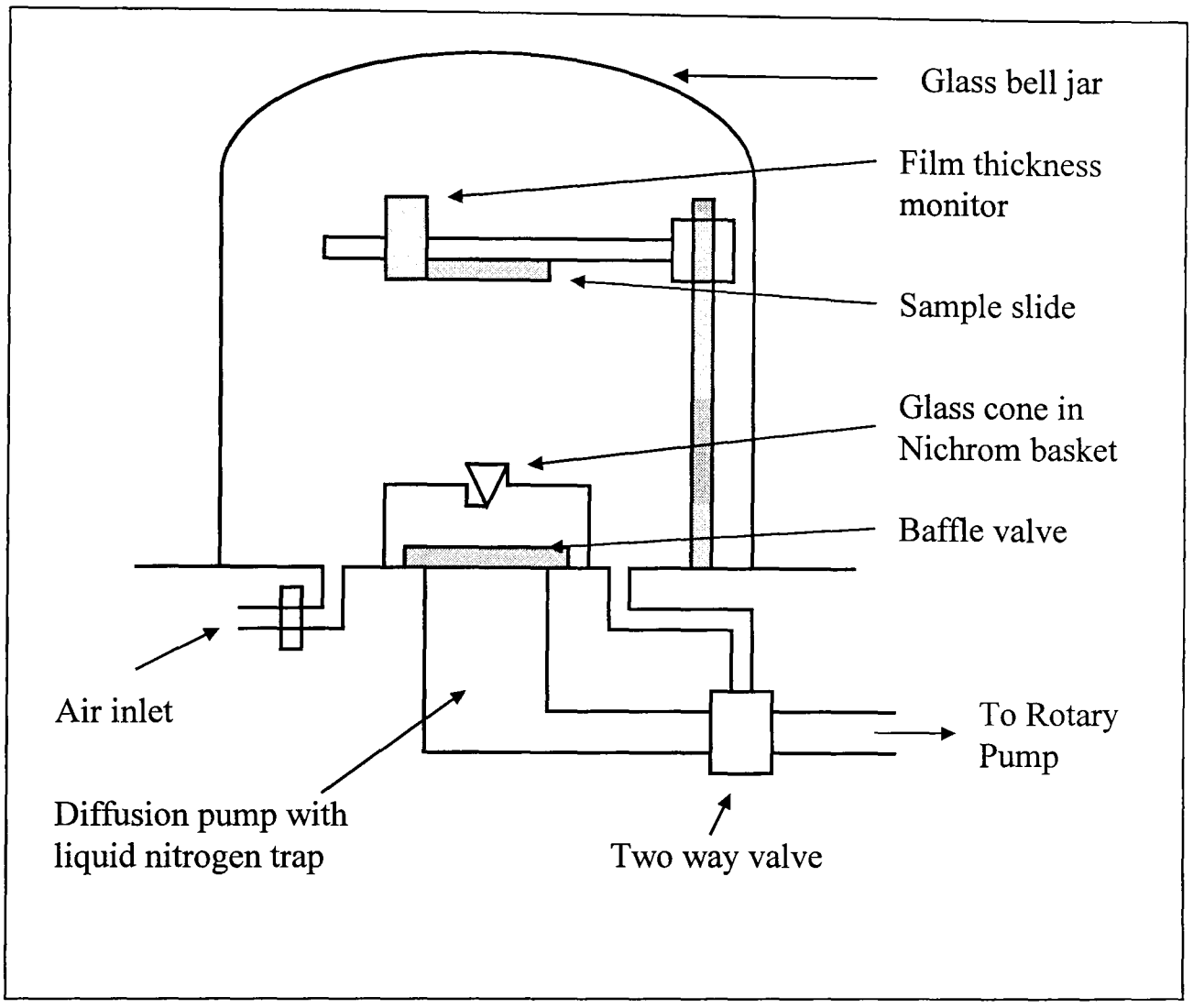

Fig 4.3:- Edwards E306 vacuum coating unit.

Operation of the sublimation unit

The glass substrates were mounted in the unit with the appropriate masks and they were placed 20-25cm from the heating source. A Sloan 200 film thickness monitor was placed next to the slides. The system was evacuated using an oil diffusion pump backed by a rotary pump to a pressure less than $8x10^{-6}$ mbar. The liquid nitrogen trap ensures that the chamber is kept free of oil contamination. Organic materials were sublimed using a glass cone in a

Nichrom basket whilst a molybdenum boat was used for gold. When the chamber was at the operating pressure, the materials were evaporated by resistive heating of the boat/ basket and the thickness of the film was measured by the film thickness monitor.

Evaporating the layers

The cleaned glass slides were mounted in the evaporator and masks made from steel or cardboard were placed above the slide. Masks were ideally kept a few millimetres above the slide so that the evaporated films did not have any sharp edges. The organic layers were deposited at a rate of 2-3Å s^{-1}. After each deposition, the samples were left to cool for at least an hour under vacuum. The thickness of each organic layer was between 500Å and 1500Å. As only one heating element was used, the chamber was opened and the samples were exposed to air between each deposition. The top gold (supplied by Alfa, 99.995% pure) electrode was laid in short bursts of less than 10 seconds, to prevent heating of the sample, to a thickness of 300Å. The sample was left for about 10 minutes between each burst. This reduced the number of samples that shorted. For some organic materials (e.g. BTQBT), it is necessary to reduce the substrate material distance as it is easily pumped away by the system.

When the samples had been prepared, thin copper wires were attached by applying Electrodag silver conducting paint to make a connection. The wires were secured using quick-set Araldite. An alternative design where small crocodile clips replaced the attached wires was later used.

4.5 Device Measurements

Three main tests were performed on each sample. The sample was mounted in an Oxford Instruments PTC-500 cryostat fitted with Spectrasil windows. It was held in place on a copper cold finger with Blu-Tak. The cryostat was attached by 1.5m steel bellows to an Edwards E02 cold-trapped diffusion pump backed

by an Edwards Rotary pump, fitted with a bypass line. The system could be pumped out to 10^{-5} mbar.

4.5.1 Current/ Voltage plots

The following circuit was used to test the samples:

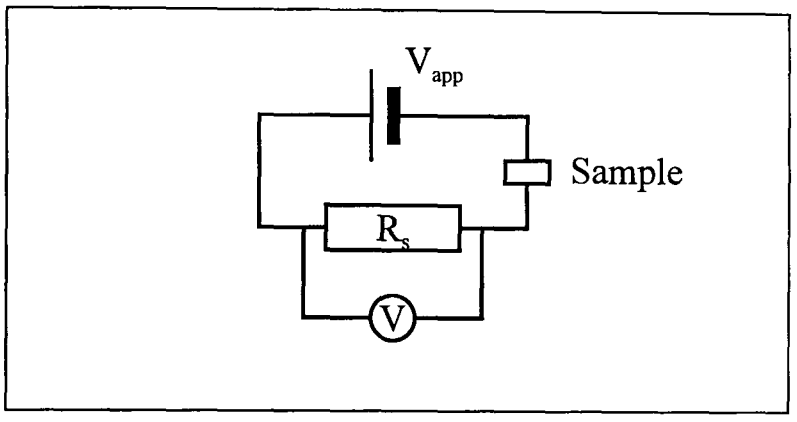

Fig 4.4: Circuit for current/ voltage measurements.

The sample was connected in series with d.c. power supply (Thurlby PL320 - 30V/2A) and a standard resistor (R_s). The standard resistor is chosen so that it has a much lower resistance than the sample ensuring that the applied voltage is effectively equal to the voltage across the sample. The applied voltage was varied between -0.6 and 0.6V and this was checked with a Keithley 195 multimeter. The voltage across the sample was measured by a Keithley 616. The sample was illuminated by a 24V, 250W tungsten-halogen projector bulb focused by two quartz lenses so that the light illuminated the whole of the sample. The intensity of the incident light was measured using a Macam light meter (unit Q102X with a SD112 detector fitted with a RFF Cos-112). Alternatively, the white light source was replaced by a 0.5-2.5 mW, 670nm, 0-95% intensity modulated, 1-1x10^5 Hz diode laser (obtained from LASER 2000).

4.5.2 Action spectra

To measure the wavelength dependence of the short circuit current of the sample (or action spectra), a Spex Minimate monochromator was placed in front of the white light source. Three quartz lenses were used to focus the light onto the monochromator, collimate the output and focus it onto the sample. The monochromator was scanned from 300nm to 1000nm at 20nm intervals and the intensity of light at each wavelength was measured by the Macam light meter and this was used to normalise the readings. The short circuit current was measured using a Keithley 616 to record the voltage across a standard resistor. All the action spectra were corrected for the intensity of the incident radiation.

4.5.3 Chopped light measurements

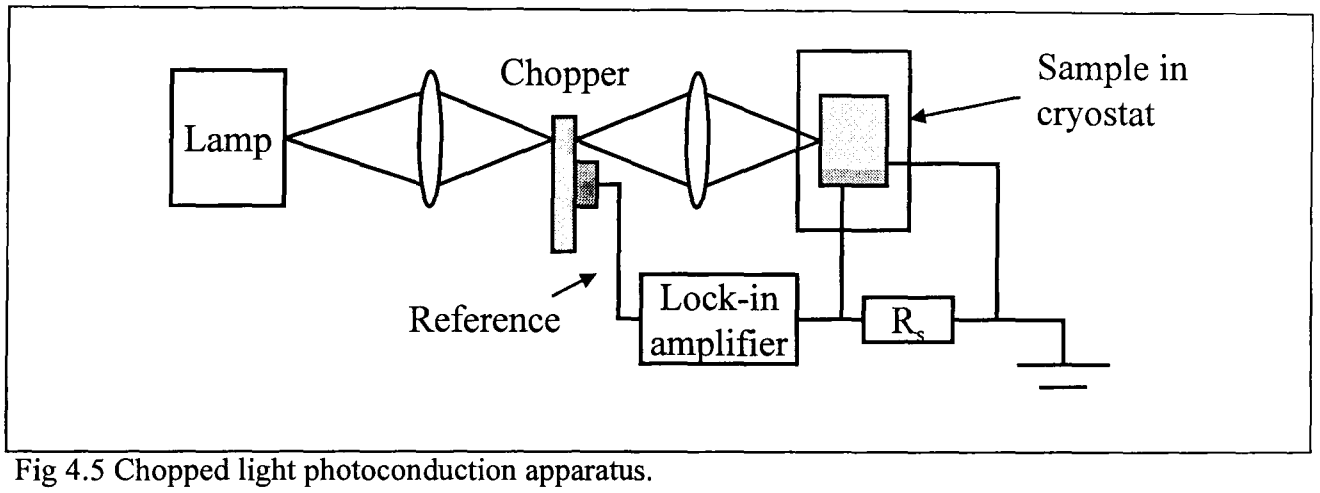

Fig 4.5 Chopped light photoconduction apparatus.

The white light source was used at a low intensity to avoid heating. This was collimated and focused using a quartz lens so that the beam was small enough to pass through the sectors of the chopper ensuring a square wave resulted. There was the choice of a 2 or 12 sectored aluminum disk which was rotated by a Velodyne motor and allowed chopping speeds between 0 and 500 Hz to be measured. A photodiode was mounted on a movable arm in close proximity to the chopping disk which monitored the frequency of chopping and acted as the reference signal for the lock-in amplifier. The lock-in amplifier was a Brookdeal 9503E with a microprocessor and it was operated manually.

The modulated 670nm diode laser was also used instead of the white light source. This produced a square wave output with a frequency range from 5-20000 Hz. A reference beam is produced which was fed directly into the lock-in amplifier and an oscilloscope (Hitachi VC-6024) was used to measure its frequency.

Chapter 5:- Results

5.1 Introduction

The idea of bilayer cells was proposed in the 1970's with several different materials suggested. In 1986, Tang[29] suggested a cell based on the combination between a perylene tetracarboxylic acid derivative and copper phthalocyanine. Since then there has been considerable work on related systems, though there has been very few suggestions of new combinations of potential pairs. To this end, many different materials were tried (mostly as potential partners for a phthalocyanine). All the systems tried used ITO conducting glass and gold as the electrodes with the phthalocyanine contacting the gold electrode because it has been shown that they form a neutral contact[104]. ITO is also an ideal electrode because of its high transmissivity to visible light. Even most so called semi-transparent metal electrodes cut out around 90% of the incident light so dramatically reducing the conversion efficiency.

When quoting conversion efficiencies for devices, different authors make corrections for factors such as light absorbed by the first electrode/layer and the amount of light that passes through the device. All the values quoted in this chapter for conversion efficiencies make no allowance for light absorbed by the electrodes or the first layer as they are calculated by measuring the energy produced by the device compared with the energy of the incident light. A blank glass slide was coated with a 300Å gold film to see its transmissivity and it was found that the film cut out 90% of white light shone on the sample whereas ITO coated glass cuts out only 15% of white light. This means that 85% of the light will get to the organic layers through ITO coated glass compared to 10% for the gold electrode so this must be remembered when considering the relative performance of the device.

It was noted that the performance of the samples left in air improved over the first few days. This maturing of the sample has been noted by several authors. The 'wine cellar effect' has been studied extensively by Whitlock et al[31] for the MPCI/ AlPcCl system. They attribute this to the formation of a simple crystalline hydrate $AlClPc.2H_2O$ which has an improved photovoltaic response. Detailed studies into the nature of the doping and attempts to optimise the conditions haven't been tried but all the samples studied were exposed to air for 2 days before being tested.

5.2 ITO - MPCI - TiOPc - Au

The first system studied was using dimethyl perylenetetracarboxylic acid diimide (MPCI) and titanyl phthalocyanine (TiOPc). These cells were made with a 1100Å MPCI layer and a 1000Å TiOPc layer. The layers were quite thick due to fabrication problems with the top gold electrode contacting the ITO electrode. This problem was later alleviated by depositing the gold electrode in short bursts as described in the experimental section. For this device, the TiOPc acted as the p- type semiconductor. Measurements were made using white light and a 2.5mW laser (λ=670nm).

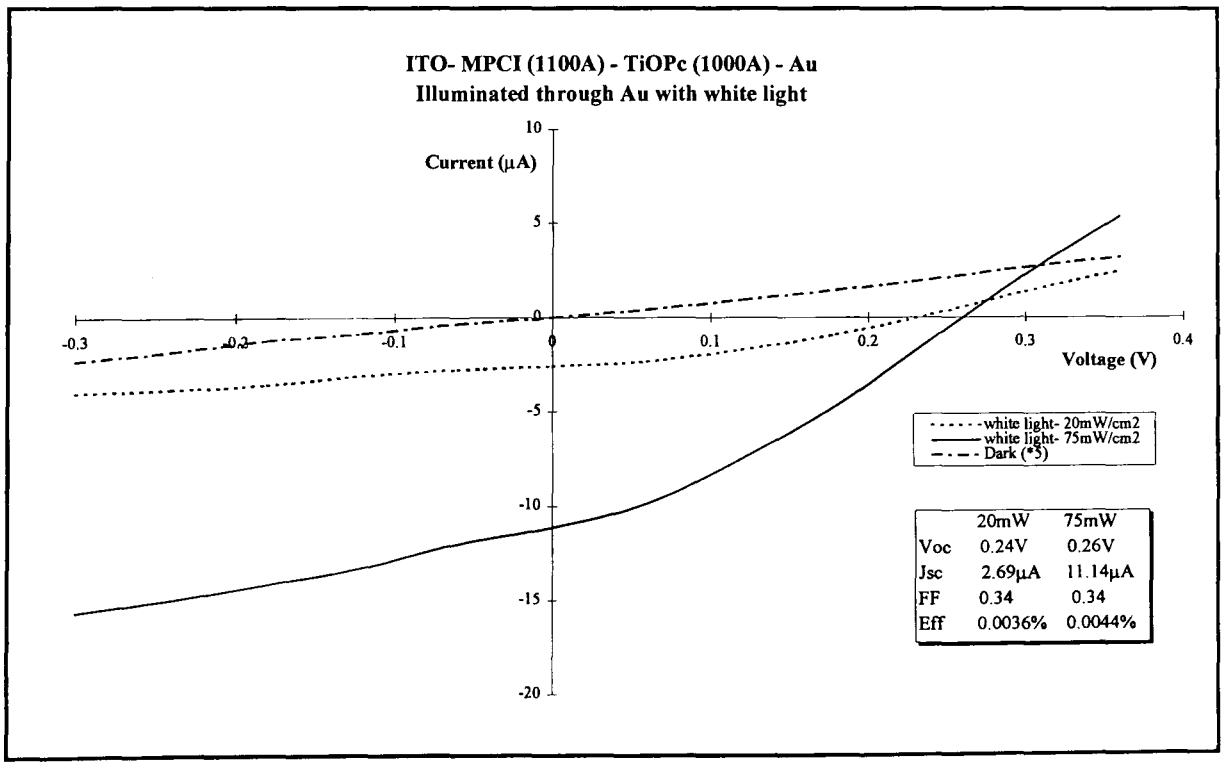

Fig 5.1:- I-V plot of ITO- MPCI- TiOPc-Au illuminated through Au

The current- voltage plot for a typical ITO-MPCI (1100Å)- TiOPc (1000Å)-Au cell is shown in figure 5.1. The plot shows little rectification in the dark though under illumination decent fill factors are found. The low efficiency values are partly due to the layers being quite thick so increasing the series resistance of the cell.

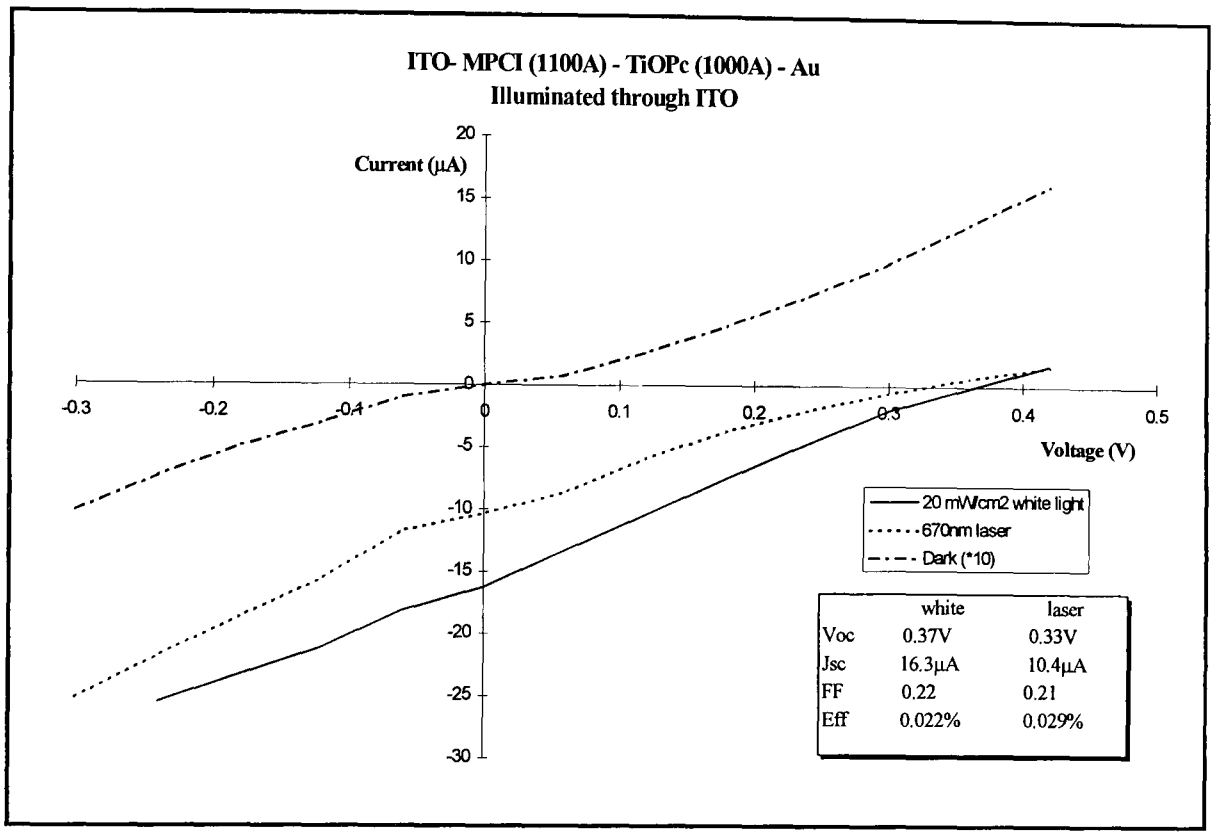

Fig 5.2 I-V plot for ITO- MPCI- TiOPc- Au illuminated through ITO.

The I-V plot for this cell illuminated through ITO is shown in figure 5.2. The values for J_{sc}, V_{oc} and the efficiency are greater than when the sample is illuminated through Au. The larger values for J_{sc} are due to the better transmissivity of ITO compared to the semi-transparent gold electrode. The increase in J_{sc} results in a larger value for V_{oc} as V_{oc} is directly proportional to $\log(J_{sc})$, though this isn't enough to explain the difference in V_{oc} when reversing the direction of illumination. The gradient of the dark I-V plot indicates that the series resistance of the device is large. This could be because the quality of the films or metal-semiconductor contacts are poor. The fill factors are significantly greater when illuminated through Au though this again could be attributed to the lower light intensity or to the MPCI film being of a better quality. The efficiency of the device is greater when measured using the

670nm laser because this wavelength coincides with high absorption by the TiOPc layer. As mentioned previously, the efficiency decreases with increasing incident light intensity. The laser has a narrow beam width ($8.0mm^2$) making the intensity of the beam $31mW/cm^2$. Thus the increase in the efficiency of the device when using the laser was due to the increased absorption of the TiOPc layer rather than the reduced light intensity.

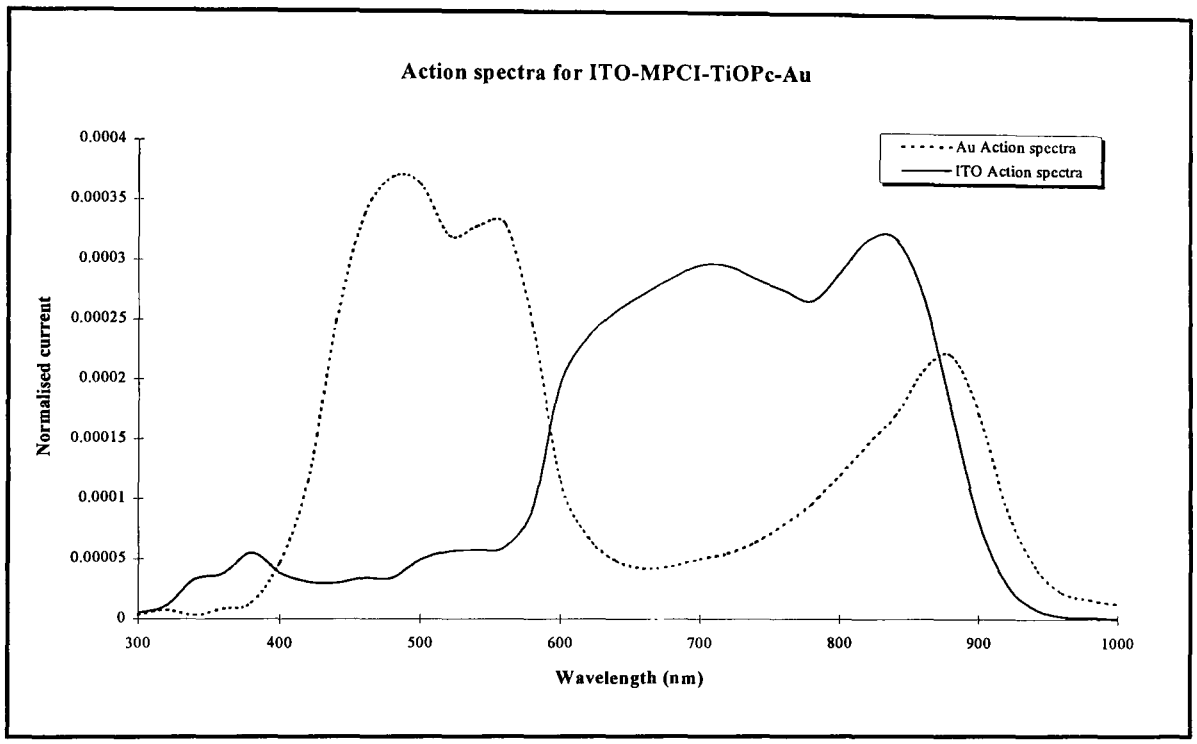

Fig 5.3:- Short circuit current wavelength dependence.

The wavelength dependence of the short circuit current is shown in figure 5.3. The action spectra of the short circuit current largely follows the absorption spectra of the second layer showing that only light which is absorbed at the interface of the 2 layers contributes to the measured photocurrent. Whilst the short circuit current has been plotted, a graph of photovoltage against wavelength has a similar form. In both spectra, there is an extra peak at around 810nm and this could correspond to light being absorbed by the phthalocyanine layer if it was in its alpha- form[39]. The action spectra shows little response in the 300nm- 400nm region because the output of the monochromator is very low at these wavelengths. The two absorption spectra make a good complementary pair as their absorption peaks cover the visible

spectrum, though the action spectra show that the cell only performs well at some wavelengths.

The kinetics of the sample were measured using white light of a low intensity to minimise any heating effects which would cause a change in the current. The data showed a good fit when fitted using the Ryvkin first order equation showing that the response of the sample is first order. Response times of 5.8ms and 4.1ms were obtained when the sample was illuminated through Au and ITO respectively. The sample had relatively slow response time which indicates a high trap density. This would cause a reduction in the exciton diffusion length and the mobility of the charge carriers which would in turn have an effect on the short circuit current. A high trap density could also reduce the open circuit voltage as generated charge carriers that have been separated by the junction which are subsequently trapped will create mirror potentials that oppose the junction. The response when illuminated through both ITO and Au is shown in Fig 5.4 with the proposed first order fit.

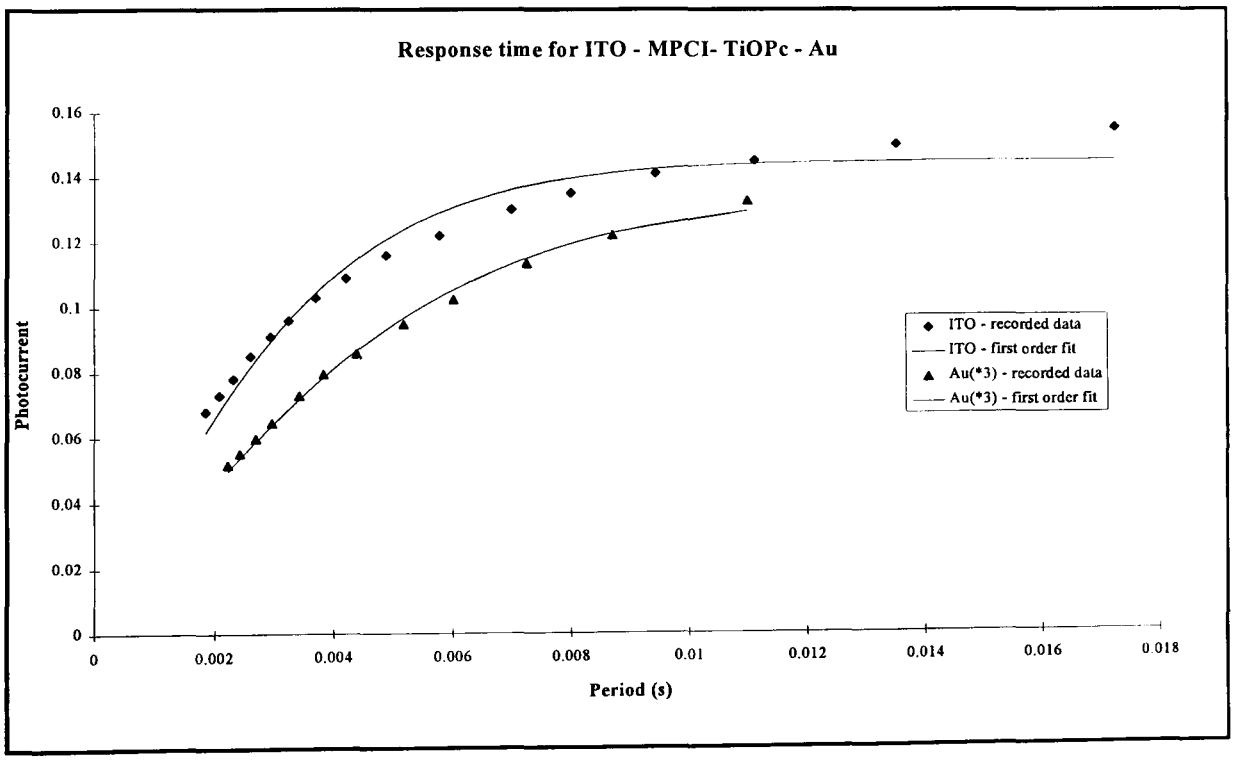

Fig 5.4 :- Response of photocurrent to chopped light of different frequencies.

5.3 ITO- MOPPCI - TiOPc -Au

These cells were made using 500Å layers of MOPPCI and TiOPc (sublimed once). Again, the TiOPc layer acted as the p-type semiconductor with the MOPPCI acting as the n-type semiconductor. Gold and ITO were used as the electrodes because they form neutral contacts with phthalocyanines and perylene tetracarboxylic acids respectively[37]. The area of the sample was 0.2 cm^2.

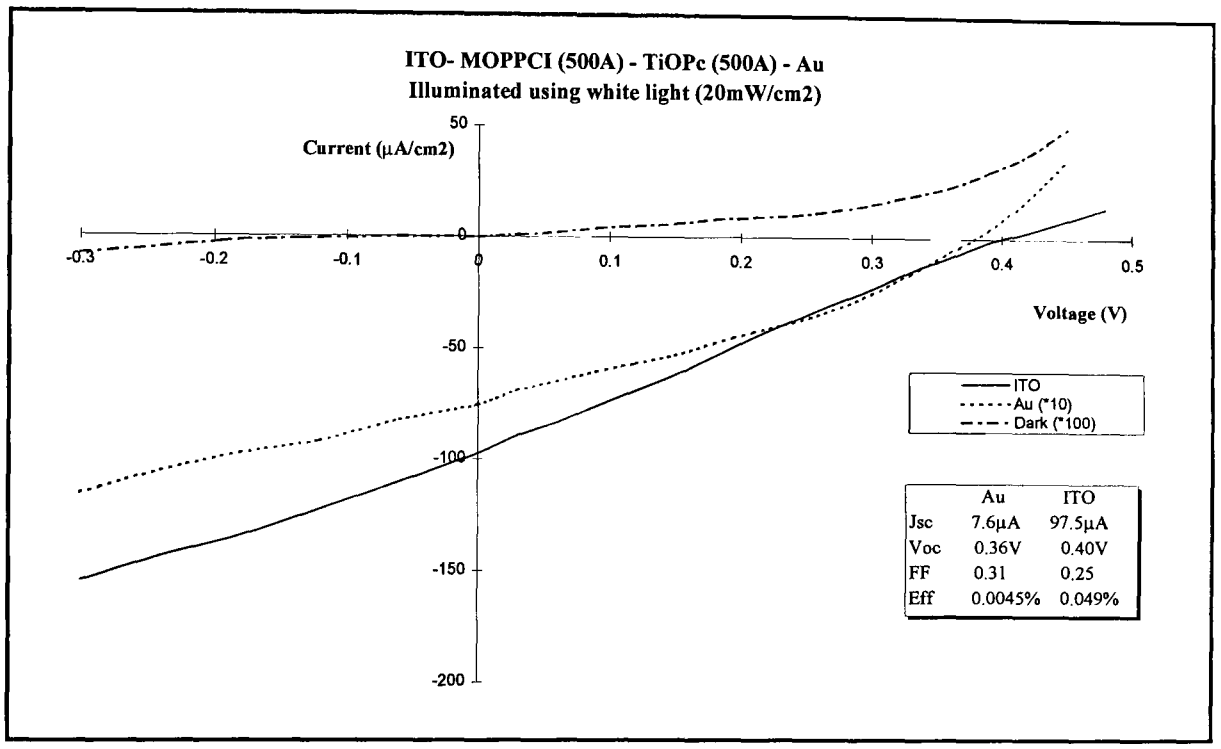

Fig 5.5 I-V plot for ITO-MOPPCI (500Å) - TiOPc (500Å) - Au

Again the I-V plot for this system (see Fig 5.5) shows that the sample is more efficient when illuminated through ITO than the gold electrode due to larger values for the short circuit current despite finding lower values for the Fill Factor. The efficiency values are better than for the MPCI - TiOPc partly due to the layers being under half as thick, so reducing the series resistance. The open circuit voltage is also slightly larger than for MPCI-TiOPc but again the fill factor is greater when illuminated through Au. The efficiency of the sample was measured through ITO using a 670nm, 2.5mW laser and found to be 0.074% which is greater than the value using white light because TiOPc absorbs strongly at this wavelength. Changing the perylene tetracarboxylic acid derivative had very little effect on the open circuit voltage which

remained at around 0.30V-0.40V. The value for V_{oc} is typical to that measured for similar systems though lower than that required for practical device applications.

The action spectra of the cell (see fig 5.6) shows that the active area is the interface between the two layers with the large peak around 700nm corresponding to the TiOPc and the one at 500nm to the MOPPCI. However, as the layers are thinner than those used for the MPCI-TiOPc sample (Fig 5.3), the action spectra do not exclusively follow the absorption spectrum of the second layer. This is because the first layer is thinner which allows some of the light which was totally absorbed by the thicker layer to reach the junction and contribute to the photocurrent. Hence, there is a small peak at 720nm when the sample was illuminated through the Au electrode in addition to the peak at 500nm corresponding to the MOPPCI layer. Tsuzuki et al[33] using MPCI and TiOPc have produced a cell whose action spectra is similar when illuminated from either direction which indicates that the cell has a very large depletion layer. It is also interesting to note that the shape of the TiOPc peak is different from the MPCI/TiOPc cell. In this case, the TiOPc layer is probably largely amorphous.

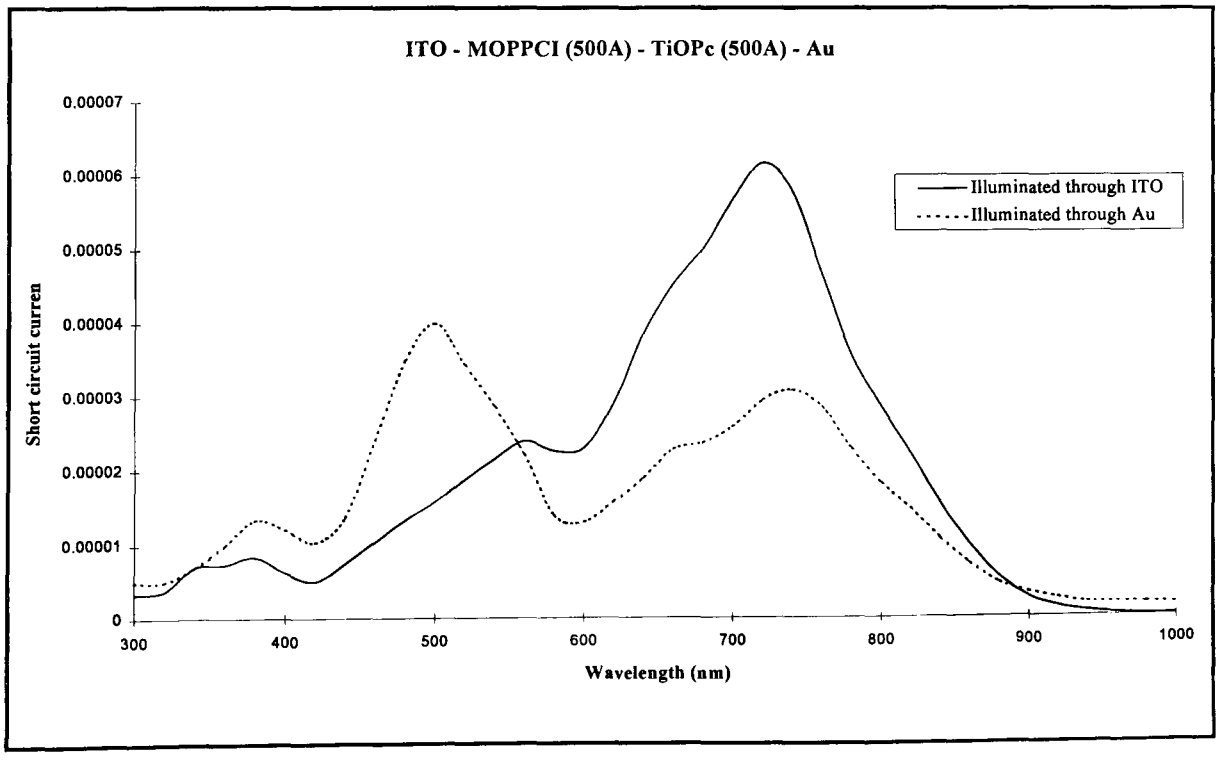

Fig 5.6: Action spectra for ITO - MOPPCI (500Å) - TiOPc (500Å) - Au

5.3.1 Annealing the sample

The sample was annealed by heating it in an oven for 16 hours at a temperature of 75°C. Repeating the I-V plot showed that the performance of the sample had improved (see fig 5.7)

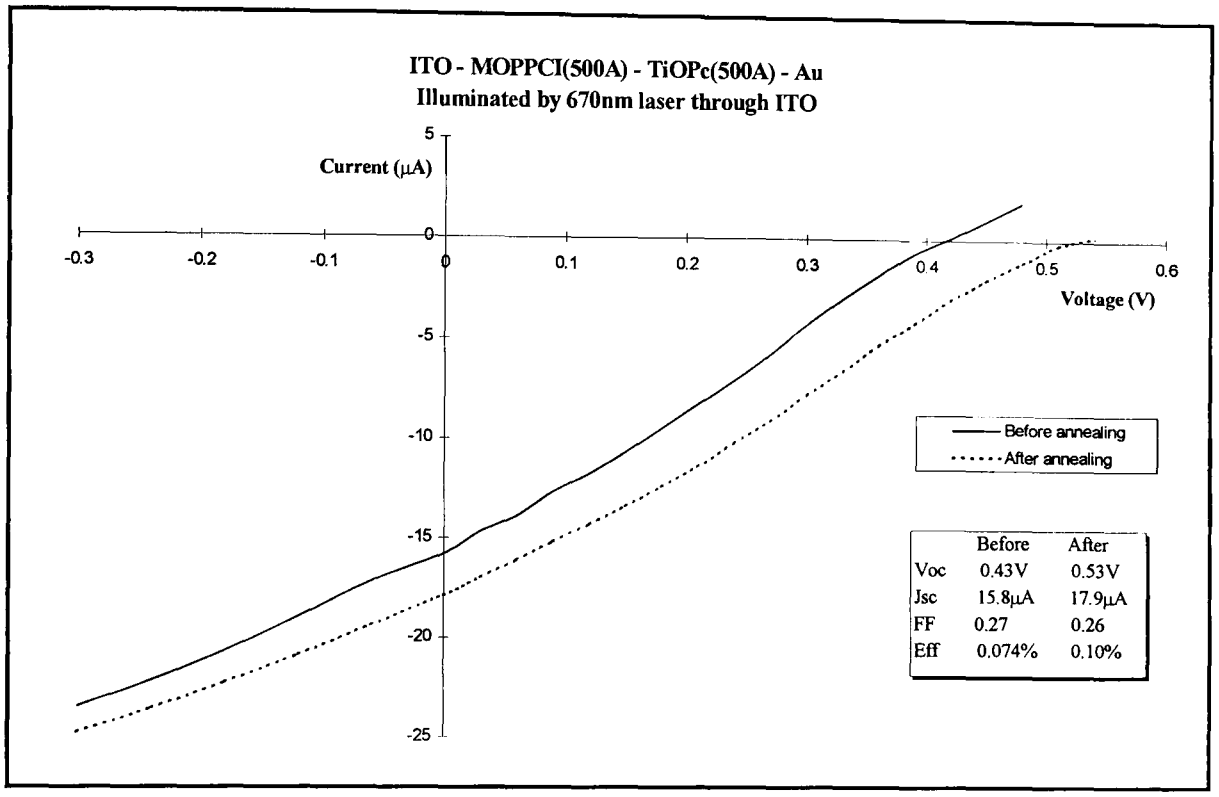

Fig 5.7:- Effect of annealing on ITO - MOPPCI - TiOPc - Au

After the sample was annealed, the open circuit voltage and the short circuit current increased, though the fill factor remained unchanged. This caused the efficiency of the sample to improve by over 30%. As the gradient of the I-V plot didn't change, the resistance of the sample must have remained constant. There was a change in the action spectra (see fig 5.8).

The change in the action spectra indicates a change in the morphology of the TiOPc layer. As mentioned above, the TiOPc layer before annealing was probably largely amorphous. After annealing, a shoulder appears on the phthalocyanine peak at around 850nm. In the MPCI/TiOPc system, this peak is larger than the peak at 700nm (see Fig 5.3) and was attributed to the TiOPc layer being in the α- form. It appears that annealing the sample causes the previously amorphous TiOPc layer to partially convert into the α- form. As the

α- form of TiOPc is more photosensitive than an amorphous film, this would explain the increase in J_{sc}. Also, as the value of the FF is small (about 0.25), this increase in J_{sc} could contribute to the increase in V_{oc}.

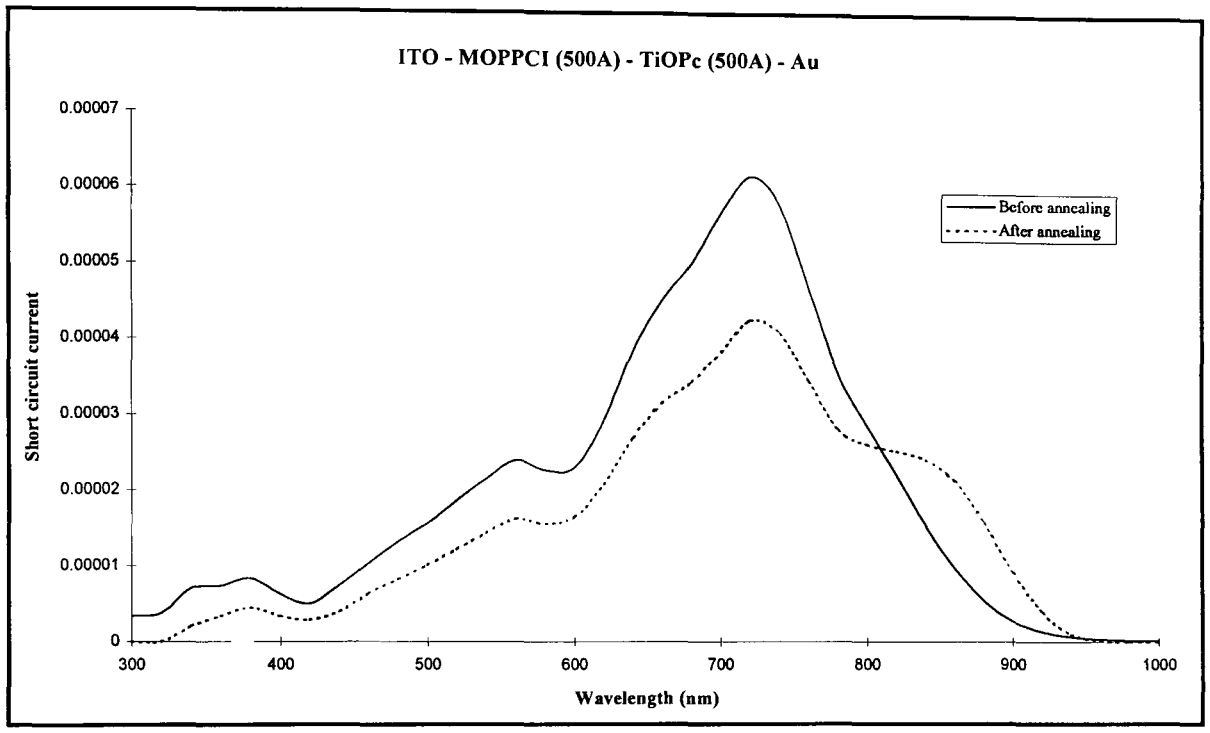

Fig 5.8: Showing the effect of annealing the sample on the action spectra of the short circuit current when illuminated through ITO.

The speed of response of the sample was measured before and after annealing for the TiOPc layer using the 670nm laser (i.e. the sample was illuminated through the ITO glass). The response of the sample was very fast (τ=0.33 ms) and this was largely unchanged after annealing (τ=0.39ms).

An attempt was made to anneal the sample at 105°C for 16 hours but this caused the resistance of the sample to drop by a factor of 100 and considerably reduce the open circuit voltage.

5.4 ITO - DBA - TiOPc - Au

Dibromoanthanthrone (DBA) is known to be a good photoconductor and because it peaks at 430nm in its absorption spectrum, it was investigated as a possible partner for TiOPc. The same electrodes were used because of the high

transmissivity for light of ITO and gold forms a neutral contact with TiOPc. The sample area was $0.2cm^2$.

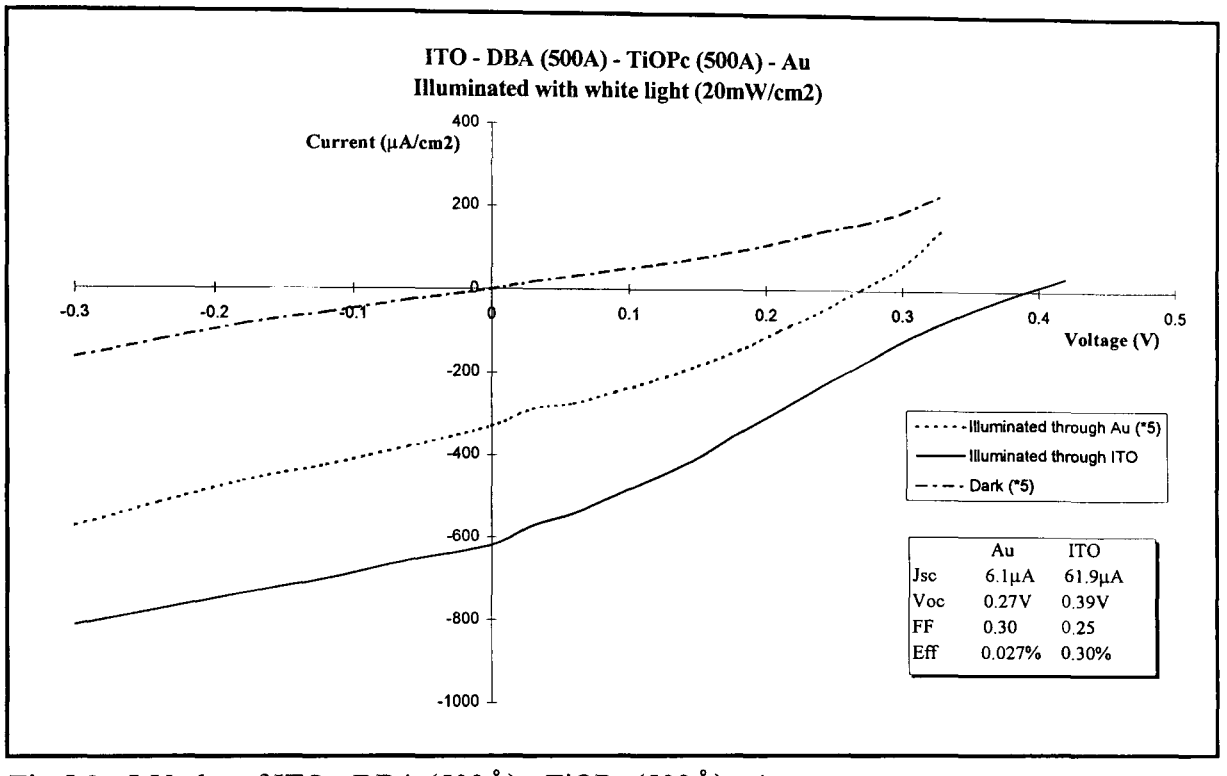

Fig 5.9:- I-V plot of ITO - DBA (500Å) - TiOPc (500Å) - Au

In the device, the DBA layer acted as the n-type layer with the TiOPc as the p-type layer. The performance of the cell is shown in fig 5.9. The efficiency of the device was a factor of 10 greater when illuminated through the ITO glass partly because of its greater transmissivity compared to gold and also because of the low absorption of the DBA layer. Increasing the thickness of the DBA layer didn't improve the performance because this increased the series resistance of the cell negating the increase in carriers generated by the DBA layer. Again, the open circuit voltage is considerably lower when illuminated through the gold electrode and this is still due to the low light intensity being transmitted by the semi-transparent gold electrode. The efficiency of this system compares well with other reported phthalocyanine systems (i.e. MPCI/TiOPc is 0.35% efficient for incident white light[33]).

The action spectra of the cell is shown in Fig 5.10. The peaks at 700nm when illuminated through ITO and 500nm when illuminated through gold show that the action spectra follows the absorption spectra of the second layer which

agrees with the junction being at the interface of the two layers. The TiOPc absorption band shows an extra peak at around 810 nm which would indicate that the TiOPc layer is in the α- form rather than being an amorphous film as seen with MOPPCI previously. The action spectra does show that when illuminated through ITO that the cell will only respond to light of a wavelength between 600-900nm which reduces the overall conversion efficiency when white light is used as half the visible spectrum does not contribute to the overall photocurrent.

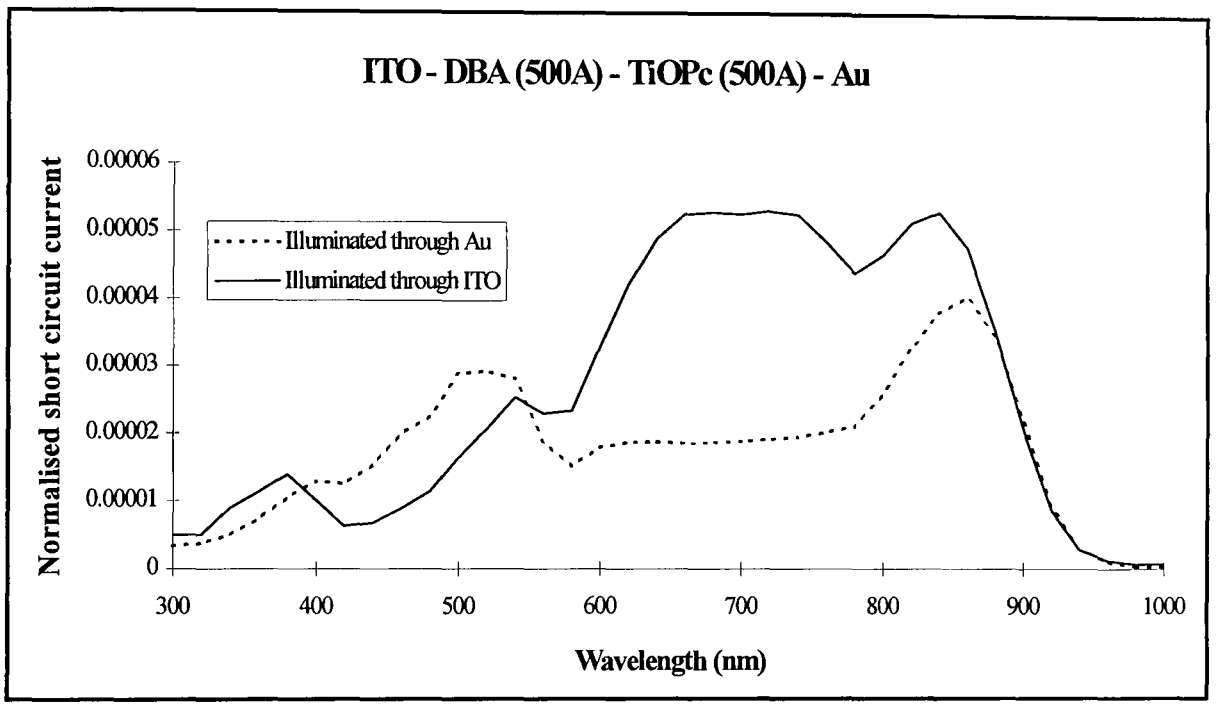

Fig 5.10:- Action spectra for ITO - DBA (500Å) - TiOPc (500Å) - Au.

5.4.1 Performance of the samples with time

A sample was left exposed to air and its performance was measured at different times (see Fig 5.11). The optimum performance came after 2 days and then there was a steady decrease until after 14 days the efficiency had dropped by a third. Devices made from MPCI/ ZnPc have been studied before by Wohrle et al[37] and they found that the short circuit current of samples that were left under constant illumination (35mW/cm^2) for 10 days decreased to half the initial value, with those kept in the dark hardly decaying at all. The MPCI/ TiOPc and MOPPCI/ TiOPc systems mentioned previously showed no sign of decaying after they had matured. This means that it could be the DBA

layer that is crystallising resulting in a poor contact with the ITO electrode. Despite the sample being left in air, it is unlikely that the initial increase in open circuit voltage and fill factor is a result of doping from oxygen or water vapour. Whilst this would cause a shift in the Fermi level in one of the layers so changing V_{oc}, the improvement in performance occurred over days whereas a doping effect would be expected to happen more rapidly. Deliberate doping of a cell made from MPCI/ H_2Pc with H_2 and NH_3 has been shown to improve the performance of the device so accidental doping that occurs in air will also have an effect on performance.

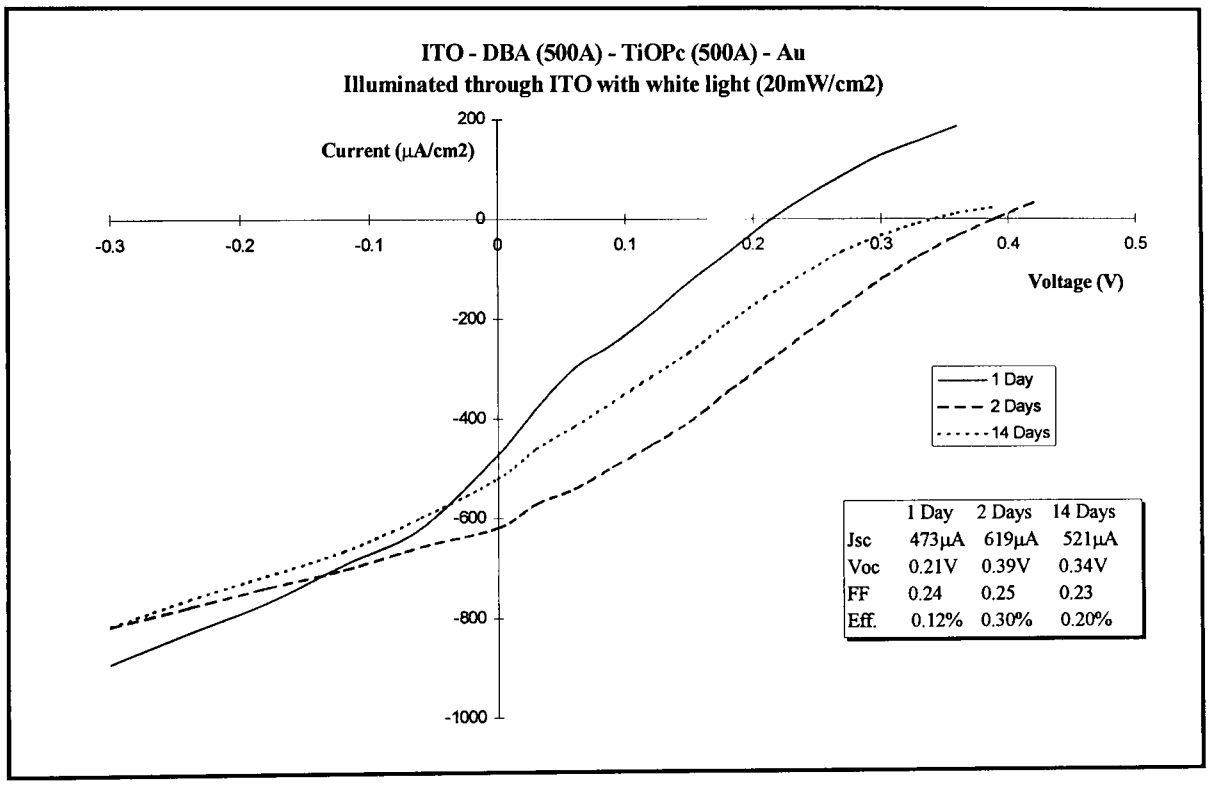

Fig 5.11:- Variation of performance of ITO - DBA (500Å) - TiOPc (500Å) -Au with time.

The speed of response of the sample did not change over time (see fig 5.12) and the response time is very fast (τ = 0.20ms after 2 days and τ = 0.21ms after 14 days). This would indicate that there is not a morphological change in the TiOPc layer over time. However, the fast response of the TiOPc layer indicates that the sample has a low trap density which correlates with the high efficiency of the device.

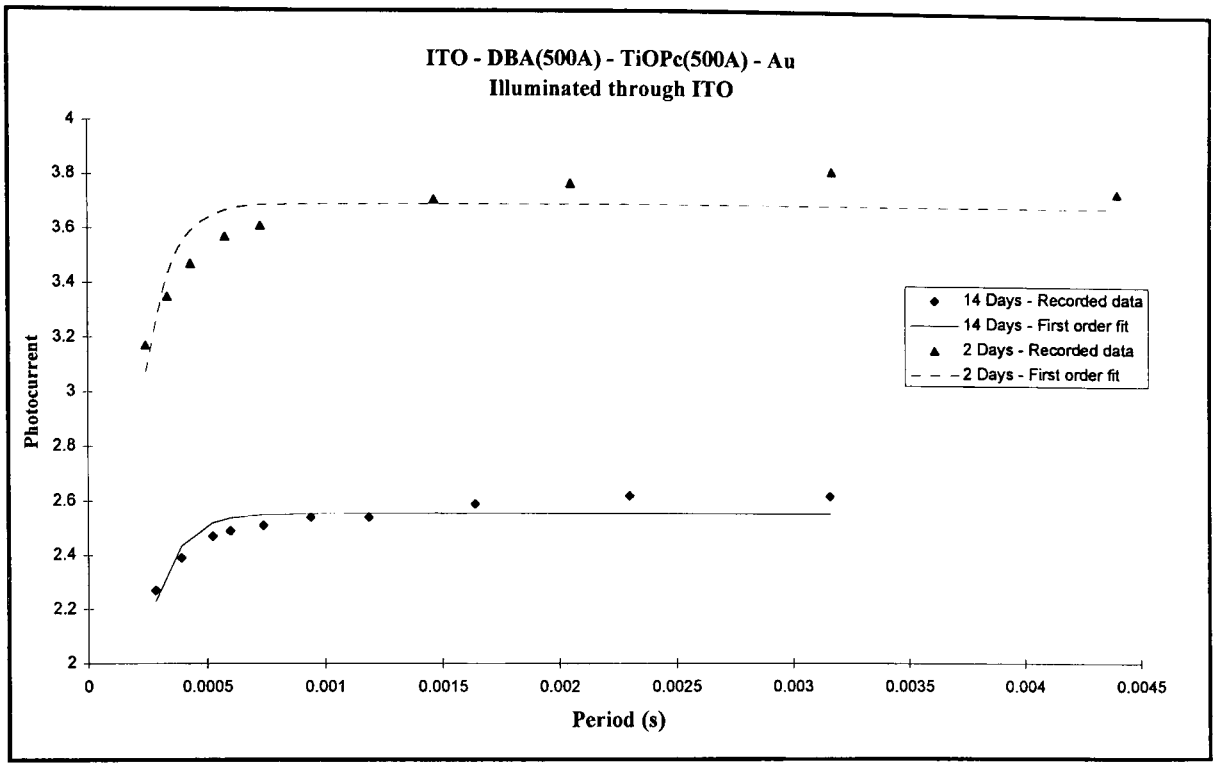

Fig 5.12:- Variation of response time of ITO - DBA (500Å) - TiOPc (500Å) -Au with time.

5.5 Proposed model for TiOPc heterojunctions

From the dark I-V plots which are symmetric (i.e. when partnered with MPCI and DBA), therefore showing no rectification, it is unlikely that there is a large built-in voltage at the junction. This would occur if the Fermi levels of the two materials are similar. There is, however, a large photoresponse so there must be a barrier to separate the photogenerated charge carriers. This can be explained if there is a barrier at the junction in the conduction and valence bands. If the barriers are of different sizes then this could be used to explain the difference in the size of the open circuit voltage when illuminated from different directions. It is however impossible to make too much comment on the height of any barriers from the measurements made because V_{oc} varies with light intensity and R_{sh}. It is also reduced if mirror charges are generated from separated charges which are not efficiently removed from the junction. The junction produces a photocurrent when illuminated because light absorbed near the interface creates an electron/hole pair. If the phthalocyanine layer absorbs the light, the electron in the conduction band may randomly diffuse to the interface and be separated when they 'fall' over the barrier. This is akin to

the p-n junction in equilibrium situation where J_{np} (made up from electrons with enough thermal energy to surmount the barrier) equals J_{pn} (electrons that diffuse to the barrier/junction). When illuminated through the ITO layer, light is absorbed at the interface by the phthalocyanine molecule generating an electron/hole pair. The extra electrons in the conduction band mean that there is a greater probability of electrons diffusing to the interface and thereby being separated by the barrier so increasing J_{pn}. J_{np} is unchanged so causing the net flow of electrons from the phthalocyanine to the perylene tetracarboxylic acid. The equivalent case is with light absorbed by the perylene layer where holes are formed in the valence band that diffuse to the barrier and are separated. The diagram for the proposed junction is shown in fig 5.13

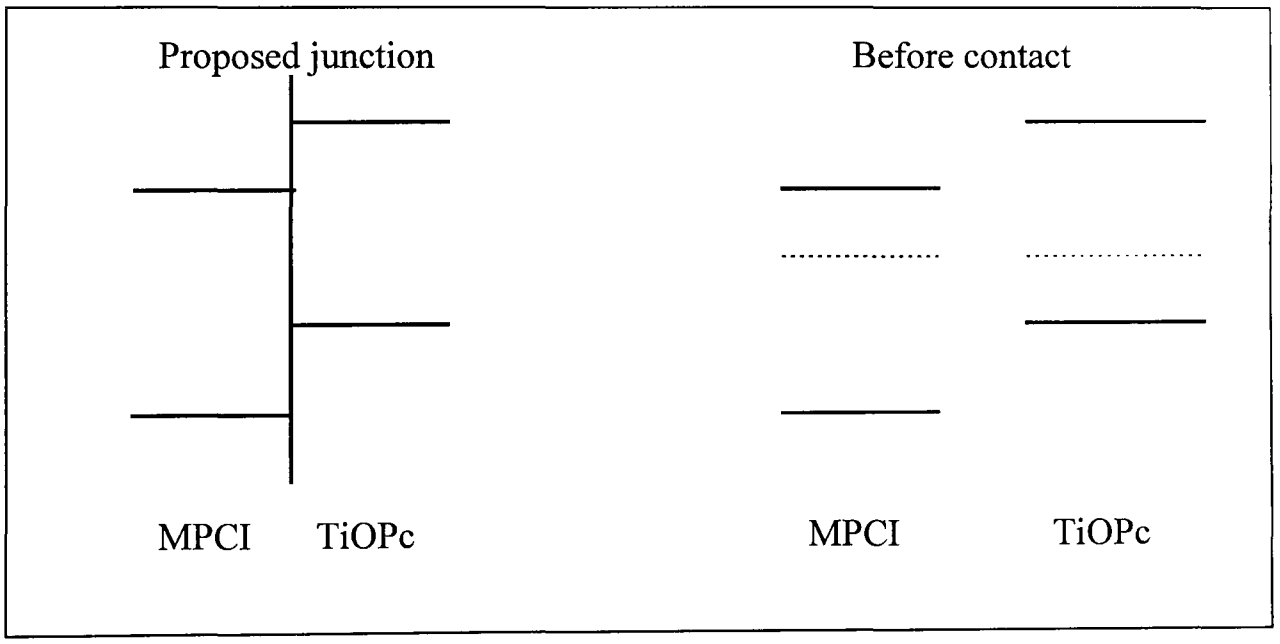

Fig 5.13: Diagram of proposed junction for our MPCI / TiOPc heterojunctions.

A similar situation arises with the DBA/TiOPc interface as the characteristics of the cell are similar. The cell is more efficient than the MPCI/TiOPc cell because R_s is over 100 times smaller (from the gradient of the dark I-V plot).

Proposed model for MOPPCI/TiOPc junction

The characteristics of a cell fabricated with MOPPCI and TiOPc is similar to those of a MPCI/TiOPc cell apart from the dark I-V plot shows rectification. This implies that there is a built-in voltage due to the difference in Fermi levels of the two materials. This is the case if the position of the HOMO and LUMO bands are different for MOPPCI or if it is more extrinsic. There is a similar mechanism for the generation of the photocurrent, though it is more efficient in this case because there is an internal field at the interface to separate the charges rather than relying on the charge carriers diffusing to the interface. This would explain why this device is more efficient than the MPCI/TiOPc junction fabricated. Again a disparity in the size of the conduction and valence band discontinuities could be used to explain the different values of V_{oc} found when illuminating through Au and ITO.

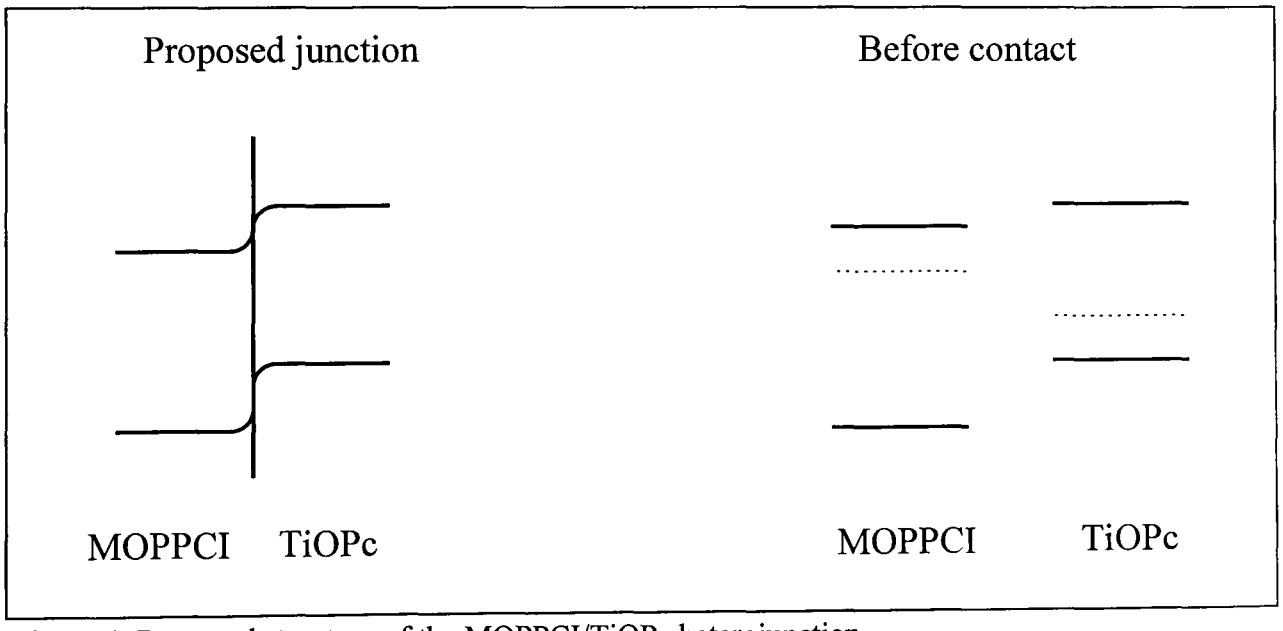

Fig 5.14: Proposed structure of the MOPPCI/TiOPc heterojunction.

5.6 Cells fabricated with Sq5 and DBA

Cells were prepared using a squaraine (Sq5) and dibromoanthanthrone (DBA), again using ITO and gold as the two electrodes. These were chosen because of their availability and because both materials have been noted to be good photoconductors. As well as this, successful devices have been made using

squaraines as layers in Schottky barrier systems[22]. It was also of interest to see the effect non-complementary absorption spectra have on the photovoltaic properties of a junction.

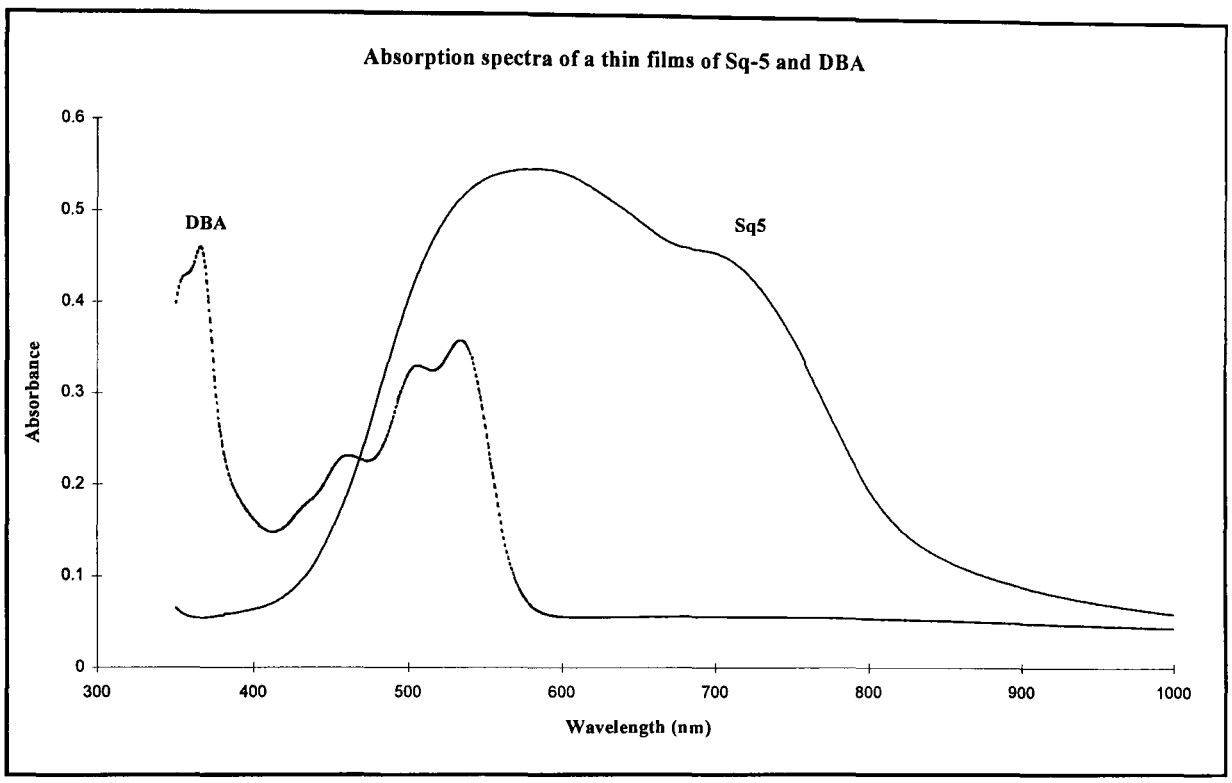

Fig 5.15: The absorption spectra of thin films (500Å) of DBA and Sq5.

The major absorption peak of DBA at ~530nm coincides with a broad absorption of the squaraine. This will cause light of this wavelength to be absorbed by the first layer so preventing it reaching the second layer and the resulting exciton being split at the junction. It is also important to note the Sq5 film has a higher extinction coefficient than the DBA film.

5.6.1 ITO - Sq5 - DBA - Au

In the above system, the Sq5 layer acts as the p-type semiconductor with the DBA as the n-type semiconductor, i.e. the ITO acts as the positive junction and the Au as the negative junction. This is the opposite polarity to the cells made with DBA or MOPPCI and TiOPc reported previously. However, this does mean that the DBA layer acts as the n-type layer which is as expected from the literature, previous cells and the position of the HOMO. Looking at

the action spectra for the system (see fig 5.17), it is clear that the samples response does not match the absorption spectra of the second layer. When the sample is illuminated through the ITO electrode, there are large peaks at 550nm and around 700nm. The response below 500nm is due to the DBA layer with the peak at 550nm made up from contributions from both layers. The peak at 700nm must be due to the Sq5 layer so it is a result of either a blocking contact between it and the ITO electrode or the excitons in the Sq5 layer being mobile. However, if a blocking contact was formed between the ITO and a p-type material, then this would cause holes to travel in the direction of contact to semiconductor, making the ITO go negative. The opposite is found so this is an impossible scenario. It is common for cells to show some contribution from the front layer (see fig 5.10) indicating that excitons can diffuse to the interface making a smaller, yet significant, contribution to the performance of the cell. When the sample is illuminated through the Au electrode, there is a stronger response at 540nm than at 700nm. This indicates that there is a greater photogeneration efficiency from the transition that gives rise to the peak around 540nm than at 700nm.

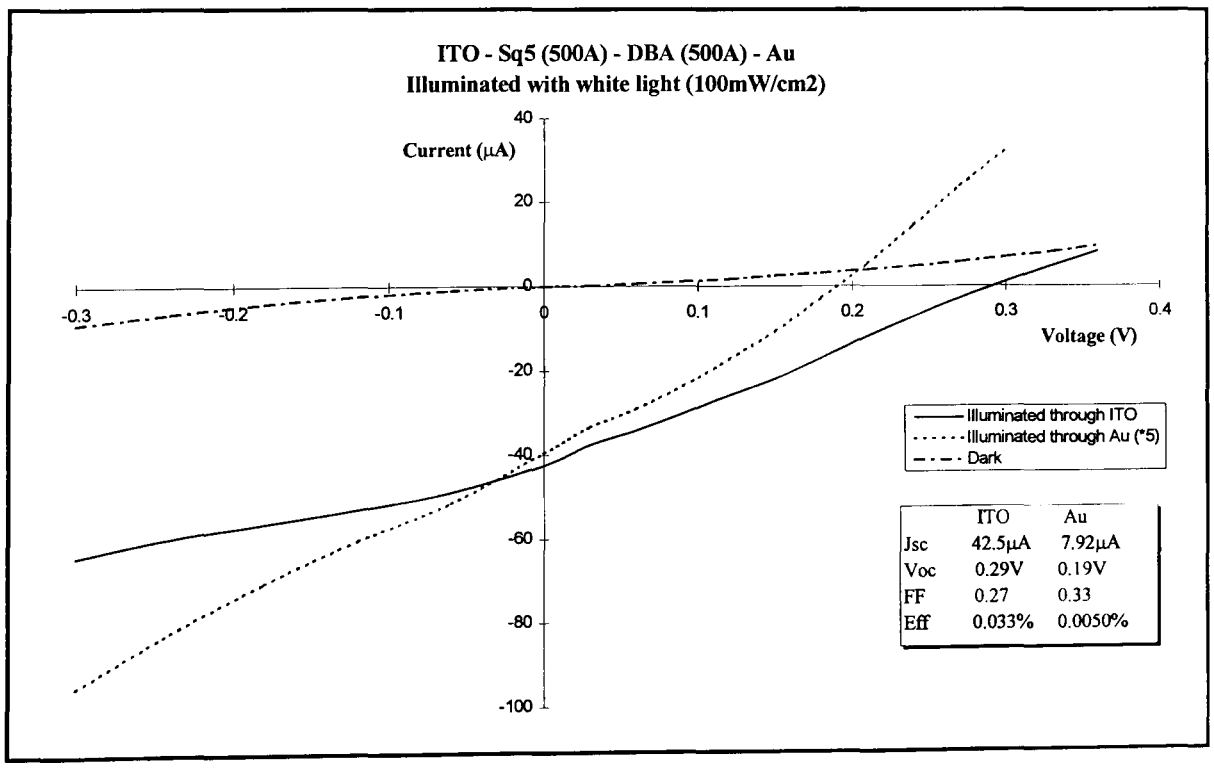

Fig 5.16: I-V plot for ITO - Sq5 (500Å) - DBA (500Å) -Au

The system performs well with similar efficiencies when illuminated from either direction once an allowance for the absorption of the semi-transparent gold electrode has been made. The rectification is better but the open circuit voltage is lower when illuminated through the gold electrode, but again, this is probably due to the lower intensity of light reaching the organic layers.

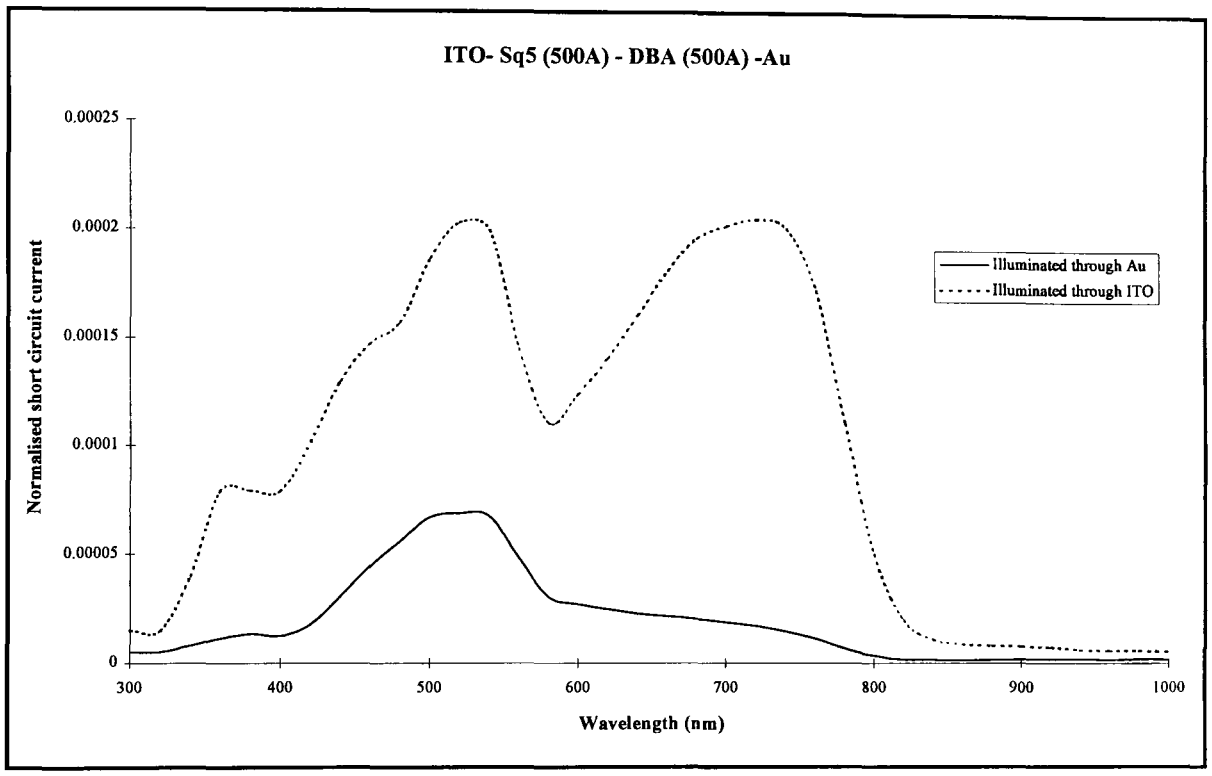

Fig 5.17:- Action spectra for ITO - Sq5 (500Å) - DBA (500Å) - Au

An analysis of the response times for the sample was completed and found to be $\tau = 0.32$ms when illuminated through ITO and $\tau = 1.1$ms when illuminated through Au. Both values were obtained using the $\lambda = 670$nm diode laser as the illumination source. Although this does not correspond to a wavelength of good response in the action spectrum when illuminated through the gold electrode, similar results are obtained using a white light source ($\tau = 1.4$ms). One possible explanation is that DBA responds more slowly than Sq5.

5.6.2 ITO-DBA-Sq5-Au

When the sample was reversed (ITO - DBA - Sq5 - Au), the polarity of the cell was also reversed with the ITO going negative and the gold electrode positive. This again means that the DBA was acting as the n-type layer and the Sq5 was the p-type layer. As the workfunction of ITO is less than Au, it is expected that this will cause an increase in the efficiency of the device. However, the performance of the cell was poor (see fig 5.18) with a low fill factor and open circuit voltage. The magnitude of the photovoltage when illuminated through Au was too small to report.

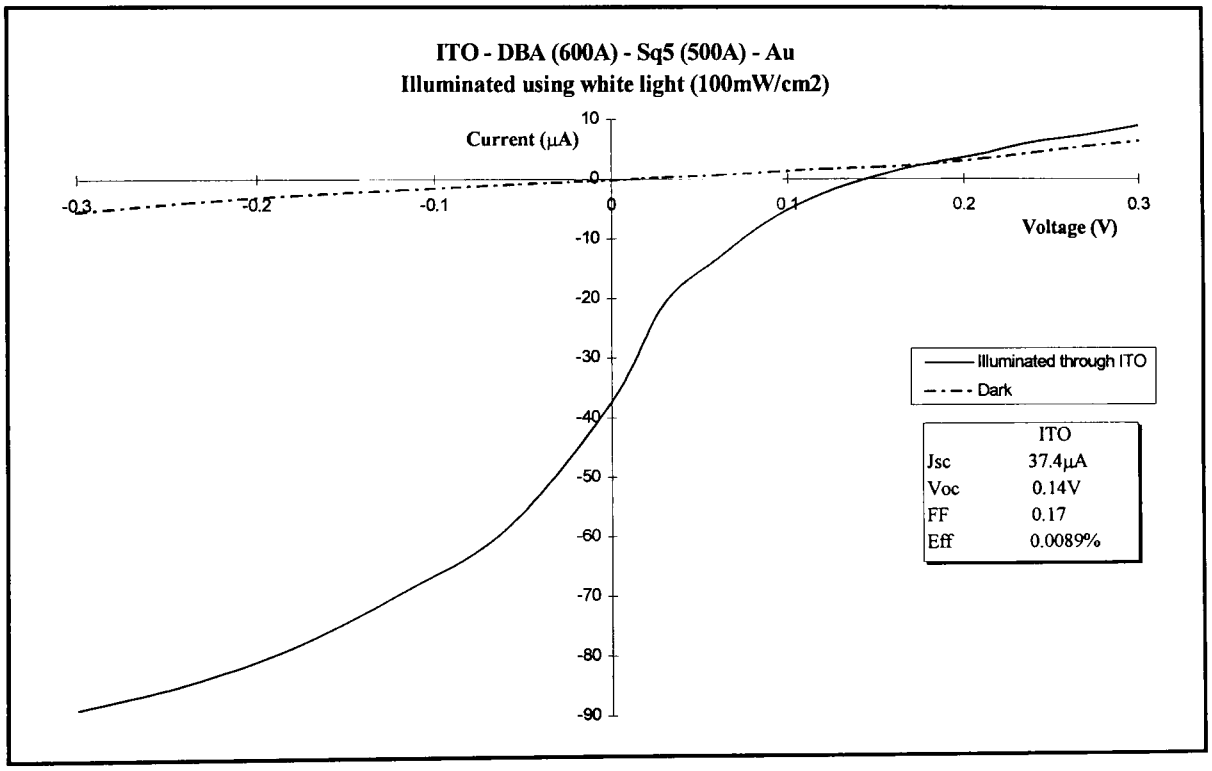

Fig 5.18: I-V plot for ITO - DBA(600Å) - Sq5(500Å) - Au.

From the I-V plot, it is clear that there is a barrier impeding current flow because of the poor rectification shown by the fill factor. The shape of the graph is also indicative of a poor contact. It is not expected to be between the ITO and DBA layer as the device made from ITO-DBA-TiOPc-Au performed well. As the squaraine behaves as a p- type semiconductor, a barrier contact will form that will cause holes to flow from the contact to the semiconductor, making the Au electrode negative, which is acting against the polarity of the cell.

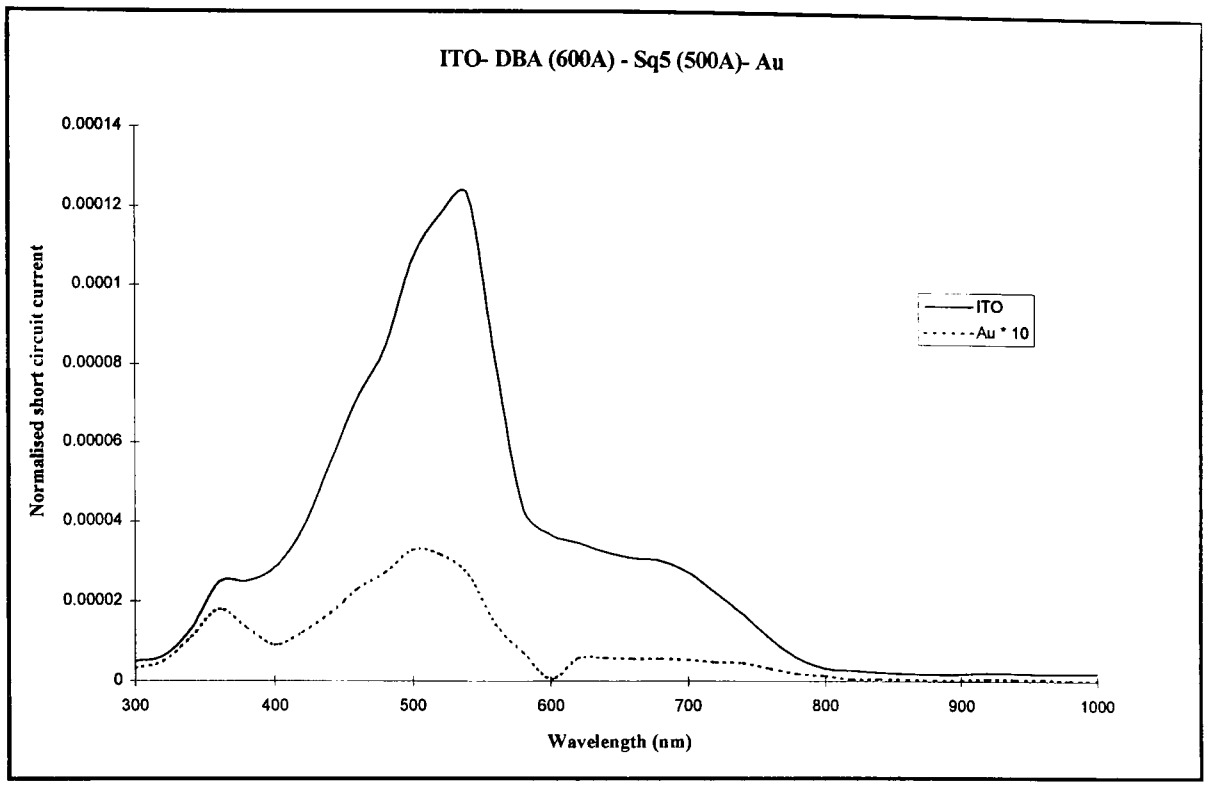

Fig 5.19: Action spectra of ITO - DBA (600Å) - Sq5 (500Å) - Au

The action spectra (see fig 5.19) when the sample is illuminated through ITO resembles the superposition of the 2 absorption spectra. This indicates that both the light that reaches the Sq5 layer and that which is absorbed by the DBA layer contributes, making the exciton mobile in the DBA layer. When the sample is illuminated through the Au electrode, the response follows that of the DBA layer but the signal is very small, partly because the amount light reaching the junction is small as the transmissivity of the Au electrode and Sq5 layer is low. The response time for the sample when illuminated through ITO was $\tau = 0.79$ms.

5.6.3 Proposed model for Sq5 and DBA cells

As expected, a rectifying junction is formed with the DBA layer acting as the n- type material and Sq5 the p-type. But the situation is complicated by the overlapping absorption spectra and electrode effects. As ITO has a lower workfunction than Au, it is expected that the better performance would come from the cell where the ITO contacts the DBA layer. But the results show that there is a barrier contact (probably between the Au electrode and Sq5) which hinders the flow of holes. Barrier contacts form between metals and p- type

semiconductors if the workfunction of the metal is above the Fermi level for the semiconductor. As the EH calculations show, squaraines have a high ionisation potential for p- type semiconductors which makes this scenario more likely. In both cells, there is a contribution from the front layer showing that the excitons were partially mobile. This system demonstrates the need for potential pairs to have complementary absorption spectra and that some attention has to be paid to the choice of electrodes.

5.7 Other materials tried

A number of alternative compounds were tried as alternative partners to TiOPc. These were C_{60}, BTDA, BTQBT and PBD. In each case, ITO glass and Au were the electrodes used with TiOPc contacting the Au electrode.

5.7.1 C_{60}

Previous work by Kinge[104] and others has shown that C_{60} behaves as an electron acceptor (or an n-type semiconductor) and that it is a very efficient photoconductor. The absorption spectra of C_{60} has a peak between 400 - 500nm making it complementary to TiOPc. Kinge tested this combination using a liquid contact as the top electrode and achieved an open circuit voltage of 0.3V with an efficiency of $4x10^{-3}$%. A cell was made to the design ITO - C_{60} (1200Å) - TiOPc (1100Å) - Au and it was found to have a very low open circuit voltage and efficiency (V_{oc} = 0.09V and Eff = $5.1x10^{-4}$% when illuminated through ITO with 20mW/cm^2 white light). The response time of the sample was also very slow (τ = 6.4ms when illuminated with white light through ITO). Yonehara and Pac[105] have recently reported work on an Al/C_{60}/TiOPc/ITO system with conversion efficiencies of 0.347% for 720nm light that was transmitted through the Al electrode. However, when white light of intensity 28.2mW/cm^2 was used, the efficiency dropped to 0.00231% which the authors relate to the degradation of the Al electrode. The above results indicate that a barrier contact is formed between C_{60} and Al which isn't formed

between ITO and C_{60}. This is backed up by the action spectra reported by Yonehara. It also indicates that a p-n junction is formed between C_{60} and TiOPc.

5.7.2 BTQBT

Due to the problem of the high series resistance of bilayer cells made from organic semiconductors, it was of interest to try any material with an unusually high conductivity. Yamashita et al synthesised BTQBT which absorbed light in the 500-650 nm region though there was no knowledge of its electrical properties. Cells were made where it was tried as a potential partner for TiOPc but these were unsuccessful due to the films of BTQBT crystallising, so breaking contact with the electrode and TiOPc layer. This problem wasn't solved.

5.7.3 PBD

Gregg[52] had reported success in producing a device made from TPD (a hole transport layer) and MePCI. This utilised a Dember type photovoltaic effect which produced a large open circuit voltage ($V_{oc} \approx 1.0V$). A similar system was attempted using PBD (known to be an electron transport layer[106]) and TiOPc but this was unsuccessful due to the PBD layer crystallising.

5.7.4 BTDA

Yamashita et al. synthesised BTDA. It absorbs in the 400nm region so was partnered with TiOPc. There was no previous knowledge of its electrical behaviour. The BTDA was sublimed once before use. The following cell was made ITO - BTDA (800Å) - TiOPc (500Å) - Au. The performance of the cell after one week is shown in fig 5.20.

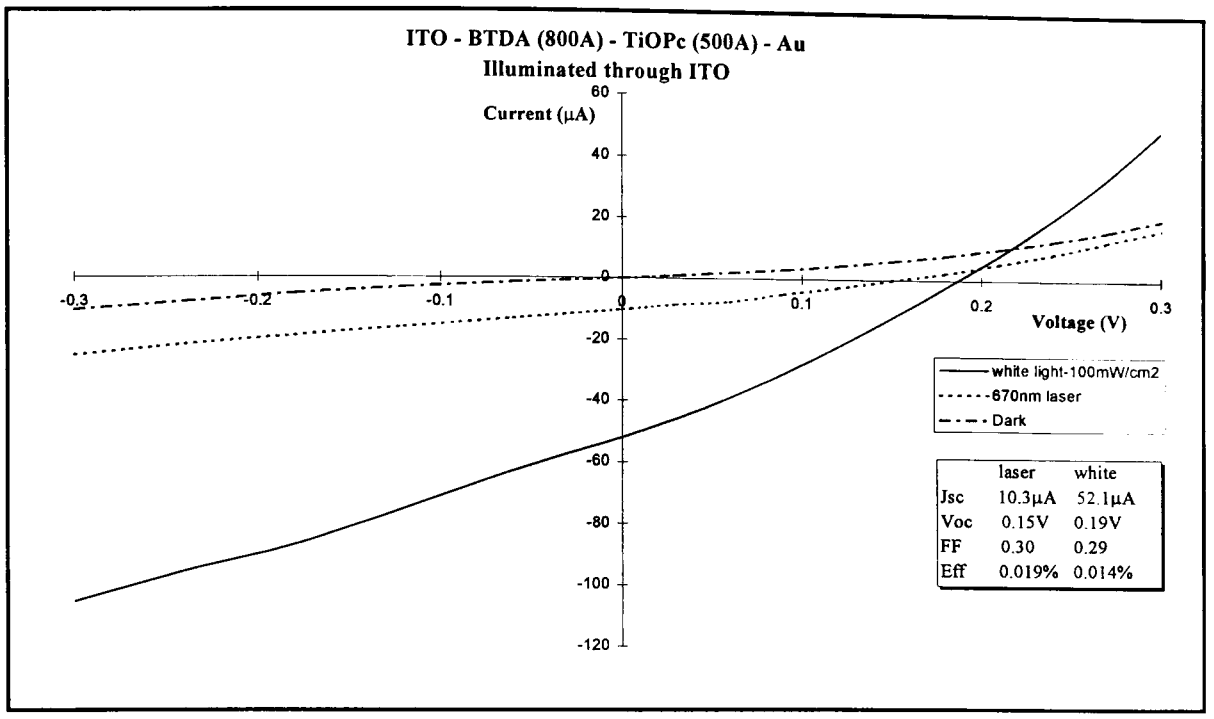

Fig 5.20:- I-V plot of ITO-BTDA-TiOPc-Au illuminated through ITO

The I-V plot shows some rectification and more than any other corresponding plot for a cell illuminated through ITO. The dark current also shows rectification with a rectification ratio at 0.3V of 2. The size of the open circuit voltage is small, however, and this limits the usefulness of the device thought the small absorption of the BTDA layer (only between 400-500nm) makes it potentially useful as a front layer in a heterostructure type device.

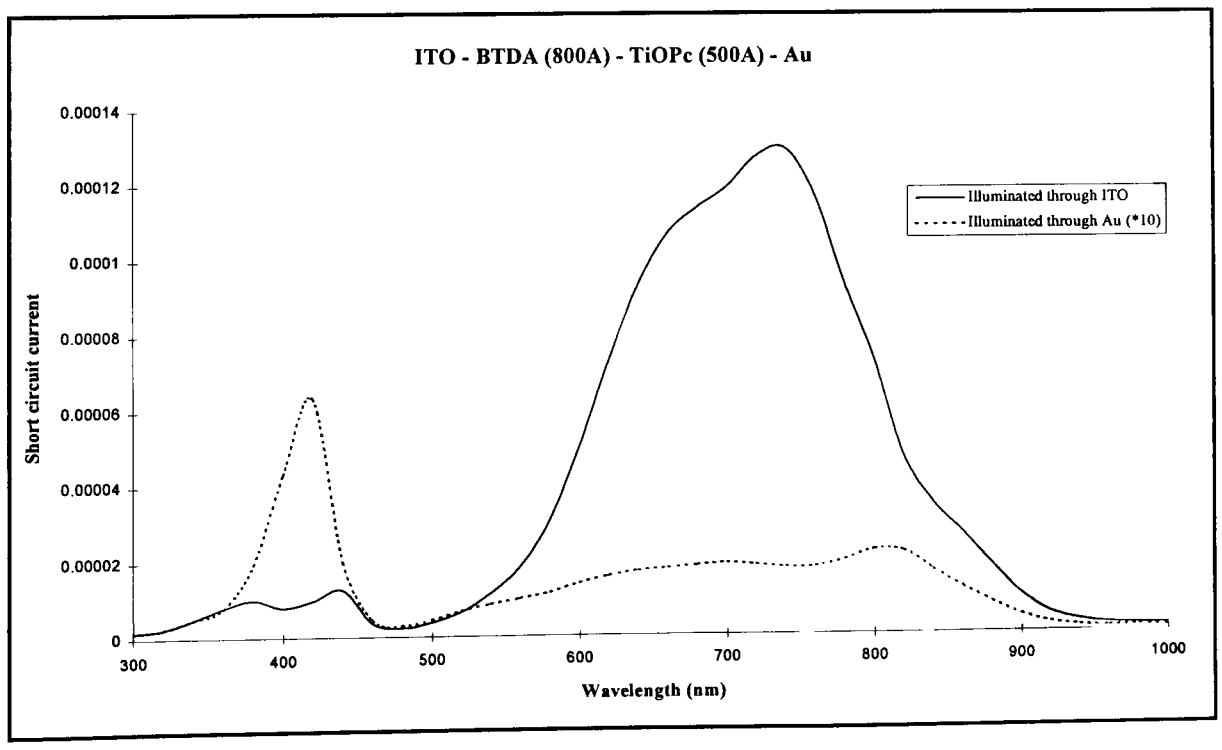

Fig 5.21: Action spectra of ITO - BTDA (800A) - TiOPc (500A) - Au

The action spectra (see fig 5.21) shows that the active region is the interface between the 2 layers showing that a junction is formed. The TiOPc layer acts as the p-type layer and the BTDA acts as the n-type layer. The cell response time is also quite fast when illuminated through ITO at 670nm with τ=0.37ms.

5.7.5 Mixed layer cells

The action spectra of the cells fabricated showed that the response of the cell closely matched the absorption spectra of the second layer. In an effort to improve the performance of the cell, an attempt was made to fabricate a cell where the first layer covered a minimum amount of the visible spectrum, with the second layer comprising of two different materials that would cover the visible spectrum between them. C_{60} and TiOPc were chosen for the mixed layer for spectral reasons and a cell fabricated using them as the two layers provided a low open circuit voltage indicating similar Fermi levels. DBA was used as the front layer. The action spectra for this cell and a cell with only a TiOPc layer is shown in Fig 5.22

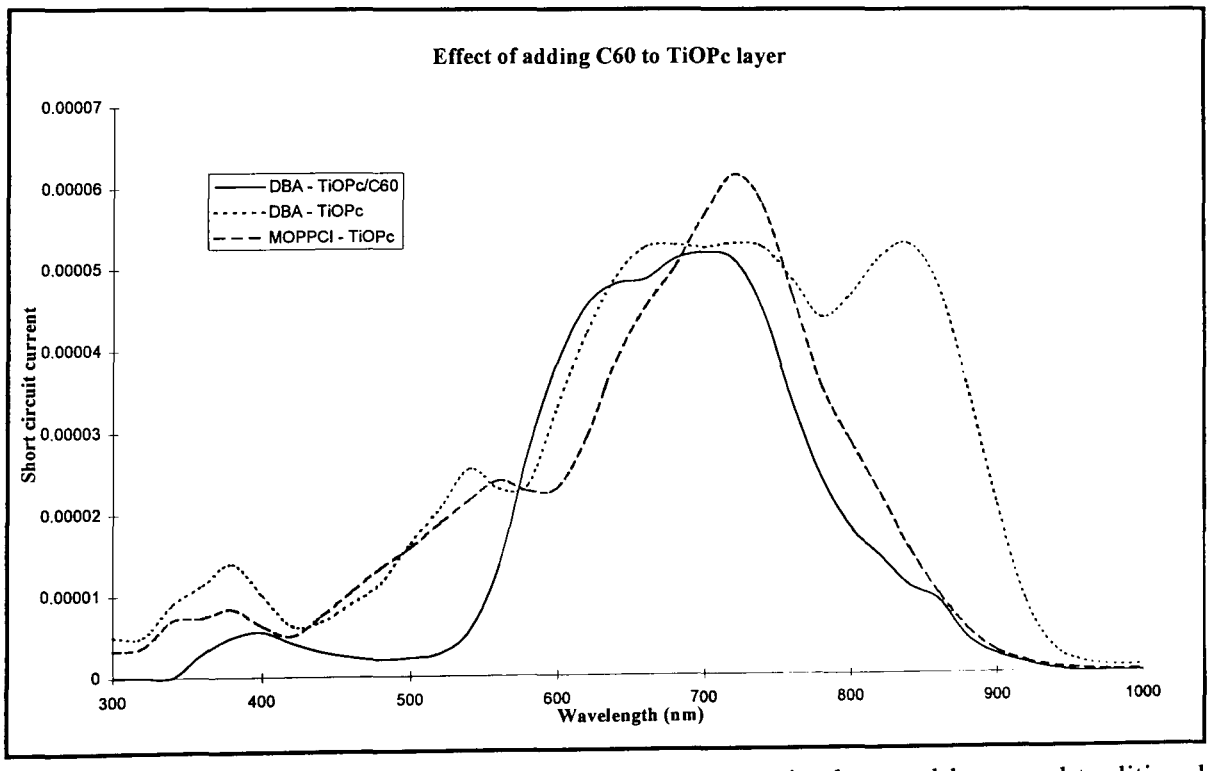

Fig 5.22: Graph comparing action spectra of a cell with a mixed second layer and traditional bilayer cell.

The result wasn't successful when comparing the cell DBA-TiOPc without C_{60} with the mixed layer. However, when compared with the response of the cell with the mixed layer with that of MOPPCI-TiOPc, then the response the absorption peak of the TiOPc layer has been increased. This is probably due to the TiOPc layer being largely amorphous in the mixed layer cell and the MOPPCI-TiOPc cell whereas in the DBA-TiOPc cell it appears to be in the α-form. Adding the mixed layer did reduce the efficiency of the cell by a factor of 50. There is potential in this idea though more careful consideration is needed in the choice of partners.

Chapter 6:- Calculations of the Band Structure for Organic Semiconductors

The aim of this work was to do a series of calculations on the band structure of different photoconductors with the aim of using the information obtained to assist the choice of potential pairs for the bilayer systems. It was hoped that the calculations would provide information on the position of the Fermi level, conduction and valence bands of the materials enabling a more systematic approach to the choice of potential pairs for bilayer devices. Due to the size of the molecules (e.g. metal free phthalocyanine has 58 atoms), *ab initio* calculations are impractical so the more approximate extended Huckel (EH) method was chosen[107].

The EH method has been used extensively to calculate the band structures of organic metals, and has given considerable insight into their behaviour. Because the method makes no specific allowance for electron-electron interactions, the absolute values of the energies of the valence and conduction bands and the HOMO and LUMO from which they are derived, are inaccurate. Nevertheless, it is hoped that

(a) the relative band positions of a pair of photoconductors will be meaningful.

(b) Improved energy values may be obtained by a judicious choice of parameters.

6.1 The Extended Huckel Method

The simplest Huckel theory was introduced in 1931 to describe the π- electron system in conjugated molecules. Its great advantage was its ease of application whilst still providing useful results. It was extended to include a σ framework by Hoffmann, Lohr and Lipscomb[108-110], thus making it include all valence electrons. Since then, it has been widely used and its parameters have often

been adjusted to fit the particular system being investigated. Its use has grown alongside the development of more powerful computers which enable the resulting large matrices to be solved.

The EH theory is best summarised by explaining how a calculation is carried out[111].

A. **Input atomic coordinates**

The molecular coordinates are inputted in Angstroms. It is convenient to input the data so that Cartesian and symmetry axes coincide though it doesn't effect the final MO's.

B. **The Basis Set**

It is necessary to choose a set of normalised valence Atomic Orbitals to describe the MO's. The EH method normally uses single-zeta Slater Type Orbitals (STO's). The radial part of the wavefunction is described by

$$R(n,Z,s) = r^{(n-1)}e^{(-(Z-s)r/n)} \qquad (1)$$

where n is the principal quantum number

Z is the nuclear charge in atomic units

s is a 'screening constant' which is used to reduce the nuclear charge, Z, seen by an electron. This is 1 for a 1s electron, and less for all others as the nuclear charge is effectively shielded by the inner electrons. A list of the screening constants are given by Slater[112].

The programme used has the values for Slater type orbitals as its default setting though it is possible to alter these and use a different set for a particular calculation. It is possible to use double zeta Slater type orbitals which are of similar form but with two exponential terms, one reproduces the wavefunction at short distances, the other at longer ones. Whilst this creates a more accurate form for the wavefunction, the programme only contains the values for carbon so reducing the usefulness of this.

C. **The Overlap Matrix**

Now that the AO functions and their relative positions have been inputted, the overlaps between them can be calculated and these are stored in the form of a matrix called the Overlap Matrix, S. This matrix is symmetric and the diagonal elements are unity because the AOs are normalised. The matrix is calculated within the unit cell and for the overlap between atoms within different unit cells. These results are also used to calculate the Hamiltonian matrix.

D. **The Hamiltonian Matrix**

The Hamiltonian matrix is generated in a very similar way to Huckel theory. The energy integral H_{ii} in the EH method (the α in Huckel theory) is taken to be equal to the energy of an electron in the *i*th AO of the isolated atom in the appropriate state. The ionization potentials of atoms are well known so these are easily inputted, though the problem comes with finding the appropriate state. For example, for carbon in methane in the sp^3 configuration, there are many different physical states (corresponding to different spin and orbital angular momenta) which will yield different ionisation potentials. The EH method averages the real ionisation potentials for all different physical states. This leads to different authors suggesting alternative sets of parameters for use in different situations. This allows for a degree of freedom in choosing the different parameters to fit the required data. There have also been many different forms proposed for the off- diagonal elements. Initially, they were calculated using the Wolfsberg- Helmholtz relationship

$$H_{ij} = KS_{ij}(H_{ii} + H_{jj})/2 \qquad (2)$$

where K is an adjustable parameter which is usually a constant and taken to be 1.75 or 1.875. This was then adjusted so that K was no longer a constant but took the form:

$$K_{ij} = \tfrac{1}{2}\kappa + \tfrac{1}{2}\Delta^2 + \Delta^4\left(\tfrac{1}{2} - \kappa\right) \qquad (3)$$

where $\Delta = \dfrac{H_{ii} - H_{jj}}{H_{ii} + H_{jj}}$

κ is a constant, usually 0.875

This is the weighted Wolfsberg Helmholtz formula.

E. **Solving for the Eigenvalues and Eigenvectors.**

Now that matrices for H and S have been generated, it is possible to solve the secular equation

$$H_{ij}(\underline{k})C_{ij}(\underline{k}) = S_{ij}(\underline{k})C_{ij}(\underline{k})E_{ij}(\underline{k}) \qquad (4)$$

The coefficients of the MOs are given by the columns in the matrix C and the energy levels are given by the diagonal elements in the matrix E. The number of valence electrons is known so the HOMO and LUMO are found by filling the energy levels.

The energy levels generated are one electron energy levels as the calculation takes no account of the electron-electron interactions (i.e. it determines the motion of an electron in the periodic array). This means that whilst the results are presented as conventional two electron energy levels, a calculation on a positive ion, for example, will still give the same results.

Band structure calculations are completed using the standard tight- binding approximation. From the basis set of Slater type orbitals, χ_u, for the atoms defined within the unit cell, a set of Bloch basis orbitals, $b_u(k)$, can then be formed

$$b_u(k) = N^{-½} \sum e^{ikR} \chi_u(r - R) \qquad (5)$$

where k = wavevector

R = l . a where a is the primitive vector.

Then the LCAO (Linear combination of Atomic Orbitals) for the crystals, $\Psi_n(k)$, is expressed as

$$\Psi_n(k) = \sum c_{nu}(k) b_u(k) \qquad (6)$$

The coefficients, $c_{nu}(k)$, are found using the secular equation (4), along with the eigenvalues $E_n(k)$. The elements of the Hamiltonian and Overlap matrices are calculated as explained previously. Thus the calculation is repeated at several different points in k space which cover the first Brillouin Zone. From these results, the density of states diagrams can be drawn.

When a band calculation is performed, the overlap matrix, S_{ij}, is calculated between the different unit cells but only one Hamiltonian matrix is used which is calculated from the overlap matrix within the unit cell. This is because the transfer integrals, t, are calculated from the intermolecular overlap integrals, S, using the following equation

$$t = ES \qquad (7)$$

where E is a constant (usually taken to be the energy of the relevant band). Hence the amount of band broadening is directly proportional to the intermolecular overlap, thereby making the size of the bandwidths depend on the intermolecular overlap integrals. The bandwidth also depends on the energy of the band (see fig 6.1). The same calculation was repeated (so S remains constant) for different values of k_1 and k_2 from equation 8 (which is the alternate form for the off-diagonal elements proposed by Anderson), thereby changing the energy of the HOMO and LUMO and the resulting bandwidths

vary linearly with this energy. Using this fact, it should be possible to alter the parameters so that an optimum set is found to provide accurate values for the bandgap and bandwidth of phthalocyanines.

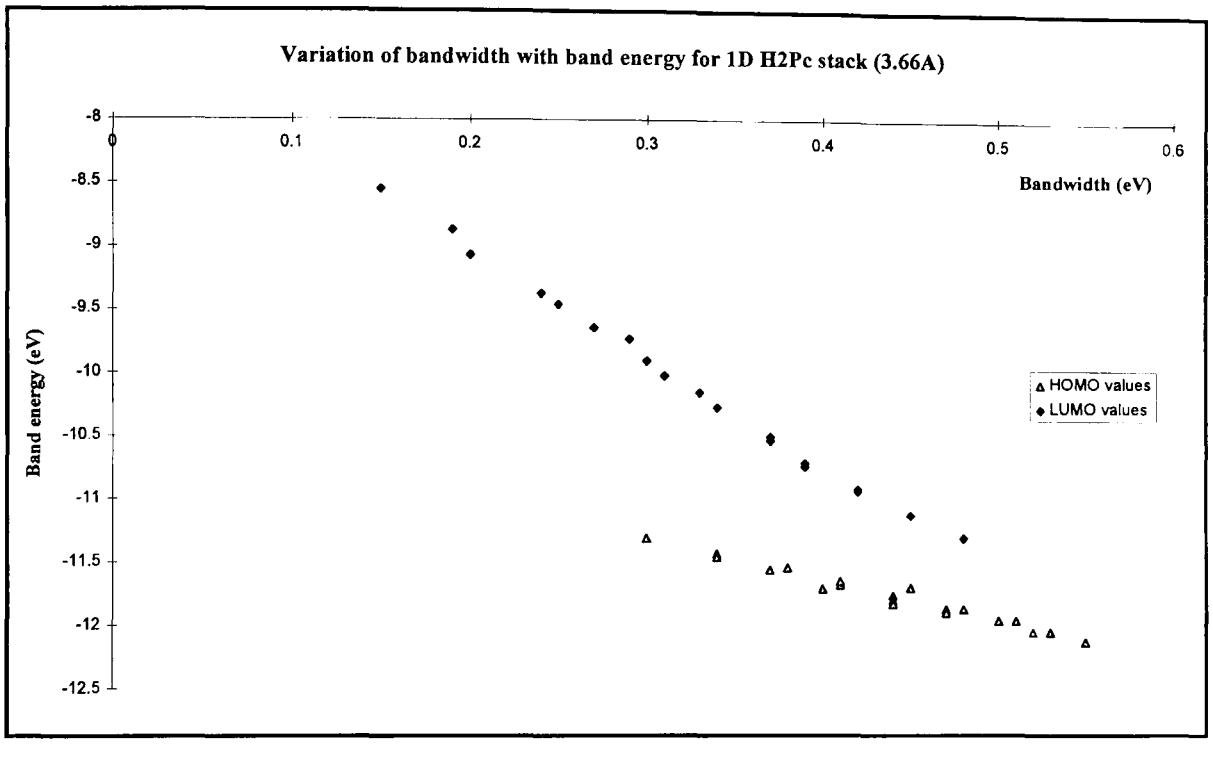

Fig 6.1: Showing variation of bandwidth with band energy for a 1D H_2Pc stack.

The EH method has been likened to using a table cloth which is just too small to cover a table so you have to move the cloth (i.e. adjust the parameters, form of off- diagonal elements etc.) to fit the situation that you are investigating. Hence, it was necessary to reoptimise the parameters to get a set that gave the most useful information on bandgaps, bandwidths and the relevant band positions for heterocyclic structures.

6.2 Development of the Extended Huckel method

When the extended Huckel method was first proposed by Hoffmann, it was designed to provide information on the geometry of hydrocarbon molecules. The simpler Huckel method had proved valuable for conjugated hydrocarbons but inaccurate in many other cases. In 1975, Anderson[116] proposed that the

form of the off- diagonal elements be changed to include an exponential term which varied with the distance between the atoms.

$$H_{ij} = k_1(H_{ii} + H_{jj})\exp(-k_2 d_{ij})S_{ij} \qquad (8)$$

where $k_1 = 2.25$

$k_2 = 0.13$ Å^{-1}

d_{ij} is the distance between atom i and atom j.

S_{ij} is the overlap matrix.

It was introduced because the binding levels for covalent molecules were usually too deep so this term reduced their magnitude. It was found that this improved the dissociation energies without affecting the determination of bond lengths or force constants. The constants were then optimised by Hong and Marynick[115] for one dimensional conductors and found to be 1.41 and 0.13Å^{-1} respectively. It was also noted that k_1 was considerably more sensitive than k_2.

An alternative form of the off- diagonal elements was proposed by Calzaferri et al.[117] to overcome a deficiency in the distance-dependent off-diagonal element formula proposed by Anderson. They found that the formula was inaccurate at large bond distances so they proposed an alternative form (for K in equation (2))

$$K = 1 + (\kappa + \Delta^2 - \Delta^4\kappa)\exp[-\delta(R - d_0)] \qquad (9)$$

where κ = positive parameter (usually 0.75)

$\Delta = (H_{ii} - H_{jj}) / (H_{ii} + H_{jj})$

δ = positive parameter (usually 0.35)

R = distance between atoms i and j

d_o= sum of the orbital radii.

This has allowed Morse potentials to be successfully simulated in several cases.

Other modifications have concerned the choice of basis set. These have been reoptimised by Roetti and Clementi[118] in 1974. These are the values used in the EHMACC programme. Jerrard et al[114] approached the problem of getting accurate ionisation potentials for benzene and naphthalene differently. They reparameterised the EH method to include distinct π and σ values for the atomic orbitals of carbon. Using these parameters, they had considerable success by predicting energy levels more accurately than by using MNDO methods. This idea was introduced because the EH method only introduces one set of parameters per atom as the off-diagonal elements are calculated from the values for the diagonal elements. Simple Huckel theory has two different parameters (one for the diagonal elements and one for the off- diagonal elements).

6.3 Previous work

The EH method has often been used in molecular and band structure calculations of organic semiconductors. EH calculations were first carried out on metal phthalocyanines and tetraporphins by Schaffer et al[119] in 1973. These were performed using the form for the off- diagonal elements described in equation (2). They predicted band gaps of around 1eV (about half the correct value) with the ionisation potential being -11eV which is larger than the expected value of around -7eV. Band structures of conjugated 1 and 2D polymers were investigated by Whangbo et al[120]. They investigated how the band structure was affected by the positions of atoms within the unit cell and the unit cell vectors. The authors noted that whilst the calculations provided information on the ideal scenario, it made no allowance for structural defects or chemical impurities. Other systems which have been investigated using the EH method include the band structure of DEBP $(TCNQ)_4$[121], and organic thin film transistor materials[122]. In both cases, the calculations have provided information on the band structure of the materials which gives an insight into some of their solid state properties.

There have been several calculations on the band structure of phthalocyanines. The first was done by Chen[113] in 1969 who reported calculations on β - H_2Pc. A more comprehensive study was undertaken by Canadell and Alvarez[123] in 1984 who looked at the electrical behaviour of 1D metallophthalocyanines. To reduce the computational effort they used a truncated ring e.g.

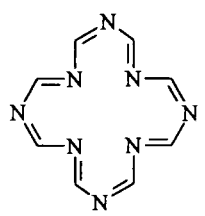

They found that the size of the bandwidths depended on the inter- ring overlap between neighbouring vertically stacked molecule. As a result, they found very little difference in going from α - NiPc to β - NiPc. They noticed a sizable band gap but could not compare it to experimental values owing to the disparity in reported values. They also commented that any increase in electrical conductivity by partial oxidation of the valence band would be small due to the narrowness of the band. Hence they attributed the increase in conductivity for NiPcI to the change in stacking angle to an ideal face to face assembly. For phthalocyanines with bridging ligands, they noted that the conductivity/ bandwidths were larger because the ligand ensured face to face stacking and sometimes reduced the inter- ring separation.

This line of study was continued by Gomez-Romero et al[124] who looked at the band structure of extended 1 and 2D phthalocyanine polymers. e.g.

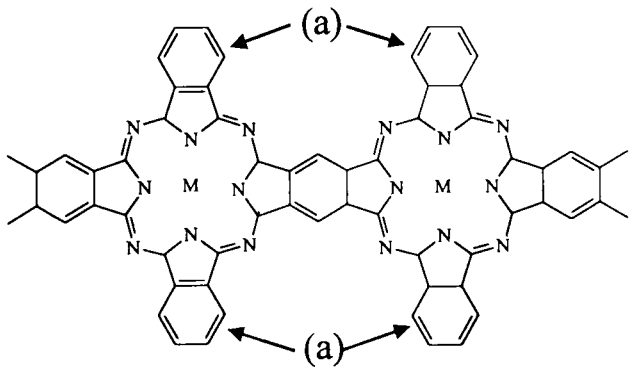

Fig 6.2: 1D phthalocyanine polymer simulated by Gomez- Romero et al.

They found that the 1D structure above (fig 6.2) would go from being a poor conductor to a good one by the inclusion of the benzene rings marked (a). This is because the partially filled band in the case without the benzene rings is very narrow. Adding the benzene rings causes the perturbation of a broad, empty band to cross this partially filled band allowing a broader conduction path for the electrons. They make similar predictions for 2D conductors.

Cain et al[125] attempted to correlate the theoretical results of EH band calculations with practical results by recording Differential Pulse Voltammograms (DPV) on a (phthalocyaninato)siloxane polymer $\{Si[(t\text{-}Bu)_4Pc]O\}_n$ and comparing them to the calculations on a truncated phthalocyanine. DPV are equivalent to density of valence states plots. Their results correlated well demonstrating that it is useful for checking the accuracy of the calculations.

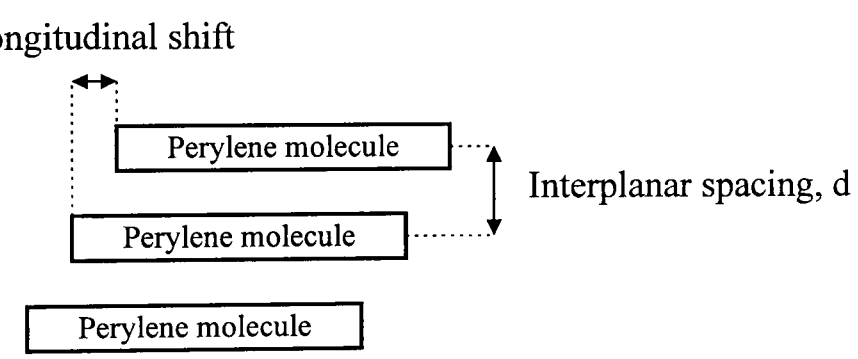

Fig 6.3: Diagram showing the side view of the stacking of perylene molecules used by Hoffmann and Kazmaier.

The crystallochromy of perylene pigments was theoretically studied by Kazmaier and Hoffmann[126] using EH band calculations. They used the EH method to demonstrate how the variation of bandwidths for perylene pigments is a quantum interference effect. By considering a 1D stack of perylene molecules (see fig 6.3), a distance of 3.5Å apart and gradually slipping the stack longitudinally, they plotted the variation of bandwidth against offset. The graph showed several nodes corresponding to nodes in the HOMO/LUMO

structures. They then compare how the bandwidth correlates with photocurrent and photogeneration efficiency. A large bandwidth stabilises an exciton so increasing the exciton lifetime and diffusion length. They are presently attempting a similar study on phthalocyanines. This suggests that the materials used for photovoltaic cells should exhibit a large bandwidth to improve the exciton lifetime and diffusion length.

Other approaches have been used by to investigate solid state properties of phthalocyanines. In 1984, Bohm[127] completed a crystal orbital study on SiO and GeO bridged tetraza porphines displaying the results as DOS histograms. Another technique which has been used is the Discrete Variational X-α method by Kutzler[128] and others[129]. The other important method is the Valence Effective Hamiltonian (VEH) which was developed by Durand and others and has been used extensively on phthalocyanines by Bredas and Orti[130-4].

6.4 Operational details

The extended Huckel calculations were performed using the extended Huckel Molecular, Crystal and Properties package (obtained from the Quantum Chemical Programme Exchange, QCPE 571) and were run on the DEC ALPHA computer at the Cripps Computing Centre of Nottingham University. The crystal structures were found using the chemical database at Daresbury (cds1) and these were converted into atomic coordinates with the help of Dr. Sandy Blake. For all the band calculations, a 1 dimensional system was considered for clarity of understanding and because a 3 dimensional calculation on a 40-50 atom system is prohibitively large. It is also justified as by far the largest intermolecular interactions occur are the π-π interactions between the molecules. This is shown by the bandwidths of metal free phthalocyanine which are around 100meV along the stacking direction and less than 10meV otherwise[113]. So by considering a vertical stack which is translationally slipped by the appropriate amount, information on the band structure can be found.

Instructions for running the calculations on the computer in A26 are given in Appendix 1.

Three different parameter sets were tried. Initially, the Slater type orbitals were used with the weighted Wolfsberg- Helmholtz formula for the off diagonal elements. The Slater type orbitals were then adjusted to those used by Jerrard et al[114] which were normalised to fit the ionisation potentials of naphthalene and benzene. (A full list of the parameters used in all the calculations is given in Appendix 2). Finally, the formula of the off- diagonal elements was changed to that used by Hong and Marynick[115] (Slater type orbitals were used). The two constants were optimised for a cofacially stacked phthalocyanine by performing calculations over a range of different values for k_1 and k_2 (see figs 6.5 and 6.6).

For band calculations, the repeat unit is added along with the unit cell vectors when the data is inputted and the calculations are repeated over a range of different points in k space. This mesh should cover the first Brillouin Zone. At each point the interaction between different unit cells is calculated, producing a new set of one electron energy levels. EHPC then orders the one electron energy levels from all the n calculations over k space and selects the appropriate ones when prompted for the metallic Fermi level (i.e. it selects the numbers n, 2n, 3n, ... from the list of all the electron levels). The results are displayed as the Fermi level as a function of the number of electrons. From this list, the bandwidths/ bandgaps can be found by locating the edge of the conduction and valence bands. The density of states diagram is calculated by multiplying each electron energy level by a gaussian of a width chosen by the user. If the calculation is run over enough points in the first Brillouin zone (usually 20 or more depending on the bandwidth but more if it is large), then a smooth 1D band is formed.

Alternatively, EH calculations on molecules were performed using the CACAO- Computer Aided Composition of Atomic Orbitals[149] program run on

a 386 Pc with a maths co- processor. This program has plotting routines which allow the user to view the nodal characteristics of all the calculated energy levels.

6.4.1 Calculation details

Calculations were performed on 4 different classes of semiconductors: phthalocyanines, perylene tetracarboxylic acids, squaraines and anthanthrones. In all cases, the simplest molecule of the type was chosen and a full list of the coordinates used is printed in Appendix 3. Fig 6.4 shows the structure of these molecules.

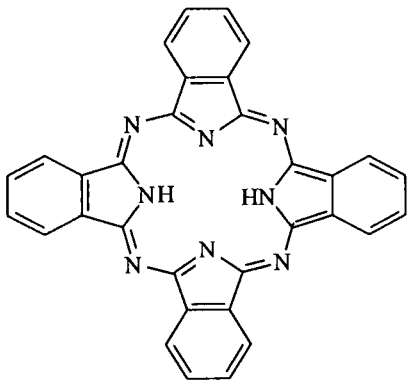

Phthalocyanine

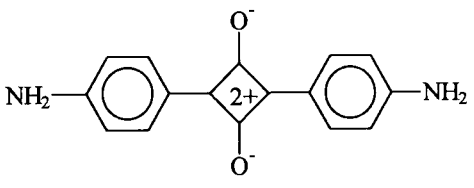

Squaraine

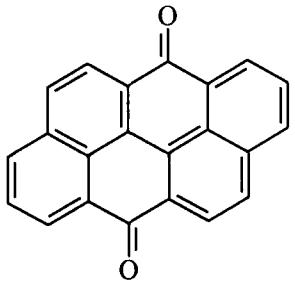

Anthanthrone

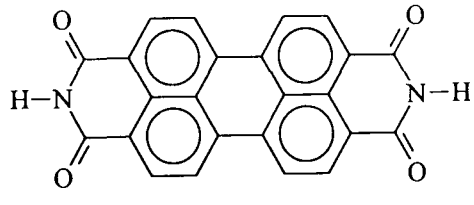

Perylene tetracarboxylic acid

Fig 6.4: The structures of the models used for the Extended Huckel calculations.

Geometry optimisations were performed using MOPAC (ver7.0) running on the Granby (Unix) computer at the University of Nottingham's Cripps Computing Centre. All the calculations used the AM1 Hamiltonian (Austin Model 1) which is a recent parameterisation of the NDDO (neglect of diatomic differential overlap) designed to overcome the weaknesses of MNDO in that it successfully treats hydrogen bonding[135].

6.4.2 Optimising k_1 and k_2

We wanted to generate a set of parameters that was relevant for phthalocyanines as Hong and Marynick[114] had based their parameters in the distance dependent form for the off diagonal elements to fit conducting polymers. To do this, a 1D stack of metal free phthalocyanine, 3.66Å apart was considered as a model for AlFPc which has a bandwidth of around 0.3eV[141] and a bandgap of around 2.0eV[5] (the bandgap was measured as the middle of the HOMO to the middle of the LUMO). When choosing a value for the bandgap of a phthalocyanine, it is necessary to find one where the bandwidth is small and where the d orbitals of the central metal atom don't infringe into the bandgap. This is the case for metal-free and transition metal phthalocyanines up to zinc (e.g. β-H_2Pc and β-CuPc have a value of ΔE=2.0eV). When using the values proposed by Hong and Marynick (k_1 = 1.41 and k_2 = 0.13), a bandgap of 1.70eV and a bandwidth of 0.44eV for the HOMO were found. The parameters k_1 and k_2 were then varied and optimum values for k_1 and k_2 were obtained graphically (see Figs 6.5 and 6.6).

From the graphs, it was found that the value of the parameters that gave the desired values for the bandgap and bandwidth were k_1 = 1.16 and k_2 = -0.06. It is clearly undesirable that k_2 is negative so the condition that the bandwidth = 0.3eV was relaxed as the accuracy of the experiment means that the error in the figure is large. The value for the bandgap was allowed to rise just above 2.0eV as the value measured experimentally is from the top edge of the HOMO to the bottom edge of the LUMO, thereby making the value differ from the value

calculated theoretically by the size of the bandwidth. Whilst the magnitude of the bandwidths are small, it will still result in the value of the calculated bandgap being smaller than the experimental value. The values chosen were k_1 = 1.41 and k_2 = 0.05 which yielded values of 2.08eV for the bandgap and 0.35eV for the bandwidth of the HOMO. These parameters were used for all calculations unless otherwise stated.

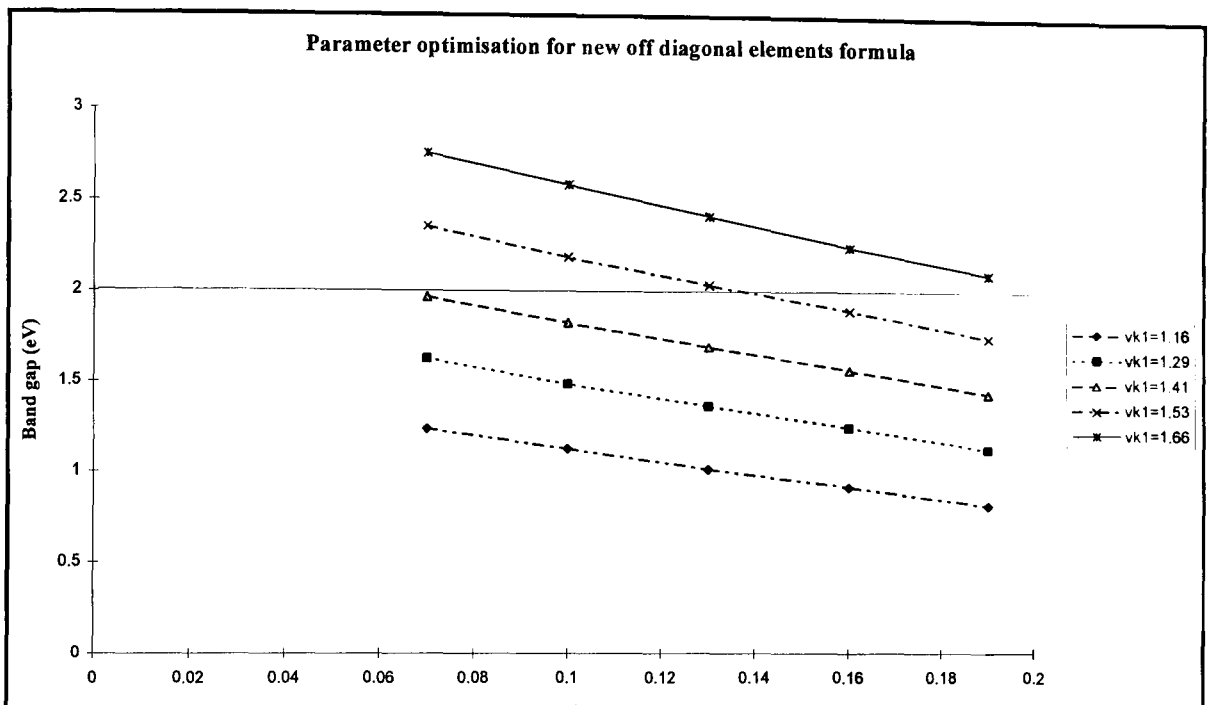

Fig 6.5: Optimising k_1 and k_2 for a band gap of 2.00eV

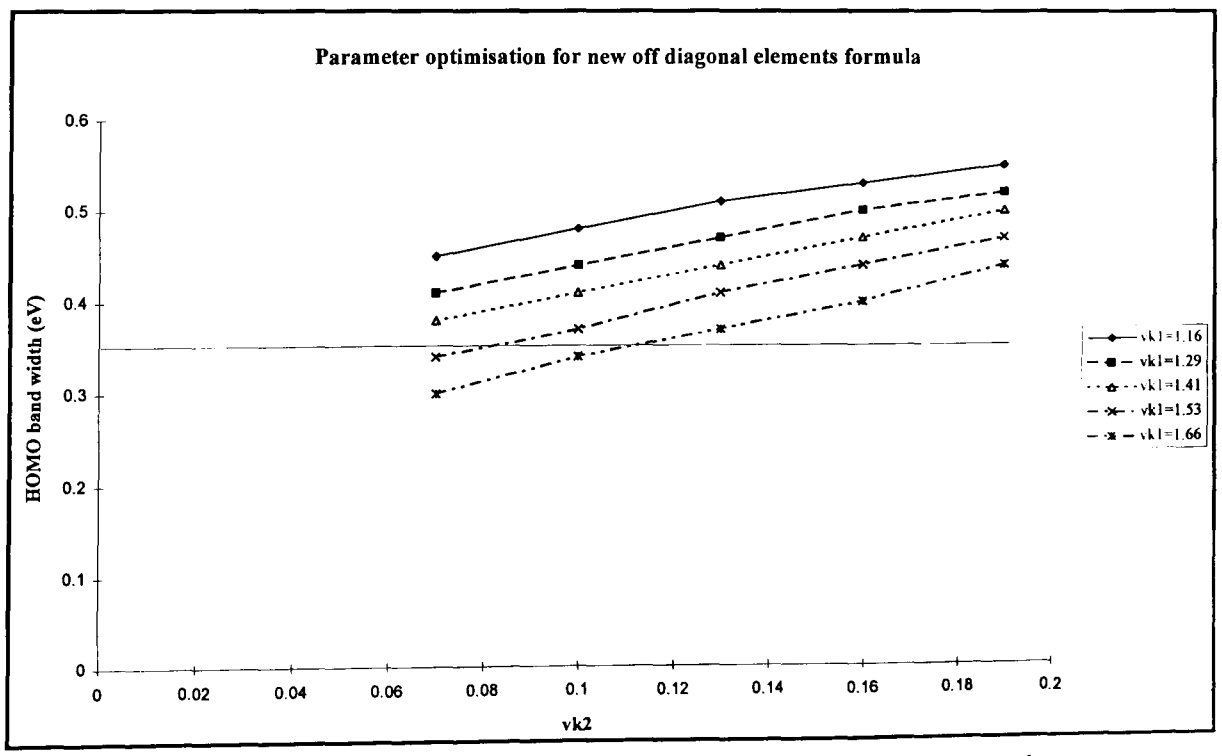

Fig 6.6: Optimising k_1 and k_2 for the bandwidth of the HOMO of a 1D H_2Pc stack.

6.4.3 Verifying the results of the calculations

To check the programme was working, calculations were performed on the band structure of a perylene tetracarboxylic acid 1D stack and this was in agreement with the one published by Kazmaier and Hoffmann[126]. Table 6.1 shows the position of the HOMO and LUMO band edges. The minor discrepancies in the energies are due to differences in the internal coordinates used. Both of these calculations were carried out using single zeta Slater type orbitals as the atomic orbitals and the weighted Wolfsberg-Helmholtz form for the off-diagonal elements in the Hamiltonian matrix.

Level	Our Calculation (eV)	Published Calculation (eV)
Top of HOMO	**-12.21**	**-12.19**
Bottom of HOMO	**-11.58**	**-11.58**
Top of LUMO	**-10.99**	**-11.02**
Bottom of HOMO	**-10.40**	**-10.42**

Table 6.1: Comparing the results of a band calculation with published results.

6.4.4 Comparing different approximations for metal free phthalocyanine

Calculations on a molecule of metal free phthalocyanine were carried out using the different approximations in order to see which provided the best results for this system. As a result, calculations were performed using the single-zeta Slater type orbitals as the basis set with the Wolfsberg-Helmholtz formula for the off-diagonal elements as well as the optimised distance dependent form. The results of the calculations are shown in figure 6.7. They show the increase in the size of the bandgap that the optimised distance dependent formula has compared to the weighed Wolfsberg-Helmholtz formula whilst keeping the order of the orbitals the same. The distance dependent formula has most effect on the orbitals around the bandgap with these levels being spread out causing the bandgap to increase. The form of the two formulas are similar with the K/2

in equation (2) being replaced with $k_1 \exp(-k_2 d)$. With K usually taken to be 1.75, this means that the optimised distance dependent form yields larger values for H_{ij} at short distances though the values reduce quickly as the distance between the atoms increases due to the exponential term coupled with the reduced overlap.

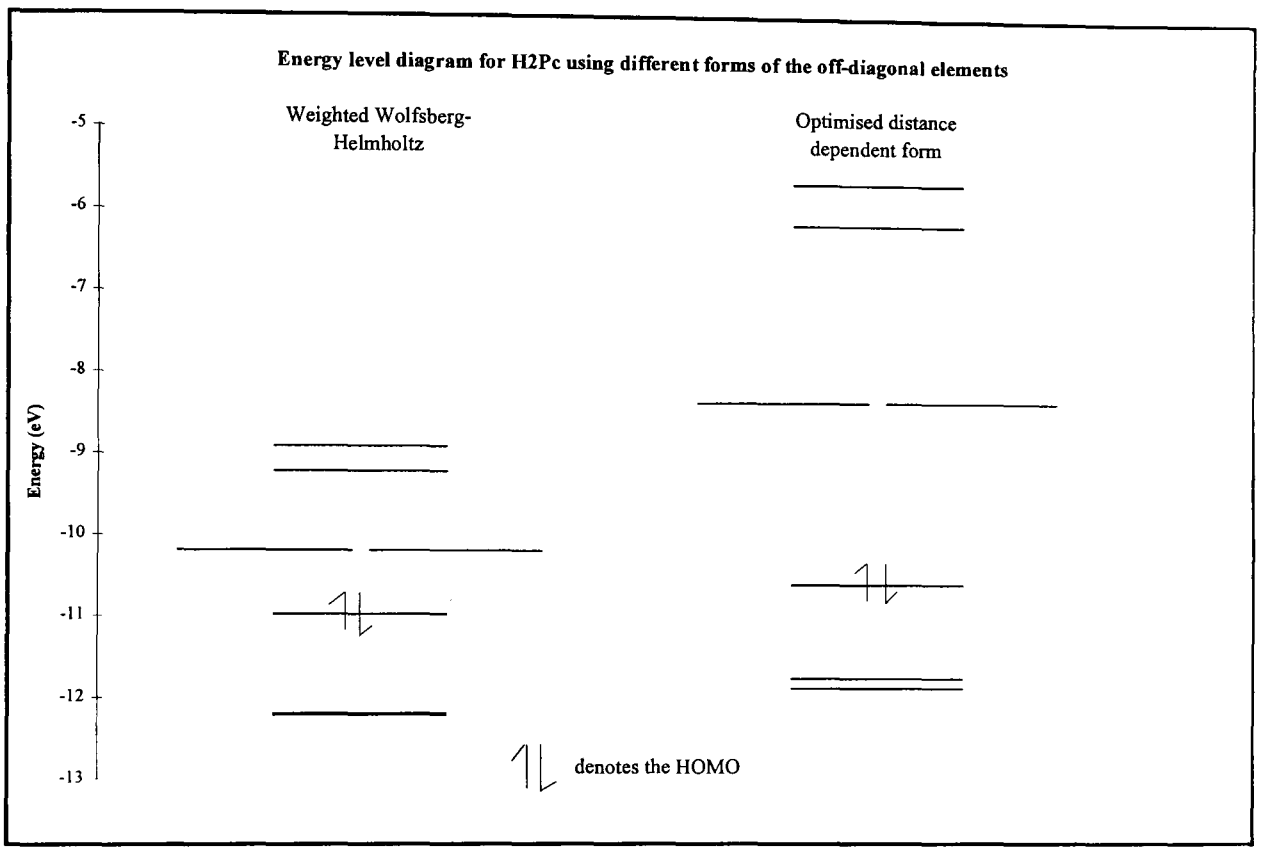

Fig 6.7: Energy level diagram comparing the results for H_2Pc using the weighted Wolfsberg-Helmholtz and the optimised distance dependent form for the off-diagonal elements.

6.4.5 Effect of changing basis set

A series of calculations were done on a molecule of metal free phthalocyanine in order to establish the best basis set for our purposes. The three basis sets used were the single zeta Slater type orbitals (STO) using the initial values, the alternative set proposed by Jerrard et al[114] and a set that included the double zeta STO's for carbon. The results are shown in fig 6.8.

The results show that using the double zeta STO's has decreased the energy of the HOMO so that the values are nearer those obtained from measuring the

ionisation potentials. There is very little effect on the size of the band gap and the ordering of the bands. However, the programme has only the double zeta values for carbon so necessitating the use of the conventional single zeta STO's for the other atoms. Whilst this hasn't caused a problem in this case, when the double zeta STO of carbon was used for a molecule of perylene, the bandgap was lost. As we only require the relative position of the bands for different molecules, the single zeta STO basis set was used. Using the set of exponents proposed by Jerrard et al caused the band gap to increase to about 2.90eV (c.f. experimental value is about 2.0eV) and had a significant effect on the relative position of the bands. As a more accurate value for the band gap was obtained using the single zeta STO, these were taken as the basis set for all calculations.

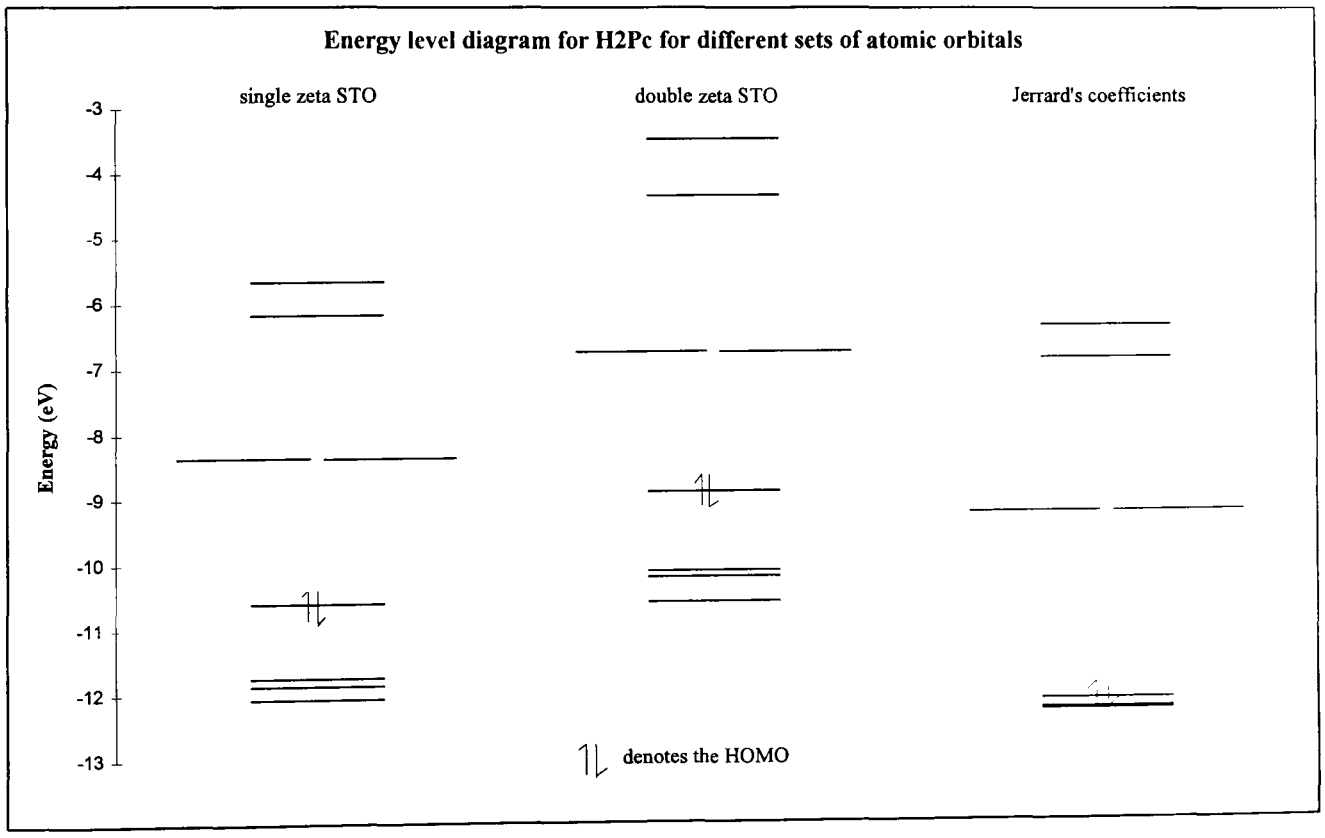

Fig 6.8: Energy level diagram for metal free phthalocyanine using different basis sets.

6.5 Calculations on other molecules

Calculations were performed on other photoconducting materials in an attempt to help explain the properties of junctions formed between them. Calculations

were done on molecules of a perylene tetracarboxylic acid, a squaraine, anthanthrone and BTQBT as band structure calculations would only reveal information on the bandwidths. Atomic coordinates were found from the crystal database at Daresbury (cds1) and are given in Appendix 3.

6.5.1 Anthanthrone

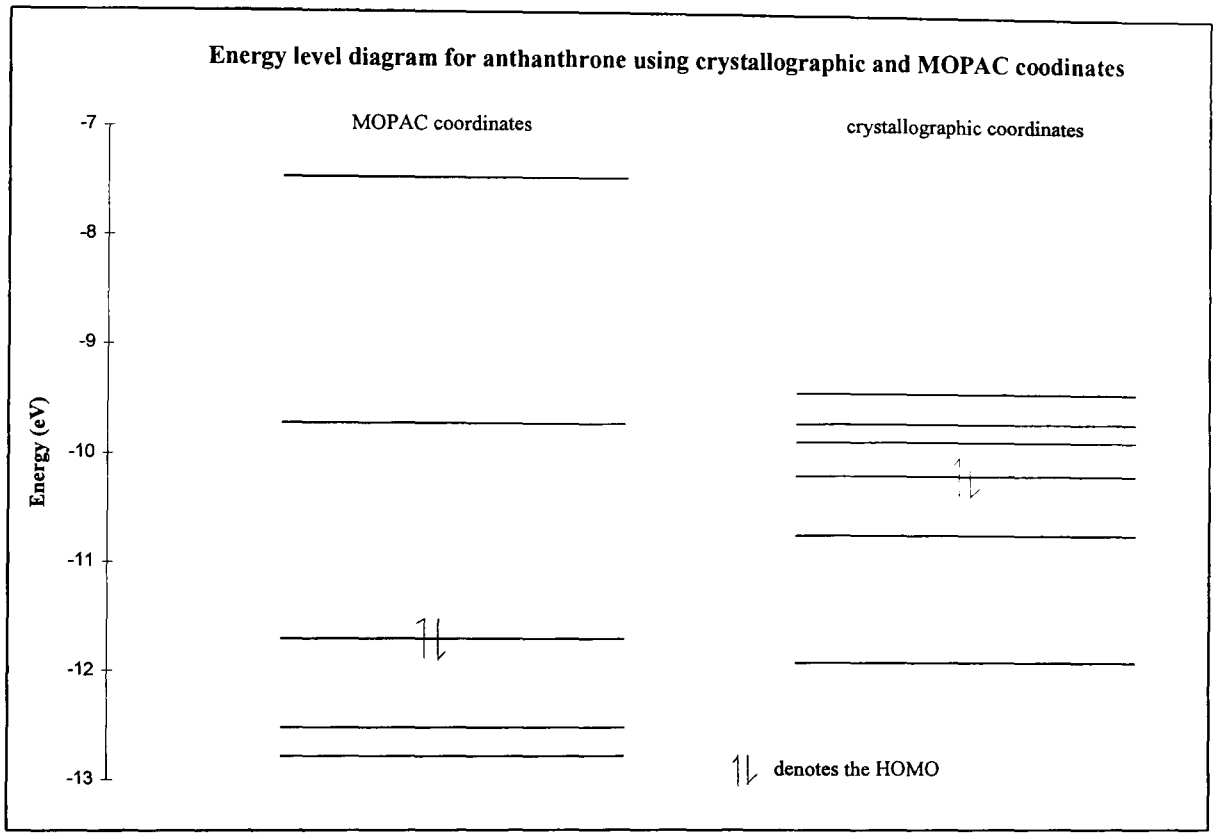

Fig 6.9: Energy level diagram for anthanthrone using two different sets of atomic coordinates obtained experimentally and theoretically.

When an extended Huckel calculation was performed on a molecule of anthanthrone, a problem was found with the positioning of the Fermi level. This was investigated further by examining the nodal character of the energy levels around the band gap. When the calculation was repeated for anthanthrone with the oxygen atoms replaced by hydrogen atoms, the order of the energy levels around the band gap changed. This revealed that the Fermi level was being incorrectly assigned and it seemed that there was a problem with the electron count. As the number of electrons in the system is fixed, it was assumed that an unfilled orbital was lying below the band gap, so causing

the problem when the energy levels were filled. A closer inspection of the atomic coordinates[151] revealed that the data collected was refined to a high residual value (R=13.7%) which meant that the standard deviation of the atomic coordinates was 0.03Å. To see if the molecular geometry was a problem, an optimised geometry was calculated using MOPAC. When this structure was used, the problems with the assignment of the Fermi level disappeared and a band gap of 1.98eV resulted. The energy level diagrams of the two calculations are shown in fig 6.9. This, shows that the results of the calculation are sensitive to the starting coordinates.

Other molecular calculations were performed on a perylene tetracarboxylic acid diimide, a squaraine and BTQBT using the optimised distance-dependent off-diagonal elements formula. The results of the calculations of the relative positions of the HOMO and LUMO for the different photoconductors used for bilayer solar cells are shown in fig 6.10. These results were used when describing the junctions formed between the materials.

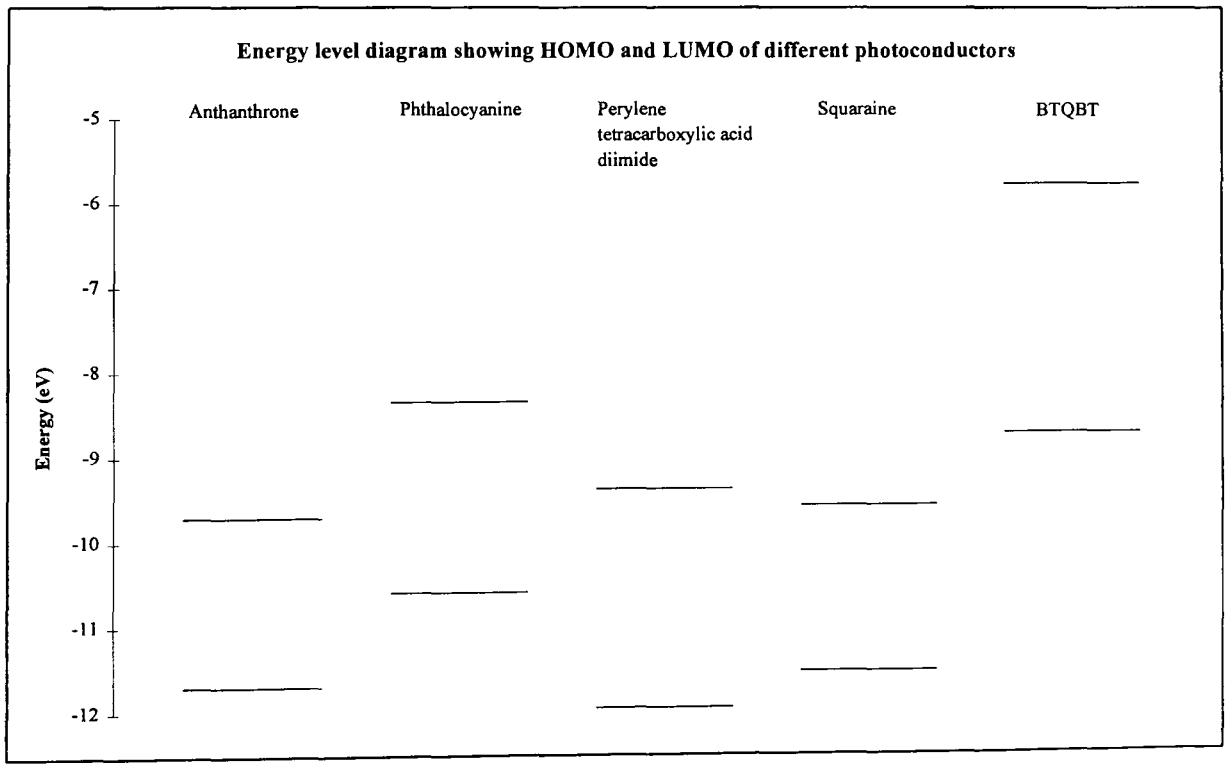

Fig 6.10: The relative positions of the HOMO and LUMO for the different photoconductors in the bilayer solar cells.

6.5.2 Predictions on conduction type based on calculations

The calculations only predict values for the metallic Fermi level (i.e. indicating the position of the energy levels). If these calculations are to be useful in predicting the results of the junctions formed between 2 semiconductors, then an estimate of the Fermi level is necessary. From the calculated positions of the HOMO/LUMO or ionisation potentials/electron affinities, it should be possible to predict whether a material is likely to exhibit n- or p- type conduction. As n-type conductors are electron acceptors, they should show a high electron affinity. Hence, the LUMO energy should be low. Conversely, p- type semiconductors are electron donors which indicates that a low ionisation potential is expected (i.e. the HOMO energy is high). Table 6.2 shows the HOMO and LUMO energy levels and the conduction type of the different materials.

class of molecule	HOMO energy (eV)	LUMO energy (eV)	Predicted conduction type	Actual conduction type
Anthanthrone	**-11.70**	**-9.72**	**n**	**n**[a]
Phthalocyanine	**-10.60**	**-8.36**	**p**	**p**[b]
Perylene deriv.	**-11.97**	**-9.39**	**n**	**n**[b]
Squaraine	**-11.55**	**-9.58**	**n**	**p**[c]
BTQBT	**-8.73**	**-5.78**	**p**	**p**[d]

Table 6.2: Showing the link between calculated HOMO/LUMO energies and conduction type where (a) from ref 96, (b) from ref 142, (c) from ref 22 and (d) from ref 136.

As can be seen from the table, there is a strong correlation between HOMO/LUMO energy and conduction type. The only molecule incorrectly predicted is the Squaraine which is on the borderline (i.e. in terms of the order of electron donating properties, it is third). This then allows predictions to be made on the conduction type from the calculated positions of the energy levels. Once this has been done, predictions can be made about the position of the Fermi level. For an n- type material, if it is assumed that the acceptor states lie midway between the valence band edge and the intrinsic Fermi level (i.e. the

middle of the band), then the Fermi level must lie midway between the acceptor states and the valence band edge. This puts it an eighth of the way up the band gap. The converse argument can be used for p- type conductors. The error involved in the assumptions made in the positioning of the acceptor/donor states are likely to lead to a small error in the predicted Fermi level. For example, if the acceptor states lie a third of the way up the band gap making the Fermi level a sixth of the way up, then this will cause an error of less than 0.1eV for a material where E_g =2.0eV.

It is possible to test the predicted values for the Fermi levels against measured values for the phthalocyanines and perylene derivatives. The results are shown in the table below. They show that this is a useful tool to get 'rule of thumb' values for the Fermi levels of materials if they are unknown.

Molecule	Predicted position of Fermi level w.r.t. valence/conduction band	Actual position of Fermi level w.r.t. valence/conduction band
Phthalocyanine	0.25eV[a]	0.31eV[c]
Perylene deriv.	0.31eV[b]	0.14eV[d]

Table 6.3: Comparing predicted and measured values for E_f - E_v (for perylene deriv.) and E_c - E_f (for phthalocyanine) where (a) assumed E_g = 2.0eV, (b) assumed E_g = 2.5eV, (c) value for ZnPc [142] and (d) value for dimethyl perylene tetracarboxylic acid diimide [142].

6.6 Calculations on substituted phthalocyanines

Calculations were performed on substituted phthalocyanines in an attempt to alter the position of the HOMO and LUMO bands. Being able to move the position of these bands would assist in the choice of potential pairs as it will be possible to reduce the size of ΔE_c, the discontinuity in the conduction band. To test this hypothesis, molecular calculations were carried out on H_2Pc, $H_2Pc(CN)_8$ and H_2PcF_8. i.e.

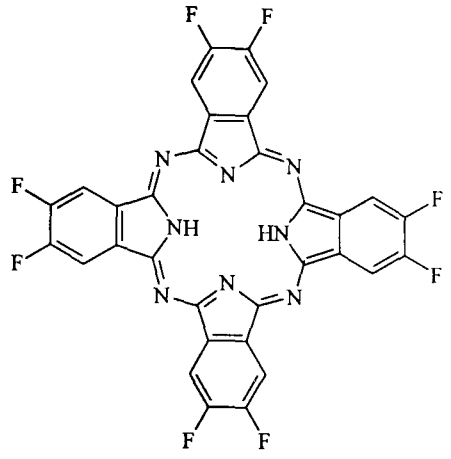

H_2PcF_8

On each benzene ring, 2 hydrogen atoms were replaced by fluorine atoms (C-F distance of 1.30Å) or a CN group (with a C-C bond distance of 1.44Å and a C-N distance of 1.158Å). The replacement of the hydrogen atoms with fluorine atoms or cyanide groups should not alter the ordering of the energy levels dramatically but it will mean that the energy of the levels will shift. As both act as electron withdrawing groups, it is expected that substitution would lower the position of the HOMO and LUMO whilst keeping the band gap approximately constant. The calculations were performed using the optimised formula for the off-diagonal elements. This idea has been attempted practically as Anderson et al[138] made a rectifying p-p junction between CuPc and $CuPcF_8$. This system exhibited rectifying behaviour in which the forward bias existed when the $CuPcF_8$ side is positive. This would happen if fluorination lowers the ionisation potential. Molecular orbital calculations using the all-electron DV-Xα have been done on $Si(Pc)(OH)_2$, $Si[Pc(CN)_8](OH)_2$ and $Si(PcF_8)(OH)_2$ by Hale et al[137] (using a C-F bond length of 1.328Å, C≡N of 1.14Å and C-(C≡N) of 1.45Å) though the authors note that there is no experimental evidence to test their results against. Their calculated ionisation energies are shown in table 5.4. The authors did note that their was an increase in the optical absorption transition (i.e. the HOMO to LUMO band gap) with substitution.

Molecule	Ionisation energy (HOMO)/ eV	Calculated optical transition, nm (expt)
$SiPc(OH)_2$	**6.8**	**673 (671)**
$Si[Pc(CN)_8](OH)_2$	**8.1**	**685 (690)[a]**
$Si(PcF_8)(OH)_2$	**8.8**	**756 (730)[b]**

Table 6.4: Calculated Ionisation energies for substituted phthalocyanine molecules using the discrete-variational local exchange (DV-Xα) formalism where (a) is for $Zn[Pc(CN)_8]$, (b) is for $NiPcF_{16}$.

An energy level diagram displaying the results is shown in fig 6.11. The results show that peripheral substitution does cause a shift in the position of the energy levels around the band gap with only minor changes to the band gap. It shows that the position of the HOMO is raised by 0.240eV with the LUMO raised by 0.249eV for H_2PcF_8. For $H_2Pc(CN)_8$, the HOMO was lowered by 0.090eV with the LUMO lowered by 0.280eV. One possibility that needed eliminating was that the addition of the fluorine atoms significantly changed the coordinates of the rest of the phthalocyanine molecule. No information could be found on the structure of either H_2PcF_8 or $H_2Pc(CN)_8$, so the structures of H_2Pc, H_2PcF_8 and $H_2Pc(CN)_8$ were optimised using MOPAC. The results showed that these peripheral substitutions had little effect on the bond lengths within the phthalocyanine molecule (changes were <0.02Å) so eliminating this possibility.

MOPAC calculates the ionisation potential of the geometrically optimised molecule using the AM1 Hamiltonian. The results of these calculations, ones using the EH method and those by Hale et al are shown in table 6.5. The three methods agree that the octocyano phthalocyanine will have a larger ionisation potential than the unsubstituted one, though the EH method indicates a small increase whereas the other methods indicate a much larger effect of about 1.3eV. The octofluoro phthalocyanine has a lowered ionisation potential predicted by the EH method which is contrary to the other methods which

show an increased value. However, the two methods disagree over the size of the effect with the AM1 method showing less of a change than for the octocyano phthalocyanine. In the EH method, the results for the octofluoro phthalocyanine could be simulated if the values for the fluorine basis set is changed.

molecule	DV-Xα[a]	EH	AM1
H_2Pc	**6.8**	**10.60**	**7.17**
H_2PcF_8	**8.8**	**10.36**	**7.85**
$H_2Pc(CN)_8$	**8.1**	**10.69**	**8.40**

Table 6.5: The calculated ionisation potentials (in eV) for the peripherally substituted phthalocyanines using different methods. (a) calculations performed on the silicon dihydroxide phthalocyanine[137].

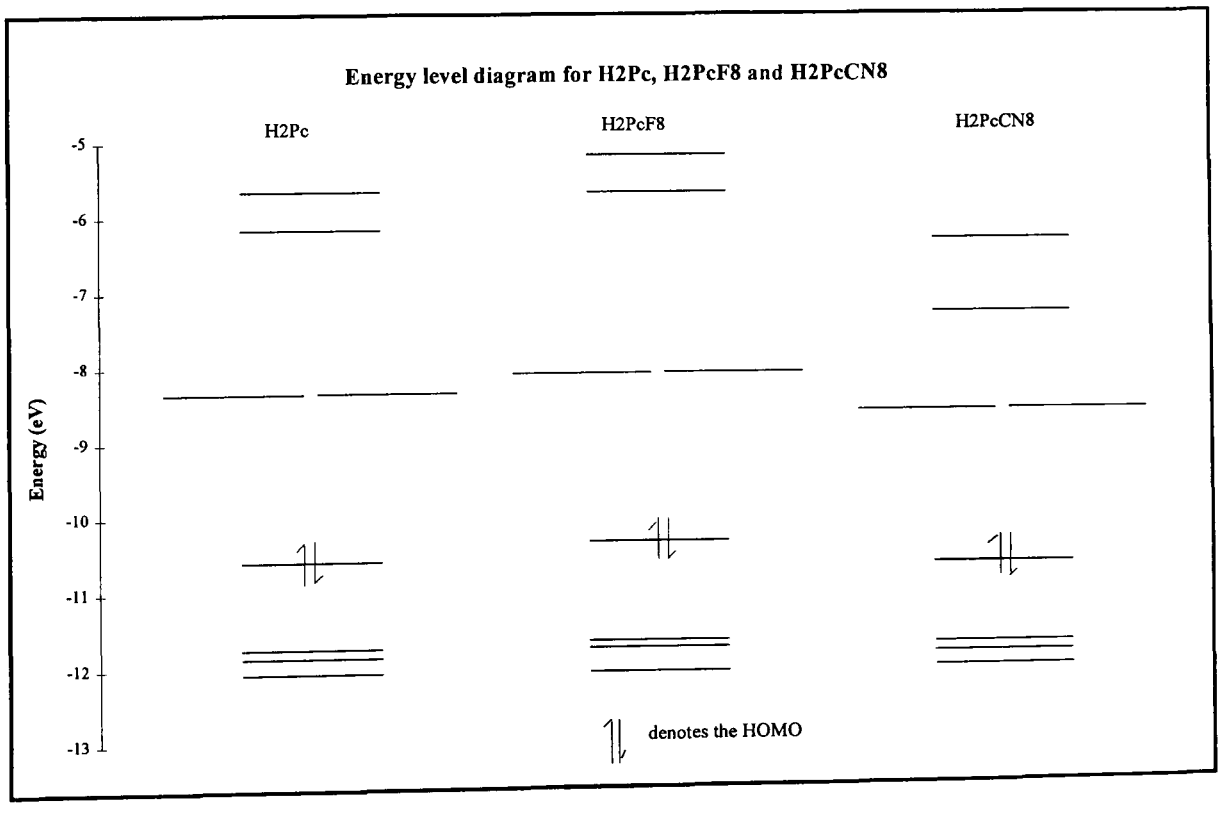

Fig 6.11: Energy level diagram for metal free phthalocyanine, octofluoro metal-free phthalocyanine and octocyano metal-free phthalocyanine calculated using the EH method.

As there is little experimental evidence to confirm any of the predicted values quoted above, it is impossible to make comments on the success of any of the methods. The direction of rectification in a junction formed between CuPc and $CuPcF_8$ does indicate that fluorine substitution will increase the ionisation potential[138]. Practical measurements using UPS on the HOMO peak for various substituted phthalocyanines have been reported by Schlettwein et al[139]. These showed that the HOMO peak was lowered in energy for thin films of $CuPc(CN)_8$ compared to CuPc by 0.5eV. This indicates that none of the theoretical techniques effectively demonstrate the effects of substitution.

6.7 Structure of the HOMO and LUMO for a phthalocyanine

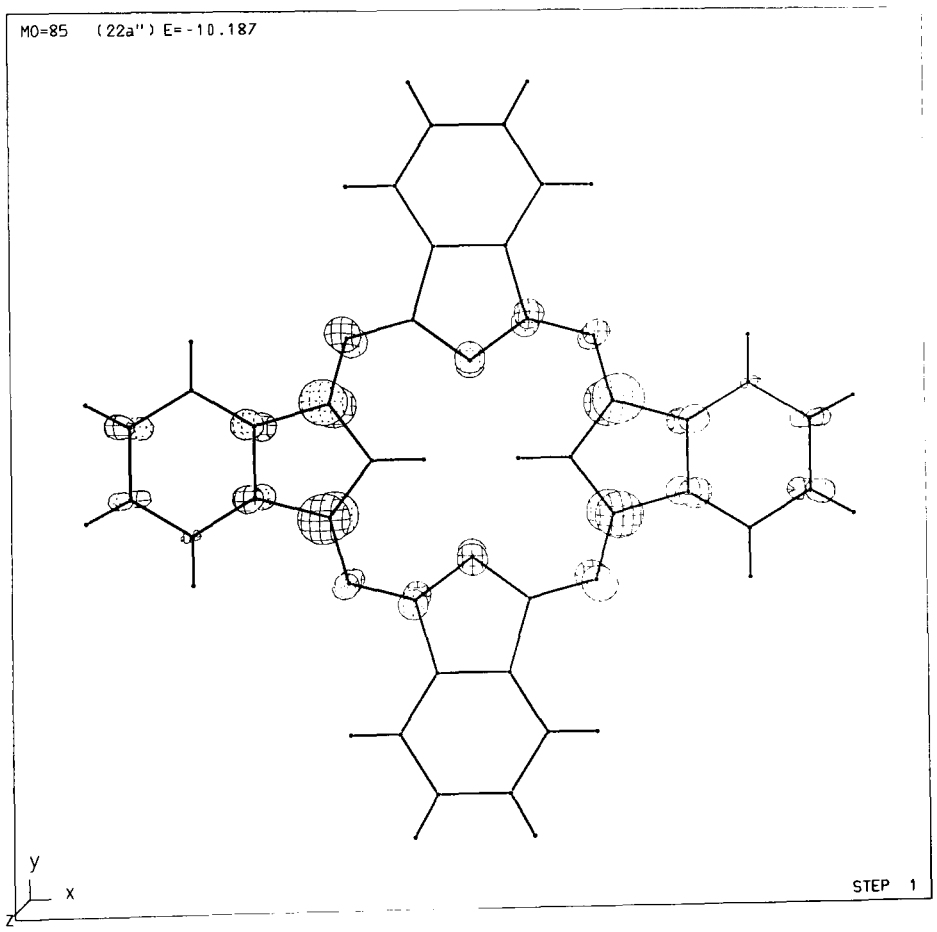

Fig 6.12: LUMO of H_2Pc

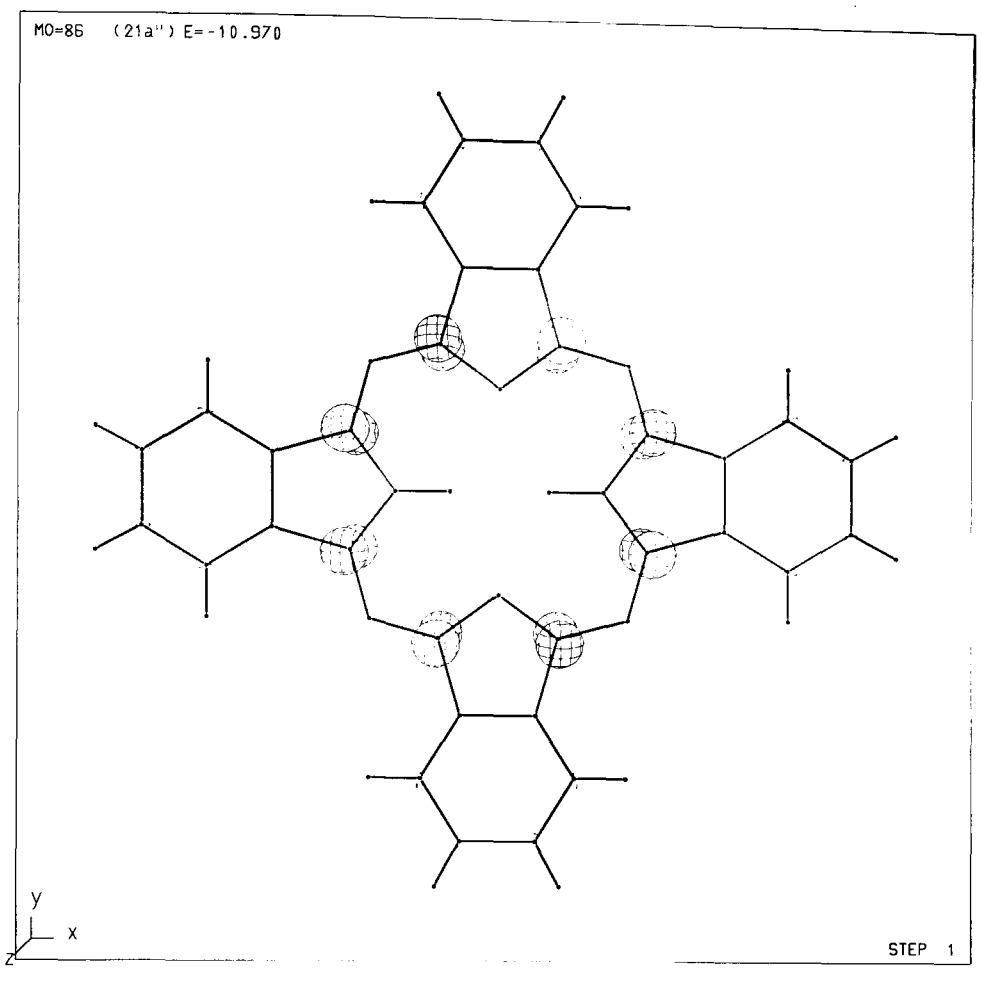

Fig 6.13: HOMO of H_2Pc

The structure of the HOMO and LUMO for metal free phthalocyanine (calculated using the single zeta Slater type orbitals and the weighted Wolfsberg-Helmholtz formula for the off-diagonal elements) are shown in figs 6.12 and 6.13. Note the nodes in the HOMO and LUMO. Notice also that the LUMO level is doubly degenerate, hence the nodal diagram has two equivalent patterns. When the calculation is repeated using titanyl phthalocyanine (TiOPc), the structure of the HOMO and LUMO are largely unchanged.

6.8 Band structure of alpha and beta metal-free phthalocyanine

The structure of phthalocyanines was first reported in 1935 when it was studied by x-ray diffraction measurements. Three polymorphic forms of metal-free phthalocyanine are known and they are referred to by the letters α, β and χ. The electrical properties of the different forms are known and whilst they are

dominated by the relative ability to absorb oxygen, it is of interest to see any differences in band structure and see if they are of any relevance. It is found that the α form has a much greater dark conductivity and its photoconductivity is 10^5 greater than the β form. The electronic structure of β-H_2Pc has been done before using the Pariser-Parr-Pople method and SCF method[113]. From these, the author found that the bandwidth was of the order of 100meV for electrons and 10meV for holes and that the bandwidth was largest in the b^{-1} direction.

Calculations were done on 1D stacks of α and β metal free phthalocyanine. The structures of α and β H_2Pc form a dog-tooth pattern which can be simplified to a 1D slipped stack as the largest intermolecular interactions will occur between the molecules that stack face to face. The α form stacks with the molecules at an angle of 23.7° to the normal with an intermolecular distance of 3.78Å. This corresponds to a stack where the atoms are 3.48Å apart, which has been slipped by 1.48Å in the direction between two benzene rings. Similarly, the β form can be modelled to a stack with molecules 3.43Å apart, slipped by 3.43Å. These calculations were performed using the optimised distance dependent off-diagonal elements formula. The results are shown in figure 6.14

The first thing to notice is the respective size of the conduction and valence bands. For the α form, the conduction band is larger than the valence band. This is also the case for the β form, though the opposite is true for a 1D stack as is the case for the cofacially stacked phthalocyanines. This can be understood by looking at the nodal pattern of the HOMO and LUMO for metal free phthalocyanine (see Figs 6.12 and 6.13). The nodal character of the HOMO and LUMO orbitals determines the oscillations in the bandwidth. Notice that the HOMO is created from only the porphyrin ring in the middle whereas the LUMO has a significant contribution form the benzene rings. For the valence band, when the phthalocyanine molecules stack cofacially, there is a large overlap between the two porphyrin rings resulting in a large bandwidth. As the stack is slipped, the amount of overlap between the nodes decreases rapidly resulting in a reduced bandwidth. With the conduction band, when the

stack is slipped, the overlap decreases more slowly than for the HOMO due to the contribution of the benzene rings. Thus as the offset increases, in going from a cofacially stacked phthalocyanine to the α then β forms, the relative sizes of the HOMO and LUMO change so that the LUMO is the larger in the β form. The overall size of the bandwidths is smaller in the β form due to the reduced overlap coming from the larger stacking angle.

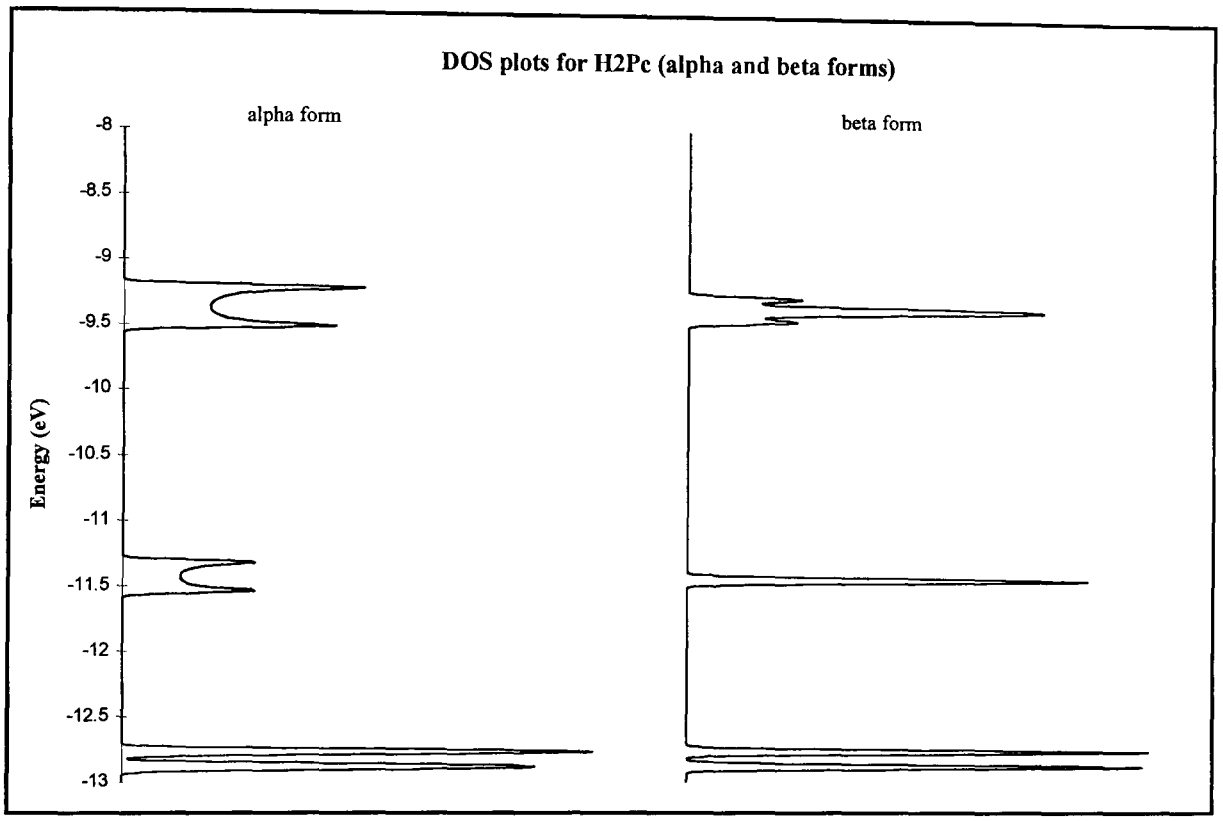

Fig 6.14: Band structure of α and β metal free phthalocyanine

6.9 Variation of bandwidth with overlap

The variation of bandwidth with inter-ring separation for a chain of cofacially stacked phthalocyanines was calculated. The bandwidths of these materials have been measured by several authors, with a trend between the bandwidths and inter-ring spacing being noted by Willis[140]. These metallophthalocyanines have a bridging ligand between the phthalocyanine rings making the materials stack as a linear chain (see fig 6.15). The phthalocyanine molecules can stack so that the benzene rings are directly above each other (the eclipsed formation) or staggered by an angle. Different metals and bridging ligands alter the distance between the phthalocyanine rings hence also the amount of π–π

overlap between adjacent rings. This will then change the size of the bandwidths. To model this situation, a series of calculations were performed on an eclipsed and a stack staggered by 45° of metal free phthalocyanine where the inter-ring separation was varied between 3.2 and 3.9Å. The results generated were then compared with experimental data (see Fig 6.16).

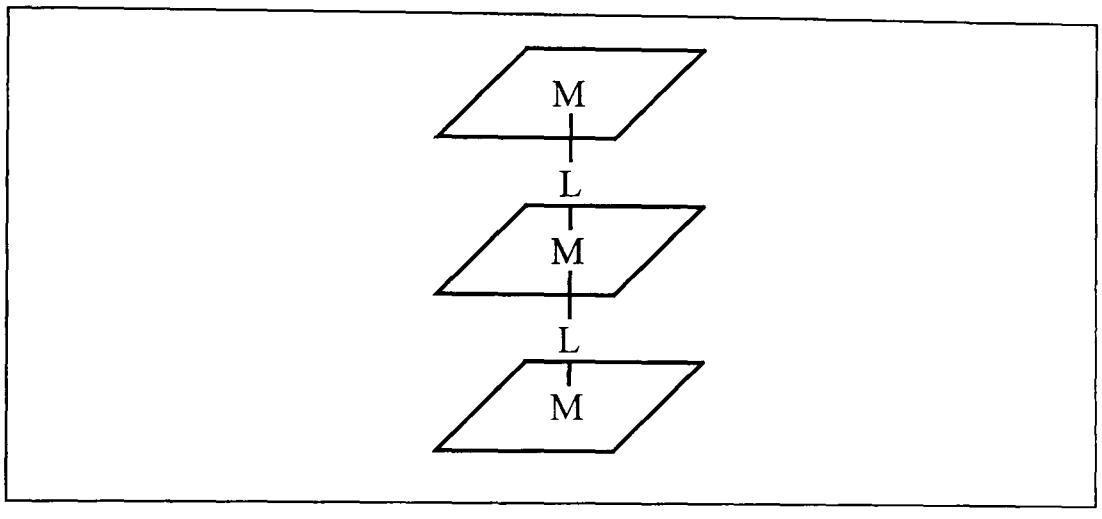

Fig 6.15: Structure of a cofacially stacked phthalocyanine

A comment is needed on the collection of the experimental data. The bandwidths were calculated from the IR reflectance spectra and then fitted using either the Drude or the Lorentz equation. Fujimoto[141] showed that a better fit resulted from using the Lorentz model and this has been used on AlFPc (separation 3.66Å) and GaFPc (separation 3.82Å) whereas previously the Drude model was used. Hence, the values of some of the values for the bandwidth at low inter-ring separation may be artificially high (i.e. the point at 3.24Å). There is also a large error involved with the experimental measurements of the bandwidth. It is known that AlFPc and GaFPc stack in an eclipsed formation.

The results of the calculation show a good fit between the experimental data and the trend predicted by the calculations. This shows that the form of the orbitals is correct in the 3-4Å range, which is the important part when considering the intermolecular overlaps which determine the bandwidths. This

shows that the EH method can provide useful insight into the solid state properties of materials and not just molecules. Whilst the calculation were performed using the weighted Wolfsberg-Helmholtz formula, it is important to remember that the form used for the off-diagonal elements is irrelevant as long as the resulting energy of the HOMO is constant. The variation is purely due to the change in the overlap matrix resulting from the different inter-ring spacing. To change the slope of the line on the graph, it is necessary to alter the coefficients and exponentials in the atomic orbitals so that the energy of the HOMO/LUMO are varied.

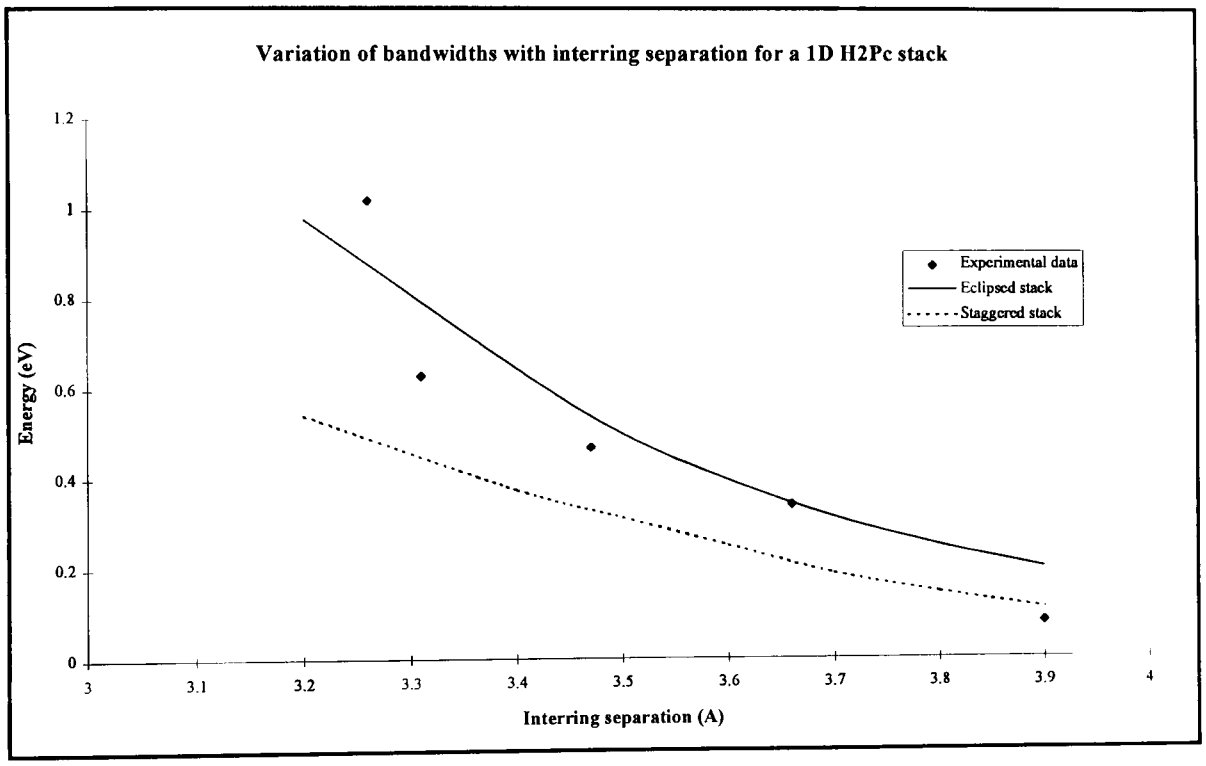

Fig 6.16: Graph demonstrating the variation of bandwidth with inter-ring spacing for a 1D stack of metal free phthalocyanine.

6.10 Simulating the Photoelectron Spectra of H_2Pc

To simulate the photoelectron spectra of H_2Pc, a calculation of the band structure of the material was completed. In the output, the bands were convoluted with a gaussian of width 0.6eV in order to broaden the bands to simulate the low resolution obtained practically. The band edge is taken to be the edge of the HOMO band. In the band calculations so far, we have only been interested in the position and bandwidth of the valence and conduction bands.

As a PES looks at the sigma bonded orbitals, this is another test of the method. The predicted spectra for a 1D stack of H_2Pc (d=3.66Å) and the one obtained practically for AlFPc are shown in figure 6.17

The predicted spectra matches the shape of the experimentally obtained spectra very well, though the values of the binding energy are incorrect. However, the ratio of the energy that the peaks appear at is constant (i.e. at energies of 2.6eV, 5.0eV and 7.5eV experimentally and at 3.3eV, 6.3eV and 9.1eV theoretically from the band edge). In order to more correctly simulate this spectra, the parameters could be optimised again. However, other simulations[133] of these spectra have also used a constant to multiply the energy scale.

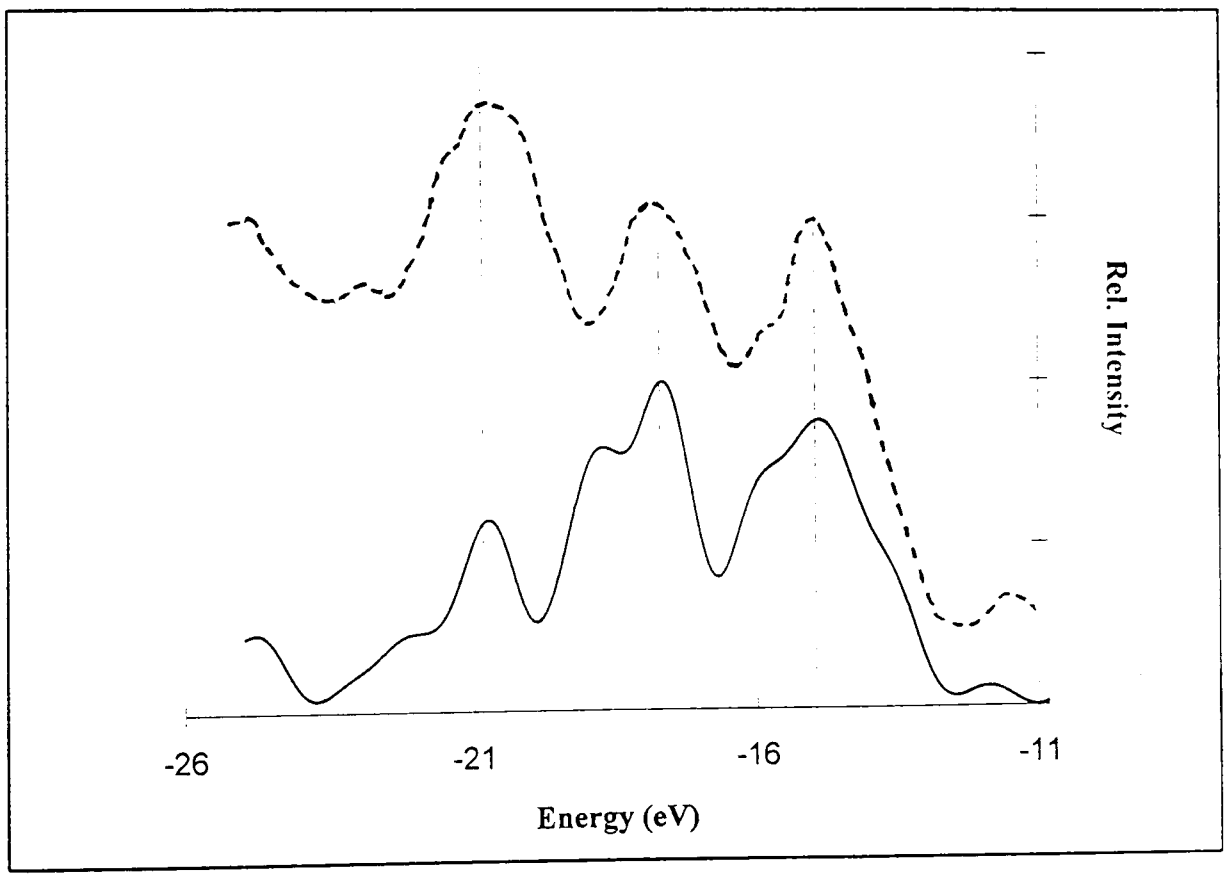

Fig 6.17: Simulated PES for a 1D H_2Pc stack (solid line). The energy axis is multiplied by 1.25 for the experimental spectrum (ref 152) in the dotted line.

Chapter 7:- Discussion

7.1 Applicability of band theory to organic thin films

Band theory is based on the assumption of a perfectly ordered crystalline lattice. Sublimed organic films are polycrystalline or amorphous. The effect of this disorder is to broaden the bands. In other respects, the band structure and location of the Fermi level are largely unaltered. Thus equilibrium properties, which are required for the formation of a p-n junction are similar.

The major difference between ordered and disordered semiconductors lie in their transport properties. In an ordered semiconductor, such as silicon, where conduction can properly be described by the band model, the mean free path is greater than the lattice spacing and the mobility is >1 $cm^2\ V^{-1}\ s^{-1}$. In an organic single crystal, the mobility is typically ~1 $cm^2\ V^{-1}\ s^{-1}$, which implies that such materials are on the borderline for the applicability of band theory. In amorphous or polycrystalline organic films, the mobility is typically 10^{-4}-10^{-6} $cm^2\ V^{-1}\ s^{-1}$, which places it outside the applicability of band theory. Thus, tunneling, hopping between traps and polaron models must also be considered.

To summarise, it is proper to discuss junction formation in band terms, but some caution must be exercised when discussing bandwidths and conduction mechanisms.

7.2 The nature of the junction

Previous authors have commented that organic bilayer solar cells are similar to p-n junctions. Whilst this idea can explain why a voltage is generated, it is not the most accurate description of the interface between two organic semiconductors. A classical p-n junction is formed between an intrinsic semiconductor that has been doped with an acceptor on one side and a donor on

the other to make the layers act as n-type or p-type respectively. When two different materials are used, as in the heterojunction case in inorganic systems, the positions of the conduction and valence bands as well as the Fermi level have to be considered. In inorganic heterojunctions where the lattices are highly ordered and if there is good lattice matching between the two materials, discontinuities in the conduction band can be seen as spikes in an I-V plot[16]. For organic semiconductors, where conduction mechanisms are less accurately described by the band model, predictions of the carrier flow through the junction are less valid. However, it is still possible to predict that discontinuities at the junction will impede carrier flow though more quantitative predictions are inappropriate. Thus when considering potential pairs it is necessary to consider not only the positions of the Fermi levels (i.e. choosing an electron acceptor and a donor molecule) but also the positions of the bands.

According to equation 2.3, the magnitude of V_{bi} for a heterojunction is dependent upon the difference in the Fermi levels in the two materials and is unaffected by the magnitude of any discontinuities in the conduction or valence band. So, a junction between two materials with the same Fermi level should not produce a voltage. However, a chemist's view of such a junction is different. If an electron was excited at the interface (molecule (b) in Fig 7.1), then it is energetically favourable for it to move on to molecule (c) rather than molecule (a). This would then result in a photovoltage being produced.

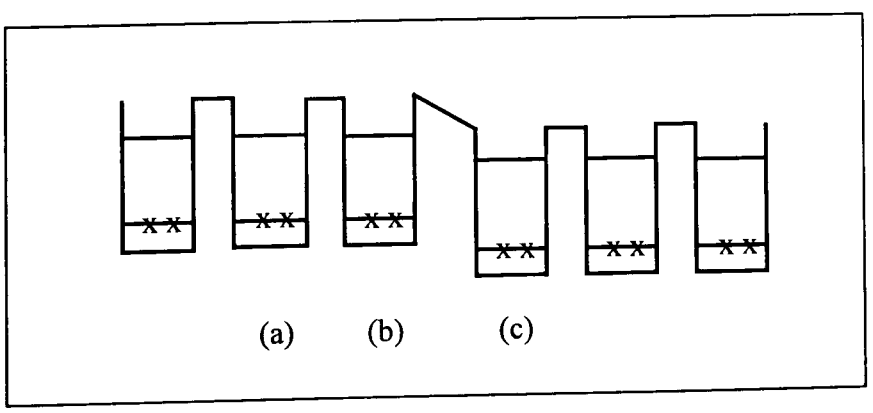

Fig 7.1: A molecular view of a p-n junction

As the size of the discontinuities in the conduction and valence band could be different, this would cause the size of V_{oc} to vary when the sample is illuminated through either electrode. This view only considers the molecules that lie next to the interface and provides no mechanism for carrier separation elsewhere in the system. This limits the efficiency drastically as a monolayer with an absorption coefficient of $\alpha = 1.5 \times 10^5$ cm^{-1} will absorb only 0.5% of the incident photon flux. Thus, the field created by the movement of charge when the Fermi levels equalise will more efficiently separate photogenerated charge carriers so only this process need be considered.

In the inorganic system, heterojunctions are usually designed so that the front layer has a large band gap (E_{G1}) and the second layer has a narrow band gap (E_{G2}). Thus when the sample is illuminated, light with energy less than E_{G1} and greater than E_{G2} will be absorbed in the depletion region and separated as in a p-n junction cell. Light of energy greater than E_{G1} will be absorbed by the front layer and carriers generated within a diffusion length of the junction or in the depletion region will be collected. This makes heterojunctions more efficient than p-n junctions as heterojunctions show enhanced short wavelength spectral response.

When choosing a potential pair for an organic solar cell, complimentary absorption spectra has always been an important criteria. This allows light which was strongly absorbed by the second layer to pass through the first to be absorbed at the interface of the two. As is the case with heterojunctions, light which is absorbed by the front layer only contributes if the exciton diffuses to the depletion region. As the exciton diffusion lengths are short in organic thin films, the contribution from this process is usually small. Thus the device is considerably more efficient at some wavelengths when compared to others. So to improve the efficiency of organic cells, a cell with a front layer that has a large band gap (i.e. transparent) and a second layer which absorbs large amounts of the visible spectrum (i.e. black) is preferable. As large band gap materials are usually highly resistive, it is common to dope the front layer to

improve the conductivity. When choosing the dopant, it is important not to affect the front layers light transmission characteristics and remember that any effect on the Fermi level of the material will change the size of V_{bi}.

7.3 Comparison of experimental results with the calculations

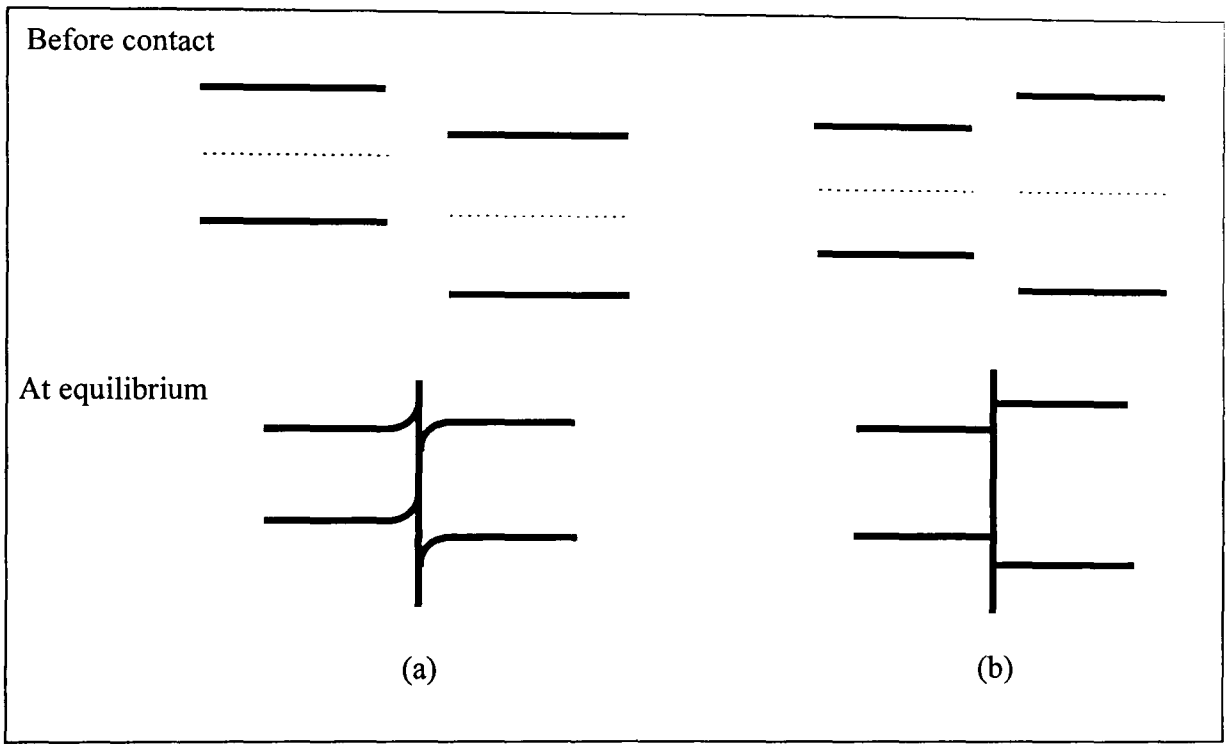

Fig 7.2: The junctions formed between two intrinsic materials where the Fermi levels are (a) different and (b) equal.

In the results chapter, models were proposed for the junctions formed between the different layers. It is also possible to propose junctions based on the EH calculations by assuming the position of the Fermi level. If we use highly pure materials and assume they behave as intrinsic semiconductors (i.e. that they are undoped, be it deliberately or accidentally by air) then the following junctions can be drawn. If the position of the Fermi levels are different, then discontinuities form in the conduction and valence bands which will hinder the flow of electrons and holes (fig 7.2a). Whilst this system is expected to show rectification (and would behave like a p-p isotype heterojunction), the separation of charge carriers will be poor so reducing its photovoltaic

efficiency. If the position of the Fermi levels is equal then a barrier is formed as in fig 7.2b. In this case the barrier acts to send generated holes and electrons in the same direction so failing to separate them. So even if the position of the bands are shifted, there is no position that will separate charge carriers without generating discontinuities. This shows that for a bilayer junction to efficiently separate the generated charge carriers, the two materials must be extrinsic. This is akin to the chemical view where a junction is only formed if one of the materials is a donor and the other is an acceptor.

If we now consider the junction formed between two extrinsic materials. Even under ultra-high vacuum conditions, the presence of impurities and oxygen cause the materials to behave extrinsically resulting in the Fermi level shifting from the middle of the band. The largest values of V_{bi} result when an n- type and a p- type material are brought into contact. To be able to draw out accurately the resulting junction, the positions of the Fermi levels within the materials need to be known. These have been determined by thermoelectric measurements of the Seebeck coefficient for thin films of zinc phthalocyanine (ZnPc) and dimethyl tetracarboxylic acid diimide (MPCI) by Meyer et al[142]. A search of the literature did not reveal similar studies on DBA or any squaraines, though it is known that squaraines behave as p-type semiconductors[22] and DBA as an n- type semiconductor[96].

7.3.1 Perylene tetracarboxylic acid derivative/phthalocyanine junction

Meyer et al[142] found that the Fermi level was 0.31eV above the valence band for ZnPc (making it a p-type conductor) and 0.14eV below the conduction band for MPCI (making it an n-type conductor). Using these values and the position of the HOMO/LUMO calculated using the EH method a junction can be formed (see fig 7.3).

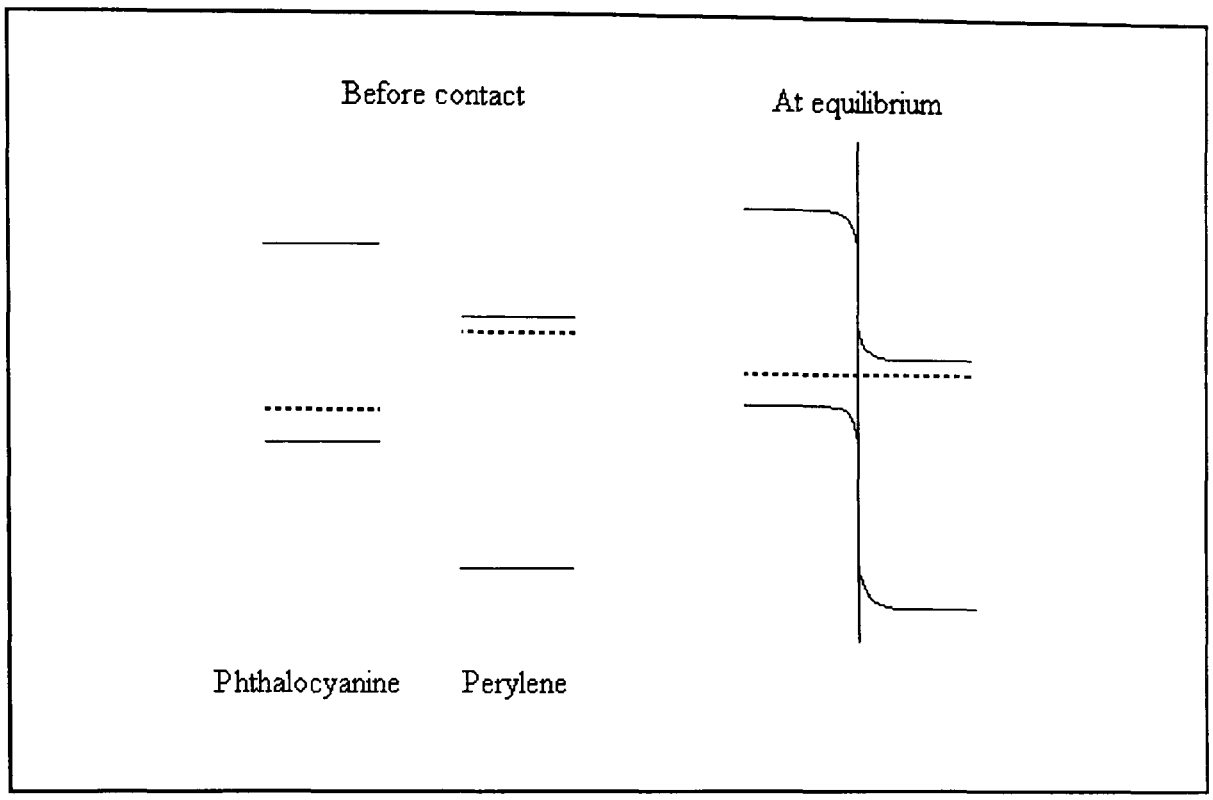

Fig 7.3: Phthalocyanine/Perylene junction based on EH calculated band structures

Thus when an exciton dissociates at the interface of the two layers, the electron and hole are separated by the internal field at the junction. The electron travels towards the perylene layer and the hole towards the phthalocyanine layer making the perylene layer/ITO electrode negative. Another point to note is that the width of the depletion layer in this picture is arbitrary.

From the diagram, it is possible to estimate V_{oc}. The HOMO for the phthalocyanine layer is at -10.60eV with the LUMO for MPCI at -9.39eV. These are the results from a molecular calculation and so take no account of the bandwidths of the materials. Our calculations show that the bandwidth of a phthalocyanine in a thin film (e.g. the bandwidth of the α- or β- form) is ≈0.20eV. Using this bandwidth for MPCI allows us to predict the onset photoionisation potentials as follows: HOMO for the phthalocyanine layer -10.50eV and the LUMO for the perylene layer -9.49eV. Thus by using the positions of Fermi levels for ZnPc and MPCI quoted above gives the following values for the Fermi level in our calculated model: E_F at -10.19eV for the phthalocyanine and E_F at -9.63eV. This gives a value of 0.56eV for V_{bi}. This

compares with the values of between 0.35eV and 0.53eV for V_{oc} obtained experimentally. As expected, the values of V_{oc} are less than those for V_{bi} as V_{bi} is the maximum possible voltage and takes no account of any mirror charges that might build up and oppose the junction or the high series resistance which can reduce V_{oc}.

The shape of the junction is very similar to the one deduced by Sato et al[143] based on the measurement of ionisation potentials and estimations of the bandgap from the optical absorption (see Fig 7.4). This was measured for an AlClPc/MPCI interface. This experimentally obtained picture is remarkably similar to the diagram proposed above based on the band structures calculated by EH method.

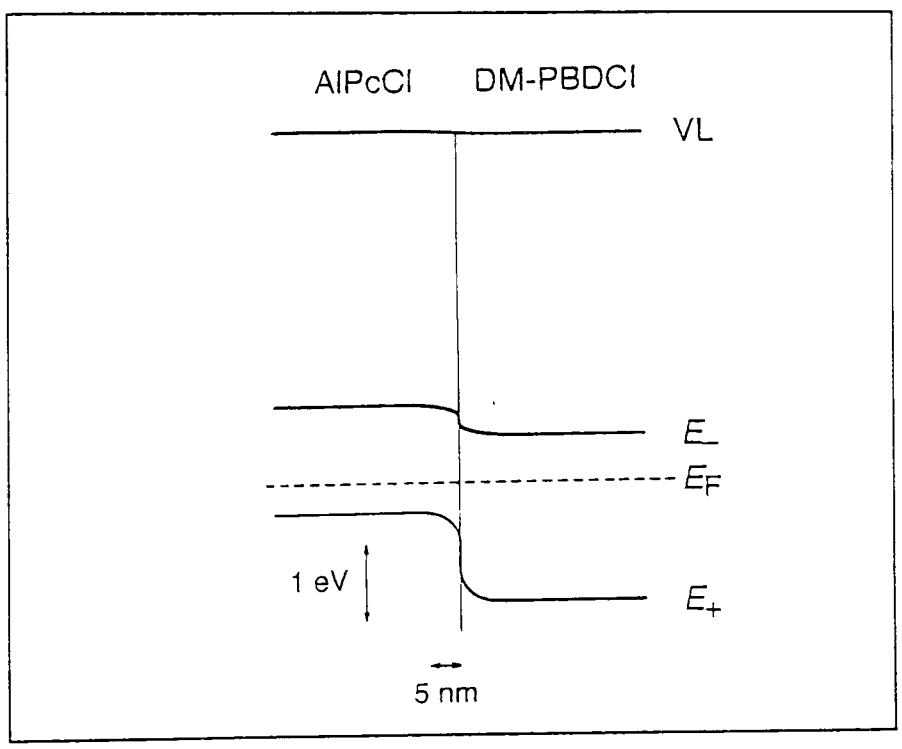

Fig 7.4: Diagram of MPCI/AlClPc junction proposed by Sato[143].

At this point, a comment should be made about the model proposed in the results section to describe the experimental results for the MOPPCI/TiOPc and MPCI/TiOPc devices. In this model, it was stated that the MPCI/TiOPc junction had no built in voltage as there was no rectification in the dark I-V plot. This would be the case if the Fermi levels of the two materials were

similar. As the junction proposed above (fig 7.3) was constructed using values of the Fermi levels of similar materials and the doping was accidental (i.e. due to impurities in the air like O_2, H_2O etc.), it is possible that the Fermi levels were different to those quoted above. When changing the perylene derivative to MOPPCI, the I-V plot showed rectification in the dark. The change in endgroup will have altered the position of the HOMO/LUMO and the doping characteristics so possibly causing a shift in the Fermi level. This could have changed V_{bi} and hence also the dark conductivity.

7.3.2 Anthanthrone/phthalocyanine junction

Another junction studied practically was between DBA and TiOPc. On illumination, the performance of the junction was similar to that of the MOPPCI/TiOPc junction, with the TiOPc acting as the electron donor in both cases. There has been no published data concerning the position of the Fermi level for DBA, though the calculated positions of the HOMO (-11.70eV) and the LUMO (-9.70eV) are similar to those for a perylene tetracarboxylic acid derivative. The polarity of the cell indicates that a junction akin to that drawn for the phthalocyanine/perylene interface exists though as the position of the LUMO for DBA is lower in energy than for the perylene derivative (-9.70eV for DBA and -9.49eV for the perylene derivative), a smaller value for V_{bi} is expected. This correlates with the experimental results as the maximum value for V_{oc} obtained in a DBA/TiOPc cell was 0.39V compared with the value of 0.53V for the MOPPCI/TiOPc cell after annealing.

From the picture of the proposed junction, it should be possible to suggest ways of substituting the base materials to increase the size of V_{oc}. V_{oc} depends mostly on the difference in the Fermi levels of the two materials though when this is small, the size of the discontinuity in the conduction band (ΔE_c) can be used to explain the generated photovoltage. However, junctions which have a large built-in voltage and a small value for ΔE_c will be more efficient because light that is absorbed at the interface will be separated by the junction rather

than relying on diffusing to the junction and being separated by 'falling' over the barrier. This was shown by the improved performance of the MOPPCI/TiOPc cell over that of the MPCI/TiOPc cell. As the former showed rectification in the dark, this implies that the junction showed a built-in voltage unlike the latter which showed no rectification in the dark. To increase the value of V_{bi} requires increasing the difference in the Fermi levels of the two materials. This can be done by doping or substitution. The values found for the Fermi level show that they are already close to the conduction/valence band making the prospect of doping unappealing. Substitution (on the benzene rings of the phthalocyanine, for example) is the other alternative, causing the position of the HOMO/LUMO to move. So if the position of the HOMO/LUMO for the phthalocyanine were lowered without altering the position of the Fermi level with respect to the HOMO, the value for V_{bi} would increase making the junction more efficient and increasing V_{oc}. The same effect will result if the position of the HOMO/LUMO for the perylene is increased.

7.4 Criteria for 'ideal' heterojunction solar cells

The following criteria are recommended for heterojunction solar cell (assuming that the second (absorbing) layer is p- type):

- The absence of conduction band spikes to impede the flow of generated charge carriers (i.e. $\Delta E_c = \chi_2 - \chi_1 < 0$).
- ΔE_c should be as close to zero as possible (to maximise V_{bi}).
- E_{G2} should be in the range 1.4 - 1.6eV for the maximum solar efficiency.
- E_{G1} as large as possible to allow the maximum amount of the solar spectrum to pass.

If the second layer is an n- type material, then substitute ΔE_v for ΔE_c. Fig 7.4 shows three n-p heterojunctions formed where χ_1 is varied.

Fig 7.5b shows the ideal situation where the maximum value of V_{bi} is obtained. Obviously, the largest values are found when the Fermi levels of the semiconductors are as close to the valence/conduction bands as possible. This is dependent upon the nature of the impurity and the position at which they lie within the band gap.

All the criteria listed above can be predicted from the band EH calculations. This allows for a less random approach to the selection of suitable pairs for bilayer cells and then of ways to optimise the system.

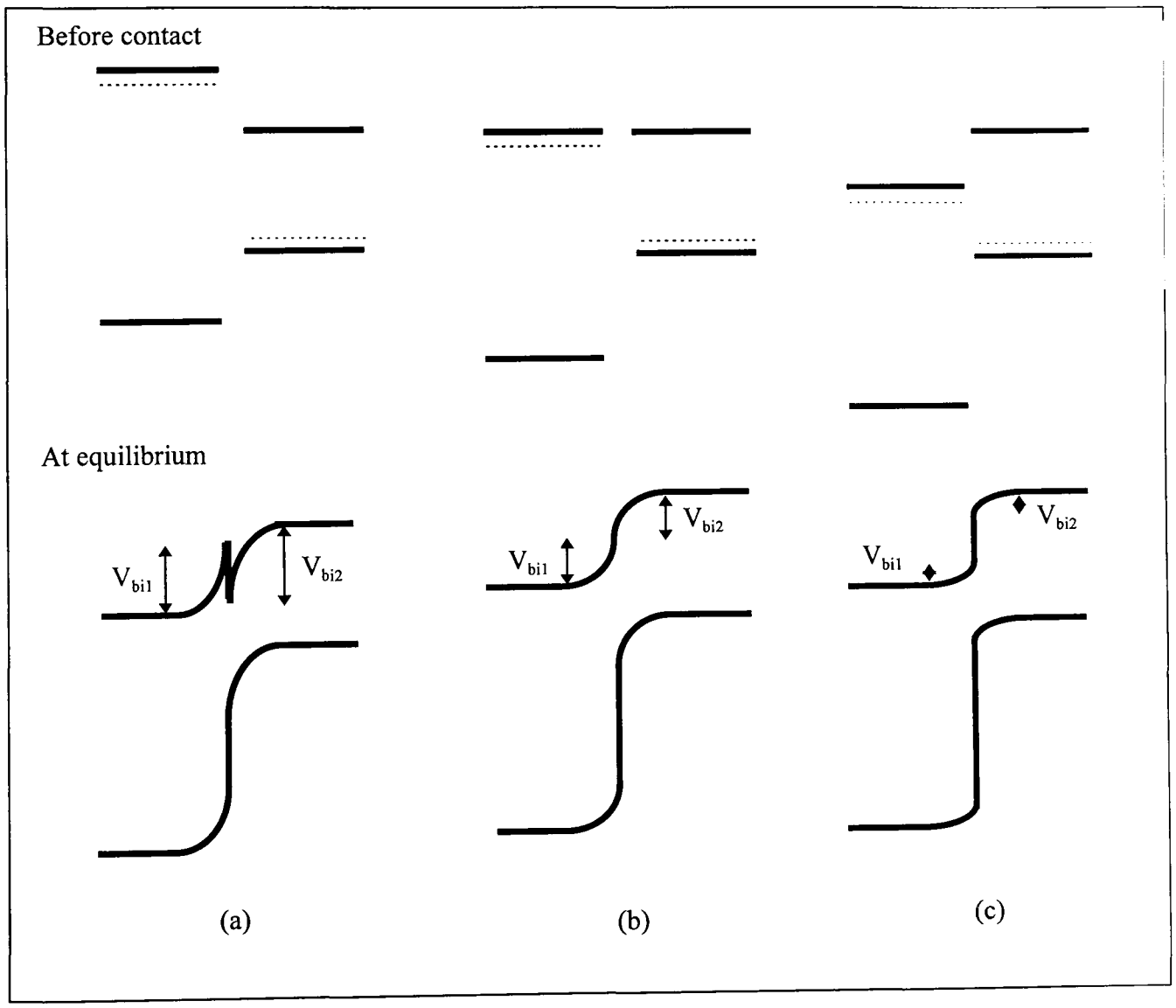

Fig 7.5: Showing effect of relevant positions of the conduction band on the heterojunction formed ($V_{bi} = V_{bi1} + V_{bi2}$)

(a) $\Delta E_c < 0$; a spike in the conduction band is formed which will impede the photogenerated carrier flow through the junction.

(b) $\Delta E_c = 0$; allows maximum value for V_{bi} without impeding carrier flow.

(c) $\Delta E_c > 0$; shows a reduced value of V_{bi}.

In order to obtain the maximum value for V_{oc}, it is necessary to alter the position of the conduction and valence bands. As mentioned in the theoretical chapter, this can be done by peripherally substituting the materials with electron donors or acceptors. The theoretical efforts at predicting the effect of substituting on the position of the energy levels around the band gap using the EH method were not conclusive. However, measurements of ionisation potentials show that the addition of an electron withdrawing group (e.g. -F or -CN) will cause the ionisation energy to increase or in other words lower the HOMO/LUMO. Thus, a junction between a phthalocyanine substituted with an electron withdrawing group and perylene should perform better than one between a phthalocyanine and a perylene by increasing the value of V_{bi}.

To maximise the efficiency of a cell, the effect on J_{sc} of substituting one of the layers must be considered. Substitution could affect the photoconductivity of the molecule. Firstly, it may change the stacking pattern of the molecule, thereby changing the amount of intermolecular overlap/bandwidth of the material so possibly the photosensitivity. Secondly, the amount of accidental doping may change. This is most clearly shown by seeing the effect changing the central metal atom has on the photoconductivity of the phthalocyanines as the influence of the complexed metal ions on the performances of the organic solar cell strictly follows their O_2 binding ability. Therefore substituting an electron donating/withdrawing group may have a similar effect. So to improve the performance of the cell, it is necessary to use a substituted material that alters the position of the bands without adversely affecting the photoconductive properties.

This approach has been attempted practically. Gunster et al[34] completed a series of experiments using different porphyrinic and aromatic tetracarboxylic acid diimide compounds though the authors failed to comment on the results. However the order of the size of V_{oc} was maintained for the diimide compounds when partnered with different porphyrinic partners. A similar study was also carried out by Yanagi et al[45]. They noted that the molecular

modification in p-type phthalocyanine derivatives changed the cell photovoltage. A substitution with electron withdrawing groups, which lowered the HOMO energy of the molecules, increased the photovoltage. It was also noted that an extension of the macrocyclic ring from phthalocyanine to naphthalocyanine lowered the photovoltaic efficiency. Thus the most promising approach for optimising the performance of the perylene/phthalocyanine junctions is to substitute the outer benzene rings of the phthalocyanine molecule so that the HOMO energy is lowered (i.e. substitute with an electron acceptor). This should not adversely affect the electrical properties as the nodal characteristics of the HOMO/LUMO are dominated by the inner porphyrin ring, so largely unchanged by peripheral substitutions.

Increasing the size of V_{oc} is one of the most significant challenges involved in improving the performance of a cell. The energy required to promote an electron across the band gap is greater than 2.0eV for all the materials studied. So if the cell produces a V_{oc} of 0.5V, this means that it can only be 25% efficient even if every photon absorbed generates an electron/hole pair that is separated (c.f. a silicon p-n junction solar cell has a value of V_{bi} =0.94V with the indirect band gap for silicon being 1.12eV). Any increase in V_{bi} will also extend the depletion region further into the semiconductor layer. This allows more absorbed photons to be harvested by the junction. However, the greatest problem is the low conductivity of the materials used that limits the thickness of the layers and the width of the depletion region by reducing the number of free charge carriers. This limits the amount of the incident light that is absorbed by the active part of the device, hence reducing the overall efficiency.

The calculations on DBA and a squaraine show that the position of the HOMO and LUMO for both are similar (-11.70eV and -9.70eV for DBA, -11.58eV and -9.59eV for the squaraine). Thus, the junction between these layers should provide a large value of V_{bi} as there will be only a small ΔE_c. The actual performance of the device was hindered by non-complimentary absorption spectra and a poor choice of electrodes.

7.5 Use of EH calculations for other applications

EH calculations could provide useful information for the choice of materials in other device applications. One such area is electroluminescent cells[144], which convert electricity into light which is the opposite of solar cells. The most promising approach involves a two layer system which uses a hole transport layer (HTL) and an electroluminescent layer (EL).

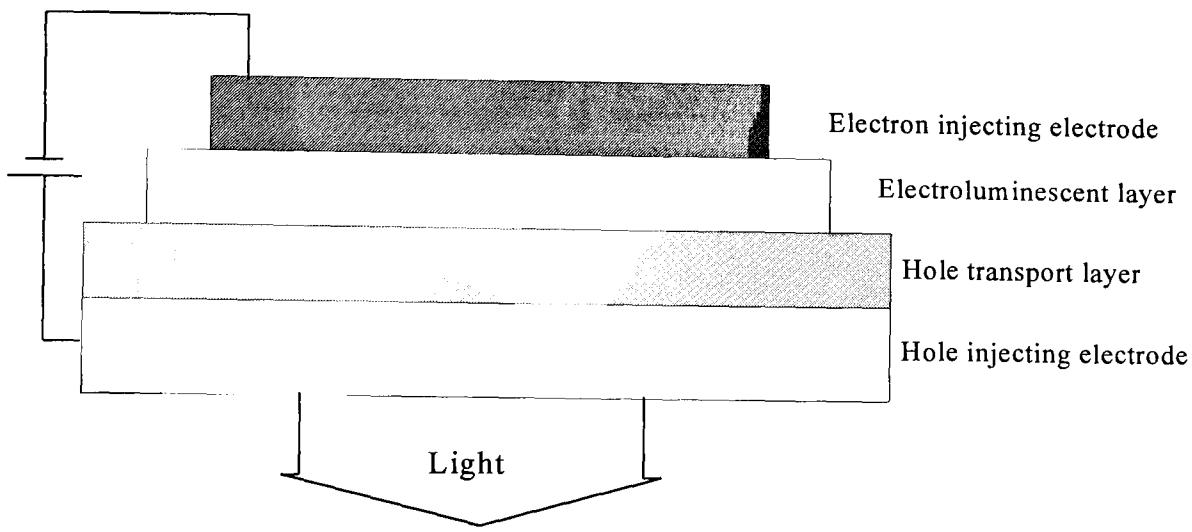

Fig 7.6: Schematic design of a bilayer electroluminescent cell

Holes are injected into the HTL and recombine in the EL with electrons to generate light. For this process to be efficient, there needs to be a high density of free electrons and holes in the EL to increase the recombination rate. So a structure for the junction should demonstrate a mechanism for trapping electrons and holes in the same part of the EL when a voltage is applied.

Fig 7.7 shows the structure of a common bilayer electroluminescent cell. It was constructed using the position of the bands for TPD (a HTL) and Alq_3 (an EL) as measured by Mori et al[145]. This diagram explains the luminescent characteristics of such cells. At low current densities, the device emits light in the EL near the cathode (EIL), as electrons reside in the middle of the band due to the field near the interface. At higher current densities (or applied voltages), the site for the emission moves closer to the interface as the applied voltage causes band bending (effectively, the workfunction of HIL is increased and EIL

decreased which, in turn, increases the ionisation potential of the HTL and decreases the IP of the EL). This leads to electrons building up at the interface as they are stopped by the barrier in the conduction band (a). Hence, the holes that make it into the EL recombine with these electrons.

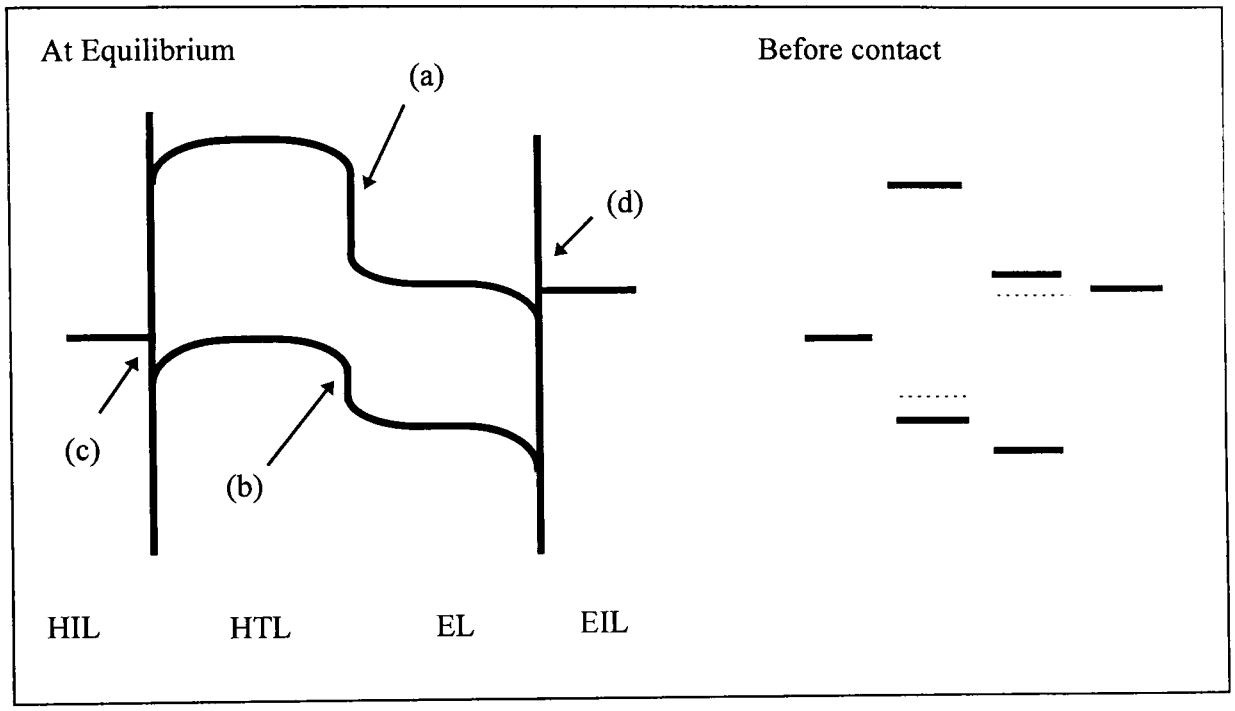

Fig 7.7: Schematic diagram of a bilayer electroluminescent cell

where (a) barrier in the conduction band to prevent electrons entering the HTL

(b) barrier in the valence band (should be much smaller than (a))

(c) barrier contact between HIL and HTL

(d) ohmic contact between EIL and EL.

From the diagram (fig 7.7) for the electroluminescent cell, it appears that to improve the efficiency of the device requires reducing the size of the barrier in the valence band (barrier (b)) to allow the injected holes an easier passage into the EL. This can be done by raising the HOMO energy in the EL or lowering the HOMO energy for the HTL. Matsumura et al[146] did this when they substituted the EL with methyl, chloro and fluoro groups. These substitutions lowered the HOMO energy and a corresponding decrease in efficiency was observed.

7.6 Performance of the cells

Overall, the performance of the cells reported in the results chapter were good though the efficiency was limited by the low fill factors. The production of efficient solar cells is highly dependent upon the quality of the deposited films. Practically, this is a field where experience is as important as the method so the efficiencies of the cells produced increased with experience. This makes direct comparisons between different cells more problematic. The quality of the film largely determines the mobility of charge carriers (i.e. the fill factor and J_{sc}) rather than the electrostatic potential in which they move (leaving V_{oc} largely unchanged). As a result, the discussion is valid as it mostly centres around the position of the bands and how this alters V_{oc}. Another significant affect on the performance of the device was the aging or 'wine cellar' effect. This is thought to be due to atmospheric dopants (probably water) but may include annealing effects, and it can alter the characteristics of some cells dramatically (see cells made from DBA and TiOPc). Again, this is a factor that is hard to control so the devices were tested over several days and the optimum performance reported.

As explained in chapter 2, one reason for the low fill factors is that R_s is too high. If this is the case, then V_{oc} will be smaller than expected as well. It was noticed that in all cases, the fill factors were larger when illuminated through the gold electrode. This could be due to the reduced light intensity reaching the sample due to its low transmissivity or to leakage currents through the TiOPc layer. From the shape of the I-V plots, the reason for the low fill factors when illuminated through ITO is that the gradient of the curve decreases as it crosses the x axis making the I-V plot s-shaped. This is typical of a low value of R_{sh} which causes the I-V plot to tend to a maximum of $1/R_{sh}$ at applied voltages greater than V_{oc} or of a poor semiconductor-metal contact. To increase R_{sh} (which is ideally equal to infinity) requires reducing the surface leakage currents. This could be done by improving the quality of the films so reducing the number of pinholes in either layer which results on the electrodes contacting through only one layer.

Efficiency losses due to non- or quasi-ohmic contacts are often overlooked. The creation of true ohmic contacts in practice is something of a black art. Indeed, one author[147] commented 'the history of ohmic contacts is still rather like that of a primitive society as it consists mostly of unrecorded reports passed around informally among experimenters...'. The most significant cause for non-ideal ohmic contacts is the effect of surface states in the semiconductor. These cause the 'pinning' of the Fermi level of the semiconductor at a distance above the valence band and can create contacts with an electron barrier when an ohmic contact is expected.

The efficiency of the cells for device purposes is still low with the best efficiency measured being 0.30% for the DBA/TiOPc cell (against intensity of incident light). Owing to the intensity dependence of the short circuit current, this value is lower than several other values quoted as this is for incident white light at 20mW/cm^2. The efficiency of a similar cell in room light (100 μW/cm^2) would be greater.

The annealing of the MOPPCI/TiOPc device had a significant effect on its performance. This wasn't repeated on the other samples because the improvement was attributed to the reordering of the molecules in the TiOPc layer. The action spectra of the other cells made with TiOPc all showed that the phthalocyanine layer was not largely amorphous so annealing of these was not attempted.

From the xerographic data, it was expected that the squaraine would be a promising partner in bilayer solar cells and it had performed well in a Schottky cell. The practical results showed that the cells did not perform exceptionally, though it is unclear whether this was due to the unavailability of a suitable partner or that the squaraine used was not pure enough. As mentioned in chapter 3, the xerographic properties are highly dependent on the purity of the squaraine with the photosensitivity varying with different synthetic routes. So whilst the squaraine used had already been sublimed twice, the purity of the

sample could have been low enough to reduce the photosensitivity significantly. Squaraines still deserve further investigation as they have the advantage of being able to adjust the position of the HOMO/LUMO without significantly affecting the photoconductive properties. This is possible because the stacking pattern is dominated by the anilino group substitutes whilst the phenyl ring substitutes change the positions of the HOMO and LUMO. This makes it easier to optimise a system to get the largest value for the open circuit voltage.

7.7 Response time of cells

The response time of the TiOPc layer was measured in different cells and compared to the efficiency of the device. As the response time is linked with the mobility of the charge carriers and hence also the amount of traps in the TiOPc layer, it should give an insight into the quality of the device made. Firstly, the efficiency of different cells made with TiOPc and a partner (acting as the n-type layer) were compared with the response time. ITO and Au were the electrodes in all cases and the organic layers were 500Å thick. These were measured using monochromatic light (λ=670nm) with the TiOPc layer as the second (absorbing) layer. The results are shown in Table 7.1

Partner	Efficiency (%)	Response time (ms)
MPCI	0.029	4.1
MOPPCI	0.074	0.33
DBA	0.30	0.20
BTDA	0.019	0.37

Table 7.1: Showing the response times and efficiencies of cells made with TiOPc and tested using the 670nm laser.

The results show that there is a strong link between the response time of the sample and the device efficiency. If the sample has a slow response time, then

it shows that the generated charge carriers are being separated slowly, implying that there is a small internal field at the junction or that the mobility of the charge carriers is low. The former implies that the device choice of partners is poor as an inefficient junction is formed. The latter implies that the quality of the device made is poor (i.e. the materials used are impure or that the metal-semiconductor contact is poor).

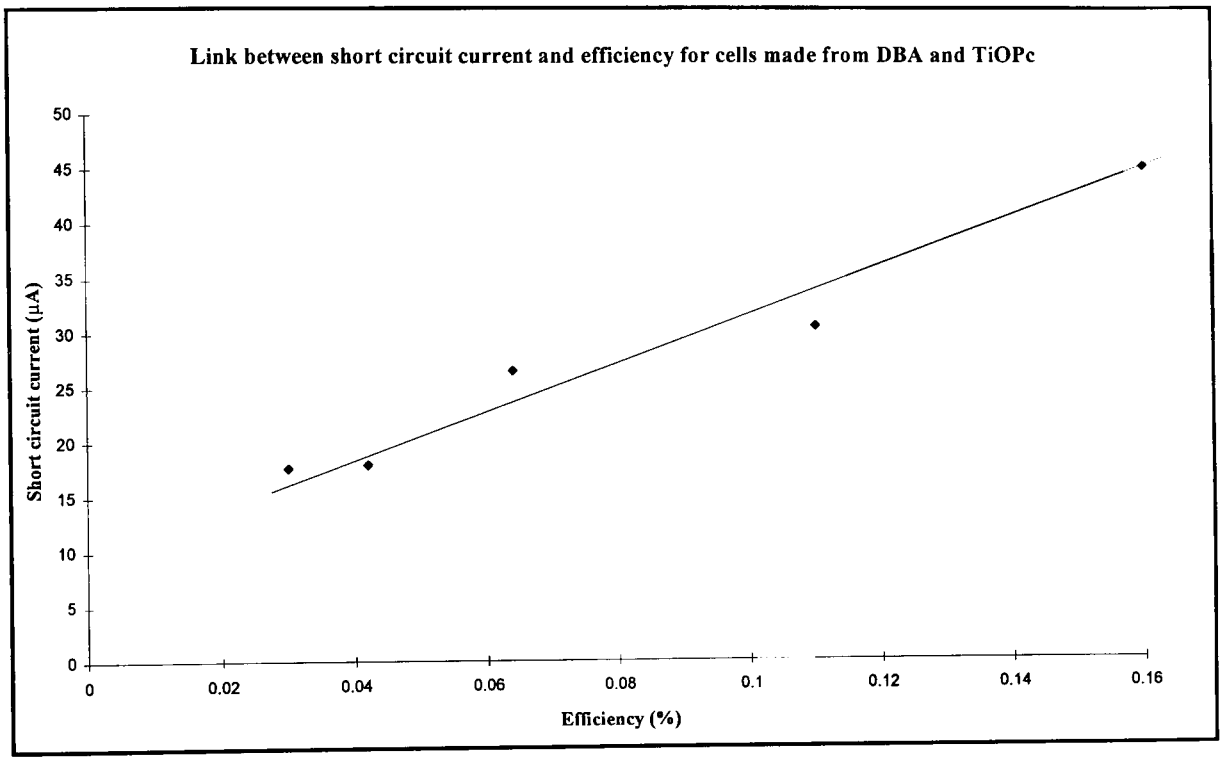

Fig 7.8: Showing link between J_{sc} and efficiency for devices made from DBA-TiOPc.

It is also of interest to see if there is a link between the response time, efficiency and short circuit current for a range of samples prepared under identical conditions. Five different devices [ITO-DBA(500Å)-TiOPc(500Å)-Au] which were prepared identically were tested and their efficiency and response time were measured. The samples were illuminated through the ITO electrode using the $\lambda = 670$nm laser.

The efficiency is directly proportional to J_{sc}, V_{oc} and FF so it is expected that there will be a direct link between the efficiency and J_{sc}. This is what is found (see fig 7.8), as V_{oc} remains constant. The difference in the values for J_{sc} is largely due to different concentrations of traps between the samples. This trap

density should be demonstrated by looking at the response times of the samples.

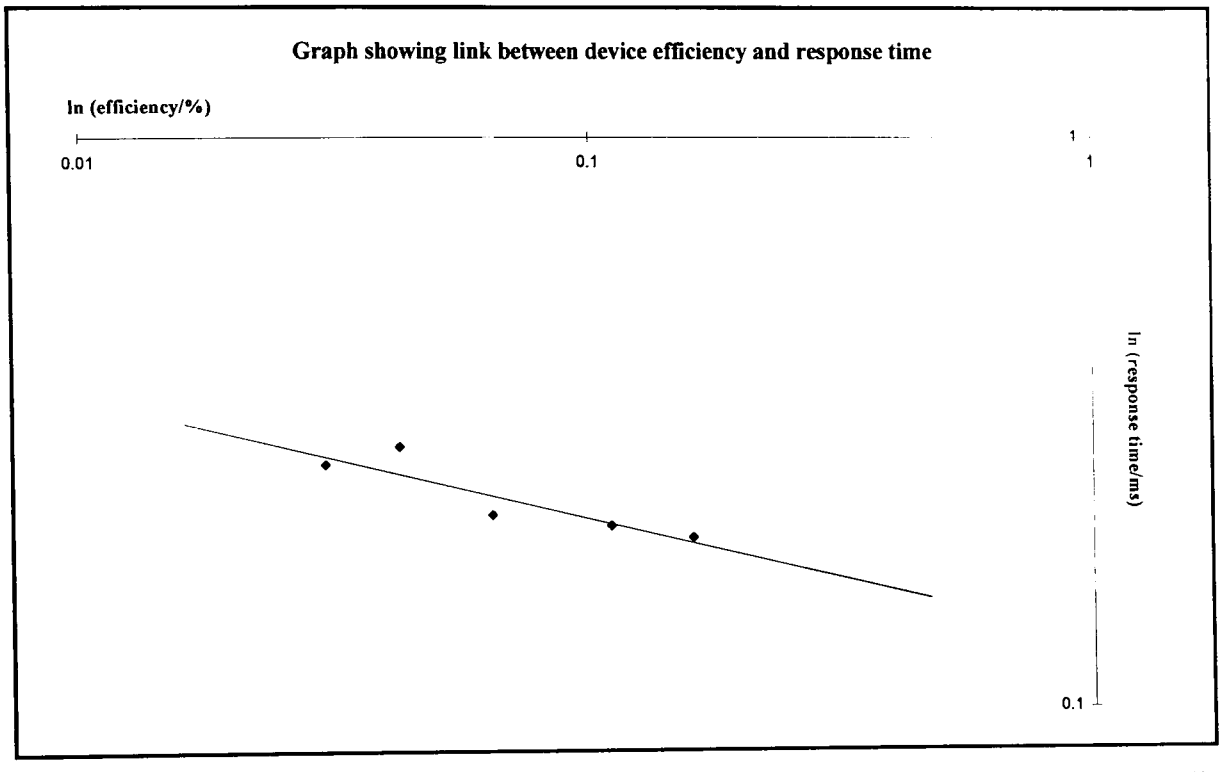

Fig 7.9: Showing the trend between device efficiency and the response time for 5 identically prepared, yet different samples.

The link between the efficiency and the response time of the sample is shown in figure 7.9 with the efficiency against J_{sc} in fig 7.10. These graphs show that for efficient devices, a low trap density is required. This allows for the efficient removal of the photogenerated charge carriers.

The efficiency of these devices can be compared to the photoconductive gain. The photoconductive gain depends upon the mobility, μ, the response time, τ, and the electric field gradient, E/L.

$$G = \mu.\tau.\frac{E}{L} \qquad (1)$$

As mentioned previously, the photoconductive gain can be compared to the efficiency, the mobility to the short circuit current and the gradient of the electric field should remain constant. Thus, a plot of efficiency against the

product of the short circuit current and the response time should be linear. This is found for the DBA-TiOPc cells and is shown in fig 7.11

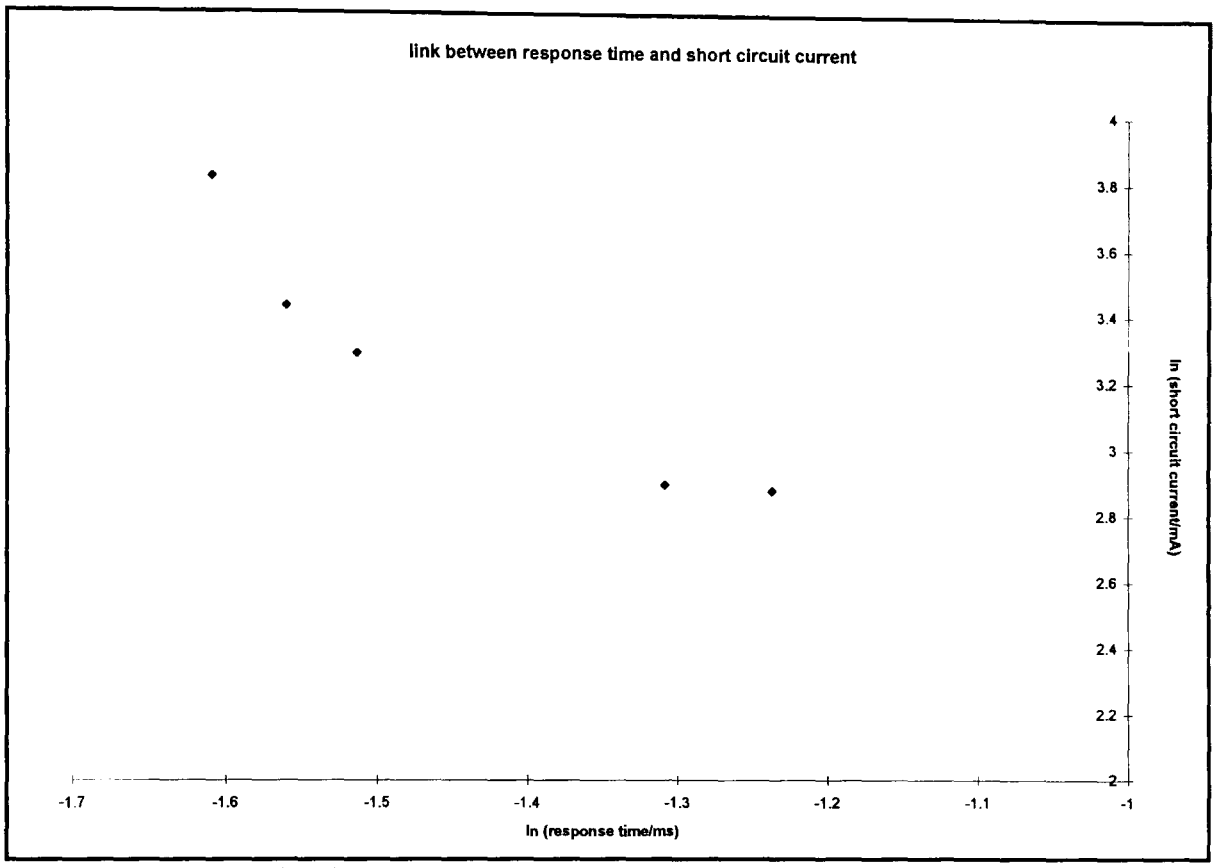

Fig 7.10: Showing link between short circuit current and response time for different DBA-TiOPc samples.

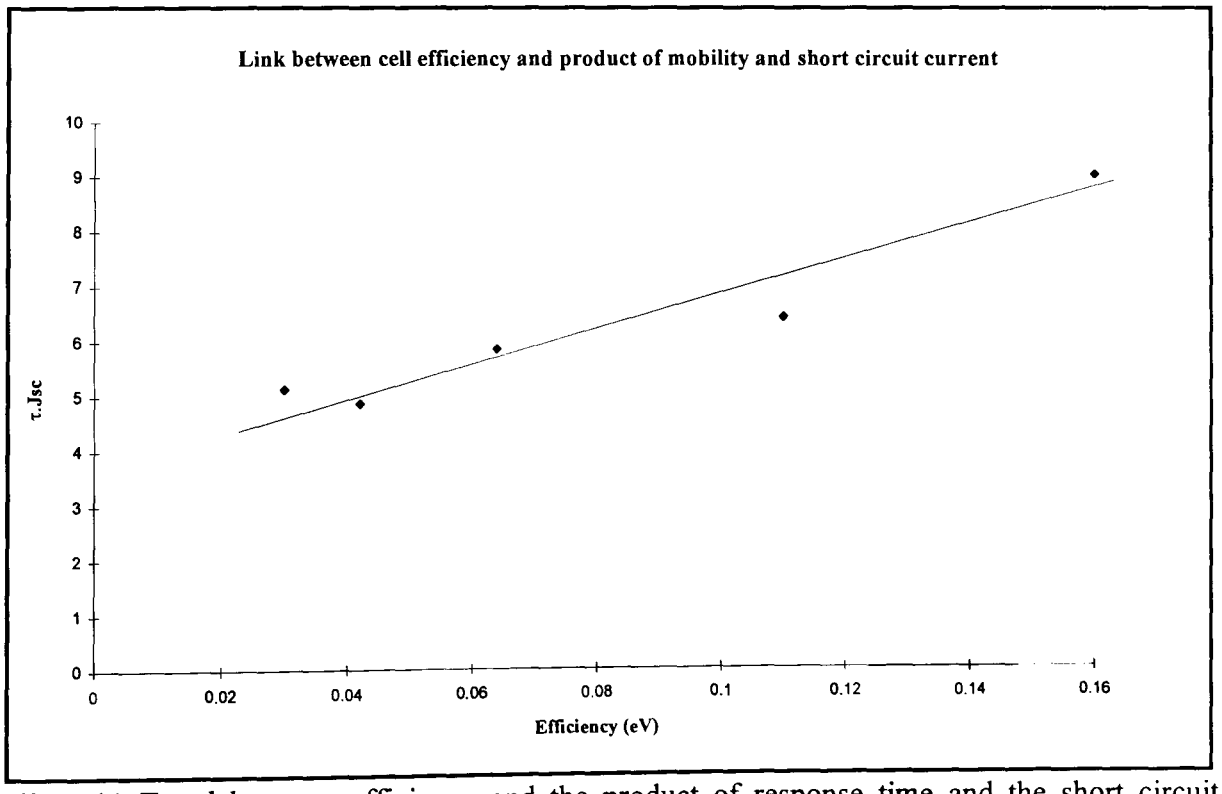

Fig 7.11 Trend between efficiency and the product of response time and the short circuit current for cells made from DBA-TiOPc.

This link was also shown by measurements of the efficiency of samples made from ITO-MPCI-TiOPc-Au. The results are shown in table 7.2

Efficiency (%)	Response time (ms)
0.000012	64
0.0049	30
0.022	4.1

Table 7.2:The link between efficiency and response time for samples of ITO-MPCI-TiOPc-Au.

The only other measurement of the response time for a bilayer cell was by Bakurji[148] who found the response time of an ITO-MPCI-TiOPc-Au cell (made by Shirota) was τ = 0.5ms. This is considerably faster than the value of 4.1ms found in our devices. The relatively efficiency of our device is low compared to the published values for similar devices made by Shirota[33]. Conversely, the response time of the DBA-Sq5 device was fast (τ=0.79ms) despite the poor efficiency. This makes it an important diagnostic tool which indicates whether the quality of the device is poor or if it is a bad combination of materials.

Conclusions

Requirements for organic bilayer solar cells

The following procedure is recommended for deciding the appropriateness of different materials for use in bilayer solar cells:

- Materials should be, or structurally related to, good photoconductors.
- Materials should be thermally stable and sublime (for good film preparation).
- MO calculations should be performed on the materials to find the position of the HOMO and LUMO. Band structure calculations are usually unnecessary unless strong intermolecular interactions are expected which would cause the positions of bands to shift.
- Select a pair of materials, one of which is an electron donor (low ionisation potential) and the other an electron acceptor (higher ionisation potential). Assume that the materials are extrinsic and that the Fermi level is located $E_g/8$ from the relevant transport band.
- Construct a heterojunction band diagram.
- Find a combination which have complimentary absorption spectra.
- Consider substituting one of the layers to make ΔE_c (if the second layer is p-type) as small as possible or make the electron affinities equal.
- Choose electrodes that will make ohmic contacts.
- The front layer and electrode should adsorb as little as possible of the solar radiation.

The extended Huckel method has proved valuable in understanding the reasons why some devices work better than others. This means it should be a useful tool which can be used in deciding which potential partners should be paired together. However, it has only been used to explain results for a system, not to predict the success of a combination. So the real test of the merit of the calculations will be the success in predicting the properties (V_{oc} etc) of a bilayer device made from two unknown materials. The calculations could be

used to assist in the material requirements in other areas, notably electroluminescence and further work in this area is merited.

The variation of the performance of the devices with time merits further investigation. The practical setup used required that the samples were exposed to air before being tested. Testing the samples before breaking the vacuum would help to eliminate some possible dopants, though as the performance increase with time for the first few days, the efficiency may not improve. The response time of the cell has been shown to be a useful tool for measuring the quality of bilayer devices.

References

(1) E. Becquerel *C. R. Hebd. Seances Acad. Sci.* **9** P561 (1839)

(2) W. Adams, R. Day *Proc. R. Soc. London, Ser. A* **25** P113 (1877)

(3) D. Chapin, C. Fuller, G. Pearson *J. Appl. Phys.* **25** P676 (1954)

(4) D. Jenny, J. Loferski, P. Rappaport *Phys. Rev.* **101** P1208 (1956)

(5) 'Molecular Semiconductors' by J. Simon, J. Andre, Springer-Verlag, (1985)

(6) 'Electrical Transport in Solids' by K. Kao, W. Hwang, Pergamon Press (1981)

(7) 'Photoconductivity of Solids' by R. Bube, John Wiley and Sons (1960)

(8) A. Sommerfield *Z. Phys.* **47** P1 (1928)

(9) 'Chemical bonding in solids' by J. Burdett Oxford University Press (1995)

(10) M. Hiramoto, K. Ihara, H. Fukusumi, M. Yokoyama *J. Appl. Phys.* **78** P7153 (1995)

(11) M. Hiramoto, K. Ihara, M. Yokoyama *Jap. J. Appl. Phys.* **34** P3803 (1995)

(12) 'Physics of Semiconductor Devices' by S. Sze John Wiley & Sons (1981)

(13) R. Anderson *IBM J. Res. Dev.* **4** P283 (1960)

(14) 'Fundamentals of Solar Cells' by A. Fahrenbruch, R. Bube, Academic Press (1983)

(15) A. Riben, D. Feucht *Int. J. Electron.* **20** P583 (1966)

(16) D. Cheung, S. Chiang, G. Pearson *Solid State Electron.* **18** P263 (1975)

(17) A. Fahrenbruch, J. Aranovich In 'Topics in applied physics' Vol.31 P257 (1979)

(18) J. Wagner, T. Fritz, H. Bottcher *Phys. Stat. Sol (a)* **136** P423 (1993)

(19) Y. Harima, T. Kodaka, H. Okazaki, Y. Kunugi, K. Yamashita, H. Ishii, K. Seki *Chem. Phys. Letts* **240** P345 (1995)

(20) J. Whitlock, P. Panayotatos *Thin Solid Films* **205** P69 (1991)

(21) S. Ryvkin *Sov. J. Exp. Theor. Phys.* **20** P139 (1950)

(22) V. Merritt, H. Hovel *Appl. Phys. Letts* **29** P414 (1976)

(23) D. Morel, A. Ghosh, T. Feng, E. Stogryn, P. Purwin, R. Shaw, C. Fishman *Appl. Phys. Letts* **32** P495 (1978)

(24) G. Sharma *Synth. Met.* **74**(3) P227 (1995)

(25) Y. Pan, L. Chen, Y.Wang, Y. Zhao, F. Li, A. Wagiki, M. Yamashita, T.Tako *Appl. Phys. Letts* **68**(10) P1314 (1996)

(26) F. Fan, L. Faulkner *J. Chem. Phys.* **69** P3334 and P3341 (1978)

(27) S. Yoshida, K. Kozawa, N. Sato, T. Uchida *Bull. Chem. Soc. Japan* **67** P2017 (1994)

(28) S.A. Chen, Y. Fang *Synth. Met.* **60** P215 (1993)

(29) C.W. Tang *Appl. Phys. Letts* **48** P183 (1986)

(30) S. Siebentritt, S. Gunster, D. Meissner *Synth. Met.* **41-43** P1173 (1991)

(31) J. Whitlock, P. Panayotatos, G. Sharma, M. Cox, R. Sauers, G. Bird *Opt. Eng.* **32** P1921 (1993)

(32) N. Karl, A. Bauer, J. Holzapfel, J. Marktanner, M. Mobus, F. Stolzle *Mol. Cryst. Liq. Cryst.* **252** P243 (1994)

(33) T. Tsuzuki, N. Hirota, N. Noma, Y. Shirota *Thin Solid Films* **273** P177 (1996)

(34) S. Gunster, S. Siebentritt, J. Elbe, L. Kreienhoop, B. Tennigkeit, D. Wohrle, R. Memming, D. Meissner *Mol. Cryst. Liq. Cryst.* **218** P117 (1992)

(35) J. Danziger, J.P. Dodelet, P. Lee, K.W. Nebesny, N.R. Armstrong *Chem. Mat.* **3** P821 (1991)

(36) T. Tsutsui, T. Nakashima, Y. Fujita, S. Saito *Synth. Met.* **71** P2281 (1995)

(37) D. Wohrle, L. Kreienhoop, G. Schnurpfeil, J. Elbe, B. Tennigkeit, S. Hiller, D. Schlettwein *J. Mat. Chem.* **5** P1819 (1995)

(38) M. Hiramoto, Y. Kishigami, M. Yokoyama *Chem. Letts* **1** P119 (1990)

(39) T. Tsuzuki, Y. Kuwabara, N. Noma, Y. Shirota, M. Willis *Jap. J. Appl. Phys. Pt2-Letts* **35** PL447 (1996)

(40) M. Hiramoto, H. Fukusumi, M. Yokoyama *Appl. Phys. Letts* **61** P2580 (1992)

(41) T. Shichiri, M. Suezaki, T. Inoue *Chem. Letts* **9** P1717 (1992)

(42) M. Hiramoto, H. Fujiwara, M. Yokoyama *Appl. Phys. Letts* **58** P1062 (1991)

(43) S. Antohe, V. Ruxandra, L. Tugulea, V. Gheorghe, D. Ionescu *J. de Physique III* P1133 (1996)

(44) M. Hiramoto, M. Suezaki, M. Yokoyama *Chem. Letts* **3** P327 (1990)

(45) H. Yanagi, N. Tanura, S. Taira, H. Furuta, S. Douko, G. Schnurpfeil, D. Wohrle *Mol. Cryst. Liq. Cryst.* **267** P435 (1995)

(46) S. Antohe, L. Tugulea *Phys. Stat. Sol. (a)* **128** P253 (1991)

(47) Y. Harima, K. Yamashita, H. Suzuki *Appl. Phys. Letts* **45** P1144 (1984)

(48) N. Noma, T. Tsuzuki, Y. Shirota *Adv. Mat.* **7** P647 (1995)

(49) K.Uehara, A. Maekawa, A. Sugimoto, H. Inoue *Thin Solid Films* **215** P123 (1992)

(50) N. Noma, K. Namba, Y. Shirota *Synth. Met.* **64** P227 (1994)

(51) K. Yamashita, Y. Kunugi, Y. Harima, A. Chowdhury *Jap. J. Appl. Phys. Pt 1* **34** P3794 (1995)

(52) B. Gregg, Y. Kim *J. Phys. Chem.* **98** P2412 (1994)

(53) B. Gregg *Appl. Phys. Letts* **67** P1271 (1995)

(54) V. Agranovich, G. La Rocca , F. Bassani *JEPT Letts* **62** P418 (1995)

(55) H. Yanagi, H. Kataura, Y. Ueda *J. Appl. Phys.* **75** P569 (1994)

(56) J. Takada, H. Awaji, M. Koshioka, W. Nevin, M. Imanishi, N. Fukada *J. Appl. Phys.* **75** P4055 (1994)

(57) B. Gregg *Chem. Phys. Letts* **258** P376 (1996)

(58) G. Sharma, S. Mathur, D. Dube *J. Mat. Sci.* **26** P6547 (1991)

(59) B. O'Regan, M. Gratzel *Nature* **353** P737 (1991)

(60) A. Braun, J. Tcherniac *Berichte Deutsche Chemie Gesellschaft* **40** P2709 (1907)

(61) G. Bryne, R. Linstead, A. Lowe *J. Chem. Soc.* P1017 (1934)

(62) C. Dent, R. Linstead, A. Lowe *J. Chem. Soc.* P1027 (1934)

(63) C. Dent, R. Linstead, A. Lowe *J. Chem. Soc.* P1033 (1933)

(64) J. Sharp, M. Lardon *J. Phys. Chem.* **72** P3230 (1968)

(65) A. Ebert, H. Gottlieb *J. Am. Chem. Soc.* **74** P2806 (1952)

(66) J. Byrne, P. Kurz *U.S. Patent 3,357,989* (1969)

(67) T. Enokida, R. Hirohashi, S. Mizukami *J. Imag. Sci.* **35** P235 (1991)

(68) T. Enokida, S. Ehashi *Chem. Letts* **2** P179 (1988)

(69) P. Ghosez, R. Cote, L. Gastonguay, G. Veilleux, G. Denes, J. Dodelet *Chem. Mat.* **5** P1581 (1993)

(70) T. Enokida, R. Hirohashi, T. Nakamura *J. Imag. Sci.* **34** P234 (1990)

(71) A. Lever *Adv. Inorg. and Radiochem.* 7 P27 (1965)

(72) C. Liang, E. Scalco *J. Electrochem. Soc.* **110** P779 (1963)

(73) J. Bornmann *J. Chem. Phys.* **27** P604 (1954)

(74) P. Day, R. Williams *J. Chem. Phys.* **37** P567 (1962)

(75) H. Yasunaga, K. Kasai, K. Takeya *J. Phys. Soc. Jap.* **46** P839 (1979)

(76) K. Gamo, K. Masuda, J. Yamaguchi *J. Phys. Soc. Jap.* **25** P431 (1968)

(77) A. Twarowski *J. Chem. Phys.* **76** P2640 (1982)

(78) E. Menzel, K. Jordan *Chem. Phys.* **32** P223 (1978)

(79) E. Menzel, Z. Popovic *Chem. Phys. Letts* **55** P177 (1978)

(80) R. Loutfy, E. Menzel *J. Am. Chem. Soc.* **102** P4967 (1980)

(81) R. Ahuja, K. Hauffe *Ber. Bunsen-Ges. Phys. Chem.* **84** P68 (1980)

(82) Z. Popovic *Chem. Phys.* **86** P311 (1984)

(83) Y. Fujimaki *IS&T Proceedings, 7th International Congress on Advances in Non-Impact Printing Technologies* P269 (1991)

(84) R. Regensburger, J. Jakubowski *U.S. Patent 3,904,407* (1975)

(85) M. Hiramoto, T. Imahigashi, M. Yokoyama *Appl. Phys. Letts* **64** P187 (1994)

(86) T. Maki, H. Hashimoto *Bull. Chem. Soc. Jap.* **25** P411 (1952)

(87) G. Klebe, F. Graser, E. Hadicke, J. Berndt *Acta Cryst.* **B45** P69 (1989)

(88) K. Law *Chem. Revs.* **93** P449 (1993)

(89) Z. Popovic, A. Hor, R. Loutfy *Chem. Phys.* **127** P451 (1988)

(90) H. Sprenger, W. Ziegenbein *Angew. Chem. Int. Ed. Eng.* **6** P553 (1968)

(91) K. Law, F. Bailey *Can. J. Chem.* **64** P2267 (1986)

(92) R. Wingnard *IEEE Ind. Appl.* **37** P1251 (1982)

(93) N. Allen, E. Robinson, C. Stott, F. Thompson *Dyes Pigm.* **10** P183 (1989)

(94) A. Karishan, D. Kustol *Zh. Obshch. Chim.* **31** P1655 (1961)

(95) H. Goldstein, P. Francy *Helv. Chim. Acta* **15** P1367 (1932)

(96) L. Viaene, H. Vanmingroot, P. Vanhaver, M. Vanderanweraer, F. Deschryver, A. Itaya, H. Masuhara *J. Photochem. & Photobiol.* **A66** P1 (1992)

(97) R. Elliot-Martin Ph.D. Thesis University of Nottingham **1994**

(98) Y. Yamashita, T. Suzuki, T. Mukai, G. Saito *J. Chem. Soc. Chem. Comm.* **15** P1044 (1985)

(99)Y. Yamashita, S. Tanaka, K. Imaeda, H. Inokuchi, M. Sano *J. Org. Chem.* **57** P5517 (1992)

(100) G. Tamizhmani, J. Dodelet, R. Cote, D. Gravel *Chem. Mat.* **3** P1046 (1991)

(101) K. Law, F. Bailey *Can. J. Chem.* **64** P2267 (1986)

(102) 'Textbook of practical organic chemistry' *(4th Ed.)* by A.Vogel Longman, London and New York (1978)

(103) H. Wagner, R. Loutfy, C. Hsiao *J. Mat. Sci.* **17** P2781 (1982)

(104) S. Kinge Ph.D Thesis University of Nottingham (1994)

(105) H. Yonehara, C. Pac *Thin Solid Films* **278** P108 (1996)

(106) J. Kido, C. Ohtaki, K. Hongawa, K. Okyama, K. Nagai *Jap. J. Appl. Phys. Letts* **32** PL917 (1993)

(107) R. Hoffmann *Angew. Chem. Int. Ed. Eng.* **26** P846 (1987)

(108) R. Hoffmann, W. Lipscomb *J. Chem. Phys.* **36** P2179 (1972)

(109) L. Lohr W. Lipscomb *ibid.* **38** P1607 (1963)

(110) R. Hoffmann *J. Chem. Phys* **39** P1397 (1963)

(111) For a review, see 'Quantum Chemistry' by J. Lowe Academic Press (1993)

(112) J. Slater *Phys. Rev.* **115** P1216 (1959)

(113) I. Chen *J. Chem. Phys.* **51** P3241 (1969)

(114) R. Jerrard, A. Amos, P. Brook *Theo. Chim. Acta* **61** P163 (1982)

(115) S. Hong, D. Marynick *J. Chem. Phys.* **96** P5497 (1992)

(116) A. Anderson *J. Chem. Phys.* **62** P1187 (1975)

(117) G. Calzaferri, L. Forss, I. Kamber *J. Phys. Chem.* **93** P5366 (1989)

(118) C. Roetti, E. Clementi *J. Chem. Phys.* **60** P4725 (1974)

(119) A. Schaffer, M. Goutermann, E. Davidson *Theo. Chim. Acta* **30** P9 (1973)

(120) M. Whangbo, R. Hoffmann, R. Woodward *Proc. R. Soc. Lond. A* **366** P23 (1979)

(121) M. Willis, T. Mori, H. Inokuchi *Bull. Chem. Soc. Jpn.* **61** P2211 (1988)

(122) R. Haddon, T. Siegrist, R. Fleming, P. Bridenbaugh, R. Laudise *J. Mat. Chem.* **5** P1719 (1995)

(123) E. Canadell, S. Alvarez *Inorg. Chem.* **23** P573 (1984)

(124) P. Gomez-Romero, Y. Lee, M. Kertesz *Inorg. Chem.* **27** P3672 (1988)

(125) S. Cain, D. Gale J. Gaudiello *J. Phys. Chem.* **95** P9584 (1991)

(126) P. Kazmaier, R. Hoffmann *J. Am. Chem. Soc.* **116** P9684 (1994)

(127) M. Bohm *Chem. Phys.* **86** P17 (1984)

(128) F. Kutzler, D. Ellis *J. Chem. Phys.* **84** P1033 (1986)

(129) P. Hale, M. Ratner *J. Chem. Phys.* **83** P5277 (1985)

(130) E. Orti, J. Bredas *J. Chem. Phys.* **89** P1009 (1988)

(131) E. Orti, J. Bredas *Synth. Met.* **33** P27 (1989)

(132) E. Orti, R. Crespo, M. Piqueras, J. Bredas *Synth. Met.* **42** P2647 (1991)

(133) E. Orti, J. Bredas *J. Am. Chem. Soc.* **114** P8669 (1992)

(134) E. Orti, J. Bredas, C. Clarisse *J. Chem. Phys.* **92** P1228 (1990)

(135) M. Dewar, E. Zoebisch, E. Healy, J. Stewart *J. Am. Chem. Soc* **107** P3902 (1985)

(136) K. Imaeda, Y. Li, Y. Yamashita, H. Inokuchi, M. Sano *J. Mat. Chem.* **5** P861 (1995)

(137) P. Hale, W. Pietro, M. Ratner, D. Ellis, T. Marks *J. Am. Chem. Soc.* **109** P5943 (1987)

(138) T. Anderson, G. Komplin, W. Pietro *J. Phys. Chem.* **97** P6577 (1993)

(139) D. Schlettwein, N. Armstrong *J. Phys. Chem.* **98** P11771 (1994)

(140) M. Willis *Mol. Cryst. Liq. Cryst.* **171** P217 (1989)

(141) H. Fujimoto, A. Dann, M. Fahy, J. Lequesne, M. Willis *J. Mat. Chem.* **6** P1361 (1996)

(142) J. Meyer, D. Schlettwein, D. Wohrle, N. Jaeger *Thin Solid Films* **258** P317 (1995)

(143) N. Sato, M. Yoshikawa *J. Elect. Spect.* **78** P387 (1996)

(144) J. Kido, K. Hongawa, K. Okuyama, K. Nagai *Appl. Phys. Letts* **64** P815 (1994)

(145) T. Mori, K. Miyachi, T. Mizutani *J. Phys. D: Appl. Phys.* **28** P1461 (1995)

(146) M. Matsumura, T. Akai *Jap. J. Appl. Phys.* **35** P5359 (1996)

(147) B. Gossick *Surf. Sci.* **25** P465 (1971)

(148) E. Bakhurji Ph.D Thesis University of Nottingham (1993)

(149) C. Mealli, D Proserpio *J. Chem. Ed.* **67** P399 (1990)

(150) G. Williams, R. Mason, S. Mason, P. Fielding *J. Chem. Soc. Dalton* P1688 (1980)

(151) I. Edwards, H. Stadler *Acta. Cryst.* **B27** P946 (1971)

(152) M. Fahy, H. Fujimoto, A. Dann, H. Hoshi, H. Inokuchi, Y. Maruyama, M. Willis *Phys. Scripta* **41** P550 (1990)

Appendix 1:- Instructions for the operation of QCPE. 571

This package is made up of three programs called EHMACC (which calculates the energy levels of the molecule or crystal over a range in k-space), EHPC (which orders the energy levels for a Band calculation and calculates a metallic Fermi level) and EHPP (which plots out the results in the form of DOS plots). EHPC and EHPP are only used for band calculations and run using files generated by EHMACC. When running a molecular calculation, only the EHMACC program is used. The programs (written in FORTRAN) are run on the Alpha computer at the Cripps Computing Centre.

EHMACC

This program completes the molecular orbital calculations for molecules or band structures using the extended Huckel method. The results of the calculations are stored in the output files filename.eh1, filename.eh2 (which are used by EHPC) and filename.eho which lists the results of the calculation in output form. The program requires an input file (filename.ehi) which lists the coordinates of the atoms and options for the calculation. The atomic coordinates can be input using Cartesian coordinates or bond lengths and angles. For band calculations, it is necessary to define the unit cell. This is done by including the coordinates of an atom in the next unit cell at the end of the list of atoms within the unit cell and then telling the program which atom within the unit cell that it is equivalent to. It is also necessary to create a mesh in k-space over which band calculations will be performed. If the calculation is in 1D (i.e. only one equivalent atom is defined), then the mesh needs only to range over 1D (i.e. only one coordinate needs to be varied). For the calculation to be successful, the mesh should cover the first Brillouin Zone evenly. This means that if the unit cell vector is 5 Angstroms, then the value of k should range between zero and the reciprocal of the unit cell vector (i.e. it should be

evenly spaced from 0.0 to 0.2 in this case). For a full list of all the other options, refer to the manual.

EHPC

This program converts the results of the band calculations into a more useful form giving values for the Fermi level and atomic orbital populations etc. The program requires the input files filename.eh1 and filename.eh2 (generated by EHMACC) as well as filename.ehpi which contains the options for the calculations. Two output files are generated, filename.ehpo which lists the results of the calculations along with filename.eh5 which is used by EHPP to plot the results. The values of the Fermi level quoted are metallic Fermi levels (i.e. the position of the nth energy level) hence it is only possible to calculate the intrinsic Fermi level by averaging the upper edge of the HOMO and the lower edge of the LUMO. The program requires the user to input a value for the smoothing used in DOS plots. The lower the number used, the narrower the Gaussian distribution used on each band. For DOS plots a value of 0.02eV was used as this was found to be sufficiently small to not distort the shape of the curves. A larger value of 0.60eV was used to simulate the PES spectra because the resolution obtained practically makes the smoother curves more accurate.

EHPP

This program converts the data in filename.eh5 into a set of points which were plotted using EXCEL.

Running the programs from the computer in A26

The following instructions are for logging on to the computer in A26 using Decce which means that the editor for files is ECCE. This is an old editor so people with experience of other editors will probably prefer to use them.

Turn on the computer and type '*netstart*'. This turns on the network card inside the computer and links the computer to Cripps Computing Centre.
Type '*Decce*'
At the 'PAD>' prompt type '*call alpha*'.
Input the username and password when prompted (ask Dr. Willis for these).

There are two main directories called EHMACC which stores the programs and EHDAT which contains the input files. There is also a temporary directory called pc_temp which has a large filestore where programs can be run but as it is a temporary filestore set up for all the chemistry department. Note that you aren't allowed to go over your filestore limit. If you do, then the program that is running will terminate immediately.

Some useful commands on the alpha system are:

set def [directory name]	This changes the current directory to the one named in the bracket. i.e. to change from EHDAT to EHMACC, type '*set def [pcxjplq.ehmacc]*'
as (short for assign)	This assigns a filename to a channel. The channel remains assigned until the command is superseded or you log off.
Show quota	Tells you the amount of filestore used/ free
Delete filename;no	When deleting a file, it is necessary to say which version you are deleting. To delete all files with the same name then use '*', e.g. to delete all generations of filename.dat, type '*filename.dat;**'

Dir	Shows all files in the current directory. To see the size of all the files in a directory, type '*dir/siz*'
Purge	Deletes all older generations of files (up to 3 generations of the same filename can be stored).

Running EHMACC

Before running the program, you need to assign (type) the following (at a $ prompt):

as [pc_temp]filename.eh1 for001
as [pc_temp]filename.eh2 for002
as [pcxjplq.ehdat]filename.ehi for005
as [pcxjplq.ehdat]filename.eho for006
as sys$output for010
run ehmacc/ ehmacc2

Filename.eh1 and .eh2 are usually assigned to the directory pc_temp because they tend to be large programs and this is a much larger directory. There are 2 versions of the EHMACC program. EHMACC has the traditional Wolfsberg-Helmholz formula for the off- diagonal elements, whereas EHMACC2 contains the form proposed by Hong and Marynick[115] (Note that the keyword uwij should never be included in an input file when using EHMACC2).

Running EHPC

Before running EHPC, it is necessary to assign/type the following:

as [pc_temp]filename.eh1 for001
as [pc_temp]filename.eh2 for002

```
as [pcxjplq.ehdat]benb.ehpi for005
as [pcxjplq.ehdat]filename.ehpo for006
as [pcxjplq.ehdat]filename.eh5 for007
run ehpc
```

The file that contains the options for this calculation is called benb.ehpi. It is important to set the output for the metallic Fermi levels so that it covers those around the band gap. The number of electrons in the system is printed in the output file filename.eho. The same is true for the energy range over which the density of states plot is performed. The number of points in a graph (usually set at 1000) and the smoothing are also varied in the input file.

Running EHPP

Before running EHPP, it is necessary to type/assign the following:

```
as [pcxjplq.ehdat]graphite-prop.ehpli for001
as sys$output for002
as sys$output for004
as [pcxjplq.ehdat]filename.eh5 for005
as [pcxjplq.ehdat]filename.dat for006
run ehpp
```

When the program runs, you are prompted for several options. Firstly, choose number 1 ('Density of states' plot) and after a long list of numbers have come up on the screen, several options are given. To get a 'traditional' DOS plot, it is necessary to switch the axes. All other options can be ignored (i.e. the default options are correct). The output of the program is in the form of pairs of data points in filename.dat. The file has 10 lines of garbage at the top and 3 lines at the bottom which are best deleted. The file can then be transferred to the hard disc of the computer and plotted out using a graph drawing package. Alternatively, there is a program (called graph) which uses the simple plot

routine to print out the results but this program doesn't run on the alpha computer so the files have to be transferred to the Vax computer and it is found in the EHMACC directory in Dr. M.R. Willis's account. Because the program is written in FORTRAN, it is necessary to check that the spacing of the pairs of numbers matches that written in the input file.

Using the ECCE editor

This editor always overwrites so any extra spaces must be inserted. To delete, use the delete key rather than the backspace key.
To edit a file, type 'ecce filename'

A '>' will appear. At this point, the following commands are useful:

m10	moves 10 lines down
m-*	move to the top of the file
k10	deletes the next 10 lines
f/fred/	finds the first time fred appears in the file
(f/fred/s/bill/)*	replaces all fred's with bill (note that the case is important)

To view the file, press CTRL + V. The following then apply:

CTRL + W	Adds a space
CTRL + S	Adds a line
CTRL + D	Deletes a line
CTRL + C	Ends viewing session. This returns you to the '>' prompt.

To end the session, either type:

%a	this abandons the editing session and leaves the file unchanged

%c this saves the changes to the file, then quits.

If the file you wish to edit is a larger than the filestore remaining, then the error message 'Unable to open output file' will appear.

Other points:

To change the values of the constants used in EHMACC2, then edit EHMACC2.FOR and the values are found at lines 5084 and 5085. When they have been changed, it is necessary to re-format the program by typing '*for ehmacc2*' then '*link ehmacc2*'. This creates the files EHMACC2.OBJ and EHMACC2.EXE. As these files are large, it is sometimes necessary to delete the old generations of the file before formatting the new version.

Appendix 2:- List of parameters used in calculations

Single-zeta Slater Type Orbitals

C	2s.	H_{ii} = -21.400	zeta1 = 1.625	c1 = 1.000
	2p.	H_{ii} = -11.400	zeta1 = 1.625	c1 = 1.000
N	2s.	H_{ii} = -26.800	zeta1 = 1.950	c1 = 1.000
	2p.	H_{ii} = -13.400	zeta1 = 1.950	c1 = 1.000
O	2s.	H_{ii} = -32.300	zeta1 = 2.275	c1 = 1.000
	2p.	H_{ii} = -14.800	zeta1 = 2.275	c1 = 1.000
F	2s.	H_{ii} = -40.000	zeta1 = 2.425	c1 = 1.000
	2p.	H_{ii} = -18.100	zeta1 = 2.425	c1 = 1.000
S	3s.	H_{ii} = -20.000	zeta1 = 2.122	c1 = 1.000
	3p.	H_{ii} = -13.300	zeta1 = 1.827	c1 = 1.000
H	1s.	H_{ii} = -13.600	zeta1 = 1.300	c1 = 1.000

Double zeta parameters

C	2s.	H_{ii} = -21.400	zeta1 = 1.831	c1 = 0.762
			zeta2 = 1.153	c2 = 0.263
	2p.	H_{ii} = -11.400	zeta1 = 2.730	c1 = 0.260
			zeta2 = 1.257	c2 = 0.803

Parameters proposed by Jerrard[114]

C	2s.	H_{ii} = -19.700	zeta1 = 1.658	c1 = 1.000
	2p.	H_{ii} = -13.250	zeta1 = 1.618	c1 = 1.000
H	1s.	H_{ii} = -11.690	zeta1 = 1.300	c1 = 1.000

Appendix 3: Listings of the coordinates used for the extended Huckel calculations

Coordinates used for calculations on metal free phthalocyanine (H_2Pc)[150]

N	0.000000	0.000000	1.906000
C	1.097000	0.000000	2.719500
N	2.369790	0.000000	2.369790
C	2.719500	0.000000	1.097000
N	1.906000	0.000000	0.000000
C	2.719500	0.000000	-1.097000
N	2.369790	0.000000	-2.369790
C	1.097000	0.000000	-2.719500
N	0.000000	0.000000	-1.906000
C	-1.097000	0.000000	-2.719500
N	-2.369790	0.000000	-2.369790
C	-2.719500	0.000000	-1.097000
N	-1.906000	0.000000	0.000000
C	-2.719500	0.000000	1.097000
N	-2.369790	0.000000	2.369790
C	-1.097000	0.000000	2.719500
C	-0.692500	0.000000	4.149000
C	-1.413500	0.000000	5.331000
H	-2.358400	0.000000	5.327600
C	-0.693800	0.000000	6.507200
H	-1.146200	0.000000	7.342000
C	0.693800	0.000000	6.507200
H	1.146200	0.000000	7.342000
C	1.413500	0.000000	5.331000
H	2.358400	0.000000	5.327600
C	0.692500	0.000000	4.149000
C	4.149000	0.000000	0.692500
C	5.331000	0.000000	1.413500
H	5.327600	0.000000	2.358400
C	6.507200	0.000000	0.693800
H	7.342000	0.000000	1.146200
C	6.507200	0.000000	-0.693800
H	7.342000	0.000000	-1.146200
C	5.331000	0.000000	-1.413500
H	5.327600	0.000000	-2.358400
C	4.149000	0.000000	-0.692500
C	0.692500	0.000000	-4.149000
C	1.413500	0.000000	-5.331000
H	2.358400	0.000000	-5.327600
C	0.693800	0.000000	-6.507200
H	1.146200	0.000000	-7.342000
C	-0.693800	0.000000	-6.507200
H	-1.146200	0.000000	-7.342000
C	-1.413500	0.000000	-5.331080
H	-2.358400	0.000000	-5.327600
C	-0.692500	0.000000	-4.149000
C	-4.149000	0.000000	-0.692500
C	-5.331000	0.000000	-1.413500
H	-5.327600	0.000000	-2.358400
C	-6.507200	0.000000	-0.693800
H	-7.342000	0.000000	-1.146200

C	-6.507200	0.000000	0.693800
H	-7.342000	0.000000	1.146200
C	-5.331000	0.000000	1.413500
H	-5.327600	0.000000	2.358400
C	-4.149000	0.000000	0.692500
H	0.000000	0.000000	0.906000
H	0.000000	0.000000	-1.906000

Coordinates used in calculations on a perylene[87]

C	0.700000	0.000000	-1.212000
C	-0.772000	0.000000	-1.212000
C	-1.502000	0.000000	-2.408000
C	-2.904000	0.000000	-2.391000
C	-3.586000	0.000000	-1.238000
C	-2.904000	0.000000	0.023000
C	-3.621000	0.000000	1.221000
C	-2.948000	0.000000	2.415000
C	-1.549000	0.000000	2.430000
C	-0.800000	0.000000	1.277000
C	0.672000	0.000000	1.279000
C	1.399000	0.000000	2.476000
C	2.801000	0.000000	2.462000
C	3.485000	0.000000	1.309000
C	2.806000	0.000000	0.048000
C	3.525000	0.000000	-1.149000
C	2.854000	0.000000	-2.345000
C	1.457000	0.000000	-2.420000
C	-1.481000	0.000000	0.015000
C	1.379000	0.000000	0.054000
C	-5.086000	0.000000	-1.227000
O	-5.699000	0.000000	-2.294000
N	-5.690000	0.000000	-0.020000
H	-6.650000	0.000000	0.000000
O	-5.628000	0.000000	2.321000
C	-5.045000	0.000000	1.254000
C	5.025000	0.000000	-1.129000
O	5.651000	0.000000	-2.179000
N	5.614000	0.000000	0.094000
H	6.574000	0.000000	0.094000
O	5.580000	0.000000	2.419000
C	4.954000	0.000000	1.360000
H	-1.042000	0.000000	-3.251000
H	-3.394000	0.000000	-3.217000
H	-3.437000	0.000000	3.241000
H	-1.042000	0.000000	3.251000
H	0.938000	0.000000	3.318000
H	3.290000	0.000000	3.288000
H	3.394000	0.000000	-3.217000
H	1.023000	0.000000	-3.276000

Coordinates for the calculations on a Squaraine

C	1.050000	0.000000	0.000000
O	2.273000	0.000000	0.000000
C	-0.009000	0.000000	-1.041000
C	-0.009000	0.000000	-2.468000
C	1.203000	0.000000	-3.222000
H	2.169000	0.000000	-2.715000
C	1.203000	0.000000	-4.619000
H	2.180000	0.000000	-5.106000
C	-0.009000	0.000000	-5.374000
N	-0.009000	0.000000	-6.778000
H	0.923000	0.000000	-7.345000
H	-0.941000	0.000000	-7.345000
C	-1.222000	0.000000	-4.619000
H	-2.198000	0.000000	-5.106000
C	-1.222000	0.000000	-3.222000
H	-2.187000	0.000000	-2.715000
C	-1.068000	0.000000	0.000000
O	-2.291000	0.000000	0.000000
C	-0.009000	0.000000	1.041000
C	-0.009000	0.000000	2.468000
C	1.203000	0.000000	3.222000
H	2.169000	0.000000	2.715000
C	1.203000	0.000000	4.619000
H	2.180000	0.000000	5.106000
C	-0.009000	0.000000	5.374000
N	-0.009000	0.000000	6.778000
H	0.923000	0.000000	7.345000
H	-0.941000	0.000000	7.345000
C	-1.269000	0.000000	4.701000
H	-2.211000	0.000000	5.252000
C	-1.361000	0.000000	3.308000
H	-2.359000	0.000000	2.866000

Coordinates used in calculations on Anthanthrone (MOPAC version)

C	0.000000	0.000000	0.000000
C	1.452400	0.000000	0.000000
C	-0.715600	1.191300	0.000000
C	2.168000	1.191300	0.000000
C	-0.696000	-1.247300	0.000000
C	2.148400	1.247300	0.000000
C	-2.113300	-1.255700	0.000000
C	3.565700	1.255700	0.000000
C	0.008400	-2.486200	0.000000
C	1.444000	2.486200	0.000000
C	1.483900	-2.502400	0.000000
C	-0.031500	2.502400	0.000000
C	-0.690400	-3.678500	0.000000
C	2.142800	3.678500	0.000000
C	-2.104600	-3.682800	0.000000
C	3.557000	3.682800	0.000000
C	-2.801400	-2.500400	0.000000
C	4.253800	2.500400	0.000000

C	-2.813700	-0.021100	0.000000
C	4.266100	0.021100	0.000000
C	-2.133100	1.170600	0.000000
C	3.585500	-1.170600	0.000000
O	2.122300	-3.566300	0.000000
O	-0.669900	3.566300	0.000000
H	-0.139800	-4.634600	0.000000
H	1.592200	4.634600	0.000000
H	-2.633700	-4.647900	0.000000
H	4.086100	4.647900	0.000000
H	-3.902800	-2.493700	0.000000
H	5.355200	2.493700	0.000000
H	-3.914700	-0.037800	0.000000
H	5.367100	0.037000	0.000000
H	-2.667700	2.135600	0.000000
H	4.120000	-2.135600	0.000000